Functions of the midline thalamic nucleus reuniens

Dolleman-van der Weel, M.J.

2018

document version
Publisher's PDF, also known as Version of record

FUNCTIONS OF THE MIDLINE THALAMIC NUCLEUS REUNIENS

A combined anatomical, electrophysiological and behavioral study in the rat

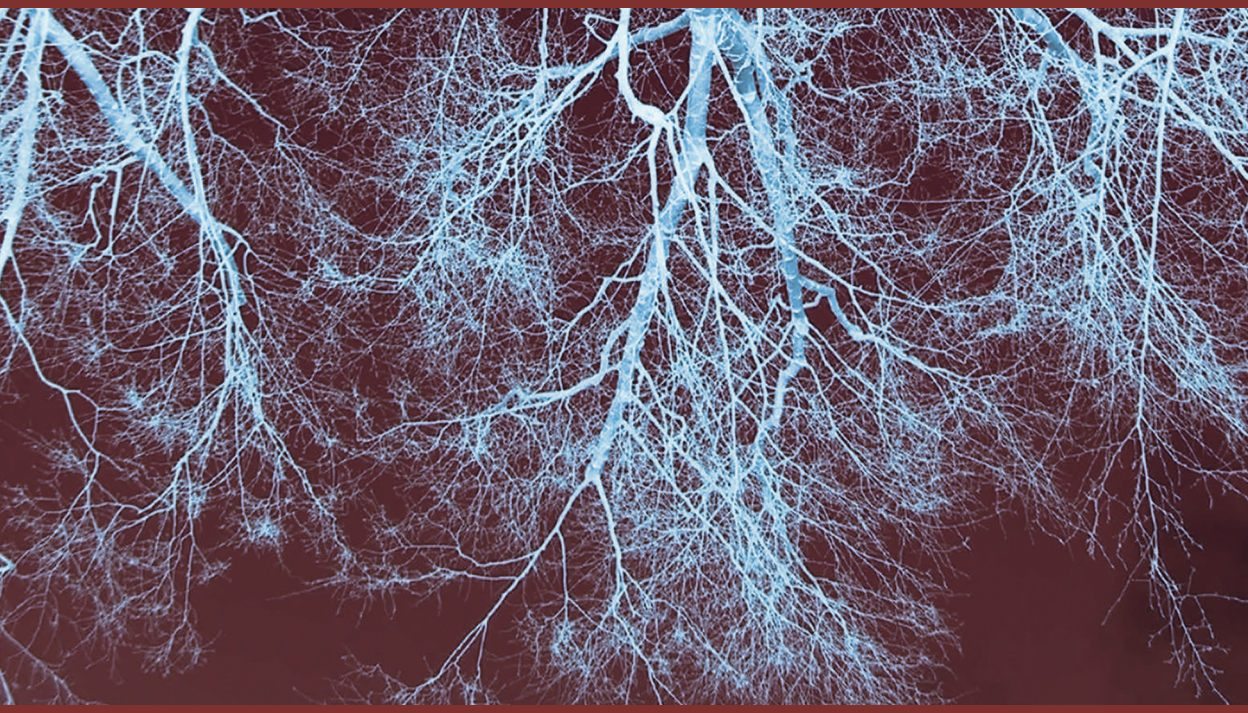

Margriet Dolleman-van der Weel

FUNCTIONS OF THE MIDLINE THALAMIC NUCLEUS REUNIENS

A combined anatomical, electrophysiological and behavioral study in the rat

ISBN: 978-90-828478-0-2 (hard copy)
ISBN: 978-90-828478-1-9 (electronic version)
Cover design / layout: Margriet Dolleman-van der Weel, Natasja Akkerman
Printing: Drukkerij Haveka bv, Alblasserdam

VRIJE UNIVERSITEIT

Functions of the midline thalamic nucleus reuniens

A combined anatomical, electrophysiological and behavioral study in the rat

ACADEMISCH PROEFSCHRIFT

ter verkrijging van de graad Doctor
aan de Vrije Universiteit Amsterdam,
op gezag van de rector magnificus
prof.dr. V. Subramaniam,
in het openbaar te verdedigen
ten overstaan van de promotiecommissie
van de Faculteit der Geneeskunde
op woensdag 30 mei 2018 om 13.45 uur
in de aula van de universiteit,
De Boelelaan 1105

door
Margrieta Johanna Dolleman-van der Weel
geboren te Reeuwijk

promotor:	prof.dr. H.J. Groenewegen
copromotoren:	prof.dr. M.P. Witter
	prof.dr. F.H. Lopes da Silva

Contents

Chapter 1

GENERAL INTRODUCTION

The thalamus, a centrally located region of the brain, consists of over 30 nuclei in each hemisphere. These nuclei were initially considered to be simple relay stations, transmitting sensory information from peripheral organs to the cortex, and relaying motor functions in the opposite direction. Anatomical observations by Lorente de Nó (1938) and electrophysiological characteristics of thalamic nuclei formed the basis of the classic concept that thalamocortical connections involved two projection systems, i.e., a 'specific' and a 'non-specific' system. Specific thalamocortical projections, arising from sensory, motor and associational relay nuclei, were thought to form a dense terminal arborisation in layer IV of a restricted cortical target area; non-specific thalamocortical projections, arising from the intralaminar and midline nuclei, were thought to innervate layer I of a relatively large part of the cortical mantle. Different cortical responses could be evoked by either high or low frequency stimulation of the thalamus. Low frequency stimulation of specific nuclei resulted in short-latency augmenting responses in a restricted cortical area. In contrast, low frequency activation of non-specific nuclei elicited widespread long-latency recruiting responses and the gradual development of cortical slow waves, whereas high frequency stimulation resulted in desynchronization of cortical waves (e.g., Dempsey and Morison, 1942; Ajmone Marsan, 1965).

Nowadays, it is well known that specific as well as non-specific thalamic nuclei have an anatomical specific in- and output organization (Bentivoglio et al. 1991; Jones 1998; Van der Werf et al, 2002; Groenewegen and Witter, 2004; Cassel et al. 2013; Vertes et al. 2015). In addition, all thalamic neurons display similar electrophysiological characteristics (i.e., a bursting or a tonic activity mode; llinás and Jahnsen 1982; Jahnsen and llinás 1984), and thus specific as well as non-specific thalamocortical projections are supposed to be involved in maintaining the levels of cortical activity (Jones, 1985). In combination with behavioral paradigms, this has resulted in renewed views on the function of thalamic nuclei as integral parts of multiple neural circuits, playing distinct roles in relaying information derived from brainstem, diencephalic, neocortical and subcortical areas onto specific cortical and subcortical targets. Hence, thalamic dysfunction (e.g., due to neurodevelopmental abnormalities, brain injury, stroke, intoxication) results in various neuropathological conditions. Among these are disturbances in higher-order processes, such as anterograde and retrograde amnesia, as well as impairments in planning, executive functions, attention, inhibition control, and emotional responding (e.g., Van der Werf et

al, 2002; Van der Werf et al. 2003a,b). However, thalamic lesions in patients are seldom if at all restricted to one nucleus. Experimental studies in animals are therefore needed to clarify how a particular thalamic nucleus participates in (aspects of) behavior and/or in cognitive processes.

Using the rat as a model, the research described in this thesis focusses on the ventral thalamic midline nucleus reuniens (RE) and its connectivity with the hippocampus and adjacent cortices, structures of crucial importance for learning and memory. Historically, RE is considered to be part of the non-specific system. In the rat, the thalamic midline nuclei (i.e., the paratenial, paraventricular, intermediodorsal, reuniens/perireuniens, and rhomboid nuclei) form a narrow band of small nuclei along the dorsal-to-ventral midline, extending throughout approximately 2/3 of the rostral-to-caudal length of the thalamus (Fig. 1).

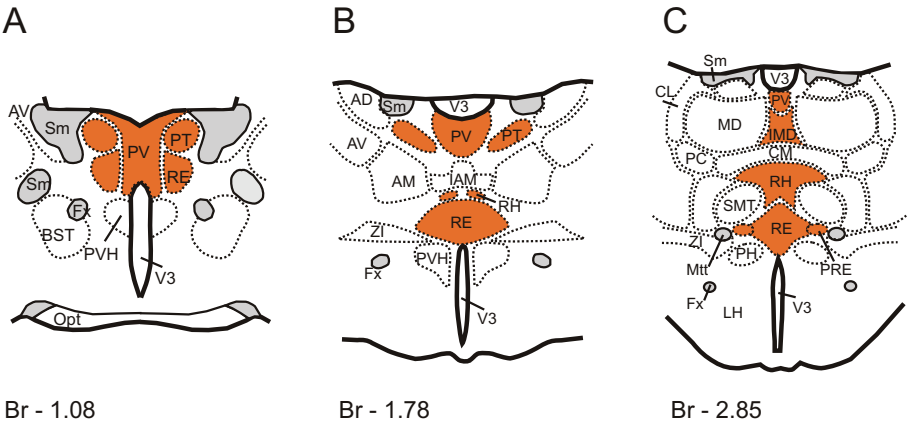

Fig. 1. Transverse sections through the rostral-to-caudal thalamus. Midline nuclei are in orange, fiber tracts are in grey. A. The most rostral part of RE is divided into a right and left nuclear mass by the paraventricular nucleus/3rd ventricle. B. More caudally, RE is fused into a mass of cells overlying the 3rd ventricle. C. The caudal RE is accompanied by small bilateral extensions called the perireuniens nucleus.
Abbreviations: AD=anterodorsal; AM=anteromedial; AV=anteroventral; BST=bed nucleus stria terminalis; CM=central medial; CL=centrolateral; IAM=interanteromedial; IMD=intermedialdorsal; LH=lateral hypothalamus; MD=mediodorsal; PC= paracentral; PH=posterior hypothalamic; PT=paratenial; PRE=perireuniens; PV=paraventricular; PVH=paraventricular hypothalamic nucleus; RE=reuniens; RH=rhomboid; SMT=submedial thalamic; ZI=zona incerta; Br=bregma; Fx=fornix; Mtt=mammillothalamic tract; Opt=optic tract; Sm=stria terminalis; V3= 3rd ventricle. Adapted from Swanson (2004).

Overall, the small size of these nuclei may have presented difficulties in investigating their connectivity, physiological characteristics, and individual contributions to behavior and higher order cognitive functions, rendering the group of midline nuclei the least studied region of the thalamus. In fact, until recently, RE has received very limited attention. For instance, a PubMed search (October 2017) for 'nucleus reuniens' resulted in just over 1050 hits, whereas the search term 'hippocampus' yielded more than 140000 publications.

The first systematic study of RE in- and output structures was conducted by Herkenham (1978). He provided evidence for a direct RE-hippocampal (i.e., CA1/subiculum) pathway, as well as for a dense RE innervation of the entorhinal cortex. He also reported that almost all RE efferent projections appeared to target structures of the limbic system. In the early nineties, the RE connectivity with the hippocampus and entorhinal cortex was further investigated at the light- and electron microscopic level (Wouterlood et al. 1990; Wouterlood 1991). Around that time, Braak and Braak (1991) reported that the entorhinal cortex, hippocampal field CA1 and RE were among the first structures to display characteristic degenerative features in a relatively early stage of Alzheimer's disease. This raised the interest for the possibility that RE may play an important role in the functioning of the medial temporal lobe memory system. Subsequently this idea formed the basis for the multidisciplinary research presented in this thesis.

Anatomical description and terminology of nucleus reuniens

An early, comprehensive anatomical description of the thalamus in the brain of the albino rat was given by Gurdjian (1927). With regard to the assembly of cells in the ventral thalamic midline, Gurdjian adopted the name nucleus reuniens (RE), which together with the dorsally adjacent rhomboid nucleus form the ventral group of the thalamic midline nuclei. Almost two decades later, Krieg (1944) created a 'three-dimensional mental picture' of the thalamus in a series of graphic reconstructions of the thalamic nuclei and fiber systems (see Fig. 2).

He also questioned the terminology of RE, arguing that:

"……. Gurdjian (1927) seemingly had interchanged the applications of the terms nucleus rhomboidalis and reuniens. In most transverse sections the reuniens is strikingly rhomboidal in shape, while the rhomboidalis changes its shape greatly. Correspondingly, it is the rhomboidalis which merits etymologically the name of reuniens, for it is truly a joining or reuniting structure…….".

Nonetheless, Krieg (1944) and most authors after him used the terminology of the rhomboid and reuniens nuclei as adopted by Gurdjian (1927). Some authors, however, have used the name medioventral nucleus (MV) instead of RE (e.g., McAllister and Das,

1977; Jones, 1985; Morel et al, 1997), on account of derivation of the medioventral (=RE) and mediodorsal (MD) nuclei from one pronucleus. Yet, the term medioventral nucleus may easily lead to considerable confusion with the ventral medial (or ventromedial) thalamic nucleus. In this thesis the term nucleus reuniens will be used throughout.

In the rat brain, RE is approximately 2 mm in length in rostro-caudal direction, and has a maximal width of about 0.6 mm (Wouterlood et al, 1990). In the horizontal plane RE has the shape of a letter Y (Fig. 2B). In the transversal plane the rostral RE is composed of a left and right part, divided by the paraventricular nucleus/3rd ventricle (Fig. 2C). More caudally these bilateral components are fused to form a dense mass of cells lying over the 3rd ventricle (Fig. 2D,E). The bilateral wing-like extensions of the caudal RE consist of the perireuniens nucleus (see Fig. 1C).

Embryonic and postnatal development of the thalamic midline and thalamocortical connectivity

Briefly, in the embryonic rat brain the thalamic midline cell groups start as paired (i.e., bilateral symmetrical) structures, projecting to the ipsilateral forebrain. In early postnatal life these cells in the midline fuse to form a 'massa intermedia' (MI), yet they retain the bilateral symmetry and laterality in their output connections. In fact only very few cells seem to have axons that cross the fused midline (Bentivoglio et al, 1991). Already at postnatal day 3, large numbers of thalamo-cortical matrix axons from multiple thalamic nuclei, including RE, converge onto cortical layer I (Galazo et al 2008), and may thus have an important influence on the early postnatal development of cortical circuits (Hartung et al 2016).

In human embryos, a dense and extensive accumulation of cells adjacent to the wall of the 3rd ventricle will differentiate into the intralaminar and midline nuclei. At 13-14 weeks the medial borders of both thalami, including RE, will fuse to form a bridge of grey matter, i.e., the MI or adhaesio interthalamica, and at 21 weeks all thalamic nuclei are present (Dekaban 1954). It has even been suggested that the MI in humans consists entirely of the fused RE nucleus (Rabl 1982). However, the MI between the two thalami will not always develop. It will be formed in approximately 78% of females and in 68% of males, and is on average about 50% larger in females than in males. Therefore, the MI may be a sexual dimorphic structure, underlying the sex differences in the functioning of the normal as well as the pathological brain (Allen and Gorski, 1991). It has also been suggested that either a shorter or smaller MI, or its absence, may play a role in schizophrenia/psychiatric disorders (e.g., Trzesniak et al. 2011, 2012; Landin-Romero et al 2016; for a potential involvement of RE in schizophrenia, see below, and General discussion).

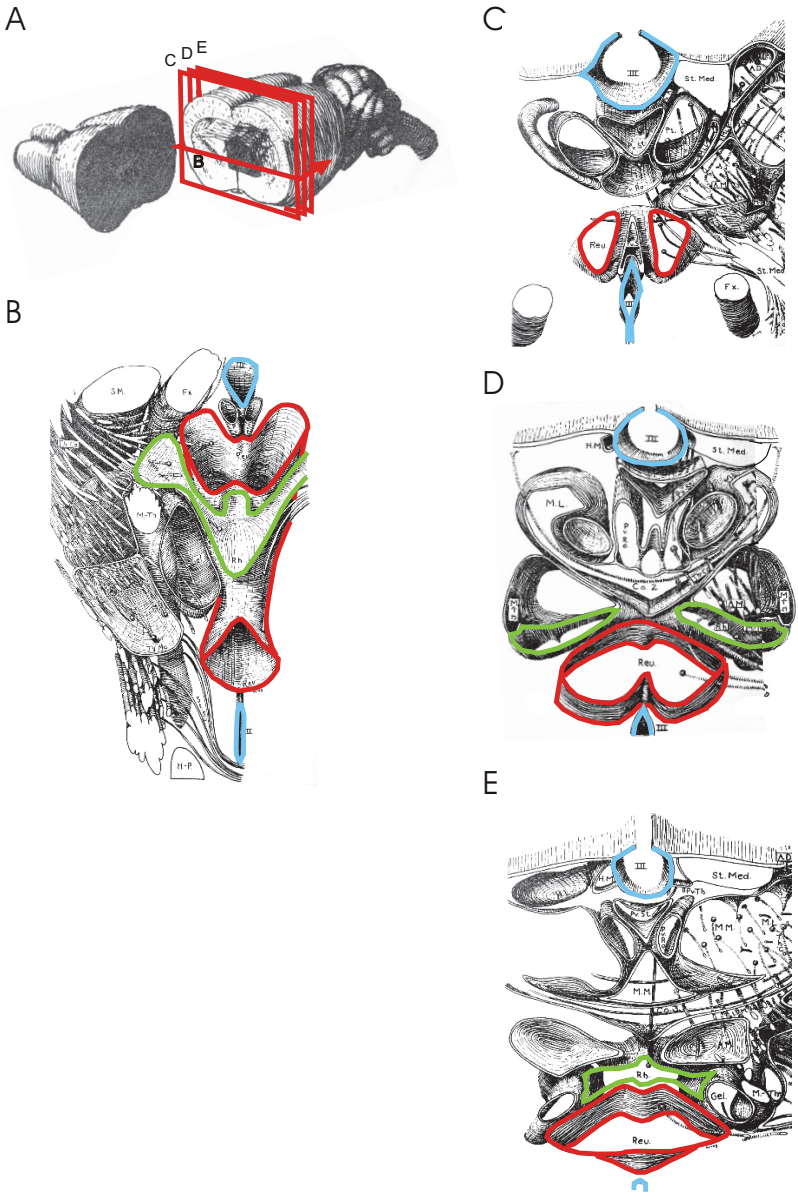

Fig. 2. 'Three-dimensional' graphic reconstructions of thalamic nuclei and fiber systems, adapted from Krieg (1944). A. The rat brain; red lines indicate the horizontal and transversal sections through the thalamus illustrated in B and C-E, respectively. Nucleus reuniens is outlined in red, and the rhomboid nucleus is outlined in green; the 3rd ventricle is indicated in blue.

Normal development of thalamo-cortical connectivity in neonates and during early childhood (i.e., first 2 years) was investigated by Alcauter et al. (2014). They emphasized that, in relation to the development of cognitive processes, the early presence of thalamic projections to the salience and default networks are important for various functional roles in the cognitive domain and in self-awareness, respectively. Specific thalamocortical connections with higher-order cortical networks, for instance associated with executive control, might develop later. Fair et al. (2010) studied the functional development of thalamocortical projections in healthy children, adolescents, and adults. They reported that the functional connectivity between the frontal cortex and dorsal/anterior subdivisions of the thalamus was greater in adults than in children. In contrast, the functional connectivity of the temporal lobe with ventral/midline/posterior thalamic subdivisions was systematically weakened with increasing age. These differential changes in functional connectivity are likely reflected in age-related changes in behavior and/or cognitive abilities.

Overall, it is noteworthy that RE is well developed in rodents, but is relatively small in carnivores and particularly small, yet recognizable in primates. In addition, even among genera of the same order, there exists considerable variation in size/extent of the RE nucleus (Jones 1985).

In- and output connections of nucleus reuniens

From the 1970's onwards, the use of modern retrograde and anterograde tracers in various animal models has contributed significantly to our knowledge of the anatomical connectivity of the brain. Nonetheless, it should be kept in mind that generally the 'strength or efficacy' of a projection is not synonymous with the 'traced density' of a projection, because the latter relies on just anatomical quantitative measures such as the numbers of retrogradely labelled neurons, or anterogradely labelled fibers and synaptic terminations (e.g., Rockland 2015). Instead, the synaptic efficacy of a projection is much more complex and depends on multiple factors, as for instance differences in distribution of specific receptors, location of synaptic contacts on the postsynaptic neuron, amount of terminal divergence, and the inhibitory or excitatory nature of the transmitter in the presynaptic neurons.

Reuniens afferents

RE receives input from a wide array of brain areas and is thereby a convergence zone of telencephalic, diencephalic, and brainstem derived information. In an early neuroanatomical tracing study, Herkenham (1978) investigated the input structures of

RE. His findings were largely confirmed by Ohtake and Yamada (1989). Later studies provided a detailed description of more than 90 input structures (Dolleman-van der Weel et al. 1993; McKenna and Vertes 2004). Following injections with a retrograde tracer in RE, the highest density of retrogradely labelled neurons was found in infralimbic, prelimbic, anterior cingulate, medial orbital, agranular insular, and agranular secondary motor cortices, as well as in the claustrum, subiculum, preoptic area, lateral septum, anterior and lateral hypothalamic area, posterior hypothalamus, premammillary and supramammillary nuclei, zona incerta, central gray, commissural nucleus, laterodorsal tegmental, parabrachial and pedunculopontine nuclei, precommissural nucleus, and medial pretectum (McKenna and Vertes 2004; for all afferents, see their Table 1). It was concluded that RE receives a widespread, mainly limbic-associated topographically organized input, with an ipsilateral predominance.

Whether RE receives input via collateralized projections has been hardly investigated. Recently Varela et al. (2014) reported that a small percentage of neurons in the ventral subiculum projects via collaterals to both RE and the medial prefrontal cortex (mPFC). In addition, they found that a few cells in the anterior lateral septum project through collateralized axons to mPFC and RE.

Reuniens efferents

In comparison to the abundance of input structures, the total output of RE is slightly less numerous, comprising just over 70 projections (Herkenham 1978; Wouterlood et al. 1990; Wouterlood 1991; Dolleman-van der Weel and Witter 1996, see *Chapter 2*; Bokor et al. 2002; Van der Werf et al. 2002; Vertes et al. 2006, for all efferents see their Table 1). In particular, a high density of RE axons was found in the medial prefrontal polar, the medial and ventral orbital, the anterior cingulate, anterior piriform, pre- and infralimbic, insular, ectorhinal, perirhinal, and entorhinal cortices, tenia tecta, claustrum, dorsal and ventral subiculum, pre- and parasubiculum and hippocampal field CA1. Thus, major RE output is almost entirely directed to structures in the hippocampus and limbic-associated cortices. In addition, RE projects also, yet more sparsely, to many subcortical structures such as the amygdala, nucleus accumbens, lateral and medial septum, bed nucleus of stria terminalis, diagonal band nuclei, preoptic area, reticular thalamic nucleus, zona incerta, hypothalamic area, supramammillary nucleus, central grey, ventral tegmental area, pretectum, and superior colliculus. As initially suggested by Herkenham (1978), reciprocity of connections between RE and most of its limbic-related target structures is quite common (for a comparison of in- and output structures: see Herkenham 1978; McKenna and Vertes 2004, RE afferents Table 1; Vertes et al. 2006, RE efferents Table 1).

As yet, it has rarely been studied whether RE neurons project via collateralized axons to more than one target area. Previously, only very small numbers of RE cells have been

reported to project to both the hippocampus and nucleus accumbens, and to both the hippocampus and amygdala (Su and Bentivoglio, 1990; Otake and Nakamura, 1998). More recently, Hoover and Vertes (2012) reported that a small percentage of RE-CA1 projecting neurons also projects via axon collaterals to mPFC. In contrast, it has been shown that RE efferents to the hippocampal formation and adjacent cortices (i.e., CA1, subiculum, entorhinal and perirhinal cortex), as well as to CA1 and medial septum, are non-collateralized projections arising from distinct, topographically organized RE cell clusters (Dolleman-van der Weel and Witter 1996, see *Chapter 2*; Bokor et al. 2002).

Role of nucleus reuniens in cognitive functioning

Considering its wide array of (often reciprocal) in- and output structures it is not surprising that RE is supposed to play a role in a variety of behaviors such as feeding, metabolism, reproduction, seasonable adaptations, nociception, stress and anxiety (for review, see Cassel et al. 2013). In this thesis, however, we focus on RE and its presumed role in (aspects of) cognitive functioning (Pereira de Vasconcelos and Cassel 2015).

Initially, neuronal degeneration in an early phase of Alzheimer's disease (Braak and Braak 1991, 1998) in the interconnected areas CA1, entorhinal cortex, and RE, was regarded as an indication for the potential involvement of RE in hippocampal-dependent memory processes. However, in an early behavioral study by Flämig and Klingberg (1978), a RE lesion had no effect on learning and memory in a conditioned avoidance task in a Y-maze. Instead, these investigators reported an increase in anticipatory behavior in a jumping test. Surprisingly, nearly 40 years elapsed until the next behavioral RE studies were published (Dolleman-van der Weel et al. 2009, see *Chapter 6*; Davoodi et al. 2009). Our study was the first to show that rats with a neurotoxic RE lesion displayed normal spatial (i.e., hippocampal-dependent) learning and memory in a standard water maze task, whereas behavioral flexibility (e.g, strategy shifting) was affected. This effect pointed to the importance of RE regarding mPFC-related aspects of cognitive functioning. Subsequently, a growing number of behavioral studies in rodents, employing RE lesions, reversible inactivation and/or optogenetic stimulation of RE, has provided further evidence for the involvement of RE in (aspects of) a variety of memory-related processes such as working memory (Davoodi et al 2009; Hembrook and Mair 2011; Hembrook et al. 2012; Hallock et al. 2013, 2016; Griffin et al. 2015; Duan et al. 2015; Layfield et al. 2015), memory consolidation/remote memory (Loureiro et al. 2012; Ali et al 2017; Sierra et al 2017), fear memory (Carvalho-Netto et al 2010; Kincheski et al. 2012), impulsive behavior/behavioral flexibility/strategy shifting (Flämig and Klingberg 1978; Dolleman-van der Weel et al. 2009; Cholvin et al. 2013; Prasad et al 2013; 2017;

Linley et al 2016), associative learning (Eleore et al. 2011), inhibitory response control (Anderson et al. 2016), passive avoidance learning (Davoodi et al. 2011), memory specificity/generalization (Xu and Südhof 2013), goal-directed navigation (Ito et al. 2015), and executive behaviors (Varela et al. 2014; Reagh et al 2017; Prasad et al 2017). Overall, these studies have strongly indicated that RE plays an important role in the communication between hippocampus and mPFC (Vertes et al. 2007; Varela et al. 2014), instead of being involved in modulating hippocampal activity alone. Interestingly, dysfunctional connectivity/communication between CA1/subiculum and PFC has also been implicated to underly deficits in brain diseases such as epilepsy, and schizophrenia (e.g., Paz and Huquenard 2015; Sigurdsson and Duvarci 2016).

Involvement of nucleus reuniens in neuropathology

RE has been suggested to be involved in several pathological conditions of the brain, e.g., Alzheimer's disease (Braak and Braak, 1991; Moretti et al, 2011; Hardenacke et al, 2013), Korsakoff's syndrome (Visser et al, 1999), autism (Ray et al, 2005), stress and depression (Kafetzopoulos et al 2017), epilepsy (Hirayasu and Wada, 1990; Bertram et al, 2001; Sloan and Bertram, 2009; Graef et al, 2009; Wang et al, 2009; Drexel et al, 2011), and schizophrenia (Cohen et al, 1998; Lambe et al, 2007; Lisman et al, 2010; Lisman 2012; Zhang et al, 2012; Saalmann 2014; Duan et al, 2015). The focus in this thesis is on the assumed involvement of RE in the latter two diseases, for which a better understanding of the role(s) RE may play in the hippocampal-PFC communication might help to develop new therapies.

Epilepsy

Epilepsy is a neurological disease with severe disturbances in brain functioning. It is characterized by hypersynchronized discharges (seizures) in large numbers of neurons, involving complex regional interactions across the brain, as well as gross motor behaviors (convulsions). Several studies have implicated a role for RE in limbic or mesial temporal lobe epilepsy (TLE), and in atypical absence seizures (AAS).

Temporal lobe epilepsy

TLE is a common and often drug-resistant epilepsy syndrome, with distinct pathological changes such as severe neuronal degeneration and sclerosis in hippocampus and entorhinal cortex (Bertram et al. 1998), hence its association with deficits in memory and cognitive performance. In animal studies of epilepsy it has been shown that neurons in the thalamic midline become hyperactive, and there is evidence that RE in particular can evoke

epileptic activity in the hippocampus. For instance, when in normal rats NMDA was injected into RE, this caused an initial hyperactivity in behavior followed by generalized tonic-clonic convulsions, which could progress to a status epilepticus with continuous EEG hippocampal discharges (Hirayasu and Wada 1992).

From an anatomical point of view, RE is well situated to play an important role in TLE (Bertram et al. 2001, 2008). RE has strong (excitatory) projections to the hippocampus (i.e., CA1, subiculum), and entorhinal cortex (e.g., Wouterlood et al. 1990; Wouterlood 1991; Dolleman-van der Weel et al. 1996, 1997, 2017, see *Chapters 2, 4, and 7*; Vertes et al. 2006). Hence, this nucleus may be involved in the development of an hyperexcitable entorhinal-hippocampal loop. Such hyperexcitability is critical for the generation and/or propagation of hippocampal seizure activity (Ang et al. 2006), and may be due to the loss of RE-induced feedforward inhibition in hippocampal field CA1 (Dolleman-van der Weel et al. 1997, 2017, see *Chapters 4 and 7*; Dolleman-van der Weel and Witter 2000, see *Chapter 5*).

Atypical absence seizures

Another type of epilepsy, mainly observed in children, consists of typical and atypical absence seizures, with each type displaying a dependency of activities in different circuits (Han et al. 2012). In general, absence seizures are characterized by synchronized oscillatory bursting of neocortical and thalamic neurons. Typical absence seizures are considered benign, with brief behavioral/motor arrest, easy to treat with drugs, and not associated with impaired cognition. In contrast, atypical absence seizures (AAS) are malignant due to a progressive nature. They are severe and associated with a prolonged twilight state with semi-purposeful movements, and commonly cause a cognitive impairment (Han et al. 2012). A possible mechanism of the latter type of absence seizures may involve the thalamic RE. This was studied in a transgenic mouse model with over-expression of the GABA-B receptor subunit R1a, that displays the characteristicts of the human syndrome of AAS. In this model, it was shown that spike- and wave discharges are initiated in mPFC, from where they propagate to the RE, which projects back to mPFC and forward to the CA1 region of the hippocampus (Wang et al. 2009; Han et al. 2012).

Schizophrenia

Schizophrenia is a severe disease, involving various brain regions including the thalamus, prefrontal cortex and the hippocampus (Small et al. 2011; Marenco et al. 2012; Godsil et al. 2013; Ghoshal and Conn 2015; Sigurdsson and Duvarci 2016). A combination of genetic, neurodevelopmental and environmental factors is assumed to contribute to the disease. Characteristic symptoms are classified as positive (e.g., hallucinations, delusions,

thought disorder), and negative symptoms (e.g., social withdrawl, anhedonia, apathy), and cognitive deficits (e.g., in attention, working memory, executive functions). The thalamus occupies a central position in multiple thalamocortical functional circuits, and plays a key role in cortico-cortical communication and higher cortical functions (Guillery 1995). Several hypotheses have been formulated with respect to the pathophysiology of schizophrenia, involving abnormalities in thalamocortical neural networks (Cronenwett and Csernansky 2010). One of these hypotheses focusses on thalamic midline nuclei, in particular RE, given its position between mPFC and hippocampal field CA1 (Lisman 2012). Moreover, the thalamic nuclei of the massa intermedia, including RE, participate in the neural circuits that mediate the effects of antipsychotic drugs (Cohen et al. 1998). Thus, unraveling the role of RE in a cortico-thalamo-hippocampal network may also have important implications for future therapeutical approaches of schizophrenia.

Outline and aim of this thesis

In view of the relative sparse knowledge of its functional anatomy, as indicated above, the aim of the present thesis was to study the anatomical organization, physiological characteristics, and functional role(s) of the ventral midline thalamic RE in a comprehensive, multidisciplinary way. Employing (combined) neuroanatomical, electrophysiological and behavioral experiments in rats, our main aim was to provide more insight into the presumed relevance of RE for hippocampal-dependent learning and memory processes. In addition, these insights might also shed some light on the involvement of RE in schizophrenia and epilepsy.

An important note is that, for a large part, the results of our anatomical and electrophysiological experiments were published around 20 years ago. As also indicated in the introductory paragraphs above, in the last decades some newer studies have appeared that mostly extend and confirm our earlier results. In the General discussion *(see Chapter 9)* we will discuss our initially and more recently published findings in the context of both early and recent literature.

Initially, we studied the totality of RE input structures, employing anatomical (i.e., combined retrograde and anterograde) tracing methods. These preliminary findings were published in abstract form (Dolleman-van der Weel et al. 1993), and were largely confirmed in a later retrograde tracing study by McKenna and Vertes (2004).
In Chapter 2, using an anterograde tracing method, the organization of RE efferents to the hippocampal formation and perirhinal/entorhinal cortices is elucidated in great detail. We provide evidence that all these RE projections arise from distinct topographically

organized, yet partly intermingled populations of RE neurons.

In Chapter 3, the terminal overlap of RE and EC projections in stratum lacunosum moleculare of CA1 was used as a model system of converging inputs. We developed a method to permanently visualize three different anterograde tracers in one brain slice, a method that in general 1) offers the opportunity to examine the distribution of fibers originating from three different input structures (e.g., within one particular brain area), and 2) may reduce the number of animals needed for anatomical tracing studies. In addition, our results also provided detailed anatomical information that was used in our subsequent electrophysiological experiments, i.e., regarding the choice of optimal sites for electrical stimulation in RE and EC, as well as establishing the appropriate recording site in CA1, showing substantial overlap of RE and EC axons in stratum lacunosum moleculare (see *Chapters 4 and 7*).

In Chapter 4, electrophysiological in vivo techniques were employed to examine the effects of RE stimulation on neuronal activity in hippocampal field CA1. This study was the first to show that the RE-CA1 input exerts a direct monosynaptic excitatory effect on pyramidal cells, as well as an (indirect) inhibitory influence through the activation of local inhibitory interneurons. In addition, using an anterograde tracing method, we revealed the existence of a projection from caudal RE (cRE)-to-rostral RE (rRE) which is assumed to underlie an additional di-synaptic RE-CA1 input. Taken together, we propose a closed loop between rRE-CA1-subiculum-cRE-rRE that allows RE to modulate the activity level in CA1 depending on its output via the subiculum.

In Chapter 5, we present evidence, at the ultrastructural level, that RE axons form asymmetrical (i.e., excitatory) synaptic contacts onto GABA-positive dendrites in stratum lacunosum moleculare of CA1. These results confirm that the inhibitory influence of RE on CA1 cell excitability, as previously shown in our electrophysiological study (see *Chapter 4*), is mediated by a monosynaptic excitatory RE input onto GABAergic (inhibitory) interneurons in CA1.

In Chapter 6, using a standard (reference memory) Morris water maze task, we examined the effects of neurotoxic RE or MD lesions on spatial learning and memory. This behavioral study revealed that neither a RE- nor a MD lesion affected spatial learning and memory per se. Instead, we found that RE and MD lesions had opposite effects on aspects of behavioral flexibility.

In Chapter 7, employing electrophysiological in vivo techniques, it was investigated whether or not RE and EC inputs in CA1 interact at the cellular level. Simultaneous activation of RE/EC resulted in a major enhancement of evoked field excitatory postsynaptic potentials (fEPSPs) in stratum lacunosum moleculare. The non-linear summation provided the first strong indications that RE and EC axons indeed converge (at least partly) onto the same dendritic branch of pyramidal cells. Next to inhibitory

effects, mediated by both inputs separately, the CSD analyses indicated an additional peri-somatic inhibition evoked by coincident RE/EC input.

In the last two Chapters 8 and 9, a comprehensive summary of the results of our experiments is given. These results are discussed in the context of historical and recent publications. In addition, the role RE may play in (aspects of) normal cognitive functioning and memory, as well as an involvement of RE in some forms of epilepsy and in schizophrenia, is discussed.

REFERENCES

Ajmone Marsan C (1965) The thalamus. Data on its functional anatomy and on some aspects of thalamo-cortical integrations. Archo Ital Biol 103: 847-882.

Alcauter S, Lin W, Smith JK, Short SJ, Goldman BD, Reznick JS, Gilmore JH, Gao W (2014) Development of thalamocortical connectivity during infancy and its cognitive correlations. J Neurosci 34:9067-9075.

Ali M, Cholvin T, Antoine Muller M, Cosquer B, Kelche C, Cassel JC, Pereira de Vasconcelos A (2017) Environmental enrichment enhances systems-level consolidation of a spatial memory after lesions of the ventral midline thalamus. Neurobiol Learn Mem 141:108-123.

Allen LS, Gorski RA (1991) Sexual dimorphism of the anterior commissure and massa intermedia of the human brain. J Comp Neurol 312:97-104.

Anderson MC, Bunce JC, Barbas H (2016) Prefrontal-hippocampal pathways underlying inhibitory control over memory. Neurobiol Learn Mem. 134 PtA:145-161.

Ang CW, Carlson GC, Coulter DA (2006) Massive and specific dysregulation of direct cortical input to the hippocampus in temporal lobe epilepsy. J Neurosci 26:11850-11856.

Bentivoglio M, Balercia G, Kruger L (1991) The specificity of the nonspecific thalamus: The midline nuclei. Prog Brain Res 87:53-80.

Bertram EH, Mangan PS, Zhang D, Scott CA, Williamson JM (2001) The midline thalamus: alterations and a potential role in limbic epilepsy. Epilepsia 42:967-978.

Bertram EH, Zhang DX, Mangan P, Fountain N, Rempe D (1998) Functional anatomy of limbic epilepsy: a proposal for central synchronization of a diffusely hyperexcitable network. Epilepsy Res 32:194-205.

Bertram EH, Zhang D, Williamson JM (2008) Multiple roles of midline dorsal thalamic nuclei in induction and spread of limbic seizures. Epilepsia 49:256-268.

Bertram EH (2013) Neuronal circuits in epilepsy: do they matter? Exp Neurol 244:67-74.

Bokor H, Csáki A, Kocsis K, Kiss J (2002) Cellular architecture of the nucleus reuniens

thalami and its putative aspartatergic/glutamatergic projection to the hippocampus and medial septum in the rat. Eur J Neurosci 16:1227-1239.

Braak H, Braak E (1991) Alzheimer's disease affects limbic nuclei of the thalamus. Acta Neuropath 81:261-268.

Braak H, Braak E (1998) Evolution of neuronal changes in the course of Alzheimer's disease. J Neural Transm Suppl 53:127-140.

Cassel JC, Pereira de Vasconcelos A, Loureiro M, Cholvin T, Dalrymple-Alford JC, Vertes RP (2013) The reuniens and rhomboid nuclei: neuroanatomy, electrophysiological characteristics and behavioral implications. Prog Neurobiol 111:34-52.

Cholvin T, Loureiro M, Cassel R, Cosquer B, Geiger K, De Sa Nogueira D, Raingard H, Robelin L, Kelche C, Pereira de Vasconcelos A, Cassel JC (2013) The ventral midline thalamus contributes to strategy shifting in a memory task requiring both prefrontal cortical and hippocampal functions. J Neurosci 33:8772-8783.

Cohen BM, Wan W, Froimowitz MP, Ennulat DJ, Cherkerzian S, Konieczna H (1998) Activation of midline thalamic nuclei by antipsychotic drugs. Psychopharmacol (Berl) 135:37-43.

Cronenwett WJ, Csernansky J (2010) Thalamic pathology in schizophrenia. Curr Top Behav Neurosci 4:509-528.

Davoodi FG, Motamedi F, Nagdhi N, Akbari E (2009) Effect of reversible inactivation of the reuniens nucleus on spatial learning and memory in rats using Morris water maze. Beh Brain Res 198:130-135.

Davoodi FG, Motamedi F, Akbari E, Ghanbarian E, Jila B (2011) Effect of reversible inactivation of reuniens nucleus on memory processing in passive avoidance task. Behav Brain Res 221:1-6.

Dekaban A (1954) Human thalamus: an anatomical, developmental and pathological study. II. Development of the human thalamic nuclei. J Comp Neurol 100:63-97.

Dempsey EW, Morison RS (1942) The production of rhythmically recurrent cortical potentials after localized thalamic stimulation. Am J Physiol 135:293-300.

Dolleman-van der Weel MJ, Ang W, Witter MP (1993) Afferent connections of the nucleus reuniens thalami: a neuroanatomical tracing study in the rat. Eur J Neurosci Suppl 6:65.

Dolleman-van der Weel MJ, Wouterlood FG, Witter MP (1994) Multiple anterograde tracing, combining Phaseolus-vulgaris Leucoagglutinin with rhodamine- and biotin-conjugated dextran amine. J Neurosci Meth 51:9-21.

Dolleman-van der Weel MJ, Witter MP (1996) Projections from the nucleus reuniens thalami to the entorhinal cortex, hippocampal field CA1, and the subiculum in the rat arise from different populations of neurons. J Comp Neurol 364:637-650.

Dolleman-van der Weel MJ, Lopes da Silva FH, Witter MP (1997) Nucleus reuniens thalami modulates activity in hippocampal field CA1 through excitatory and inhibitory mechanisms. J Neurosci 17:5640-5650.

Dolleman-van der Weel MJ, Witter MP (2000) Nucleus reuniens thalami innervates gamma aminobutyric acid positive cells in hippocampal field CA1 of the rat. Neurosci Lett 278:145-148.

Dolleman-van der Weel MJ, Morris RG, Witter MP (2009) Neurotoxic lesions of the thalamic reuniens or mediodorsal nucleus in rats affect non-mnemonic aspects of watermaze learning. Brain Struct Funct 213:329-342.

Dolleman-van der Weel, Lopes da Silva FH, Witter MP (2017) Interactions of nucleus reuniens and entorhinal cortex projections in hippocampal field CA1 of the rat. Brain Struct Funct 222:2421-2438.

Drexel M, Preidt AP, Kirchmair E Sperk G (2011) Parvalbumin interneurons and calretinin fibers arising from the thalamic nucleus reuniens degenerate in the subiculum after kainic acid-induced seizures. Neurosci 189:316-329.

Duan AR, Varela C, Zhang Y, Shen Y, Xiong L, Wilson MA, Lisman J (2015) Delta frequency optogenetic stimulation of the thalamic nucleus reuniens is sufficient to produce working memory deficits: relevance to schizophrenia. Biol Psychiatry 77:1098-1107.

Eleore L, López-Ramos JC, Guerra-Narbona R, Delgado-Garcia JM (2011) Role of reuniens nucleus projections to the medial prefrontal cortex and to the hippocampal pyramidal CA1 area in associative learning. PLoS One 6:e23538. Doi: 10.1371/journal.pone.0023538.

Fair DA, Bathula D, Mills KL, Costa Dias TG, Blythe MS, Zhang D, Snyder AZ, Raichle ME, Stevens AA, Nigg JT, Nagel BJ (2010) Maturing thalamocortical functional connectivity across development. Front Syst Neurosci 18;4:10, doi 10.3389/fnsys.2010.00010.

Flämig R, Klingberg F (1978) Participation of thalami nuclei in the elaboration of conditioned avoidance reflexes of rats. IV. Lesions of the nucleus reuniens. Acta Biol Med Germ 37:1779-1782.

Galazo MJ, Martinez-Cerdeño V, Porrero C, Clascá F (2008) Embryonic and postnatal development of the layer 1-directed ("matrix") thalamo-cortical system in the rat. Cereb Cortex 18:344-363.

Ghoshal A, Conn PJ (2015) The hippocampal-prefrontal pathway: a possible therapeutic target for negative and cognitive symptoms of schizophrenia. Future Neurol 10:115-128.

Godsil BP, Kiss JP, Spedding M, Jay TM (2013) The hippocampal-prefrontal pathway: the weak link in psychiatric disorders? Eur Neuropsychopharmacol 23:1165-1181.

Graef JD, Nordskog BK, Wiggins WF, Godwin DW (2009) An acquired channelopathy involving T-type Ca2+ channels after status epilepticus. J Neurosci 29:4430-4441.

Griffin AL (2015) Role of the thalamic nucleus reuniens in mediating interactions between the hippocampus and medial prefrontal cortex during spatial working memory. Front Syst Neurosci 9:29 doi: 10.3389/fnsys.2015.00029.

Groenewegen HJ and Witter MP (2004) Thalamus. In: The Rat Nervous System, third ed. Paxinos G, Paxinos G (Eds). Elsevier Academic Press. Pp 407-453.

Gurdjian ES (1927) The diencephalon of the albino rat. Studies on the brain of the rat no. 2. J Comp Neurol 43:1-115.

Hembrook JR, Mair RG (2011) Lesions of reuniens and rhomboid thalamic nuclei impair radial maze win-shift performance. Hippocampus 21:815-826.

Hembrook JR, Onos KD, Mair RG (2012) Inactivation of ventral midline thalamus produces selective delayed conditional discrimination impairment in the rat. Hippocampus 22:853-860.

Hallock HL, Wang A, Shaw CL, Griffin AL (2013) Transient inactivation of the thalamic nucleus reuniens and rhomboid nucleus produces deficits of a working-memory dependent tactile-visual conditional discrimination task. Behav Neurosci 127:860-866.

Han HA, Cortez MA, Snead OC III (2012) GABAB receptor and absence epilepsy. In: Noebels et al, editors. Jasper's Basic Mechanisms of the Epilepsies. 4th edition Bethesda (MD): Nat Center for Biotechnol Information (US).

Hardenacke K, Shubina E, Bűhrle CP, Zapf A, Lenartz D, Klosterkőtter J, Visser-Vanderwalle V, Kuhn J (2013) Deep brain stimulation as a tool for improving cognitive functioning in Alzheimer's dementia: a systematical review. Front Psychiatry 4:159. Doi: 10.3389/fpsyt2013.00159.

Hartung H, Brockmann MD, Pőschel B, De Feo V, Hanganu-Opatz IL (2016) Thalamic and entorhinal network activity differently modulates the functional development of prefrontal-hippocampal interactions. J Neurosci 36:3676-3690.

Herkenham M (1978) The connections of the nucleus reuniens thalami: evidence for a direct thalamo-hippocampal pathway in the rat. J Comp Neurol 177:589-610.

Hirayasu Y, Wada JA (1992) Convulsive seizures in rats induced by N-methyl-D-aspartate injection into the massa intermedia. Brain Res 577:36-40.

Hoover WB, Vertes RP (2007) Anatomical analysis of afferent projections to the medial prefrontal cortex in the rat. Brain Struct Funct 212:149-179.

Hoover WB, Vertes RP (2012) Collateral projections from nucleus reuniens of thalamus to hippocampus and medial prefrontal cortex in the rat: a single and double retrograde fluorescent labeling study. Brain Struct Funct 217:191-209.

Ito HT, Zhang SJ, Witter MP, Moser EI, Moser MB (2015) A prefrontal-thalamo-

hippocampal circuit for goal-directed navigation. Nature 522:50-55.

Jahnsen H, Llinás R (1984) Voltage–dependent burst-to-tonic switching of thalamic cell activity: an in vitro study. Acta Ital Biol 122:73-82.

Jones EG. (1985) The thalamus. Plenum Press, New York/London.

Jones EG. (1998) A new view of specific and non-specific thalamocortical connections. Adv Neurol 77:49-71.

Kincheski GC, Mota-Ortiz SR, Pavesi E, Canteras NS, Carobrez AP (2012) The dorsolateral periaqueductal gray and its role in mediating fear learning to life threatening events. PLoS One 7:e50361. Doi: 10.1371/journal.pone.0050361.

Krieg WJS. (1944) The medial region of the thalamus of the albino rat. J Comp Neurol 80:381-415.

Lambe EK, Liu RJ, Aghajanian GK (2007) Schizophrenia, hypocretin (orexin), and the thalamocortical activating system. Schizophr Bull 33:1284-1290.

Layfield DM, Patel M, Hallock H, Griffin AL (2015) Inactivation of the nucleus reuniens/rhomboid causes a delay-dependent impairment of spatial working memory. Neurobiol Learn Mem 125:163-167.

Linley SB, Gallo MM, Vertes RP (2016) Lesions of the ventral midline thalamus produce deficits in reversal learning and attention on an odor texture set shifting task. Brain Res 1649 (PtA):110-122.

Lisman JE, Pi HJ, Zhang Y, Otmakhova NA (2010) A thalamo-hippocampal-ventral tegmental area loop may produce the positive feedback that underlies the psychotic break in schizophrenia. Biol Psychiatry 68:17-24.

Lisman J (2012) Excitation, inhibition, local oscillations, or large-scale loops: what causes the symptoms of schizophrenia? Curr Opinion Neurobiol 22:537-544.

Llinás R, Jahnsen H (1982) Electrophysiology of mammalian thalamic neurons in vitro. Nature 297:406-408.

Lorente de Nó R (1938) Cerebral cortex: architecture, intracortical connections, motor projections. In: J Fulton (Ed.), Physiology of the nervous system, Oxford University Press, London, pp 291-340.

Loureiro M, Cholvin T, Lopez J, Merienne N, Latreche A, Cosquer B, Geiger K, Kelche C, Cassel JC, Pereira de Vasconcelos A (2012) The ventral midline thalamus (reuniens and rhomboid nuclei) contributes to the persistence of spatial memory. J Neurosci 32:9947-9959.

Marenco S, Stein JL, Savostayanova AA, Sambataro F, Tan HY, Goldman AL, Verchinski BA, Brnett AS, Dickinson D, Apud JA, Callicott JH, Meyer-Lindengerg A, Weinberger DR (2012) Investigation of anatomical thalamo-cortical connectivity and fMRI activation in schizophrenia. Neuropsychopharmacol 37:499-507.

McAllister JP, Das GD. (1977) Neurogenesis in the epithalamus, dorsal thalamus and

ventral thalamus of the rat: an autoradiographic and cytological study. J Comp Neurol 172:647-686.

McKenna JT, Vertes RP (2004) Afferent projections to nucleus reuniens of the thalamus. J Comp Neurol 480:115-142.

Morel A, Magnin M, Jeanmonod D (1997) Multiarchitectonic and stereotactic atlas of the human thalamus. J Comp Neurol 387:588-630.

Moretti DV, Frisoni GB, Binetti G, Zanetti O (2011) Anatomical substrate and scalp EEG markers are correlated in subjects with cognitive impairment and Alzheimer's disease. Front Psychiatry 1:152. Doi: 10.3389/fpsyt 2010.00152.

Ohtake T, Yamada H (1989) Efferent connections of the nucleus reuniens and the rhomboid nucleus in the rat: an anterograde PHA-L tracing study. Neurosci Res 6:556-568.

Paz JT, Huquenard JR (2015) Microcircuits and their interactions in epilepsy: is the focus out of focus? Nat Neurosci 18:351-359.

Peirera de Vasconcelos A, Cassel JC (2015) The non-specific thalamus: A place in a wedding bed for making memories last? Neurosci Biobeh Rev 54:175-196.

Prasad JA, Macgregor EM, Chudasama Y (2013) Lesions of the thalamic reuniens cause impulsive but not compulsive responses. Brain Struct Funct 218: 85-96.

Prasad JA, Abela AR, Chudasama Y (2017) Midline thalamic reuniens lesions improve executive behaviors. Neurosci 345:77-88.

Rabl R (1982) Structure and evaluation of the paramedian side of thalamus. Gegenbaurs Morphol Jahrb 128:12-25.

Ray A, Graham AJ, Lee M, Perry RH, Court JA, Perry EK (2005) Neuronal nicotinic acetylcholine receptor subunits in autism: an immonohistochemical investigation in the thalamus. Neurobiol Dis 19:366-377.

Rockland KS (2015) About connections. Front Neuroanat 9:61 doi 10.3389/fnana.2015.00061.

Saalman YB (2014) Intralaminar and medial thalamic influence on cortical synchrony, information transmission and cognition. Front Syst Neurosci 8:83 doi: 10.3389/fnsys.2014.00083.

Sierra RO, Pedraza LK, Zanona QK, Santana F, Boos FZ, Crestani AP, Haubrich J, de Oliveira Alvares L, Calcagnotto ME, Quillfeldt JA (2017) Reconsolidation-induced rescue of a remote fear memory blocked by an early cortical inhibition: involvement of the anterior cingulate cortex and the mediation by the thalamic nucleus reuniens. Hippocampus 27:596-607.

Sigurdsson T, Duvarci S (2016) Hippocampal-prefrontal interactions in cognition, behavior and psychiatric disease. Front Syst Neurosci 9:109. Doi: 10.3389/fnsys.2015.00190.

Sloan DM, Bertram EH 3rd (2009) Changes in midline thalamic recruiting responses in the prefrontal cortex of the rat during the development of chronic limbic seizures.

Epilepsia 50:556-565.

Small SA, Schobel SA, Buxton RB, Witter MP, Barnes A (2011) A pathophysiological framework of hippocampal dysfunction in ageing and disease. Nat Rev Neurosci 12:585-601.

Su H-S, Bentivoglio M (1990) Thalamic midline cell populations projecting to the nucleus accumbens, amygdala, and hippocampus in the rat. J Comp Neurol 297:582-593.

Swanson LW (2004) Brain maps: structure of the rat brain. Elsevier. New York.

Trzesniak C, Kempton MJ, Busatto GF, de Oliveira IR, Galvão-de Almeida A, Kambeitz J, Ferrari MC, Filho AS, Chagas MH, Zuardi AW, Hallak JE, McGuire PK, Crippa JA (2011) Adhesio interthalamica alterations in schizophrenia spectrum disorders: a systematic review and meta-analysis. Prog Neuropsychopharmacol Biol Psychiatry 35:877-886.

Trzesniak C, Schauffelberger MS, Duran FL, Santos LC, Rosa PG, McGuire PK, Murray RM, Scazufca M, Menezes PR, Hallak JE, Crippa JA, Bussato GF (2012) Longitudinal follow-up of cavum septum pellucidum and adhesio interthalamica alterations in first episode psychosis: a population-based MRI study. Psychol Med 42:2523-2534.

Van der Werf YD, Witter MP, Groenewegen HJ (2002) The intralaminar and midline nuclei of the thalamus. Anatomical and functional evidence for participation in processes of arousel and awareness. Brain Res Rev 39:107-140.

Van der Werf YD, Jolles J, Witter MP, Uylings HBM (2003a) Contributions of thalamic nuclei to declarative memory functioning. Cortex 39:1047-1062.

Van der Werf YD, Scheltens P, Lindeboom J, Witter Mp, Uylings HB, Jolles J (2003b) Deficits of memory, executive functioning and attention following infarctions in the thalamus: a study of 22 cases with localised lesions. Neuropsychol 41:1330-1344.

Varela C (2014) Thalamic neuromodulation and its implications for executive networks. Front Neural Circuits 8:69 doi: 10.3389/fncir.2014.00069.

Varela C, Kumar S, Yang JY, Wilson MA (2014) Anatomical substrates for direct interactions between hippocampus, medial prefrontal cortex, and the thalamic nucleus reuniens. Brain Struct Funct 219:911-929.

Vertes RP, Hoover WB, Do Valle AC, Sherman A, Rodriguez JJ (2006) Efferent projections of reuniens and rhomboid nuclei of the thalamus in the rat. J Comp Neurol 499:768-796.

Vertes RP, Hoover WB, Szigeti-Buck K, Leranth C (2007) Nucleus reuniens of the midline thalamus: link between the medial prefrontal cortex and the hippocampus. Brain Res Bull 71:601-609.

Vertes RP, Linley SB, Hoover WB (2015) Limbic circuitry of the midline thalamus. Neurosci Biobeh Rev 54:89-107.

Visser PJ, et al (1999) Brain correlates of memory dysfunction in alcoholic Korsakoff's syndrome. J Neurol Neurosurg Psychiatry 67:774-778.

Wang X, Stewart L, Cortez MA, Wu Y, Velazquez JC, Liu CC, Shen L, Snead OC 3rd (2009) The circuitry of atypical absence seizures in GABA(B)R1a transgenic mice. Pharmacol Biochem Behav 94:124-130.

Chapter 2

PROJECTIONS FROM THE NUCLEUS REUNIENS THALAMI TO THE ENTORHINAL CORTEX, HIPPOCAMPAL FIELD CA1, AND THE SUBICULUM IN THE RAT ARISE FROM DIFFERENT POPULATIONS OF NEURONS.

J Comp Neurol (1996) 364: 637-650.

ABSTRACT

The entorhinal cortex (EC), CA1, and the subiculum receive a major input from the thalamic midline nucleus reuniens (RE). At present, it is not known whether RE projections to these intimately interconnected regions are collateralized or arise from different cell populations. We employed the multiple fluorescent retrograde tracing technique with Fast Blue, Diamidino Yellow and Fluoro-Gold to examine the possible collateralization of RE projections to EC, CA1 and the subiculum. In addition, we studied the extent of collateralization within each target area. The results indicate that different, yet morphologically indistinguishable, populations of RE cells selectively innervate the EC, CA1, or subiculum. Within each of these areas, RE fibers display a locally restricted collateralization instead of distributing collaterals throughout the entire target structure.

The rostal two-thirds of RE is the major source of ipsilateral projections to CA1, subiculum, and EC. The periRE nucleus selectively projects to the perirhinal cortex. RE projections to CA1 and medial EC originate in the dorsolateral part and throughout the medial one-half of the nucleus, respectively. For these two projections, no topography could be established. However, subicular afferents are topographically organized such that a dorsal-to-ventral gradient in RE corresponds to a dorsal-to-ventral gradient along the subicular axis. Lateral entorhinal afferents display a subtle topography such that a lateral-to-medial shift of terminal fields in the lateral EC corresponds to a lateral-to-medial shift of projection neurons in the ventral RE.

INTRODUCTION

The entorhinal cortex (EC) and the hippocampal formation have strong reciprocal connections and are the central components of the medial temporal lobe memory system (e.g., Squire and Zola-Morgan, 1991; Eichenbaum and Otto, 1992; Squire, 1992; Jarrard, 1993; Zola-Morgan and Squire, 1993). The EC gives rise to the major cortical input to all divisions of the hippocampal formation, i.e., the dentate gyrus, fields CA3 and CA1, and the subiculum (Amaral and Witter, 1989; Witter et al., 1989; Lopes da Silva et al., 1990). In turn, field CA1 and the subiculum distribute extensive projections back to EC. The EC and the hippocampal formation have inputs from several subcortical structures in common, including an input from nuclei in the midline of the thalamus. This latter region is of interest since medial thalamic structures have been implicated in thalamic amnesia (cf. Rousseau, 1994) as well as in the early phase of Alzheimer's disease (Masliah et al., 1989; Braak and Braak, 1991, 1992; Forstl and Sahakian, 1993). The most prominent projection from the thalamic midline nuclei to EC and hippocampal formation originates in the nucleus reuniens (RE) (Segal, 1977; Herkenham, 1978; Beckstead, 1978; Baisden and Hoover, 1979; Wyss et al., 1979; Riley and Moore, 1981; Yanagihara et al., 1987; Ohtake and Yamada, 1989; Su and Bentivoglio, 1990; Wouterlood et al., 1990). Fibers from RE terminate especially in the layers I and III of EC, and in the stratum lacunosum-moleculare of CA1 and the stratum moleculare of the subiculum (Wouterlood et al., 1990; Wouterlood, 1991). Interestingly, projections from layer III of the EC terminate in the same two strata of CA1 and the subiculum. On the basis of these data, Wouterlood et al. (1990) proposed that RE is in a crucial position to influence the flow of cortical information through the EC to the hippocampal formation, as well as the processing of this information within CA1 and the subiculum. RE might thus modulate the activity in the entorhinal-hippocampal circuitry, which is critically involved in learning and memory processes (e.g., Jarrard, 1993).

The connections between the EC, CA1, and the subiculum are organized in a complex topographical manner (for review, see Witter, 1993). In view of the postulated modulatory influence of RE on these areas, at least two issues are of interest. First, do the projections from RE to interconnected parts of the EC, CA1, and the subiculum stem from different populations of neurons or are they collateralized? Wouterlood et al. (1990) suggested that within the EC and hippocampal formation the RE fibers are highly collateralized. Yet, according to Su and Bentivoglio (1990), the projections from the thalamic midline nuclei display only a low degree of collateralization to different target areas. Second, to what extent is the RE innervation of the hippocampal region topographically organized? If RE is topographically organized, what is the relationship of this topography with the organizational features of the entorhinal-CA1-subicular connectivity. Whereas Wyss et

al. (1979) did not find any topographic organization in the connections between RE and the hippocampal formation and EC in the rat, other investigators gave indications for such a topography (Riley and Moore, 1981; Wouterlood et al., 1990). They reported that the dorsal portion of RE preferentially projects to the dorsal part of the hippocampus and to the lateral portion of the EC. The ventral RE would preferentially project to the ventral hippocampus and to the medial portion of EC.

In the present study, retrograde tracing experiments were employed to elucidate the extent of collateralization and the topographic organization of the RE projections to the EC, field CA1, and the subiculum.

MATERIALS AND METHODS

Nineteen female Wistar rats (Harlan-Centraal Proefdierbedrijf, Zeist, the Netherlands), body weight 200-250 g, were used. Single and multiple injections with the fluorescent retrograde tracers Fast Blue (FB), Diamidino Yellow (DY; EMS-Polyloy, Grob-Umstadt, Germany), and Fluoro-Gold (FG; Fluorochrome Inc., Englewood, CO., USA) were placed at different sites along the dorsal-to-ventral axis of the hippocampal formation. Based on the findings by Wouterlood et al. (1990) that the most dorsal part of the hippocampus receives a weak innervation from RE, our most dorsal injections in the hippocampus were made approximately at the level of the splenium of the corpus callosum. Injections in EC were placed at different rostral-to-caudal and lateral-to-medial coordinates, and together covered most of the lateral and medial entorhinal areas. In 16 rats, tracers were applied unilaterally: either as a single injection of one tracer, or as a combination of multiple injections, each with a different tracer at a different location. In 3 rats, injections were placed bilaterally. In addition, we performed one control experiment (see below) in which a mixture of two tracers was injected. All experiments and combinations of injection sites are summarized in Table 1.

Our first interest was the precise relationship of RE with interconnected parts of the EC and the hippocampal formation. In the rat, the connections between EC, on the one hand, and CA1 and the subiculum, on the other, are topographically organized such that a lateral-to-medial axis of the EC corresponds with a dorsal-to-ventral axis in the hippocampal formation. In addition, these connections exhibit subtle organizational features along the transverse axis of CA1 and the subiculum which are reminiscent of the organization of projections from CA1 to the subiculum (Amaral and Witter, 1989; Amaral et al., 1991; Witter, 1993). Therefore, the combinations of injection sites were based on the topography of the entorhinal-hippocampal connections. Our second interest was to determine to what extent fibers from RE collateralize within a particular portion of EC or

the hippocampal formation. Therefore, we combined injections in: (1) dorsal and ventral CA1, and/or (2) dorsal and ventral subiculum, and/or (3) medial and lateral divisions of EC. To facilitate the description of the two types of collateralization, we will differentiate between so-called *inter*divisional collateralization, i.e., between divisions (e.g., CA1 and the subiculum) and *intra*divisional collateralization, i.e., between different parts of one and the same hippocampal (e.g., dorsal and ventral CA1) or entorhinal division. Additional single tracing experiments were carried out to study a possible topograpfic organization of the projections from RE to the hippocampal formation and EC (see Table 1).

Surgery. Rats were deeply anesthetized by means of an injection (i.m., 1 ml/kg body weight) of a mixture of 4 parts ketamine (1% solution of Aescoket, Aesculaap BV, Boxtel, The Netherlands) and 3 parts xylazine (2% solution of Rompun, Bayer, Leverkussen, Germany), and mounted in a stereotaxic frame. Using glass micropipettes, 100-200 nl of the tracer was injected by air-pressure. Coordinates for the injection sites were derived from Paxinos and Watson (1986). FB and DY (2%) were dissolved in 0.1 M phosphate buffer (pH 7.4) or in distilled water; FG (2%) was dissolved in 0.05 M NaAcetate (pH 5) or in distilled water.

Tissue processing. One to three weeks after surgery, the rats received an overdose of sodium pentobarbital (i.p., 60 mg/kg body weight; Nembutal, Sanofi, Maassluis, The Netherlands). The animals were transcardially perfused with 100 ml of 0.9% NaCl, which was immediately followed by 400-500 ml of 10% formaldehyde in 0.1 M phosphate buffer (pH 7.4, room temperature). Subsequently, the brains were postfixed for 1-2 hours in the same fixative and then cryoprotected overnight (4 ºC) in 2% dimethyl sulfoxide (DMSO) and 20% glycerin in distilled water. One-in-three series of coronal sections (40 µm thickness) were cut on a freezing microtome. One series of sections was directly mounted from a 0.2% gelatin solution in Tris-HCl (pH 7.6) for analysis; the remaining two series were collected in DMSO/glycerin and stored at -20 ºC.

Control experiment. In multiple retrograde tracing studies, factors such as uptake and/or transport competition between different tracers may contribute to an underestimation of the actual degree of collateralization displayed by projection fibers. Moreover, differentiation problems may arise when the fluorescence of one tracer masks that of another tracer. To exclude the possibility of an underestimation of the degree of collateralization, we performed a control experiment in which a mixture of FB and FG was injected. Because these two tracers label the cytoplasm of neurons, especially for FB and FG, co-transport could be hampered, or the differentiation between double- or single-labeled cells could be difficult. The mixture of FB and FG was injected in the medial portion of the lateral

entorhinal area; to control for an adequate transport of both tracers, FB and FG were each separately injected into the ipsilateral ventral subiculum and medial entorhinal area, respectively, in the same animal.

Analysis. With the use of fluorescence microscopy (excitation wave length 360-390 nm) the location and size of the injection sites were established. The area of necrosis, which is generally present, was considered the center of the injection site. The area into which the tracer had diffused was indicated by the halo of fluorescence around the center of the injection. The distribution of retrogradely labeled neurons in RE was analyzed using a computer-aided X-Y plotting system (Minnesota Datametrics, MD-2 digitizer and software). The extent of collateralized fibers was examined by analyzing every mounted section for the presence of single- and/or multiple-labeled neurons in RE. To establish a possible topography, we represented the distribution of labeled RE cells in a standard series of five rostral-to-caudal sections through the nucleus (see Fig. 1). Finally, the sections that had been plotted were counterstained with cresyl violet or azur B to determine cytoarchitectonic boundaries.
The five standard drawings of sections through RE (Fig.1), as well as the drawings of injections sites in representative cases (Figs. 2-4, 6, 7), were derived and modified from the brain maps of Swanson (1992).

RESULTS

Nomenclature

The hippocampal formation comprises the dentate gyrus, the Ammon's horn, which is subdivided into the fields CA1, CA2 and CA3, and the subiculum. Within the hippocampal formation, a curved, longitudinal axis runs from the dorsal to the ventral pole (Amaral and Witter, 1989). In the rat, the dorsal pole is situated near the midline, close to the septal complex, and the ventral pole abuts the amygdaloid complex. For descriptive purposes, field CA1 and the subiculum will be tentatively divided along this longitudinal axis into dorsal, intermediate and ventral portions.

The EC will be subdivided into a lateral (LEA) and a medial (MEA) entorhinal area (cf. Blackstad, 1956). Within EC, rostral-to-caudal and lateral-to-medial axes will be differentiated. The latter runs in the transverse plane from the rhinal sulcus towards the hippocampal fissure.

RE is located in the thalamic midline, just dorsal to the third ventricle (Fig. 1). In the horizontal plane, the nucleus is Y-shaped with a length of approximately 2 mm. The

most rostral portion of RE consists of two cell clusters that are separated in the midline by the most rostro-ventral extension of the paraventricular thalamic nucleus. Caudally, the two cell clusters form one fused, centrally situated nucleus. The most caudal level of RE consists of a central portion, which is accompanied by paired, ventrolateral "wing-like" extensions. The "wing" of RE, which can be distinguished from the main nucleus based on cytoarchitectonic features, is called the ventrolateral RE nucleus (Paxinos and Watson, 1986) or the periRE nucleus (Swanson, 1992). Throughout this paper we will refer to these wing-like extension as the "periRE nucleus" (see Fig. 1).

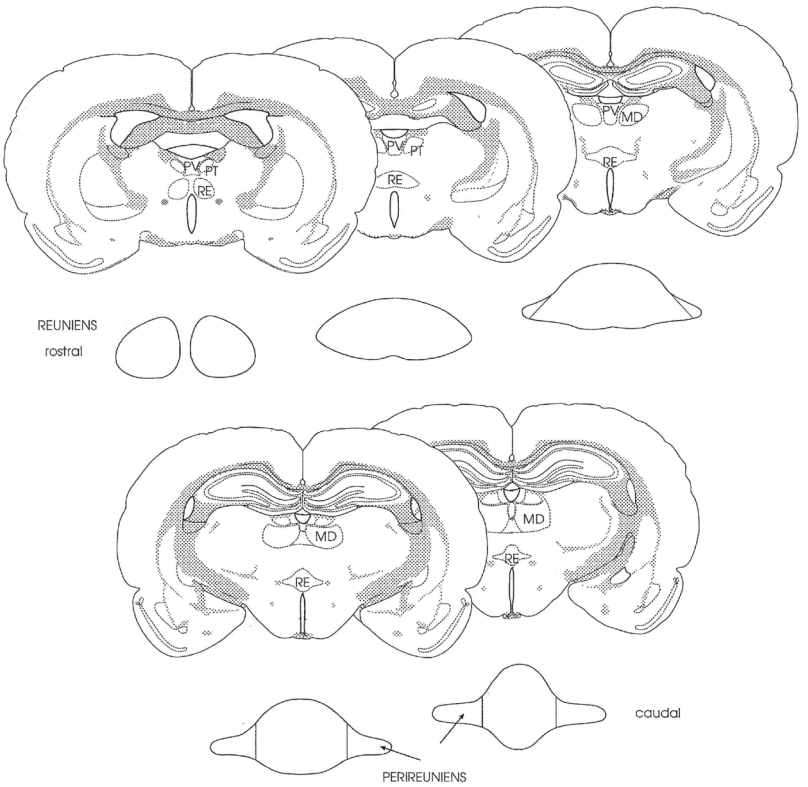

Fig. 1. Overview of five coronal sections through the rat brain and the corresponding standard drawings of the rostral-to-caudal nucleus RE/periRE that were used to illustrate the distribution of retrogradely labeled cells resulting from tracer injections into the hippocampal formation and EC. MD, mediodorsal nucleus; PT, paratenial nucleus; PV, paraventricular nucleus; RE, reuniens.

General distribution and morphology of labeled reuniens neurons

All injections with retrograde tracers in CA1, the subiculum and EC (see Table 1) resulted in labeling of neurons in RE. Labeled cells were observed throughout the ipsilateral one-half of the nucleus, whereas only a few cells were labeled contralaterally. The majority of retrogradely labeled cells was found in the rostral two-thirds of the nucleus, whereas the number of labeled cells rapidly decreased at more caudal levels. With the exception of an injection that involved the perirhinal cortex (case 387; see below) only a few cells were labeled in the periRE nucleus.

TABLE 1. Summary of experiments[1]

Case	Tracers	Injection sites
310	FB/DY	i CA1 + DG, CA3/ctr LEA
397	FG/FB/DY	i CA1/DG, CA3/l LEA
309	FB/DY	i CA1/ctr LEA
318	FG/FB/DY	i CA1/DG, CA3/l LEA + dp Prh
396	FG/FB/DY	i CA1/iCA1 + iSub/l LEA
317	FG/FB/DY	i CA1/i Sub/m LEA
386	FB/DY	i Sub/l LEA
076(l)	FB/DY	d CA1/d Sub
179	FB/DY	i CA1/i Sub + MEA
193	FB/DY	d CA1/i Sub + MEA
129	FB/DY	v Sub/MEA
275(l)	DY/FG	d CA1/v CA1 + v Sub
276(l)	DY/FG	d Sub/v Sub
275(r)	FB/DY	MEA/l LEA
121*	FB/FG/FG + FB	v Sub/MEA/m LEA
076(r)	FB	d CA1
201	FB	i CA1
178	FB	v CA1 + v Sub
122	FG	v Sub
276(r)	FB	MEA
387	DY	l LEA + sf Prh
303	DY	m LEA + dp Prh

[1]Abbreviations: FB = Fast Blue; DY = Diamidino Yellow; FG = Fluoro-Gold. CA, cornu ammonis field; Sub, subiculum; DG, dentate gyrus; Prh, perirhinal cortex; LEA, lateral entorhinal area; MEA, medial entorhinal area. d, dorsal; i, intermediate; v, ventral; l, lateral; m, medial; ctr, central; sf, superficial cortical layers; dp, deep cortical layers; (l), (r) = left, right hemisphere; * = control experiment.

In cases with injections of FB or FG, the morphology of the retrogradely labeled RE neurons was easily discerned. All labeled cells belonged to 1 of 2 classes of neurons, which were present throughout the nucleus. The first cell type had a rather large, round or multipolar, cell body and many, often up to 7, primary dendrites. The second cell type had a much smaller, oval or fusiform, cell body and 2-3 primary dendrites. Both cell types were strongly intermingled, and we were unable to establish a relationship between the cell type and a particular projection target.

Collateralization of reuniens projections

Control experiment

The analysis of case 121, in which an injection with a mixture of FB and FG was combined with injections of FB and FG alone, revealed that RE was densely packed with 3 differently labeled cell populations: numerous double FB/FG-labeled neurons, numerous single FB-labeled neurons, and single FG-labeled ones. Under high magnification and at 360 nm excitation wave length, double FB/FG-labeled neurons displayed a white-yellow color that could be distinguished from single FB-labeled (blue) and single FG-labeled (orange-yellow) ones. The color difference between FB/FG-labeled and FG-labeled neurons is, however, a subtle one. Therefore, we reexamined them under a different illumination (390 nm excitation wave length) under which FG becomes less bright and FB fluorescence appears more distinct. The effect of these different excitation wave lengths is documented in Figure 4 (A,B). Because labeled RE cells were too densely packed to make good quality high magnification photomicrographs (blurred picture due to fluorescence of cells out of focus), retrogradely labeled cells in the temporal cortex are shown. At 360 nm excitation wave length, in double FB/FG-labeled neurons the fluorescence of FG more or less masks that of FB (see Fig. 4A), whereas at 390 nm wave lengths the fluorescence of FB is dominant (see Fig. 4B).

In addition, we analyzed one experiment (case 317, not illustrated) in which the injection sites in the intermediate portion of CA1 (FG) and the adjacent subiculum (FB) showed some overlap in the subiculum. This resulted in a low number of double FG/FB-labeled neurons in RE. These findings indicate that co-transport of FG and FB in RE projection fibers had occurred.

Interdivisional collateralization

The first aim of this study was to analyze whether the RE projections to EC, CA1, and the subiculum are collateralized to 2 or 3 of these target areas, i.e., show interdivisional collateralization. Specific combinations of injections were made in those parts of the hippocampal formation and EC that, based on their topographic organization, are likely to be interconnected.

CA1-LEA: In 4 animals, an injection in CA1 was combined with an injection in LEA (see Table 1). In each animal, the injections in CA1 were placed in different positions along the dorsal-to-ventral axis, and the injections in LEA varied correspondingly along the lateral-to-medial axis. Because all four experiments gave comparable results, one representative case will be described. In case 310 (Fig. 2A,B) FB was injected into the intermediate part of CA1 and DY into the central part of LEA. The FB injection site

involved the strata radiatum and lacunosum-moleculare of CA1, and extended across the hippocampal fissure into the dentate gyrus (DG) and CA3. The center of the DY injection site was in the entorhinal layer III, with minor diffusion of the tracer into layers II and IV (Fig. 2A). Following these injections, numerous single FB- and DY-labeled cells were detected throughout RE (Fig. 2B). However, double FB/DY-labeled RE neurons were not observed. In this case, the FB injection in CA1 also involved the DG/CA3 region, which might have resulted in additional labeling of RE cells. To control for this possibility, two experiments with a selective tracer injection in the DG/CA3 region were analyzed (not illustrated). These injections in DG/CA3 did not result in any labeled cells in RE. This is in line with previous anterograde tracing results that showed that RE does not innervate the DG/CA3 region (Wouterlood et al., 1990). Therefore, in subsequent experiments diffusion of tracer into DG/CA3 is disregarded.

Subiculum-LEA: In three experiments, we combined differently positioned injections into the subiculum and LEA. Moreover, in two of those cases (396, 317) a third tracer was injected into field CA1 (Table 1). In a representative case (386), FB was injected into the stratum moleculare of the intermediate part of the subiculum, and the DY injection involved layers I and II of the lateral part of LEA (Fig. 2C). Following these injections, 2 single-labeled populations of neurons were present in RE. We did not detect any double labeling of RE cells (Fig.2D). In the other two experiments (cases 396, 317; see also below) the subicular and entorhinal injections resulted also in single DY- and FB-labeled RE cells only.

Subiculum-CA1: In case 396 (Fig. 3A,B) 3 different tracers were injected into the intermediate portions of CA1 and the subiculum, and in LEA. The FG injection in CA1 involved the strata lacunosum-moleculare and radiatum, and the FB injection was positioned in the stratum moleculare of the subiculum. This latter injection also extended into the adjacent portion of CA1, yet it did not overlap with the more dorsally positioned FG-injection in CA1 (Fig. 3A). In this case, no double labeling for FB and FG was observed, although both injections resulted in numerous single FB- and FG-labeled cells in RE (Fig. 3B).

Although these experiments indicate the probable paucity of collateral projections from RE to the hippocampal formation, a final experiment (case 076L) was performed in which the injections were placed into adjacent parts of CA1 and the subiculum in the dorsal hippocampus (Figs. 3C, 4C). In this case, RE displayed a moderate number of single DY-labeled cells and a somewhat larger number of single FB-labeled ones (Fig. 3D). Even following such closely spaced injections, no more than 4 double FB/DY-labeled neurons were observed.

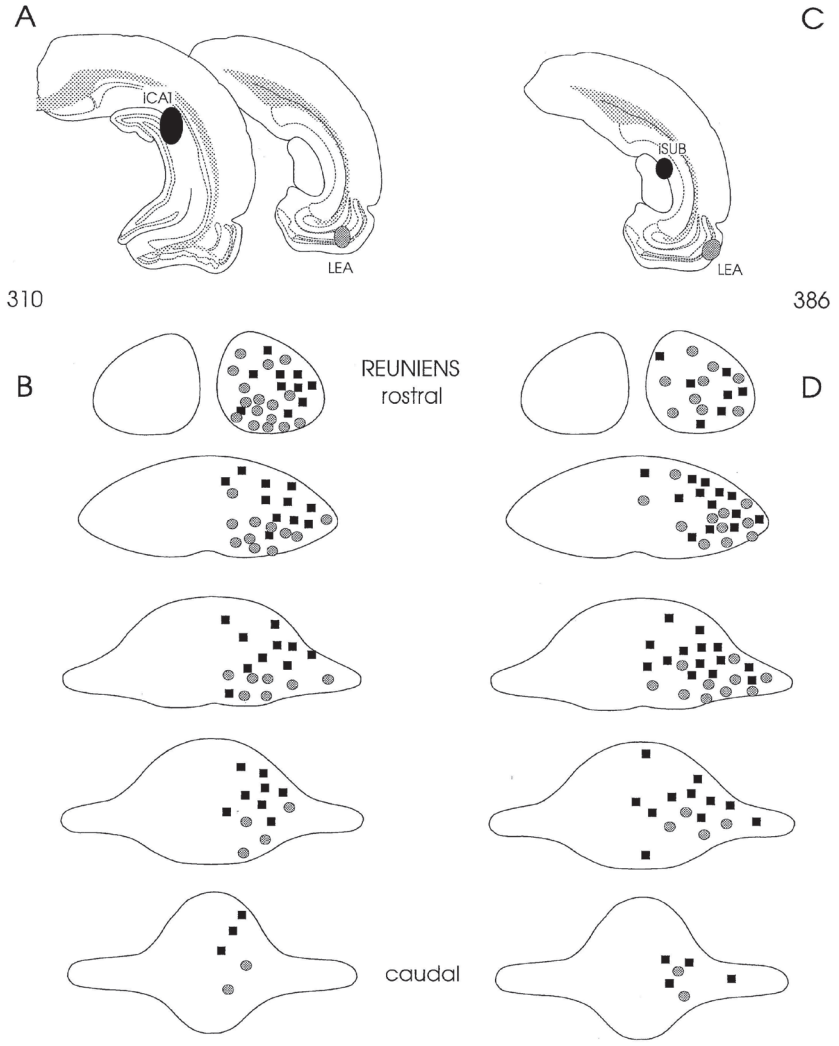

Fig. 2. Schematic representation of injection sites in the hippocampal formation and EC, and the distribution of retrogradely labeled neurons in RE. **A,B;** Labeling following a Fast Blue (FB) injection into the intermediate CA1 and a Diamidino Yellow (DY) injection centered in the caudal lateral entorhinal area (LEA). **C,D;** Labeling following a FB injection into the intermediate subiculum and a DY injection in the lateral portion of caudal LEA. FB- and DY-labeled injection sites and cells are indicated in black and grey, respectively. Each symbol corresponds to approximately 10 single-labeled neurons.

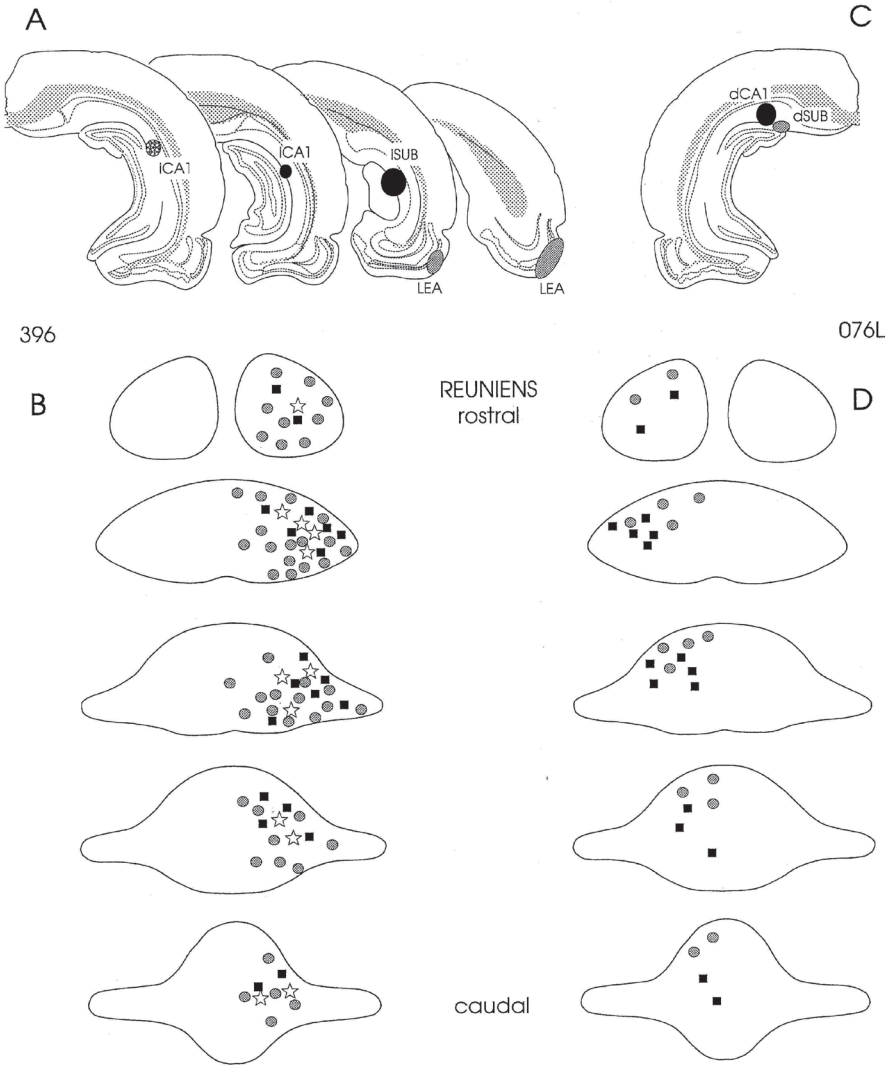

Fig. 3. Schematic representation of injection sites in the hippocampal formation and EC and the distribution of retrogradely labeled neurons in RE. **A,B;** Labeling following a FG injection into the intermediate CA1, a FB injection into the intermediate part of the subiculum and CA1, and a DY injection into the lateral part of caudal LEA. **C,D;** Labeling following a FB injection into dorsal CA1, and a DY injection into the adjacent subiculum (see Fig. 4C). The FG-labeled injection site is indicated by stippling, and the FG-labeled cells are indicates by stars. FB- and DY-labeled injection sites and cells are indicated in black and grey, respectively. Each symbol corresponds to approximately 10 single-labeled neurons.

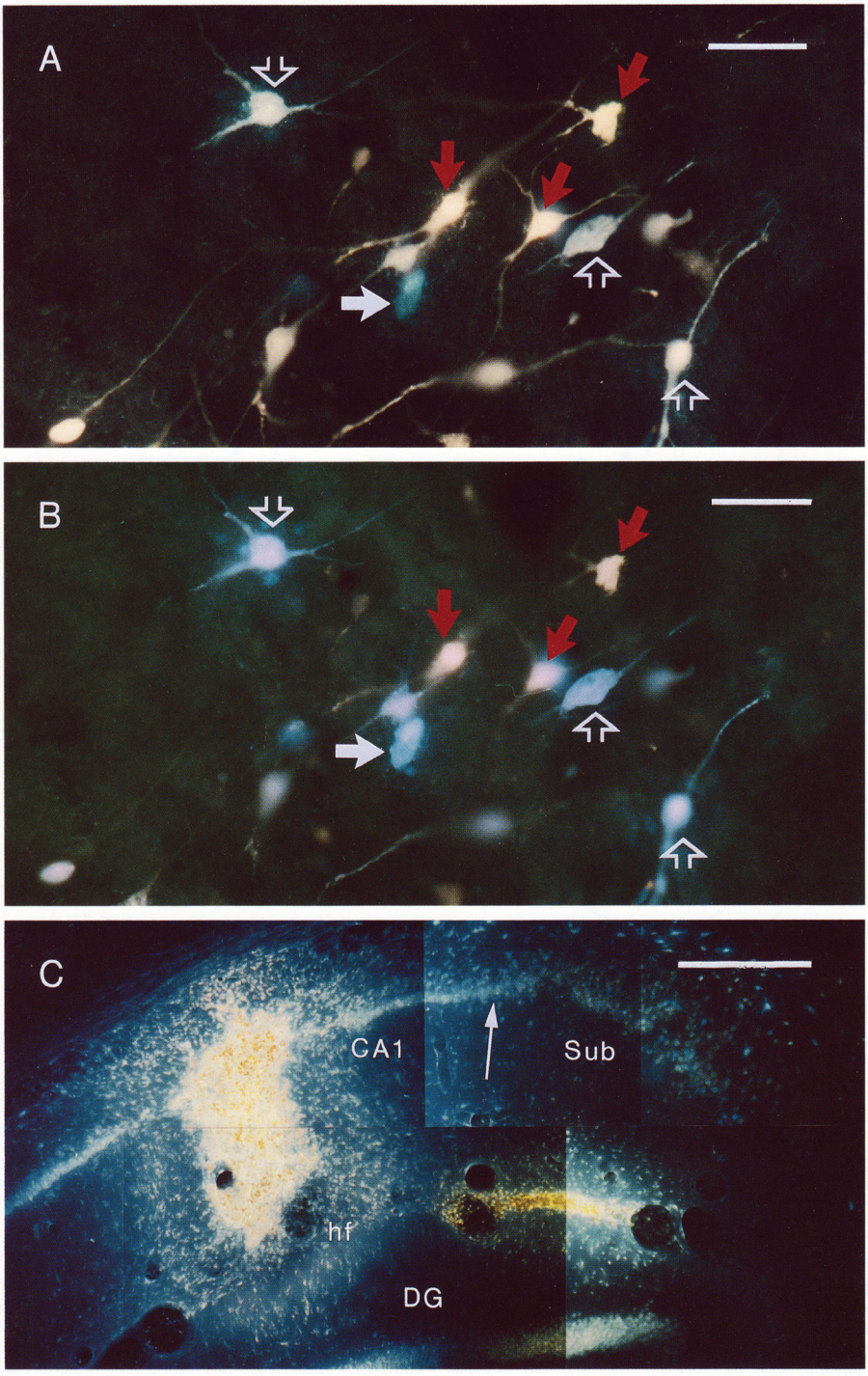
A
B
C
CA1
Sub
hf
DG

⇦ Fig. 4. **A,B.** Single FB-, single FG- and double FB/FG-labeled neurons in the temporal cortex (control experiment) under different illumination conditions. **A;** Illumination at 360 nm excitation wave length reveals a blue FB-labeled cell (white arrow), orange-yellow FG-labeled cells (red arrows), and white-yellow FB/FG-labeled ones (open white arrows). Evidently, the fluorescence of FG masks that of FB. **B;** At 390 nm wave length, the same double FB/FG-labeled cells (open white arrows) display a blue color similar to that of the single FB-labeled one (white arrow). Single FG-labeled cells appear less brightly fluorescent (red arrows). Under this illumination the fluorescence of FB dominates that of FG in the double FB/FG-labeled neurons. **C;** Photomicrograph of the dorsal hippocampus containing two closely spaced injection sites: FB was injected into CA1, DY into the subiculum. (see case 076L, Fig. 3C). These are representative examples of the selectivity of injections. The border between CA1 and the subiculum is indicated by a white arrow. DG, dentate gyrus ; hf, hippocampal fissure; Sub, subiculum. Scale bars = 50 μm in A,B, 250 μm in C.

CA1-subiculum-MEA: Following experiments in which injections into CA1 were combined with large injections covering parts of the subiculum and MEA (n=2; Table 1; not illustrated), we detected only single-labeled populations of RE neurons. Finally, in case 129, an injection with FB involving the stratum pyramidale and stratum moleculare of the ventral subiculum was combined with a DY injection in MEA involving mainly the layers I and II (Fig. 5A). Also in this experiment, we observed two populations of single-labeled RE cells (Fig. 5B).

Intradivisional collateralization

Injections of different retrograde tracers were placed into separate parts of one particular subdivision of the hippocampal formation or EC to study the extent of so-called intradivisional collateralization. A representative experiment is case 275 in which injections were placed bilaterally (Fig. 5C). In the left hemisphere, the DY injection was centered in dorsal CA1 and the FG injection in ventral CA1 and the adjacent subiculum. In the right hemisphere, the injections were placed in MEA (FB) and in LEA (DY), respectively. In both hemispheres, only single-labeled neurons were found in RE (Fig. 5D). Similar results were found in a case with injections in the dorsal and ventral subiculum (not illustrated). Moreover, as already described for case 396 (see Fig. 3A,B), non-overlapping injections with different tracers in the intermediate portion of CA1 did not result in double-labeled RE neurons.

Topographic organization

As a common result from all experiments (Table 1), we found that each retrogradely labeled cell population consisted of clustered cells in a particular location of the nucleus, accompanied by widely scattered cells throughout the nucleus. Consequently, all described cell populations were partly intermingled.

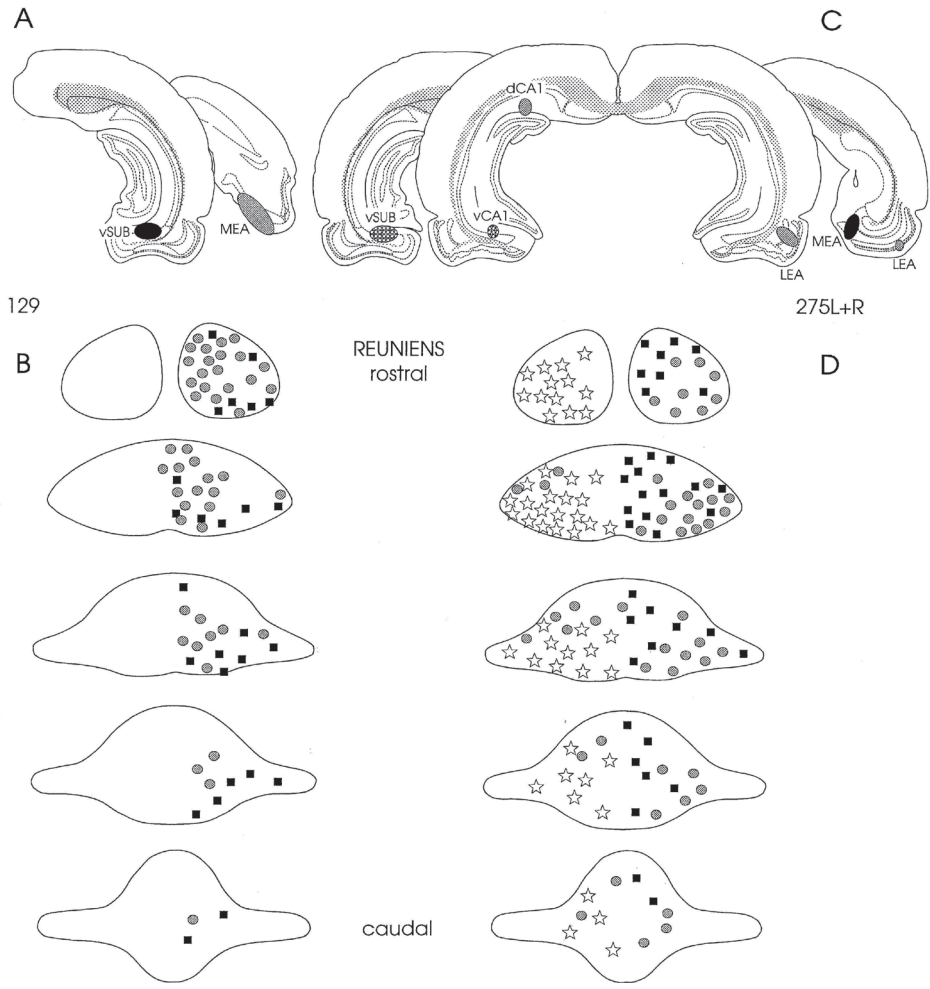

Fig. 5. Schematic representation of injection sites in the hippocampal formation and EC and distribution of retrogradely labeled neurons in RE. A,B; Labeling following a FB injection into the ventral subiculum and a DY injection centered in the medial entorhinal area (MEA). C,D; (left side) Labeling following a FB injection into dorsal CA1 and a FG injection into both ventral CA1 and ventral subiculum; FG-labeled injection site is indicated by stippling, FG-labeled cells are indicated by stars; (right side) Labeling following a DY injection into the lateral part of rostral LEA, and a FB injection into medial MEA. FB- and DY-labeled injection sites and cells are indicated in black and grey, respectively. Each symbol corresponds to approximately 10 single-labeled neurons..

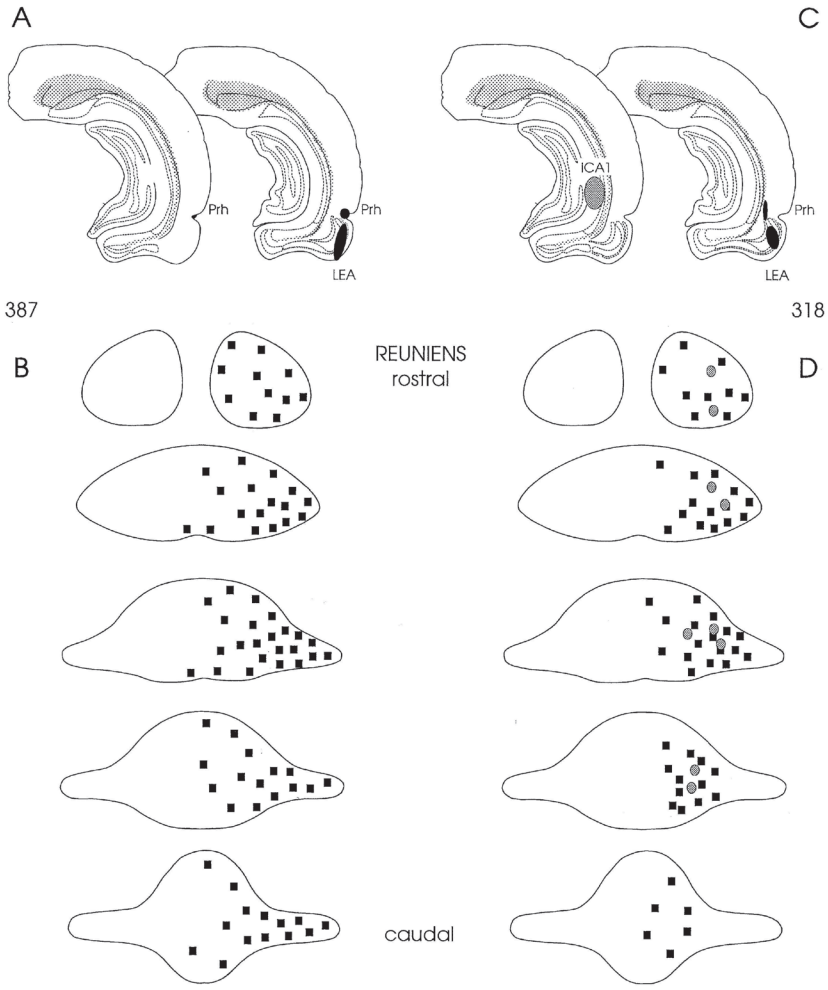

Fig. 6. Schematic representation of injection sites in the hippocampal formation and EC and distribution of retrogradely labeled neurons in RE and the periRE nucleus. A,B; Labeling following a DY injection into the superficial layers of the perirhinal cortex and in lateral LEA. Injection site and labeled cells are indicated in black. C,D; Labeling following a FB injection into intermediate CA1 and a DY injection into the deep layers of the perihinal cortex and into the lateral LEA. FB-labeled injection site and cells are indicated in grey; DY-labeled injection site and cells are indicated in black. Each symbol corresponds to approximately 10 single-labeled neurons.

CA1 projections: In general, following differently positioned injections in CA1 (n=15; see Table 1), the majority of retrogradely labeled cells clustered in the dorsolateral RE. We were unable to find an obvious difference in the preferential location of labeled RE cells following injections at different dorsal-to-ventral positions of CA1 from its ventral portion up and including the dorsal level close to the splenium of the corpus callosum. The lack of a clear topography can be easily appreciated when Figures 3 (C,D) and 6 (C,D) are compared. Figure 3 illustrates the distribution of labeled RE cells following the most dorsal CA1 injection (case 076L), and Figure 6 illustrates the results of an injection in the intermediate (close to the ventral) portion of CA1 (case 318). The most ventral CA1 injections always involved, although to a variable extent, the ventral subiculum and were therefore not included in the analysis of the topographic organization.

Subicular projections: Following differently positioned injections in the dorsal, intermediate, and ventral parts of the subiculum (n=9; Table 1), we observed gradual differences in the preferential location of clusters of labeled cells along the dorsal-to-ventral axis of RE. Whereas more dorsally situated RE neurons were labeled following injections in the dorsal subiculum (Fig. 3C,D; case 076L), injections in the ventral subiculum preferentially labeled neurons in the ventral part of the RE (Fig. 5A,B; case 129). RE neurons, labeled as a result of injections into the intermediate subiculum, were found at a mid dorsal-to-ventral position (fig. 2C,D; case 386).

Entorhinal projections: Comparison of all experiments with injections in different portions of LEA (n=11; Table 1), indicated that its lateral-to-medial position, not the rostral-to-caudal level of the injection site, was reflected in a subtle positional shift of labeled neurons in RE. This can be illustrated first by comparing case 275R (Fig. 5C,D; rostral LEA) with case 396 (Fig. 3A,B; caudal LEA); following both injections, cells were labeled predominantly in the ventrolateral part of the nucleus. In contrast, comparing a laterally placed injection (Fig. 2C,D; case 386) with a more medial injection in LEA, both at the same rostrocaudal position (Fig. 2A,B; case 310), clearly indicates a different location of labeled RE cells. In the lateral LEA case, labeled neurons were mainly present ventrolaterally in RE, whereas in the medial LEA case the labeled cells were situated more ventromedially.

The positions of the various injection sites in MEA (n=6; Table 1) were not sufficiently different from each other to further analyze the possibility of a topographic organization. However, the distribution of labeled RE cells following injections in MEA appeared strikingly different from that following injections in LEA. This difference is clearly illustrated in Figures 2, 3, and 5. A marked example is case 275R, documented in the Figure 5 (C,D), which shows that LEA-projecting neurons were predominantly present in the ventral RE, whereas MEA-projecting neurons were mainly present throughout the medial one-half of the nucleus.

Perirhinal projections: In 3 experiments, an injection into EC was accompanied by leakage of tracer in the perirhinal cortex. In 1 of those cases (Fig. 6A,B; case 387), in which only the superficial layers of the perirhinal cortex were involved, we noticed an exceptionally large number of retrogradely labeled cells in the periRE nucleus, in addition to the labeling of cells in RE. In contrast, the 2 remaining cases (see case 318; Fig. 6C,D), which involved only the deep layers of the perirhinal cortex, showed no labeling of periRE cells.

DISCUSSION

The results from the present study clearly demonstrate that the projections from RE to EC, hippocampal field CA1, and the subiculum originate from different cell populations. Moreover, we conclude that these projections predominantly originate in the rostral two-thirds of the nucleus; the caudal one-third contributes only modestly to these projections. Finally, the results indicate that the projections to the hippocampal formation and EC are ipsilateral, and that contralateral projections are extremely weak if present at all. The latter two conclusions regarding the topological origin are in accordance with those reported previously by Wouterlood et al. (1990). With the use of anterograde tracing techniques they observed that the most dense labeling in the areas presently under study was detected following injections into the rostral part of RE. Interestingly, our results further indicate that neurons in the periRE nucleus hardly innervate EC, CA1 and the subiculum but give rise to projections to the superficial layers of the perirhinal cortex. Recent anterograde tracing experiments support this observation, and indicate that the periRE nucleus also projects to the medial prefrontal cortex (own unpublished results).

Methodological considerations

The first aim of our study was to clarify whether neurons in RE give rise to collateral projections to the hippocampal formation and EC. Although the multiple retrograde tracing technique has been used succesfully in collateralization studies (Bentivoglio et al., 1980, 1981; Bentivoglio and Molinari, 1984; Su and Bentivoglio, 1990; Akintunde and Buxton, 1992a,b), at least two factors may contribute to an underestimation of the true numbers of neurons having collateralized projections. First, there is the possibility of uptake and/or transport competition between different fluorescent tracers, as has been shown for the combination of FB and DY that label the cytoplasm and the nucleus, respectively (Alheid et al., 1984). Although such a competition may lead to a decrease in

the number of double-labeled cells, it is not to be expected to result in no double-labeling at all. In fact, in one of our cases that showed a possible slight overlap of closely adjacent FB and DY injection sites in the dorsal parts of CA1 and the subiculum, a few FB/DY double-labeled RE cells were detected, indicating that co-transport of FB and DY does occur. Likewise, the presence of many FB/FG double-labeled cells in the RE resulting from the mixed FB/FG control injection, indicates that competition is not very apparent for these two tracers.

The second problem that might occur is that the intensity of fluorescence of one tracer may mask the fluorescence of another tracer. As regards the combination of FB and DY, we observed that additional labeling of the nucleus with FB and a faint cytoplasmic labeling with DY may interfere with a clearcut identification of single- or double-labeled cells. In case of FG and FB, which both result in labeling of the cytoplasm, the differentiation between single- or double-labeled cells may also be hampered (Keizer et al., 1983; Bentivoglio and Su, 1990; Akintunde and Buxton, 1992a). However, we found that in all cases switching from 360 nm to 390 nm excitation wave length allowed for a good differentiation of single- and/or double-labeled neurons (Keizer et al., 1983; Akintunde and Buxton, 1992a).

Morphology of cells of origin

A common feature of the presently analyzed RE projections is that they all arise from two, morphologically distinctive cell types. In a combined Golgi-horseradish peroxidase (HRP) study, Baisden and Hoover (1979) already described the morphology of RE cells projecting to the hippocampus as round or multipolar cells with 4-7 primary dendrites, and as smaller, fusiform cells with 2-3 primary dendrites. In our study, the FB- or FG-labeled neurons displayed similar morphologies, and both multipolar and fusiform cells were abundantly present and intermingled throughout the nucleus. Neither of the presently analyzed projections displayed an obvious selectivity for one particular cell type.

Organization of reuniens projections

The most important finding of the present study is that projections from RE to EC, field CA1, and the subiculum arise from different, albeit intermingled, populations of neurons. In only 2 experiments, a very small number of double-labeled RE neurons were noted among numerous single-labeled ones. In both these cases, an overlap of injection sites was the most likely explanation for the occurrence of this rare double labeling.

Moreover, we did not observe double-labeled RE neurons in any of the experiments in which combined injections were made in different parts of particular divisions of the hippocampal formation or EC. Thus, there is not only evidence that RE projections to CA1, the subiculum and EC are not collateralized, there is also little collateralization throughout the extent of each of these areas.

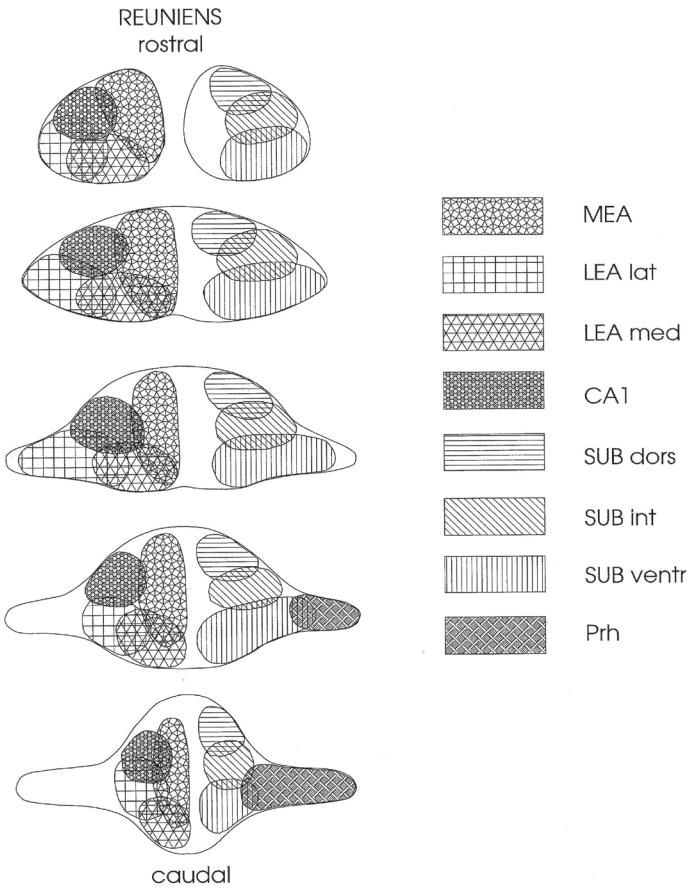

Fig. 7. Summary diagram represents the position of populations of RE and periRE neurons projecting (ipsilaterally) to a different (part of a) division of the hippocampal formation and of the entorhinal and perirhinal cortices. For the sake of clarity, populations of neurons projecting to EC or to CA1 are represented on the left side; neurons projecting to the subiculum or to the perirhinal cortex are indicated on the right side of the nucleus. Different shading patterns indicate the origin of the various projections. CA1, cornu ammonis field 1; LEA lat, lateral part of the lateral entorhinal area; LEA med, medial part of the lateral entorhinal area; MEA, medial entorhinal area; Prh, perirhinal cortex; SUB dors, dorsal subiculum; SUB int, intermediate subiculum; SUB ventr, ventral subiculum.

The RE projections to the hippocampal formation and EC are topographically organized. This organization is schematically represented in Figure 7. A dorsal-to-ventral gradient in the nucleus corresponds with a gradient in the terminal distribution along the dorsal-to-ventral axis of the subiculum. A comparable topography for the RE innervation of field CA1 could not be detected; the majority of neurons projecting to CA1 was consistently found in the dorsolateral part of the nucleus. Although the most dorsal portion of CA1 was not investigated in this study, these findings largely agree with those of Su and Bentivoglio (1990). With respect to the projections to EC, Wouterlood et al. (1990) reported that neurons in the dorsal RE project to lateral LEA, and neurons in the ventral RE project to medial LEA and MEA. In contrast, our results indicate that projections to all of LEA predominantly arise from the ventral part of the RE. Within this projection, we noted a subtle topography such that a shift in the terminal fields along the lateral-to-medial axis of LEA corresponds with a positional shift along the lateral-to-medial axis in the ventral nucleus RE. With respect to a possible topographic organization of the projections to MEA, our experiments do not allow to draw conclusions. However, we did detect a marked positional difference in MEA- and LEA-projecting cells, i.e., projections to MEA originate predominantly from neurons throughout the medial one-half of RE, whereas projections to LEA originate preferentially from the ventral part of RE.

In summary, in the dorsal part of the nucleus the distribution of neurons projecting either to the dorsal subiculum or to MEA largely overlap. In the dorsolateral RE, the populations of neurons projecting to either CA1 or the intermediate subiculum are partly intermingled. In the ventral nucleus RE, the distribution of cell populations projecting to the ventral subiculum, and to LEA, show a high degree of overlap. In the ventromedial part of the nucleus, MEA-projecting neurons are intermingled with neurons projecting to the medial portion of LEA. In addition, we conclude that neurons in the periRE nucleus project to the superficial layers of the perirhinal cortex.

Functional considerations

The present findings indicate that RE distributes selective, noncollateralized projections to the subiculum, field CA1, and EC. Unfortunately, the functional significance of such an organization is not yet clear. One might assume that this organization is related to a differential distribution of afferents to RE such that specific afferents target only certain groups of neurons, which in turn relay that information to only specific targets within the hippocampal-entorhinal complex. In a recently conducted systematic study of the afferents to RE (Dolleman-Van der Weel et al., 1993), the input structures were allocated

to three groups: strong, moderate or weak afferent projections. All major inputs appeared to originate in limbic structures such as the medial prefrontal cortex, anterior cingulate cortex, ventral subiculum, supramammillary region, and the precommissural nucleus of the pretectal region. Interestingly, all these major afferents showed a notable, different distribution of their terminal fields in RE. Whether or not this differential distribution of afferents is related to the presently described different populations of RE projection neurons remains to be established.

Acknowledgements

We thank Prof. H.J. Groenewegen for his advice and critical reading of the manuscript. This study was supported by the Graduate School Neurosciences Amsterdam (NWA grant 90-20).

REFERENCES

Akintunde, A., and D.F. Buxton (1992a) Quadruple labeling of brain-stem neurons: a multiple retrograde fluorescent tracer study of axon collateralization. J. Neurosci. Meth. 45:15-22.

Akintunde, A., and D.F. Buxton (1992b) Differential sites of origin and collateralization of corticospinal neurons in the rat: a multiple fluorescent retrograde tracer study. Brain Res. 575:86-92.

Alheid, G.F., J. Carlsen, J. DeOlmos, and L. Heimer (1984) Quantitative determination of collateral anterior olfactory nucleus projections using a fluorescent tracer with an algebraic solution to the problem of double retrograde labeling. Brain Res. 292:17-22.

Amaral, D.G., and M.P. Witter (1989) The three-dimensional organization of the hippocampal formation: a review of anatomical data. Neuroscience 31:571-591.

Amaral, D.G., C. Dolorfo, and P. Alvarez-Royo (1991) Organization of CA1 projections to the subiculum: a PHA-L analysis in the rat. Hippocampus 1:415-435.

Baisden, R.H., and D.B. Hoover (1979) Cells of origin of the hippocampal afferent projection from the nucleus reuniens thalami. Cell Tissue Res. 203:387-391.

Beckstead, R.M. (1978) Afferent connections of the entorhinal area in the rat as demonstrated by retrograde cell-labeling with horseradish peroxidase. Brain Res. 152:249-264.

Bentivoglio, M., and M. Molinari (1984) Fluorescent retrograde triple labeling of brainstem reticular neurons. Neurosci. Lett. 46:121-126.

Bentivoglio, M., and H.S. Su (1990) Photoconversion of fluorescent retrograde tracers.

Neurosci. Lett. 113:127-133.

Bentivoglio, M., H.G.J.M. Kuypers, C.E. Catsman-Berrevoets, H. Loewe, and O. Dann (1980) Two new fluorescent retrograde neuronal tracers which are transported over long distances. Neurosci. Lett. 18:25-30.

Bentivoglio, M., G. Macchi, and A. Albanese (1981) The cortical projections of the thalamic intralaminar nuclei, as studied in the cat and rat with the multiple fluorescent retrograde tracing technique. Neurosci. Lett. 26:5-10.

Blackstad, W.T. (1956) Commissural connections of the hippocampal region in the rat, with special reference to their mode of termination. J. Comp. Neurol. 105:417-537.

Braak, H., and E. Braak (1991) Alzheimer's disease affects limbic nuclei of the thalamus. Acta Neuropathol. 81:261-268.

Braak, H., and E. Braak (1992) The human entorhinal cortex: Normal morphology and lamina-specific pathology in various diseases. Neurosci. Res. 15:6-31.

Dolleman-van der Weel, M.J., W. Ang, and M.P. Witter (1993) Afferent connections of the nucleus reuniens thalami: a neuroanatomical tracing study in the rat. Eur. J. Neurosci. 6 (Suppl.):247.

Eichenbaum, H., and N.J. Otto (1992) The hippocampus - what does it do? Behav. Neur. Biol. 57:2-36.

Forstl, H., and B. Sahakian (1993) Thalamic radiodensity and cognitive performance in mild and moderate dementia of the Alzheimer type. J. Psych. Neurosci. 18:33-37.

Herkenham, M. (1978) The connections of the nucleus reuniens thalami: evidence for a direct thalamo-hippocampal pathway in the rat. J. Comp Neurol. 177:589-609.

Jarrard, L.E. (1993) On the role of the hippocampus in learning and memory in the rat. Behav. Neural Biol. 60:9-26.

Keizer, K., H.G.J.M. Kuypers, A.M. Huisman, and O. Dann (1983) Diamidino Yellow dihydrochloride (DY.2HCl); a new fluorescent retrograde neuronal tracer, which migrates only very slowly out of the cell. Epx. Brain Res. 51:179-191.

Lopes da Silva, F.H., M.P. Witter, P.H. Boeijinga, and A.H.M. Lohman (1990) Anatomic organization and physiology of the limbic cortex. Physiol. Rev. 70: 453-511.

Masliah, E., R. Terry, and G. Buzsaki (1989) Thalamic nuclei in Alzheimer disease: evidence against the cholinergic hypothesis of plague formation. Brain Res. 493:240-246.

Ohtake, T., and H. Yamada (1989) Efferent connections of the nucleus reuniens and the rhomboid nucleus in the rat: an anterograde PHA-L tracing study. Neurosci. Res. 6:556-568.

Paxinos, G., and C. Watson (1986) The rat brain in stereotaxic coordinates, 2 nd edition. New York: Academic Press.

Riley, J.N., and R.Y. Moore (1981) Diencephalic and brainstem afferents to the

hippocampal formation of the rat. Brain Res. Bull. 6:437-444.

Rousseaux, M. (1994) Amnesias following limited thalamic lesions. In J. Delacour (ed): Adv. Series Neurosci. vol 4, Singapore/London, World Scientific Publ.: pp. 241-276.

Segal, M. (1977) Afferents to the entorhinal cortex of the rat studied by the method of retrograde transport of horseradish peroxidase. Exp. Neurol. 57:750-765.

Su, H.S., and M. Bentivoglio (1990) Thalamic midline cell populations projecting to the nucleus accumbens, amygdala, and hippocampus in the rat. J. Comp. Neurol. 121:1-12.

Squire, L.R. (1992) Memory and the hippocampus: A synthesis from findings with rats, monkeys and humans. Physiol.Rev. 99:195-231.

Squire, L.R., and S. Zola-Morgan (1991) The medial temporal lobe memory system. Science 253:1380-1386.

Swanson, L.W. (1992) Brain maps: Structure of the rat brain. Amsterdam: Elsevier.

Witter, M.P. (1993) Organization of the entorhinal-hippocampal system: a review of current anatomical data. Hippocampus 3:33-44.

Witter, M.P., Groenewegen, H.J., Lopes da Silva, F.H., and Lohman, A.H.M. (1989) Functional organization of the extrinsic and intrinsic circuitry of the parahippocampal region. Prog. Neurobiol. 33:161-253.

Wouterlood, F.G. (1991) Innervation of entorhinal principal cells by neurons of the nucleus reuniens thalami. Anterograde PHA-L tracing combined with retrograde fluorescent tracing and intracellular injection with Lucifer Yellow in the rat. Eur. J. Neurosci. 3:641-647.

Wouterlood, F.G., E. Saldana, and M.P. Witter (1990) Projection from the nucleus reuniens thalami to the hippocampal region: light and electron microscopic tracing study in the rat with the anterograde tracer Phaseolus vulgaris leucoagglutinin. J. Comp. Neurol. 296:179-203.

Wyss, J.M., L.W. Swanson, and W.M. Cowan (1979) A study of subcortical afferents to the hippocampal formation in the rat. Neurosci. 4:463-476.

Yanagihara, M., K. Niimi, and K. Ono (1987) Thalamic projections to the hippocampal and entorhinal areas in the cat. J. Comp. Neurol. 266:122-141.

Zola-Morgan, S., and L.R. Squire (1993) Neuroanatomy of memory. Annu. Rev. Neurosci. 16:547-563.

Chapter 3

MULTIPLE ANTEROGRADE TRACING, COMBINING PHASEOLUS VULGARIS LEUCOAGGLUTININ WITH RHODAMINE- AND BIOTIN-CONJUGATED DEXTRAN AMINE.

J Neurosci Methods (1994) 51:9-21.

ABSTRACT

The simultaneous use of different neuroanatomical anterograde tracers provides a potentially powerful method to study the convergence of afferent systems in a particular brain area. However, a simple routine procedure to apply multiple anterograde tracers in conjunction with their simultaneous visualization is still missing. We report an easy and straightforward application of three sensitive anterograde tracers, Phaseolus vulgaris leucoagglutinin (PHA-L), rhodamine-conjugated dextran amine (RDA) and biotin-conjugated dextran amine (BDA). These tracers can be visualized simultaneously and permanently through a triple-staining procedure with nickel-enhanced diaminobenzidine (DAB-Ni), DAB and 1-naphthol/Azur B as chromogens. Our test model comprised the projections from the nucleus reuniens thalami (RE) and from the entorhinal cortex (EC). Both projection systems show a high degree of overlap in their terminal fields in the hippocampus. Two tracers were injected in the left and right EC, respectively; a third tracer was injected into RE. This combination of injections provided a good opportunity to compare the three tracers in one and the same animal. PHA-L, RDA and BDA, injected in either of the injection sites, turned out to be equally sensitive, and revealed the morphology of the involved projection systems in great detail. The triple-staining protocol yielded an excellent, simultaneous detectability of the three tracers with a remarkably low background level. Thus, the combination of the anterograde tracers PHA-L, RDA and BDA, in conjunction with the triple-staining procedure, offers a very attractive approach for neuroanatomical research.

INTRODUCTION

Connectivity of brain regions and particularly the interrelationship of converging afferent fiber systems are important issues in neuroanatomical research. One way to study the degree of overlap of different afferents to the same brain area is through simultaneous anterograde tracing and subsequent distinguishable visualization of the labeled fiber systems in one and the same section. Despite an expanding class of sensitive anterograde tracing methods, the simultaneous visualization of more than one input to a particular target area cannot yet be considered a routine procedure. The effectiveness of a combination of tracing methods depends greatly on the compatibility of the tracers used. Various technical problems may arise applying various combinations of widely used, sensitive anterograde tracers such as wheat germ agglutinin-conjugated horseradish peroxidase (WGA-HRP, e.g. Mesulam, 1982), tritiated amino acids (Cowan et al., 1972), cholera toxin B-conjugated HRP (CTB-HRP, Trojanowski, 1981; Wan et al., 1982), Phaseolus vulgaris leucoagglutinin (PHA-L, Gerfen and Sawchenko, 1984), and biocytin (King et al., 1989; Izzo, 1990; Lapper and Bolam, 1991). As a consequence of differences in optimum survival times between tracers, a rather complicated surgical procedure has to be applied (e.g. Mesulam, 1982; Smith and Bolam, 1991; Lapper and Bolam, 1991). Differences in sensitivity may further complicate the analysis. For example, anterogradely transported PHA-L visualized via immunocytochemistry results in a very fine, detailed morphology of both the cells of origin, their fiber trajectories and terminal distribution. In contrast, transported tritiated amino acids visualized by the autoradiographic method provide far less morphological detail. Moreover, the latter procedure is extremely time consuming (Gerfen, 1985). One approach to circumvent these problems uses the simultaneous application of various distinguishable forms of the same tracer such as PHA-L and PHA-L-conjugates. Unfortunately, the use of these conjugates is hampered by a reduced detection level (Antal et al., 1990). Recently developed dextran conjugates (Glover et al., 1986; Schmued et al., 1990; Nance and Burns, 1990; Chang, 1991; Veenman et al., 1992; Brandt and Apkarian, 1992; Reiner et al., 1993) are reported to combine a sensitivity similar to that of PHA-L with comparable application and survival protocols. They may thus form an attractive combination in neuroanatomical tracing using multiple tracers.

The present report describes a sensitive method that allows the permanent and simultaneous visualization of three different anterograde tracers with a newly developed triple-staining procedure. We employed PHA-L in combination with rhodamine-conjugated dextran amine (RDA, Fluoro-Ruby, Schmued et al., 1990) and biotin-conjugated dextran amine (BDA, Veenman et al., 1992; Brandt and Apkarian, 1992; Reiner et al., 1993).

Previous single-tracing studies have shown that fibers from the nucleus reuniens

thalami (RE) and from the entorhinal cortex (EC) course through and terminate in the stratum lacunosum moleculare of the hippocampal CA1 region and in the stratum moleculare of the subiculum (Herkenham, 1978; Witter et al., 1986, 1989; Wouterlood et al., 1990). Both fiber systems overlap in their terminal fields in these hippocampal subdivisions. To explore and compare the sensitivity, the specific properties, and the detectability of PHA-L, RDA, and BDA, we used this afferentiation of the hippocampus as a model.

MATERIALS AND METHODS

Experimental subjects and surgery. Twelve young adult female Wistar rats (body weight 200-250 g; Harlan-Centraal Proefdierbedrijf, Zeist, Netherlands) were used. To compare the sensitivity and detectability of PHA-L, RDA and BDA in single-color, in 2x2 color combinations or in a 3-color combination, we performed a series of tracing experiments as summarized in Table 1. The rats were deeply anesthetized with 1 ml/kg body weight of a mixture of 4 parts ketamine (1% solution of Ket, Aesco) and 3 parts xylazine (2% solution of Rompun, Bayer), and mounted in a stereotaxic frame. PHA-L (2.5% in 0.05 M Tris-buffered saline, pH 7.4), RDA (10% in 0.1 M phosphate buffer, pH 7.4) and BDA (10% in 0.01 M phosphate buffer, pH 7.4) were injected in the EC and RE in different combinations (see Table 1) (coordinates derived from Paxinos and Watson, 1986). All injections were iontophoretically applied, using glass micropipettes (internal tip diameter 15-20 μm) and a pulsed positive DC current for 10 minutes (7 s on/7 s off; PHA-L, 6-7.5 μA; RDA, 4 μA; BDA, 5-6.5 μA). In order to obtain maximal labeling of the RE and EC projection systems a rostrocaudal array of 2-3 injections was placed in the respective sites of origin. Furthermore, we took care that each of the three tracers was injected, at least once, in either RE or EC. For reasons discussed below we performed two RDA-control experiments. The first control animal was injected with RDA in the tail vein, and the second served as a blank control.

Tissue processing. Seven to 10 days after surgery, all rats received an overdose of sodium pentobarbital (Nembutal, Ceva, 60 mg/kg body weight, i.p.). The brains were fixed by transcardial perfusion of the animals with 200 ml of 0.9% saline solution (room temperature), followed by 500 ml of 4% freshly depolymerized paraformaldehyde and 0.05% glutaraldehyde in 0.1 M phosphate buffer, pH 7.4 (room temperature). After post-fixation in the same fixative for 1-3 h at 4 ºC the brain tissue was cryoprotected by immersion in 2% dimethylsulfoxide (DMSO) and 20 % glycerin in distilled water or phosphate buffer (pH 7.4) until equilibrium. On a freezing microtome, 1 in 10 series of coronal sections

(40 μm thick) were cut and collected in 0.05 M Tris-buffered saline (TBS), pH 7.6. The sections were immediately immunocytochemically processed for the visualization of the tracers or were stored in DMSO/glycerin at -20 ºC for processing afterwards.

Single-staining procedures. Each of the tracers was initially visualized in one series of sections by a single-staining procedure (see Table 2A), using nickel enhanced diaminobenzidine (DAB-Ni) as chromogen (purple-black labeling). All incubations were conducted on free floating sections, under gentle agitation, at room temperature. Before and after each incubation step the sections were rinsed 3 times for 10 min in TBS containing 0.5% Triton X-100 (TBS-TX) pH 7.6.

PHA-L and RDA were both visualized by immunocytochemistry (unlabeled antibody method of Sternberger, 1979). Sections were incubated overnight in, respectively, a goat-anti-PHA-L (1:4000) or rabbit-anti-TRITC (tetramethyl-rhodamine-isothiocyanate) antiserum (1:6000) in TBS-TX, followed by incubation (1 h) in immunoglobuline G (IgG) raised in donkey against goat (DoaG) or in swine against rabbit (SwaR), diluted 1:50 in TBS-TX. Subsequently, the sections were incubated with a peroxidase-antiperoxidase complex (PAP), raised in goat or in rabbit, respectively (dilutions: goat-PAP 1:600, rabbit-PAP 1:800 in TBS-TX) for1 h, and finally reacted with DAB-Ni (see below).

BDA was visualized with an avidin-biotin-peroxidase complex (ABC-kit, Vectastain, Vector), prepared according to the manufacturer's recommendations. Sections were incubated with ABC solution for 1.5 h and then reacted with DAB-Ni.

Double-staining procedures. Two-by-two visualization of injected tracers (PHA-L/RDA, BDA/PHA-L, BDA/RDA) was achieved employing the chromogens DAB-Ni and DAB to obtain a purple-black and brown labeling, respectively (see Table 2B).

PHA-L/RDA. Sections were incubated overnight with a mixture of goat-anti-PHA-L (1:4000, in TBS-TX) and rabbit-anti-TRITC (1:6000, in TBS-TX), followed by incubation with a mixture of DoaG and SwaR (1:50, in TBS-TX) for 1 h. Subsequently, each tracer was separately visualized (see Table 2A,B) with the use of a DAB or DAB-Ni procedure. However, for reasons discussed in the Results, we preferred staining of RDA with DAB.

BDA/PHA-L and BDA/RDA. BDA was initially visualized with DAB-Ni as chromogen, as described above for the single-staining procedure. Subsequently, PHA-L or RDA were visualized according to their respective single-staining procedures, completed with a DAB reaction.

Table 1. Summary of experiments

Tracing experiment	injection site	tracer	No. of injections	No. of experiments
triple	RE (l+r)	PHA-L	4	2
	EC (l)	BDA	3	
	EC (r)	RDA	3	
	RE (l+r)	RDA	4	1
	EC (l)	BDA	3	
	EC (r)	PHA-L	3	
double	RE (r)	PHA-L	2	5
	EC (r)	RDA	3	
single	RE (l+r)	BDA	4	2
systemic control	tail vein	RDA	1	1
blank control	---	---	---	1

Abbreviations: RE = nucleus reuniens thalami, EC = entorhinal cortex, l = left hemisphere, r = right hemisphere, PHA-L = Phaseolus vulgaris leucoagglutinin, RDA = rhodamine-conjugated dextran amine, BDA = biotin-conjugated dextran amine.

Triple-staining procedure. In order to reveal three tracers in one and the same section, we employed 1-naphthol as third chromogen. The reaction product of 1-naphthol is a grey-violet labeling that can be intensified by a reaction with basic dyes into a differently colored 1-naphthol/basic dye complex (Mauro et al., 1985). In previous studies (unpublished results) we explored several basic dyes to form a complex with 1-naphthol. Based on these results we modified the staining procedure described by Castellano et al. (1990) to combine 1-naphthol/basic dye staining with an immunostaining employing DAB as chromogen. In these experiments the basic dye Azur B (blue-green) yielded the best contrast with DAB (brown) and was therefore selected for triple staining purposes.

Triple-staining of PHA-L/RDA/BDA was performed through the following sequence of procedures (see Table 2C). PHA-L and RDA were initially visualized with DAB-Ni and DAB as chromogens, respectively (see double-staining procedure). For the subsequent visualization of BDA these double-stained sections were incubated with an ABC solution (see single BDA staining procedure), followed by extensive rinsing in TBS. The sections were then reacted with 1-naphthol/Azur B (see below).

Table 2
A: Incubation steps in single-staining procedures

Steps	PHA-L	RDA	BDA
1	goat-α-PHA-L	rabbit-α-TRITC	ABC
2	DoaG	SwaR	DAB (Ni)
3	goat-PAP	rabbit-PAP	
4	DAB-Ni	DAB-Ni	

B: Incubation steps in double-staining procedures

Steps	PHA-L/RDA		BDA/ PHA-L	BDA/ RDA
1	mix: goat-α-PHA-L/ rabbit-α-TRITC		ABC	ABC
2	mix: DoaG/SwaR		DAB-Ni	DAB-Ni
3	goat-PAP [a]	rabbit-PAP	goat-α-PHA-L	rabbit-α-TRITC
4	DAB-Ni	DAB-Ni	DoaG	SwaR
5	rabbit-PAP	goat-PAP	goat-PAP	rabbit-PAP
6	DAB	DAB	DAB	DAB

C: Incubation steps in triple-staining procedure

	PHA-L/RDA/BDA
1	mix: goat-α-PHA-L/rabbit-α-TRITC
2	mix: DoaG/SwaR
3	goat-PAP
4	DAB-Ni
5	rabbit-PAP
6	DAB
7	ABC
8	1-naphthol
9	Azur B

[a] Preferable procedure.

DAB-Ni, DAB and 1-naphthol/Azur B protocols.

DAB-Ni. 3,3'-Diaminobenzidine tetrahydrochloride (DAB, 12.5 mg) was dissolved in 25 ml 0.1 M phosphate buffer (pH 7.4) and 1 ml 1% ammonium-nickel-sulphate (Ni). Prior to use 6.7 µl 30% H_2O_2 was added. After rinsing in 0.05 M Tris-HCl (pH 7.6) and phosphate buffer, the sections were reacted with DAB-Ni for 5-15 minutes, resulting in the formation of a purple-black reaction product.

DAB. DAB (10 mg) was dissolved in 20 ml 0.05 M Tris-HCl (pH 7.6). Prior to use 6.7 µl 30% H_2O_2 was added. After rinsing in Tris-HCl, the sections were reacted with

DAB for 15-25 minutes, resulting in a brown reaction precipitate in the labeled system. Precipitation of the DAB-Ni and DAB products in labeled cells and fibers was carefully monitored at intervals during the reaction and terminated by thorough rinsing in the appropriate buffer.

1-Naphthol/Azur B. 1-Naphthol (50 mg) was dissolved in 0.5 ml ethanol, added to 89.5 ml 0.05 M TBS (pH 7.6) containing 10 ml 1% ammonium carbonate and subsequently filtered. Prior to use 6.7 µl 30% H_2O_2 was added to 20 ml of freshly prepared 1-naphthol solution. Following rinsing in TBS, sections were reacted with this solution for 20-25 minutes. In order to enhance the color contrast with the DAB-Ni and DAB reaction products, the 1-naphthol precipitate (grey-violet) was reacted with the basic dye Azur B to obtain a blue-green labeling. Free floating DAB-Ni/DAB/1-naphthol-stained sections were reacted for 30 minutes (room temperature) with 0.05% Azur B in 0.05 M TBS (pH 8), resulting in a blue-green colored 1-naphthol/Azur B complex. By that time the background had become dark blue. Differentiation of blue background and black/brown/blue-green labeling was obtained by thoroughly rinsing the sections, twice in distilled water, once in 50% alcohol for approximately 2-5 minutes, and again twice in distilled water.

All stained sections were mounted from 0.2% gelatin in Tris-HCl (pH 7.6-8), air-dried, dehydrated through increasing concentrations of alcohol, cleared in xylene and coverslipped with Entellan (Merck).

RDA control experiments. That dextran conjugates may label non-neuronal, perivascular cells has been described previously (Schmued et al., 1990; Nance and Burns, 1991; Chang, 1991, 1993), and indeed this was also noticed in our experiments. However, in addition to RDA-labeling of perivascular cells, we were confronted with a distinctive staining of vascular walls and closely associated cellular elements (see Results and Discussion) occurring in RDA-immunoreacted sections. Since blood vessel-associated RDA labeling has never been reported in RDA-fluorescence studies, we wanted to clarify whether this peculiar phenomenon might be due to (1) a difference in sensitivity between fluorescence microscopy and immunocytochemistry, or (2) an intrinsic property of the polyclonal anti-TRITC antibody used for the visualization of RDA. We also noted that whenever the RDA injection site included large blood vessels, the blood vessel-associated staining seemed particularly evident throughout the brain. Therefore, we examined the possibility that systemically transported RDA was able to cross the blood-brain-barrier, resulting in a more widespread staining of vascular walls and associated cellular elements. Two control rats were used. One rat served as a blank control. In the second rat 100 µl RDA (1% in sterile saline) was injected in the tail vein. This rat (systemic control) was killed after 7

days survival. Sections of the brains of the blank control and the systemic control rat were compared with each other and with those of the experimental RDA cases. Comparison was conducted in the following way: (1) Sample sections were studied with the use of a fluorescence microscope directly after sectioning to determine whether blood vessel-associated labeling was present. (2) The remaining sections were immunocytochemically processed for visualization of RDA to study blood vessel-associated staining.

Cross reactivity and aspecificity of antibodies. Sections obtained from brains that received injections of all three tracers were incubated according to the single-, double- and triple-staining protocols. By comparison, this provided the conditions to examine the specificity of primary and secondary antibodies used.

Tracers and antisera. PHA-L was obtained from Vector (Burlingame, CA, USA), RDA and BDA from Molecular Probes (Eugene, OR, USA). Goat anti-PHA-L and the ABC kit were obtained from Sigma (St. Louis, MO, USA). Rabbit anti-TRITC was purchased from Nuclilabs (Ede, Netherlands), and secondary and tertiary antisera from Nordic Immunology (Tilburg, Netherlands).

RESULTS

Tracer characteristics, as compared in single-stained sections. The single-staining procedure with DAB-Ni as chromogen, resulting for all three tracers in a crisp image of the labeled fiber systems, provided a good condition for an accurate comparison.

Sites of injection. Application of PHA-L, RDA or BDA to RE or EC resulted in small and well defined injection sites (Fig. 1A-D). Usually, RDA yielded the smallest injection sites. Consequently, the array of RDA applications (distances between individual injections: 0.3 mm) in the EC showed distinguishable cores, whereas arrays of PHA-L- or BDA injections tended to merge into one large spot. With each of the tracers, individual neurons were difficult to distinguish inside the densely stained centers of the injection sites, whereas at the periphery of the spots individual labeled neurons were noticed, showing a detailed morphology resembling Golgi silver-impregnation.

Transport. Following uptake in the injection sites, PHA-L, RDA and BDA were primarily transported in the anterograde direction. Although, they appeared to be retrogradely transported to various degrees as well. Retrograde transport of PHA-L was noticed only in case of injections in RE (Fig. 1D), which always resulted in the labeling of a small group

of neurons at the border of the zona incerta and the reticular thalamic nucleus (Fig. 1E). In this area anterogradely labeled, thin fibers surrounded the retrogradely PHA-L-labeled neurons. Following application of RDA, and in particular of BDA, we found retrogradely labeled cells in several regions known to project to the site of injection. As illustrated in Fig. 1F, the cell body and primary dendrites of retrogradely RDA-labeled neurons showed a granular appearance. Usually, retrogradely BDA-labeled cells displayed a solid filling, with appearances varying from densely labeled somata and primary dendrites to Golgi-like labeling (Fig. 1G). Only occasionally we did detect a granular type of labeling of BDA-positive neurons.

Sensitivity. Each of the three tracers PHA-L, RDA and BDA, displayed a similar, high degree of sensitivity. In the projection systems from both RE and EC, fibers of passage and fibers with en passant varicosities as well as with terminal boutons were excellently visualized (Fig. 2A-C).

Track labeling. In tracing studies it is desirable to minimize labeling along the injection track in order to avoid false positive labeling. For PHA-L, RDA and BDA we compared the occurrence of uptake by neurons or fibers of passage along the injection tracks. Injections were placed in RE by lowering the pipette through the septal pole of the hippocampus and dorsal thalamic nuclei. BDA, RDA and, occasionally, PHA-L injections resulted in comparable labeling of hippocampal cells that are known to project massively within the hippocampal formation (Swanson et al., 1981; Amaral and Witter, 1989). Indeed, labeling of hippocampal projection fibers was observed for BDA and RDA, but was absent for PHA-L. Examples of inadvertant hippocampal labeling by PHA-L, RDA and BDA are illustrated in Fig. 3A-C. In contrast to these hippocampal cells, almost no neurons were labeled along the tract through the thalamus. Injections placed in the EC required a long penetration through the overlying cortex. In these cases, we noticed a remarkable difference in the morphological appearance of track labeling by BDA and RDA. Whereas BDA-labeled neurons appeared in a Golgi-like fashion (Fig. 4A), RDA-labeled neurons (Fig. 4B) showed a granular-type of staining, primarily of the soma and primary dendrites. Examples of the most serious cases of such track labeling in the neocortex are documented in Fig. 4A,B. In this study, distinctive uptake of tracer by fibers of passage occurred in one case, in which a BDA injection in the EC was made by lowering the pipette through the alveus. This resulted in extensive labeling of pyramidal cells in the hippocampus (not illustrated). In general, track labeling was difficult to avoid using BDA. Neither reversal of current during penetration and withdrawl of the pipette, nor leaving the pipette in situ for at least 10 minutes after injection could reliably solve this problem.

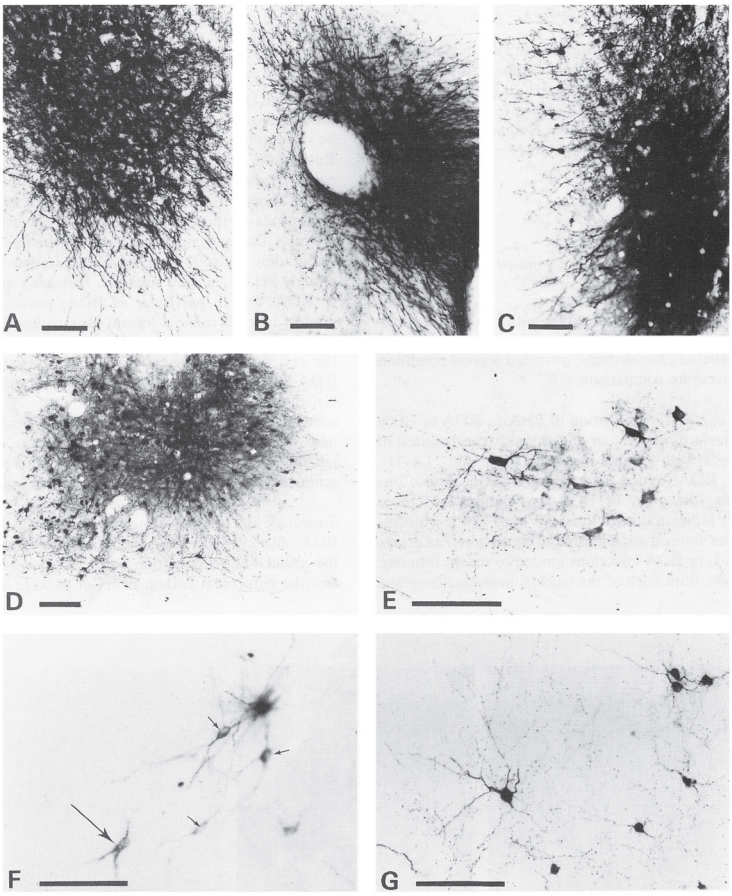

Fig. 1. Photomicrographs illustrating representative injection sites in the entorhinal cortex and nucleus reuniens thalami, and the appearance of retrograde labeling following these injections. A-C. PHA-L (A), RDA (B) and BDA (C) injection sites in the entorhinal cortex, revealing densely stained cores. At the periphery of the injection sites PHA-L-, RDA- and BDA-labeled neurons show a similar, detailed morphology. D. PHA-L injection in the nucleus reuniens, and (E) the subsequent retrograde labeling of a small group of neurons in the zona incerta/reticular thalamic nucleus, surrounded by anterogradely labeled fibers. F. Retrogradely RDA-labeled neuron (large arrow) in the horizontal limb of the diagonal band of Broca, following a RDA injection in the entorhinal cortex. This cell contains many RDA granules in the soma and primary dendrites. The small arrows mark cells that show a non-granular staining. These latter cells are occasionally found in the immediate vicinity of blood vessels throughout the brain, and represent one aspect of blood vessel-associated staining noticed in anti-TRITC-reacted sections. G. Retrogradely BDA-labeled neurons, displaying a solid filling. These cells in the subiculum are labeled following a BDA injection in the entorhinal cortex. Numerous anterogradely labeled entorhinal projection fibers course through the area. Bars: 100 μm.

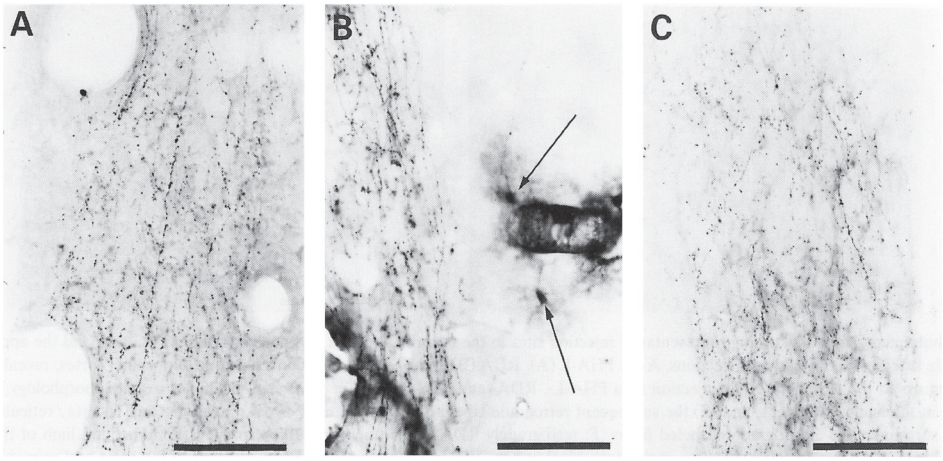

Fig. 2. Photomicrographs showing that with each tracer a detailed visualization (DAB-Ni staining) of anterogradely labeled projection fibers is obtained. All micrographs are taken in the CA1 region, after a PHA-L injection in the nucleus reuniens (A), and RDA- (B) and BDA injections (C) in the entorhinal cortex. In B the DAB-Ni staining of RDA reveals staining of vascular walls and closely associated cells with many thin, extremely arborizing processes (arrows). Bars:100 μm.

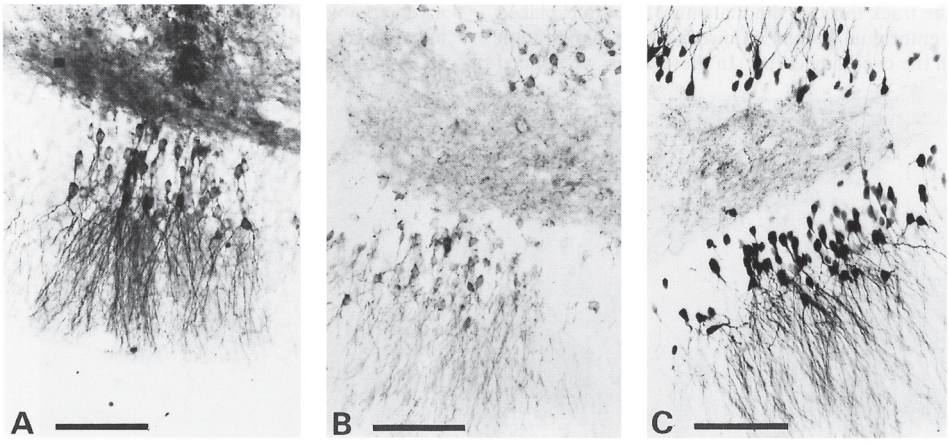

Fig. 3. Photomicrographs illustrating the labeling of cells alongside the pipette track through the septal pole of the hippocampus, following PHA-L (A), RDA (B) and BDA (C) injections in the nucleus reuniens. Although the extent of tracer uptake appears comparable in these instances, labeling of hippocampal projection fibers was observed only in case of RDA and BDA injections. Bars: 100 μm.

Non-neuronal labeling. Besides a specific neuronal uptake, both intracerebrally injected dextran amines were frequently found to be incorporated by perivascular cells. These cells, representing a particular class of brain macrophages in the vascular basal membrane (Graeber et al., 1989), as well as numerous meningeal macrophages, contained large BDA- and RDA-positive granules. Generally, BDA-labeled perivascular cells were less numerous than RDA-labeled ones, and more confined to areas near the injection site. RDA-labeled perivascular cells were found in blood vessels and meninges throughout large parts of the brain (Fig. 4C). RDA-labeling of perivascular cells was also investigated in fluorescence microscopy and compared with that in immunocytochemically stained sections. Very brightly fluorescing- and RDA-immunostained perivascular cells appeared distributed to a similar extent throughout the entire brain.

In contrast to intracerebrally injected RDA, intravenously administered RDA did not produce perivascular cell labeling. Brain sections from the systemic control rat did not show any labeled perivascular cells, neither in immunocytochemical preperations, nor in those studied with fluorescence microscopy.

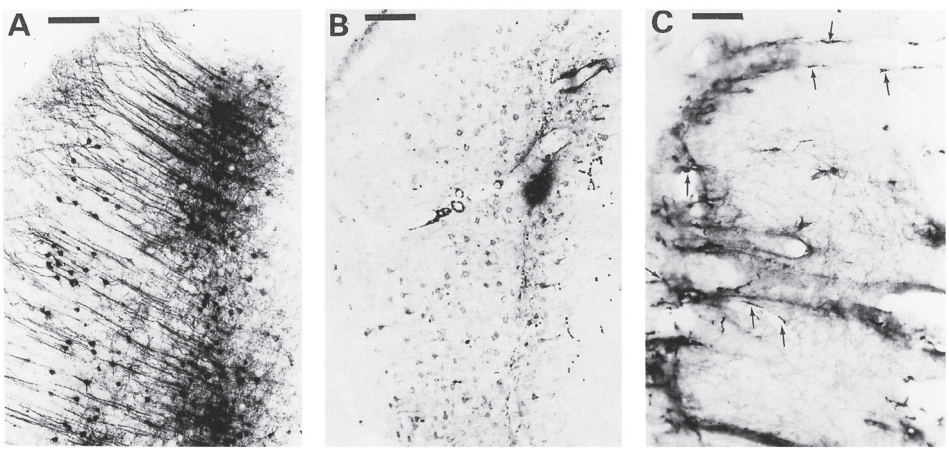

Fig. 4. Photomicrographs representing the most serious cases of track labeling in the neocortex caused by BDA (A) and RDA (B). A large contrast can be noticed between the morphology of the BDA- and RDA-labeled neurons. C. Non-neuronal uptake of dextran conjugates, as illustrated in an example of RDA-staining of perivascular cells in vascular walls and meningeal macropha-ges (arrows) in the subicular area, following a RDA injection in the entorhinal cortex. These cells contain many large RDA-positive granules. Bars: 100 μm.

Blood vessel-associated staining in RDA immunocytochemistry. Next to perivascular cell labeling by RDA, we noted a phenomenon that further will be refered to as “blood vessel-associated staining”. This peculiar phenomenon was characterized by the staining

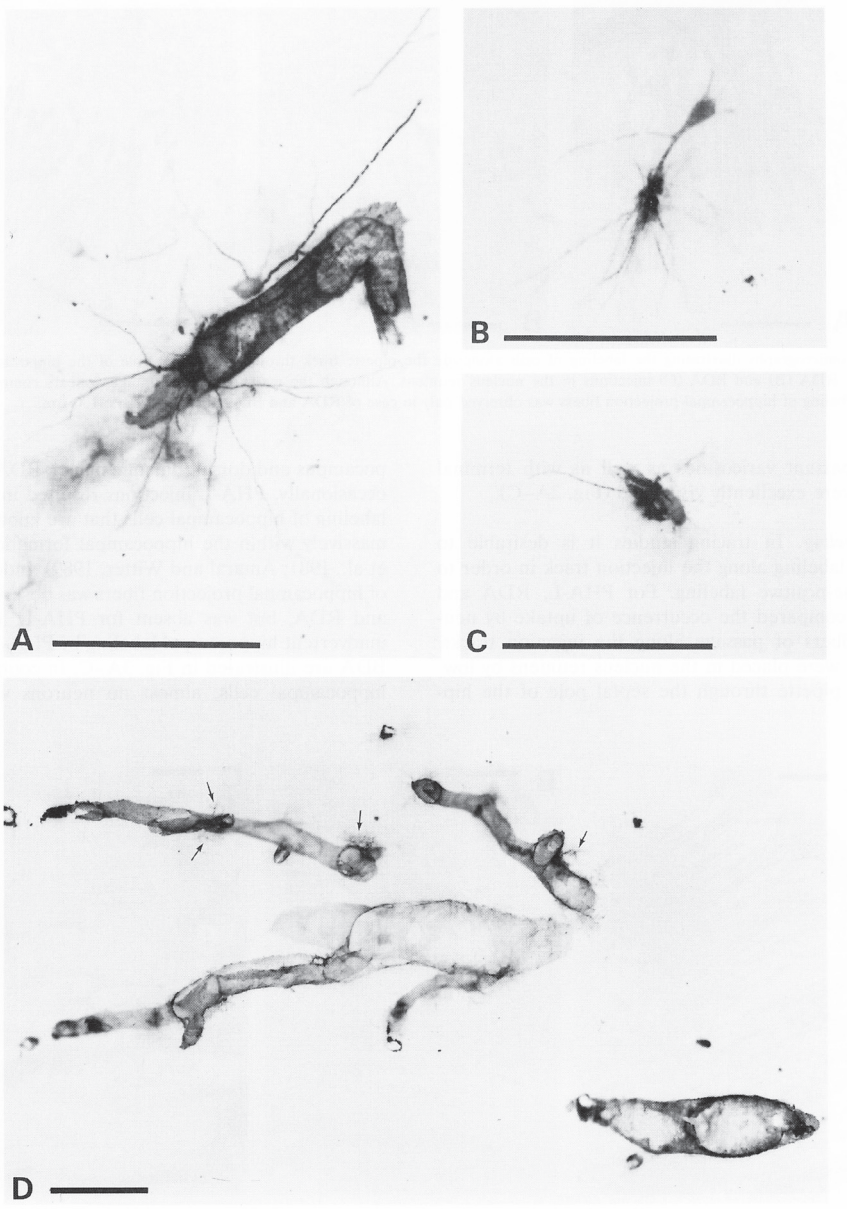

Fig. 5. Blood vessel-associated staining in RDA-immunoreacted sections. A. Section from a rat brain with an intracerebral RDA injection. Employing the DAB-Ni staining for the immunocytochemical visualization of RDA, cells with long, smooth processes are found closely associated with blood vessels that usually display staining of their walls. The same phenomenon occurs in anti-TRITC-reacted, DAB-Ni stained sections from rat brain after intraveneous administration of RDA (B), and in blank control sections (C,D). Bars: 100 µm.

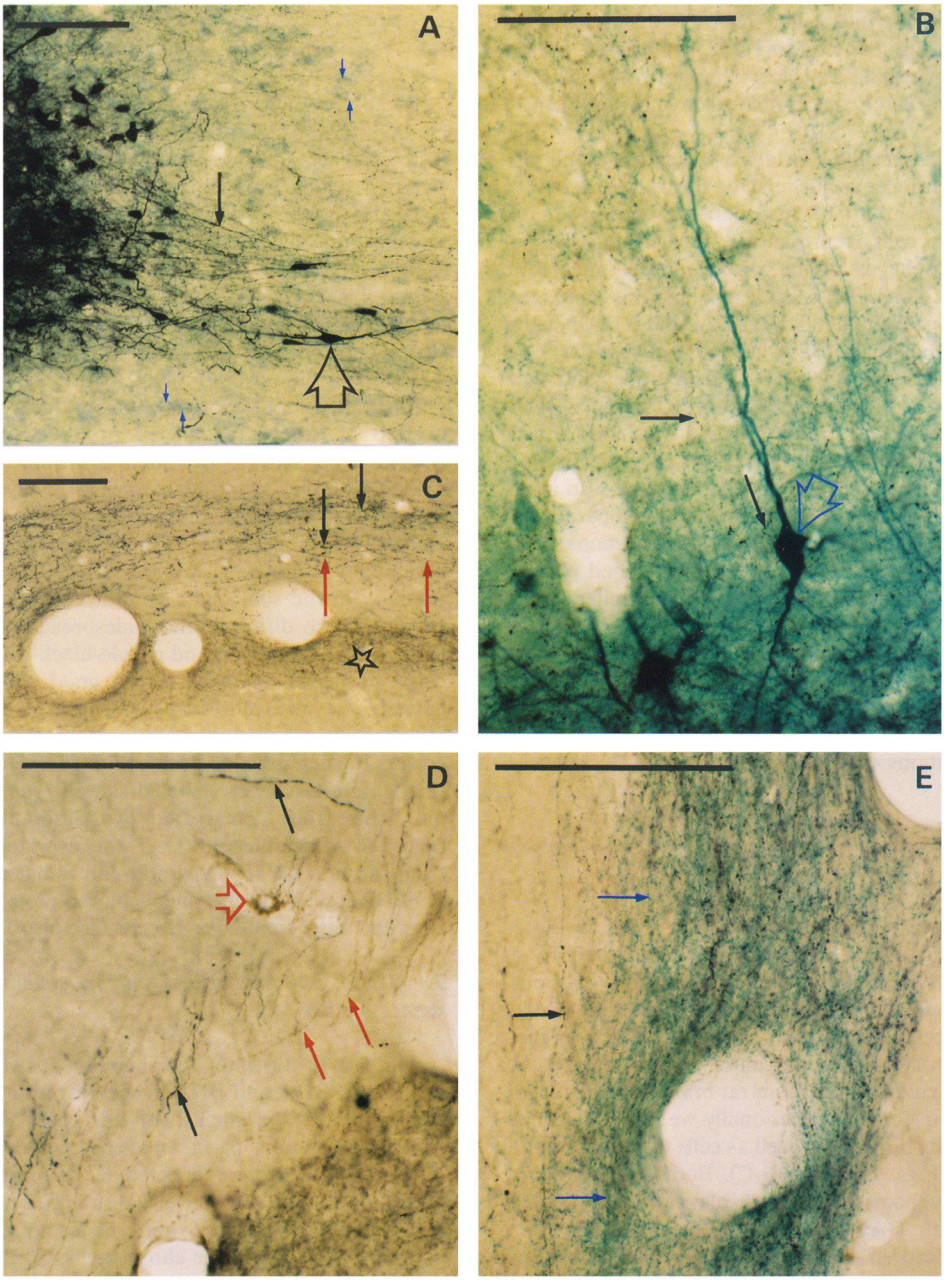
A
B
C
D
E

⇦ Fig. 6. Photomicrographs illustrating the triple labeling of fiber systems in the hippocampal formation following a PHA-L injection in the nucleus reuniens, and RDA and BDA injections in right and left entorhinal cortex respectively. PHA-L is visualized with DAB-Ni (black: black arrows), RDA with DAB (brown: red arrows) and BDA with 1-naphthol/Azur B (blue-green: blue arrows). A. (PHA-L injection site) The DAB-Ni staining yields a deep black, crisp image of labeled neurons (open black arrow), their dendrites and axons. The light-blue cell bodies (small blue arrows) result from the staining with Azur B (final step of the triple-staining procedure). B. High power micrograph of a neuron (open blue arrow) in the periphery of the BDA injection site in the entorhinal cortex, stained with 1-naphthol/Azur B. Thin, black colored reuniens fibers (black arrows) are also noticeable. C. (CA1 region of the right hippocampus) Overlap of black reuniens fibers (black arrows) and brown, RDA-labeled entorhinal projection fibers (red arrows). Brown colored perforant pathway fibers in the dentate gyrus (asterics) are also visualized. D. In less densely innervated areas than shown in C, brown and black colored fibers can be more easily distinguished. The open red arrow marks a RDA-labeled perivascular cell containing large granules. E. (CA1 region in the left hippocampus) Black reuniens fibers (black arrow) and blue-green entorhinal fibers (blue arrows) are excellently visualized. Bars: 100 μm.

of vascular walls and cellular structures, presumably glia in their immediate vicinity, and was initially detected in RDA-immunoreacted sections from rat brains with intracerebral RDA injections. Occasionally we found richly arborizing cells (Fig. 2B) as well as cells with long, smooth processes (Figs. 1 F and 5A-C). Both cell types were found throughout the brain, displaying a non-granular staining with DAB-Ni as chromogen, but they were hardly noticed in DAB stained sections. The blood vessel-associated staining was not observed as labeling in fluorescence microscopy. The difference between immunocytochemistry and fluorescence microscopy was also present in sections from the two control rats. RDA-immunoreacted sections from the systemically injected rat (Fig. 5B) and sections from the blank control rat (Fig. 5C,D), both stained with DAB-Ni, displayed the same phenomenon as described above, but again no fluorescence of blood vessels or cellular structures was noted.

Tracer detectability in double-stained sections. In all immunoreacted sections, double-stained according the procedures summarized in Table 2B, well distinguisable purple-black (DAB-Ni) and brown (DAB) reaction products were precipitated in labeled cells and in the projection fibers. However, for the visualization of RDA in combination with PHA-L we preferred to stain RDA with DAB as chromogen. Using the DAB procedure the presence of RDA-labeled perivascular cells was less obvious and blood vessel-associated staining was hardly noticed.

Despite the overall good distinction between purple-black and brown reaction products, the actual overlap of differently labeled projection systems in field CA1 of the

hippocampus was in some cases hard to establish, due to the high concentration of fibers in the relatively restricted area of the stratum lacunosum moleculare. In these cases the purple-black DAB-Ni precipitate dominated over the brown DAB reaction product. In the subiculum, in which both systems distributed more diffusely and widespread than in field CA1, individual brown and purple-black colored fibers could be better distinguished. A good differentiation between the two colors was noted in experiments with injections which included layer II of the entorhinal cortex. In such cases the projection fibers to CA3 and the dentate gyrus were labeled as well. The hippocampal fissure thus demarcated two differently colored fields: in subiculum and CA1 the overlapping fibers from the RE and EC, and in the dentate gyrus the single colored projection fibers from the entorhinal layer II cells (see also Fig. 6C).

Tracer detectability and staining stability in triple-stained sections. Fig. 6A-E illustrates the simultaneous visualization of PHA-L, RDA and BDA in sections from one of the triple-tracing experiments. In this case, PHA-L was injected bilaterally in RE, whereas RDA and BDA were injected in the right and left EC, respectively. Visualization of PHA-L, RDA and BDA in one and the same section was accomplished using three chromogens: 1) PHA-L with DAB-Ni, 2) RDA with DAB and 3) BDA with 1-naphthol/Azur B. In triple-stained sections the DAB-Ni product turned out deep black, instead of the common purple-black color. The DAB precipitate displayed a brown color, slightly different from that obtained in single- or double-staining procedures, yet clearly distinguishable from the DAB-Ni product. The 1-naphthol/Azur B complex displayed a distinctive blue-green color. In RE (Fig. 6A) black colored neurons were excellently visible, the right EC displayed brown colored cells and the left EC blue-green colored neurons (Fig. 6B). In the right hippocampus (Fig. 6C) we detected brown and black stained overlapping fibers from the right EC and RE, respectively. In this experiment, the dentate gyrus displayed brown colored projection fibers as well. The brown and black colors were easily distinguishable in less densely innervated areas, as shown in Fig. 6D. In the left hippocampus (Fig. 6E) an overlap of blue-green labeled fibers from the left EC with black labeled fibers from RE was noticed. The differentiation between the two fiber systems, particularly in areas with a high degree of overlap as in field CA1, was more easy in case of the blue-green/black staining combination than in the brown/black combination.

The crisp image of the DAB-Ni stained cells and their projection fibers was excellently preserved during the triple-staining procedure, and appeared even more distinctive by the deep black color. Both DAB and 1-naphthol/Azur B stained cells and fibers showed a slightly less crisp image, yet sufficient morphological detail was appreciable. The normally excellent stability of the DAB-Ni and DAB reaction products was unaffected by the additional 1-naphthol/Azur B staining procedure. The blue-green reaction product

of the latter procedure, however, appeared to be sensitive to light, resulting eventually in a gradual fading of the labeling. This problem was easily overcome by storage of 1-naphthol/Azur B stained sections in the dark, preferably in a freezer at -20 ºC to -40 ºC.

Background staining in triple-stained sections. The overall background level was remarkably low in triple-stained sections, and showed only a slight increase in comparison with the level of background staining in single- and double-stained (DAB-Ni/DAB) sections. Incubation with Azur B was accompanied with a blue counterstaining, which contributed also to the background level. This counterstaining could be reduced such that only a pale blue coloring of cell bodies remained. These counterstained cell bodies were easy to distinguish from blue-green labeled neurons. Thus, specific staining and counterstaining could be obtained in one and the same step, allowing for the detection of cytoarchitectonic boundaries.

Cross-reactivity. The only cross-reaction occurred between the anti-TRITC antibody and BDA. When incubated with anti-TRITC we noticed in the BDA injection sites a pale, somewhat granular staining of cell bodies and occasionally of a few fibers, presumably parts of dendrites. However, this cross-reactivity appeared to be confined to the BDA injection sites. In sections containing BDA as well as RDA that were immunoreacted with anti-TRITC, we did not observe a staining of BDA-labeled projection fibers. This observation was confirmed in anti-TRITC-immunoreacted sections, containing only BDA.

DISCUSSION

The direct comparison of PHA-L-, RDA- and BDA-labeled structures reveals that each tracer is an equally sensitive, primarily in anterograde direction transported tracer. These observations are in agreement with previous reports (e.a. Gerfen and Sawchenko, 1984; Schmued et al., 1990; Veenman et al., 1992). Moreover, in the present study we have clearly demonstrated that PHA-L, RDA and BDA are highly compatible and can thus be used in multiple anterograde tracing studies. The possibility of simultaneous and permanent visualization of these three tracers by a triple-staining procedure makes such an approach even more attractive.

Uptake and transport characteristics.
From our direct comparison between the amount of PHA-L-, RDA- and BDA-retrogradely labeled cells, we conclude that the occurrence and intensity of bidirectional transport is

highest for the dextran conjugates (Schmued et al., 1990; Wouterlood and Groenewegen, 1991; Veenman et al., 1992). Neither BDA nor RDA, however, can be considered appropriate retrograde tracers.

A common point of concern in tracing studies is uptake of tracer by neurons alongside the injection track or uptake by fibers of passage. In this study, all three tracers demonstrated track labeling, however, to varying degrees and with different consequences. For instance, especially hippocampal cells appeared very sensitive to tracer leakage and displayed a similar extent of uptake of PHA-L, RDA or BDA. Despite this similarity in uptake, labeling of hippocampal projection fibers occurred in cases of RDA- and BDA-, but was absent following PHA-L track labeling. These observations reveal that, especially in cases of RDA and BDA, the presence of anterogradely labeled fibers in a particular brain area does not necessarily imply that they originate from the actually injected structure. Although these differences in transport characteristics between PHA-L and the dextran amines cannot be adequately explained, they emphasize the need for cautious interpretations since "truly" labeled projection systems cannot be discriminated from "falsely" labeled systems. Uptake by (damaged) fibers of passage has been reported for all three tracers used in the present study (Cliffer and Giesler, 1988; Schofield, 1989; Schmued et al., 1990; Nance and Burns, 1990; Brandt and Apkarian 1992). In our study this phenomenon was noticed only once, following a BDA injection that passed through the alveus. From other experiments in our laboratory we know that indeed BDA, far more than RDA or PHA-L, is readily taken up by fibers of passage whenever the tracer is injected in a large fiber bundle.

Except for the specific neuronal uptake of all three tracers at the site of injection, BDA and especially RDA are readily incorporated by perivascular cells. This property of the dextran conjugates has also been described by others (Schmued et al., 1990; Nance and Burns, 1990; Wouterlood and Jorritsma-Byham, 1993). Yet, this feature does not disturb the detectability of labeled neuronal structures since perivascular cells, based on their morphology and specific localization, are easily recognized as non-neuronal elements.

RDA immunostaining.

The use of the anti-TRITC antibody provided the opportunity to demonstrate that the fluorescent tracer RDA is as sensitive as PHA-L and BDA, and that RDA immunostaining is as good and reliable as PHA-L- and BDA immunostaining. However, two less desirable properties of anti-TRITC should be mentioned: 1) a minor cross-reaction with BDA, and 2) blood vessel-associated staining. The cross-reactivity of anti-TRITC was restricted to a pale labeling of cell bodies at the site of BDA application, leaving projection fibers unlabeled. Thus, false positive staining of BDA-labeled projection systems is not likely to occur in RDA immunocytochemistry. With respect to the blood vessel-associated

staining, this was noticed in RDA-immunoreacted brain sections after intracerebral RDA injection, and in sections of control animals, either systemically injected or non-injected. These results indicate that the anti-TRITC antibody recognizes an endogenous antigen present in a particular class of glial cells, associated with blood vessels. Since the blood vessel-associated staining does not interfere with the detection of specifically labeled fiber systems, and is hardly noticed employing DAB instead of DAB-Ni as chromogen, we consider it appropriate to use anti-TRITC for the permanent visualization of RDA.

Tracer detectability in multiple-stained sections.

Although the level of background staining slightly increases with each additional staining procedure, the level is still remarkably low in triple-stained sections. Thus, this triple-staining procedure results in an excellent detectability of brown (DAB), black (DAB-Ni) and blue-green (1-naphthol/Azur B) labeled cells of origin and their projection fibers. The distinction between brown and purple-black colored fibers appears to be rather difficult in areas showing a high degree of overlap of projections. In such cases the distinction between black and blue-green colored fibers is much more clearcut and thus, for densely overlapping fiber systems, a combination of DAB-Ni and 1-naphthol/Azur B staining is preferable over a combination of DAB and DAB-Ni. In previous experiments, using DAB in combination with 1-naphthol/Azur B (unpublished results) the distinction between the brown and blue-green label was also very good. The sensitivity to light of the 1-naphthol/Azur B complex is considered a minor, yet solvable disadvantage. Moreover, in case of eventual fading of the blue-green complex, the labeling can be restored by a repeated incubation with the basic dye (Mauro et al., 1985).

In conclusion, the combination of the sensitive anterograde tracers PHA-L, RDA and BDA, and the possibility of permanent simultaneous visualization with DAB-Ni, DAB and 1-naphthol/Azur B as chromogens, offers a very powerful approach for triple anterograde tracing experiments.

REFERENCES

Amaral, D.G. and Witter, M.P. (1989) The three-dimensional organization of the hippocampal formation: a review of anatomical data. Neurosci., 31: 571-591.

Antal, M., Freund, T.F., Somogyi, P. and McIlhenney, R.A.J. (1990) Simultaneous anterograde labelling of two afferent pathways to the same target area with Phaseolus vulgaris-leucoagglutinin and Phaseolus vulgaris-leucoagglutinin conjugated to biotin or dinitrophenol. J. Chem. Neuroanat., 3: 1-9.

Brandt, H.M. and Apkarian, A.V. (1992) Biotin-dextran: a sensitive anterograde tracer for

neuroanatomic studies in rat and monkey. J. Neurosci. Meth., 45: 35-40.

Castellano, B., Gonzalez, B., Jensen, M.B., Pedersen, E.B., Finsen, B.R. and Zimmer, J. (1991) A double staining technique for simultaneous demonstration of astrocytes and microglia in brain sections and astroglial cell cultures. J. Histochem. Cytochem., 39: 561-568.

Chang, H.T. (1991) Anterograde transport of Lucifer yellow-dextran conjugate. Brain Res. Bull., 26: 813-816.

Chang, H.T. (1993) Immunoperoxidase labeling of the anterograde tracer Fluoro-Ruby (tetramethylrhodamine-dextran amine conjugate). Brain Res. Bull., 30: 115-118.

Cliffer, K.D. and Giesler, G.J.Jr. (1988) PHA-L can be transported anterogradely through fibers of passage. Brain Res., 458: 185-191.

Cowan, W.M., Gottlieb, D.I., Hendrickson, A.E., Price, J.C. and Woolsey, T.A. (1972) The autoradiographic demonstration of axonal connections in the central nervous system. Brain Res., 37: 21-51.

Gerfen, C.R. (1985) The neostriatal mosaic. I. Compartmental organization of projections from the striatum to the substantia nigra in the rat. J. Comp. Neurol., 236: 454-476.

Gerfen, C.R. and Sawchenko, P.E. (1984) An anterograde neuroanatomical tracing method that shows the detailed morphology of neurons, their axons and terminals: Immunohistochemical localization of an axonally transported plant lectin, Phaseolus vulgaris-leucoagglutinin. Brain Res., 290: 219-238.

Glover, J.C., Petursdottir, G. and Jansen, K.S. (1986) Fluorescent dextran-amines used as axonal tracers in the nervous system of the chicken embryo. J. Neurosci. Meth., 18: 243-254.

Graeber, M.B., Streit, W.J. and Kreutzberg G.W. (1989) Identity of ED2-positive perivascular cells in rat brain. J. Neurosci. Res., 22: 103-106.

Herkenham, M. (1978) The connections of the nucleus reuniens thalami: evidence for a direct thalamo-hippocampal pathway in the rat. J. Comp. Neurol., 177: 589-610.

Izzo, P.N. (1990) A note on the use of biocytin in anterograde tracing studies in the central nervous system: application at light and electron microscopic level. J. Neurosci. Meth., 36: 155-166.

King, M.A., Louis, P.M., Hunter,B.E. and Walker, D.W. (1989) Biocytin: a versatile anterograde neuroanatomical tract-tracing alternative. Brain Res., 498: 361-367.

Lapper, S.R. and Bolam, J.P. (1991) The anterograde and retrograde transport of neurobiotin in the central nervous system of the rat: comparison with biocytin. J. Neurosci. Meth., 39: 163-174.

Mauro, A., Germano, I., Giaccone, G., Giordana, M.T. and Schiffer, D. (1985) 1-Naphthol basic dye (1-NBD), an alternative to diaminobenzidine (DAB) in immunoperoxidase techniques. Histochem., 83: 97-102.

Mesulam, M-M. (1982) Tracing neuronal connections with horseradish peroxidase. John Wiley, New York.

Nance, D.M. and Burns, J. (1990) Fluorescent dextran as sensitive anterograde neuroanatomical tracers: applications and pittfalls. Brain Res. Bull., 25: 139-145.

Paxinos, G. and Watson, C. (1986) The rat brain in stereotaxic coordinates. 2nd edition, Academic Press, Sydney, Australia.

Reiner, A., Veenman, C.L. and Honig, M.G. (1993) Anterograde tracing using biotinylated dextran amine. Neurosci. Protocols, 93-050-14-01-14.

Schmued, L., Kyriakidis, K. and Heimer, L. (1990) In vivo anterograde and retrograde axonal transport of the fluorescent rhodamine-dextran-amine, Fluoro-Ruby within the CNS. Brain Res., 526: 127-134.

Schofield, B.R. (1989) Labeling of axons of passage by Phaseolus vulgaris leucoagglutinin (PHA-L). Soc. Neurosci. Abstr., 15: 306.

Smith, Y. and Bolam, J.P. (1991) Convergence of synaptic inputs from the striatum and the globus pallidus onto identified nigrocollicular cells in the rat: a double anterograde labelling study. Neurosci., 44: 45-73.

Sternberger, L.A. (1979) Immunocytochemistry. 2nd ed. John Wiley, New York: pp 1-354.

Swanson, L.W., Sawchenko, P.E. and Cowan, W.M. (1981) Evidence for collateral projections by neurons in Ammons horn, the dentate gyrus, and the subiculum: a multiple retrograde labelling study in the rat. J. Neurosci., 1: 548-559.

Trojanowski, J.Q., Gonatas, J.O. and Gonatas, N.K. (1981) Conjugates of horseradish peroxidase (HRP) with cholera toxin and wheat germ agglutinin are superior to free HRP as orthogradely transported markers. Brain Res., 223: 381-385.

Veenman, C.L., Reiner, A. and Honig, M.G. (1992) Biotinylated-dextran amine as an anterograde tracer for single- and double labeling studies. J. Neurosci. Meth., 41: 239-254.

Wan, X.C.S., Trojanowski, J.Q. and Gonatas, J.O. (1982) Cholera toxin and wheat germ agglutinin conjugates as neuroanatomical probes: their uptake and clearance, transganglionic and retrograde transport and sensitivity. Brain Res., 243: 215-224.

Witter, M.P. and Groenewegen, H.J. (1986) Connections of the parahippocampal cortex in the cat. III. Cortical and thalamic efferents. J. Comp. Neurol., 252: 1-31.

Witter, M.P., Groenewegen, H.J., Lopes da Silva, F.H. and Lohman, A.H.M. (1989) Functional organization of the extrinsic and intrinsic circuitry of the parahippocampal region. Prog. Neurobiol., 33: 161-253.

Wouterlood, F.G., Saldana, E. and Witter, M.P. (1990) Projections from the nucleus reuniens thalami to the hippocampal region: light and electron microscopic tracing study in the rat with the anterograde tracer Phaseolus vulgaris leucoagglutinin. J. Comp. Neurol., 296: 179-203.

Wouterlood, F.G. and Groenewegen, H.J. (1991) The Phaseolus vulgaris leucoagglutinin tracing technique for the study of neuronal connections. Prog. Histochem. Cytochem., 22: 1-75.

Wouterlood, F.G. and Jorritsma-Byham, B. (1993) The anterograde neuroanatomical tracer biotinylated dextran-amine: comparison with the tracer PHA-L in preparations for electron microscopy. J. Neurosci. Meth., 48: 75-87.

Chapter 4

NUCLEUS REUNIENS THALAMI MODULATES ACTIVITY IN HIPPOCAMPAL FIELD CA1 THROUGH EXCITATORY AND INHIBITORY MECHANISMS.

J Neurosci (1997) 17:5640-5650

ABSTRACT

The nucleus reuniens thalami (RE) originates dense projections to CA1, forming asymmetrical synapses on spines (50%) and dendrites (50%). The hypothesis that RE input modulates transmission in CA1 through excitation of both pyramidal cells and interneurons was tested using electrophysiological methods in the anesthetized rat. The RE–CA1 afferents were selectively stimulated at their origin; evoked field potentials and unit activity were recorded in CA1. RE-evoked depth profiles showed a prominent negative deflection in the stratum lacunosum-moleculare and a positive one in the stratum radiatum. The lacunosum-moleculare sink–radiatum source configuration is compatible with RE-elicited depolarization of apical dendrites of pyramidal cells. Despite a consistent and robust paired pulse facilitation of RE-evoked field potentials, population spikes in the stratum pyramidale were not detected at any tested condition. This indicates the inability of RE–CA1 input to discharge pyramidal cells. However, stimulation of RE elicited spiking of extracellularly recorded units in strata oriens/alveus and distal radiatum, indicative of the activation of local interneurons. Thus, RE seems to modulate transmission in CA1 through a (subthreshold) depolarization of pyramidal cells and a suprahreshold excitation of putative inhibitory oriens/alveus and radiatum interneurons.
RE-evoked monosynaptic or disynaptic field potentials were associated with stimulation of rostral or caudal RE, respectively. Anatomically, a projection from caudal to rostral RE was demonstrated that can account for the disynaptic RE–CA1 input. Because caudal RE receives input from the hippocampus via the subiculum, we propose the existence of a closed RE–hippocampal circuit that allows RE to modulate the activity in CA1, depending on hippocampal output.

INTRODUCTION

The involvement of thalamic midline nuclei in early stages of Alzheimer's disease (Braak and Braak, 1991, 1992) and in diencephalic amnesia (Rousseau, 1994) has recently drawn attention to the connectivity between the nucleus reuniens (RE) and structures of the medial temporal lobe (Herkenham, 1978; Wouterlood et al., 1990; Dolleman-van der Weel and Witter, 1996). In this study we focused on the RE projection to hippocampal field CA1, a crucial structure for learning and memory processes (Squire, 1992).

A few investigators have studied the contribution of RE to hippocampal functioning. Vanderwolf et al. (1985) examined whether the medial thalamic nuclei, including RE, were involved in generating hippocampal atropine-resistant theta rhythm. Their extensive radiofrequency lesions, however, resulted in little or no effect on this type of rhythmical activity. Hirayasu and Wada (1992a,b) injected NMDA in the thalamic midline of the rat. When NMDA was administered to RE, it caused tonic and/or clonic generalized convulsions associated with temporal limbic EEG seizure discharge. They proposed that RE participates in the modulation of temporal limbic excitability and seizure development. Their findings suggest that RE influences the state of activity of the entorhinal–hippocampal circuit. Yet, basic electrophysiological knowledge of RE is still lacking. A modulatory role for RE in normal functioning of the hippocampus has also been suggested based on anatomical data (Wouterlood et al., 1990; Dolleman-van der Weel and Witter, 1996). Within field CA1, RE fibers terminate in a dense laminar plexus confined to the stratum lacunosum-moleculare (L-M) and form exclusively asymmetrical (i.e., excitatory) synapses on spines (50%) and dendrites (50%) (Wouterlood et al., 1990). These data indicate that RE fibers contact the spinous apical dendrites of pyramidal cells, as well as the largely aspinous dendrites of interneurons.

Based on the latter anatomical observations and the findings by Hirayasu and Wada (1992a,b), we proposed that RE modulates transmission in CA1 through activation of both pyramidal and nonpyramidal cells. This hypothesis was tested using electrophysiological methods to stimulate the RE–CA1 afferents selectively in anesthetized rats. RE–CA1 fibers course mainly within the inferior thalamic peduncle in a rostral direction, curve dorsally around the genu of the corpus callosum, and then run caudally via the cingulate bundle (in which many hippocampal afferents and efferents course) to enter CA1 (Wouterlood et al., 1990). Within their terminal field in stratum L-M, RE axons overlap with the perforant path fibers from the entorhinal cortex (Herkenham, 1978; Wouterlood et al., 1990; Dolleman-van der Weel et al., 1994). Thus, stimulation of RE–CA1 fibers neither in the cingulate bundle nor within their terminal field in stratum L-M can provide the selectivity required. Therefore, the RE neurons had to be stimulated at their origin, and depth profiles of evoked field potentials and recordings of unit activity

were performed in CA1. Our electrophysiological observations indicated the occurrence of monosynaptic and disynaptic RE–CA1 input. To substantiate a possible intrinsic RE connectivity, which is likely to be involved in disynaptically evoked CA1 responses, a neuroanatomical tracing method was used.

MATERIALS AND METHODS

We used 30 male Wistar rats (Harlan CPB, Zeist, The Netherlands), weighing 275–375 gm. Under halothane anesthesia the trachea was intubated. The animal was then placed in a stereotaxic apparatus and throughout the experiment artificially ventilated by a mixture of O2 and N2O with 1% halothane. Body temperature was maintained using a heating pad. The skull was exposed, and two burr holes were made on the left side of the brain to accommodate placement of stimulating and recording electrodes in RE and CA1, respectively. Because the most dorsal (i.e., septal) part of CA1 is less densely innervated by RE fibers than the ventral (temporal) part (Wouterlood et al., 1990), recordings were made approximately at the level of the splenium of the corpus callosum, or slightly more caudal (see Fig. 1 A,B). Stereotaxic coordinates were derived from Paxinos and Watson (1986). They were zeroed at bregma (Br.), the midline of the sinus, and the cortical (dura) surface [stimulation electrode in RE at an angle of 15° in the coronal plane: Br., -1.80 mm; lateral (L), 2.0 mm; ventral (V), 7.0 mm; recording electrode in CA1: Br., -5.6 mm; L, 4.3 mm; V, 1.6 –3.1 mm, respectively]. To prevent the exposed brain tissue from drying, it was covered with warm paraffin oil.

Stimulation protocols and data acquisition. Electrical stimulation of RE was performed with the use of an electrode array of three stainless steel wires (diameter, 60 μm, insulated except the tip). They were glued together in a glass micropipette, with tips obliquely arranged to cover the rostrocaudal extent of the (unilateral) RE. Because this nucleus is very small (~2 mm in length and ~0.6 mm in diameter) it can be easily mechanically damaged by electrode position adjustment. We therefore followed the strategy of placing the electrode array stereotaxically and fixing it in place. Stimulation was done between different pairs of the electrode array. As it turned out during the course of experiments, this strategy also allowed for a differential stimulation of either the entire rostrocaudal RE or of the rostral or caudal portion of the nucleus, separately. The standard stimulation protocol consisted of monopolar paired pulses. The first stimulus of a pair is referred to as the conditioning pulse, the second one as the test pulse. Both stimuli were of equal strength and duration [0.2 msec; interpulse interval (IPI), 100 msec, unless stated otherwise; intensity, 150 – 650 μA; 0.13 Hz]. Occasionally, trains of single pulses were

applied at different frequencies ranging from 0.13–10 Hz.
CA1 depth profiles of evoked extracellular field potentials were typically obtained using an array of six equally spaced metal electrodes (diameter, 60 μm, insulated except the tip; interelectrode distance, 250 μm). They were arranged in the same plane, glued in a glass micropipette, and then cut at an angle of 20 –30°. In this way we were able to record simultaneously, and along a track approximately perpendicular to the curved longitudinal axis of the hippocampus, the laminar responses across CA1, from the overlying deep cortical layers and white matter down to the hippocampal fissure (Fig. 1 A,B). Evoked field potentials were amplified and digitized by way of an interface (CED 1401 plus) connected to a personal computer. They were sampled at a rate of 5000/sec, averaged (n=32, unless stated otherwise), and stored for off-line analysis.
Unit activity was recorded using a glass electrode (15–30 MΩ, filled with 2% Pontamine sky blue in 0.5 M sodium acetate buffer) that could be gradually lowered by way of a remotely controlled hydraulic manipulator. The signal was amplified and bandpass-filtered (500 –3000 Hz). A window discriminator (WPI) was used to single out spike events, the output of which was fed to a digital port of the CED interface. Unit activity was stored as individual sweeps together with simultaneously recorded field potentials.

Off-line analysis. The characteristics of CA1 field potentials to RE stimulation were studied in laminar depth profiles. Response latencies were defined as the time from the onset of the stimulus artifact to the peak of the conditioning response. Because RE– CA1 afferents are known to form axospinous and axodendritic synapses (Wouterlood et al., 1990) (M. J. Dolleman-van der Weel and M. P. Witter, unpublished observations), latencies corresponding to a monosynaptic RE input were to be expected. Our latencies, however, turned out to vary over a large range of values. Therefore, we additionally examined whether early (likely monosynaptic) and late (presumed disynaptic) responses showed a relationship with differences in recording or stimulation sites. Based on histological analysis, we sorted the experiments with regard to: (1) the site of recording in septal-to-temporal CA1, and (2) the site of stimulation in rostral-to-caudal RE. Subsequently, experiments were sorted according to latencies (early vs late) and then with respect to recording and stimulation sites.
The application of paired stimuli provided the opportunity to study a particular form of short term plasticity, termed paired pulse facilitation (PPF). PPF was expressed numerically by the ratio between test response amplitude/conditioning response amplitude and was calculated for elicited field potentials at the synaptic level (stratum L-M).
Whether stimulation of RE was sufficient to discharge pyramidal cells and/or interneurons was further analyzed in extracellular recordings of unit activity throughout the depth of field CA1. The latency of synaptic unit activity was measured as the time from the

stimulus onset to the moment of occurrence of the spike. Simultaneously recorded field potentials were averaged to provide the corresponding population response.

Technical and theoretical considerations for current–source–density analysis. A one-dimensional current– source– density (CSD) analysis estimates the sites where currents flow into or out of the extracellular space during cellular activity (Freeman and Stone, 1969; Freeman and Nichol- son, 1975). Some theoretical and practical issues, however, have to be taken into account. First, the recording should be in the plane of maximal activation, i.e., corresponding to the orientation of the apical dendrites of pyramidal cells. In this way amplitude errors of calculated currents should be minimal. A second point of importance is the distance between consecutive recording electrodes. In our experiments 100 μm interval CSD profiles were recorded using a glass electrode or, alternatively, a specially constructed array of 18 metal electrodes (diameter, 60 μm, insulated except the tip). These stainless steel wires were tightly glued together in the same plane and then cut at an angle of 20 –30° (electrode heart-to-heart distance, 100 μm). This "knife-like" electrode array, not thicker than the diameter of the wires used, caused remarkably little damage. Moreover, its shape also met the criterion for recording perpendicular to the longitudinal axis of CA1.

Histological control. At the end of the experiment, under deep anesthesia, stainless steel electrodes were marked by lesions according to a procedure (three pulses of 1 mA anodal current) that results in a blue (because of the potassium ferrocyanide in the fixative; see below) spot in the brain tissue, occasionally with a hole in the center of the lesion. Glass micropipettes were marked by passing current (20 min, electrode as cathode) to eject Pontamine sky blue. The animal was then decapitated, and the brain was quickly removed and stored for 3 d in 4% paraformaldehyde and 0.05% glutaraldehyde in 0.1 M phosphate buffer with potassium ferrocyanide. The tissue was cryoprotected by immersion in 2% dimethylsulfoxide and 20% glycerin in phosphate buffer until equilibrium. On a freezing microtome the brain was cut in coronal sections (40 μm) that were Nissl-stained and used for verification of electrode placements.

Neuroanatomical anterograde tracing. In the course of this study, we observed monosynaptic and presumably disynaptic responses in CA1 after RE stimulation. In a previous anatomical study, Wouterlood et al. (1990) found that injections of the anterograde tracer Phaseolus vulgaris leucoagglutinin in caudal RE resulted in dense fiber labeling in rostral RE. Their findings suggest a connection from the caudal to the rostral portion of RE that may form the anatomical substrate for our electrophysiological observations. To specifically elucidate this issue, we performed additional anatomical

tracing experiments, using another five Wistar rats. The neuroanatomical tracer biotin-conjugated dextran amine (BDA; Molecular Probes, Eugene, OR) was used as described in detail elsewhere (Dolleman-van der Weel et al., 1994). Briefly, rats were deeply anesthetized with a 4:3 parts mixture of Aescoket (1% ketamine; Aesculaap BV, Boxtel, The Netherlands) and Rompun (2% xylazine; Bayer, Leverkussen, Germany) and then mounted in a stereotaxic frame. At coordinates derived from those of Paxinos and Watson (1986), BDA was iontophoretically applied (pulsed positive DC current for 10 min, 5– 6.5 μA, 7 sec on/7 sec off) to the caudal portion of RE. After 7–10 d of survival, the animals received an overdose of Nembutal (sodium pentobarbital; Ceva, Paris, France) and were transcardially perfused with 0.9% saline solution, followed by 4% paraformaldehyde and 0.05% glutaraldehyde in 0.1 M phosphate buffer, pH 7.4. The brain was removed from the skull, post-fixed for 1 hr, and then cryoprotected by immersion in 2% dimethylsulfoxide and 20% glycerin in phosphate buffer. On a freezing microtome, serial coronal sections (40 μm thick) were cut and were immunocytochemically processed for visualization of BDA using an avidin–biotin–peroxidase complex (Vectastain ABC kit; Vector Laboratories, Burlingame, CA). Following 1.5 hr of incubation with ABC solution, the sections were thoroughly rinsed and reacted with nickel-enhanced diaminobenzidine as a chromogen. BDA-stained sections were then mounted, Nissl-stained, dehydrated, and coverslipped with Entellan (Merck, Darmstadt, Germany).

RESULTS

Electrophysiological observations

CA1 field response to RE stimulation

In CA1 a consistent dipole field was recorded in response to stimulation of RE in vivo. In all cases, the depth profiles, recorded with either metal or glass electrodes, were characterized by a long latency, prominent negative-going deflection in the stratum L-M that reversed polarity at the border of strata L-M and radiatum and a positive-going one in the stratum radiatum up to the alveus (Fig. 1C–E). Whenever recording electrodes were lowered into the dentate gyrus, the negative deflection of the CA1 response showed a steady decline in amplitude (Fig. 1 D). This latter observation is in line with the anatomically demonstrated absence of RE projections to the dentate gyrus and field CA3 (Herkenham, 1978; Wouterlood et al., 1990; Dolleman-van der Weel and Witter, 1996). A similar fading of the positive deflection was noticed when recordings were made in the deep cortical layers overlying CA1. Occasionally, the depth profile had a more complex waveform as documented in Figure 1 E. In those cases, the CA1 responses

consisted of two consecutive deflections (i.e., an "early," usually smaller, and a "late," larger, potential; see below) in both conditioning and test response. Yet, irrespective of waveform complexity, a common feature of the laminar depth profiles was that the largest negative peaks occurred in the stratum L-M, close to the hippocampal fissure; the largest positive peaks (as a rule smaller in amplitude than the negative ones) were recorded in the stratum radiatum. We consistently observed that a population spike could not be induced, even when the stimulus intensity was increased from 100 to 650 μA, and the frequency was raised from 0.13 to 10 Hz. In fact, during stimulation at frequencies in the theta range, the peak of the field potential markedly declined, whereas the amplitude and duration of the decay phase became enhanced (data not illustrated).

CSD analysis

Laminar depth profiles (Fig. 2 A) for CSDs, obtained either by the use of a probe with 18 metal electrodes (electrode heart-to-heart distance, 100 μm) or by stepwise lowering of a glass electrode (100 μm interval) from the white matter down to the hippocampal fissure, revealed a well-defined sink at the level of the stratum L-M and a clear source in the stratum radiatum (Fig. 2 B). The source declined in amplitude toward the strata pyramidale and oriens. This sink– source configuration is compatible with the interpretation that RE input in the stratum L-M elicits a field EPSP (f EPSP) in the apical dendrites of pyramidal cells.

Paired pulse facilitation

The short term dynamic properties of the RE–CA1 projection were studied by analyzing evoked fEPSPs to double pulse stimulation of RE (fixed IPI, 100 msec; 0.13 Hz) at different stimulus intensities. PPF was quantified by the ratio between test/conditioning peak and calculated for responses recorded in the stratum L-M, representing the summed active RE–CA1 synaptic processes.

In general, the amplitude of the conditioning deflection was quite small at low (150 –300 μA) and moderate (350 – 450 μA) intensities but was better distinguishable at high stimulus intensity (500 – 650 μA). RE-induced PPF of fEPSPs was robust at low to high intensity stimuli (low intensity: mean PPF, 1.5 ± 0.2; n=7; moderate intensity: mean PPF, 2.1 ± 0.8; n=6; high intensity: mean PPF, 1.9 ± 0.8; n=18). We also examined PPF resulting from paired stimuli (high intensity, 0.13 Hz) at IPIs ranging from 20 to 200 msec. At 200 msec IPI, PPF was comparable to that elicited by stimuli at 100 msec IPI; at IPIs shorter than 100 msec, PPF was as robust as at 100 msec IPI or displayed a slight increase in magnitude. Paired pulse depression of the test deflection under the stimulus conditions used was not observed.

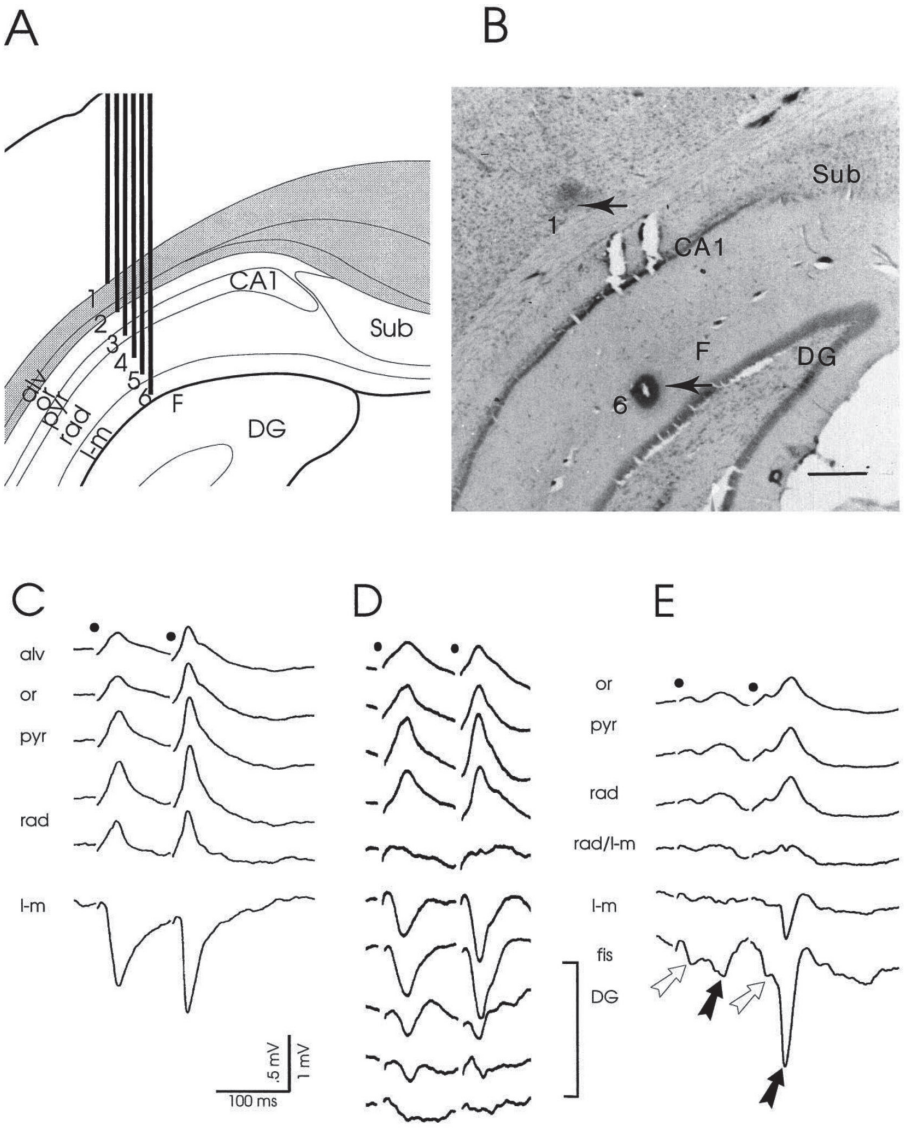
A
B
CA1
Sub
DG
F
1
2
3
4
5
6
alv
or
pyr
rad
l-m
Sub
CA1
DG
F
1
6
C
D
E
alv
or
pyr
rad
l-m
.5 mV
1 mV
100 ms
or
pyr
rad
rad/l-m
l-m
fis
DG

⇦ Fig. 1. A, B, Schematic representation of a six-channel recording probe and recording site in CA1. A, Depth profiles of the CA1 response to RE stimulation were simultaneously recorded using a probe consisting of six equally spaced metal electrodes (interelectrode distance, 250 μm). Generally, such an array of electrodes covered a track through the depth of CA1 from the alveus (alv) down to the hippocampal fissure (F). Sub, Subiculum; CA1, CA1 cell layer; or, stratum oriens; pyr, stratum pyramidale; rad, stratum radiatum; l-m, stratum lacunosum-moleculare; DG, dentate gyrus. B, Representative example of a CA1 recording site. Lesions (arrows) mark the positions of the most superficial (1) and deepest (6) electrodes in the white matter– deep cortical layer and at the fissure, respectively. Scale bar, 500 μm. C–E, Laminar CA1 field potentials to RE stimulation. C, Simultaneously recorded, typical CA1 profile evoked by paired pulse stimulation (high intensity stimuli; interpulse interval, 100 msec; 0.13 Hz) of the rostral part of RE. The dipole field consists of a prominent negative-going deflection at the synaptic level, i.e., in the stratum lacunosum-moleculare (l-m), and a positive-going deflection in strata radiatum (rad), pyramidale (pyr), and oriens (or) up to the alveus (alv). The markedly increased amplitude of the second field potential illustrates the commonly induced paired pulse facilitation. Notice also the absence of a population spike. D, Laminar CA1 responses recorded using a glass electrode that was lowered from the alveus down to the granular cell layer in the dentate gyrus (DG). The dipole field is similar to that recorded using a six-channel probe (see C). In addition, it is nicely shown that the polarity reverses at the border of strata radiatum/ lacunosum-moleculare (rad/l-m). When the electrode was lowered through the fissure (fis) into the dentate gyrus (DG), the negative deflection rapidly declined toward the granular cell level (bottom trace). E, Example of an occasionally recorded complex CA1 response, resulting from stimulation of the caudal part of RE. This CA1 dipole field displays a configuration similar to that of the profiles shown in C and D. However, early (open arrow) as well as late (black arrow) potentials are present in both conditioning and test response. The early field potentials in these complex responses are usually of small amplitude. Stimulation moments in C–E are indicated by dots.

Synaptic unit activity to RE stimulation

The consistent absence of a population spike in our CA1 profile indicated the probable paucity of pyramidal cell discharge to RE stimulation. Careful examination of all depth profiles revealed that stimulus-triggered spike events did occur, but only in two experiments. In both cases, however, the spikes were not detected at the pyramidal cell level; rather, they were superimposed on the fEPSPs recorded in the distal stratum radiatum in both conditioning and test response (Fig. 3A). Thus the radiatum spikes can be considered synaptically elicited in radiatum interneurons. The latencies of the radiatum spikes in these two experiments were remarkably similar (21 and 22 msec, respectively) and shorter than the latency of the fEPSP peak. In addition, we noticed that radiatum spikes were generated only after high intensity stimulation of RE and at low frequencies (range, 0.13–2 Hz; see Fig. 3B); they disappeared when we applied stimuli at frequencies in the theta range (5–10 Hz) but reappeared when stimulation was resumed at low rates (e.g., at 0.13 Hz).

Unit activity was systematically investigated in 11 cases by stepwise lowering of a glass

electrode across CA1 from the alveus down to the hippocampal fissure. Low to high intensity paired stimuli (IPI, 100 msec; 0.13 Hz) were applied to RE, and unit activity and fEPSPs were recorded simultaneously. In general, many spontaneously active neurons were encountered approaching the pyramidal cell layer, but they became more sparse when the electrode was lowered through strata radiatum and L-M. Only one synaptically driven neuron was recorded at the oriens/alveus border. This neuron generated a short latency (9 msec) action potential to both the conditioning and test pulses (Fig. 3C) at low as well as high intensity stimulation of RE. The simultaneously recorded, small amplitude deflection at the oriens/alveus level (Fig. 3D) shows that the RE-elicited oriens/alveus spike preceded the local field response.

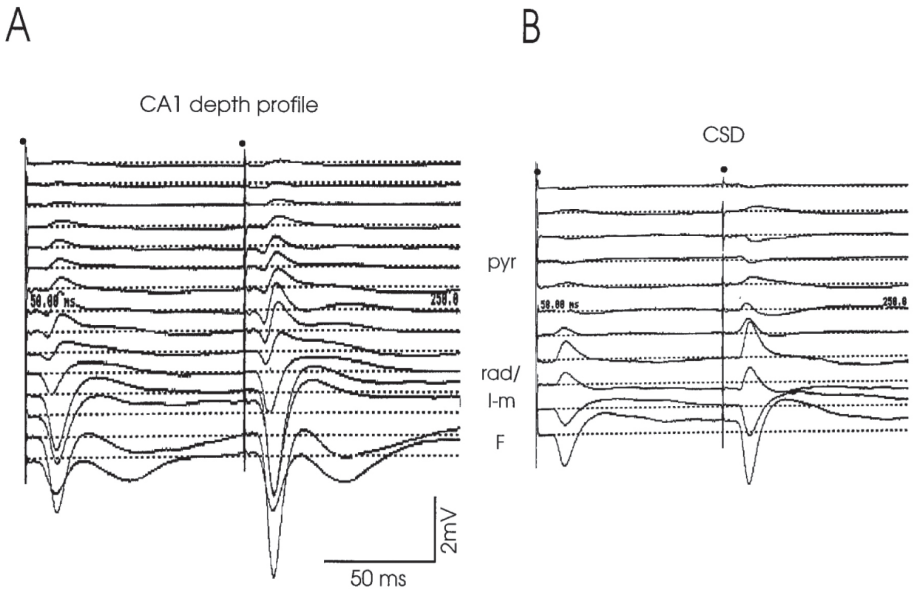

Fig. 2. Depth profile of RE-evoked field potentials in CA1 (A) with the corresponding CSD (B). A, The depth profile was recorded using a probe with 18 metal electrodes (see Materials and Methods; electrode heart-to-heart distance, 100 μm). Dots indicate the moments of the paired stimuli (100 msec interpulse interval, 0.13 Hz). The recordings from electrodes 4 –18 are depicted, covering CA1 from the white matter overlying the hippocampus down to just across the hippocampal fissure into the dentate gyrus. Indicated are the pyramidal cell layer (pyr), the radiatum/ lacunosum-moleculare border (rad/l-m), and the fissure (F). Note that in the bottom trace, recorded just below the fissure, the negative deflection is much smaller compared with the trace recorded above the fissure (also see Fig. 1 D). B, The CSD, corresponding to the depth profile shown in A, clearly demonstrates the prominent lacunosum-moleculare sink; the radiatum source rapidly declines toward the pyramidal cell layer (sinks are shown by a deflection downward, sources by a deflection upward, in arbitrary units).

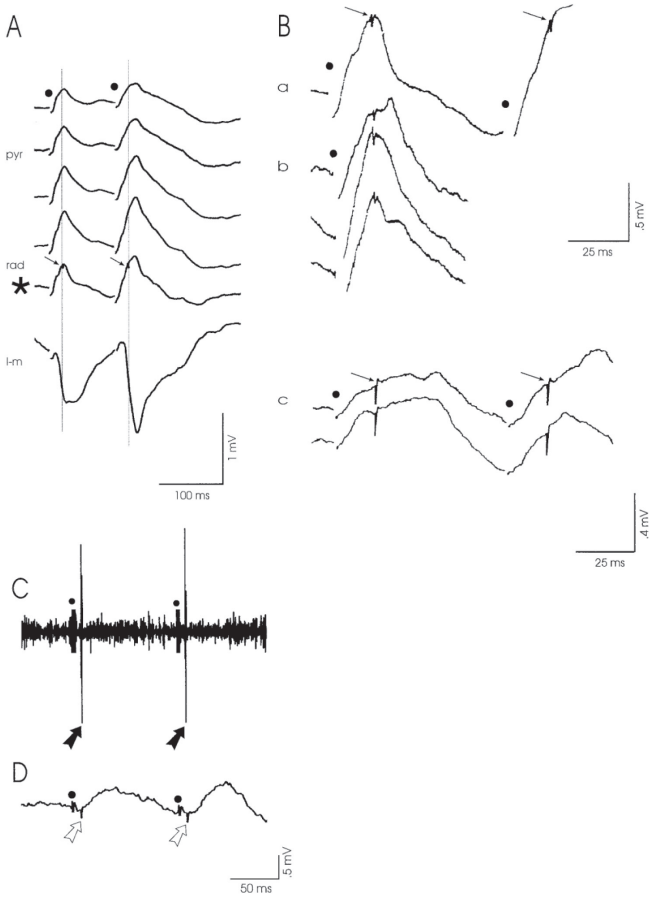

Fig. 3. RE-evoked spikes in the distal stratum radiatum and at the oriens/ alveus border, indicative of the activation of local interneurons. A, A simulta- neously recorded CA1 depth profile reveals that stimulus-triggered spikes (arrows) occurred only in the distal stratum radiatum (rad, *), in both the conditioning and test response, after high intensity stimulation of RE (0.13 Hz). pyr, stratum pyramidale; l-m, stratum lacunosum-moleculare; B, Magnifi- cation of recordings from the stratum radiatum. a, Radiatum spikes (arrows) shown in A (trace marked *). b, Radiatum field potentials to single pulses applied to RE at frequencies in the range from 0.13 to 2 Hz also exhibited spikes. c, Stimulus-triggered radiatum spikes (arrows) in both conditioning and test response, recorded in another rat. Notice that in all cases the latencies of the radiatum spikes were highly comparable. C, A synaptically driven neuron was encountered at the oriens/alveus border. A short latency action potential (black arrows) was recorded in both the conditioning and test response. D, The simultaneously recorded local field potential shows that the RE-evoked oriens/ alveus spike (open arrows) preceded the postsynaptic pyramidal cell response. Stimulation moments in A–D are indicated by dots.

Monosynaptic and disynaptic nature of RE-evoked fEPSPs in CA1

Because RE afferents in CA1 form axospinous and axodendritic contacts (Wouterlood et al., 1990), the RE input was thus expected to be of a monosynaptic nature. During the series of experiments, however, we found a rather wide range (13–39 msec) of latencies of fEPSPs to RE stimulation. Therefore, we analyzed whether these responses were monosynaptically and/or disynaptically evoked, possibly in relation to differences in recording or stimulation sites. Based on histological verification of electrode placements, the experiments were sorted for recording site (septal-to-temporal CA1) and stimulation site (rostral-to-caudal RE), respectively. By subsequent comparison with the sorting for early versus late responses, we found that so-called early (monosynaptic) responses (mean latency, 16.8 ± 3.6 msec; n=18) were evoked by stimulation of the rostral two-thirds of RE (rRE; Fig. 4 A,C); late (presumably disynaptic) responses (mean latency, 33.0 ± 3.2 msec; n=6) resulted from stimulation of caudal RE (cRE; Fig. 4 A,D). Occasionally we recorded complex responses (n=5), such as the one documented in Figure 1 E, displaying early as well as late deflections in both conditioning and test response. In those complex field potentials the early conditioning and test fEPSPs were usually of small amplitude (see Fig. 1 E). Because the (subtle) differences in CA1 recording sites could not be associated with any variation in response latency or waveform complexity, we concluded that the source of the disynaptic nature of RE– CA1 input must be within RE itself.

Anatomical observations

Intranucleus projection from caudal to rostral RE

We reasoned that an intranucleus connectivity between caudal and rostral RE might underlie the observed monosynaptic and disynaptic nature of rostral or caudal RE-evoked f EPSPs in CA1. Therefore, we investigated whether a projection that connects the caudal and rostral parts of the nucleus could be demonstrated. The neuroanatomical tracer BDA was injected in the caudal RE, where it was incorporated by neurons confined to the caudal portion of the nucleus (Fig. 5A). BDA is primarily transported in an anterograde direction. Uptake of BDA by (damaged) fibers of passage may result in some retrograde transport (Veenman et al., 1992); anterograde transport of BDA in axons of passage has not been reported. Our BDA injections resulted in many anterogradely labeled varicose fibers and terminal labeling in rostral RE (Fig. 5B,C). In comparison with the dense terminal labeling in rostral RE resulting from injections in caudal RE, we detected a sparse terminal labeling in hippocampal field CA1. This latter observation confirms previous findings (Wouterlood et al., 1990; Dolleman-van der Weel and Witter, 1996) that caudal RE gives rise to only a minor innervation of CA1. When BDA was injected in

the poorly delineated thalamic area just caudal to RE, labeled fibers were absent in both rostral RE and field CA1.

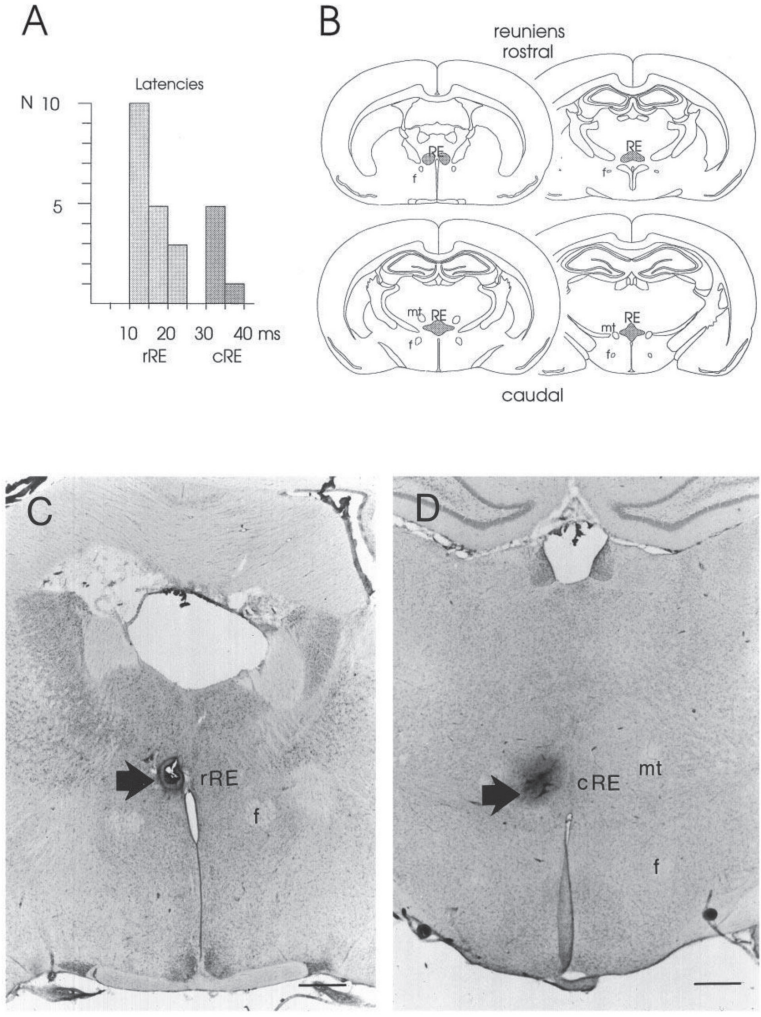

Fig. 4. Stimulation of rostral versus caudal RE and associated early versus late CA1 responses. A, The histogram represents the distribution of latencies of CA1 field potentials corresponding with early or late responses to stimulation of rRE or cRE, respectively. B, Series of rostral-to-caudal coronal sections through the rat brain, illustrating the location of the rostral (top row) and caudal (bottom row) portions of RE (shaded areas). C, Representative example of the position of a stimulation electrode in rostral RE, marked by a small lesion (arrow). D, Representative example of a stimulation site in caudal RE. The dark spot, representing the center of the lesion (arrow), indicates the position of the stimulation electrode. f, Fornix; mt, mammillothalamic tract. Scale bars, 500 μm.

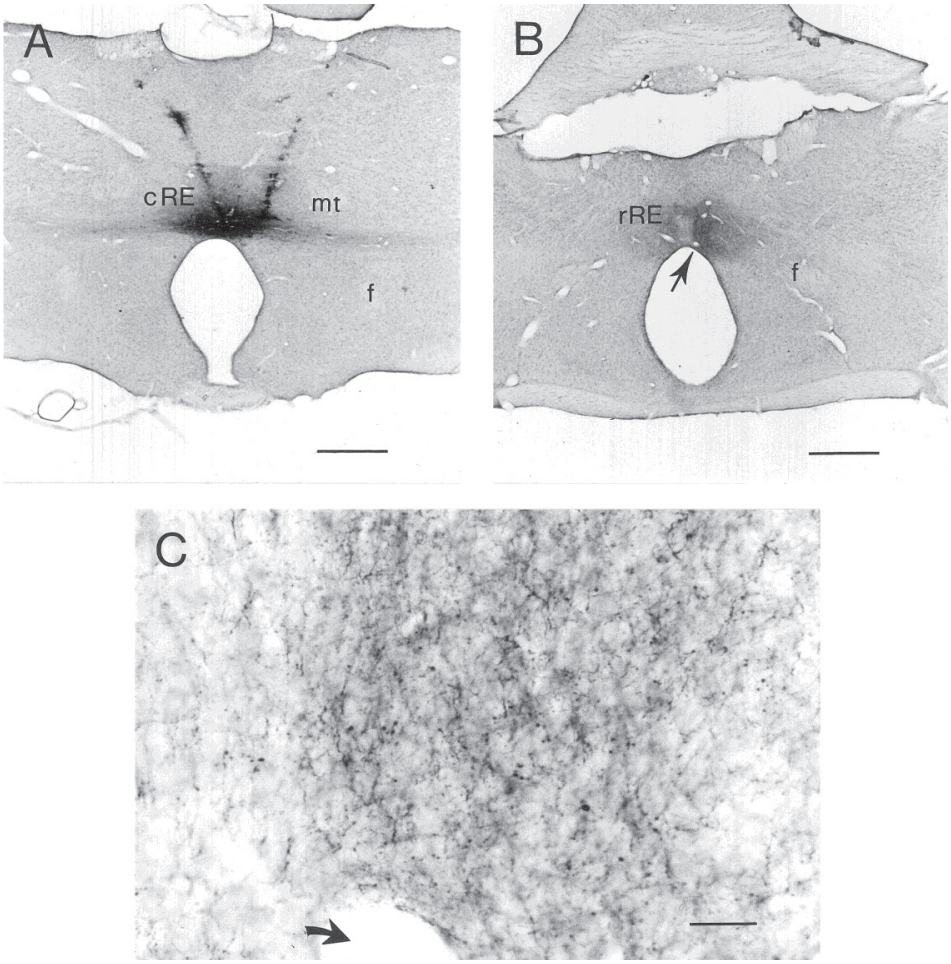

Fig. 5. Intranucleus projection from caudal to rostral RE. A, Representative example of an injection site in caudal RE; the anterograde tracer BDA has been incorporated by neurons located in the caudal part of the nucleus. B, The injection shown in A resulted in a dense plexus of BDA-positive varicose fibers and terminal labeling in the rostral part of RE. C, High magnification of the terminal labeling in rostral RE shown in B. Arrows in B and C indicate the same blood vessel. Scale bars: A and B, 500 μm; C, 20 μm. f, Fornix; mt, mammillothalamic tract.

DISCUSSION

The present study provides the first electrophysiological evidence (schematically summarized in Fig. 6) that RE is able to modulate transmission in CA1 through both excitatory and inhibitory mechanisms. First, electrical stimulation of RE–CA1 afferents at their origin causes an active (subthreshold) depolarization of the apical dendrites of pyramidal cells, which may enhance their state of excitability. Second, RE-elicited spiking of extracellularly recorded units was not detected in the stratum pyramidale but in strata oriens/alveus and radiatum, which indicates synaptic excitation of local nonpyramidal cells that are likely associated with inhibitory mechanisms (Lacaille et al., 1987; Samulack et al., 1993; McBain et al., 1994; Steffensen, 1995; Bergles et al., 1996; Maccaferri and McBain, 1996; for review, see Freund and Buzs´aki, 1996). Furthermore, evidence is provided for the existence of a projection from caudal to rostral RE that is considered to form the anatomical substrate underlying the presently observed disynaptic and complex RE-evoked responses in CA1. Because caudal RE receives input from the hippocampus via the subiculum (Herkenham, 1978; Witter and Groenewegen, 1990; Dolleman-van der Weel et al., 1993), we propose that the caudal to rostral RE connection might act to close a novel circuit (see Fig. 6) between rostral RE–CA1–subiculum–caudal RE–rostral RE, which allows RE to modulate the activity level in CA1, depending on the output of the hippocampus.

The L-M sink–radiatum source configuration is in agreement with the interpretation that stimulation of RE evokes a synaptic EPSP in the apical dendrites of pyramidal cells. However, this distal EPSP seems insufficient to elicit action potentials in these cells. This can be attributable to its spatial decay in the proximal direction, likely associated with an inhibitory action at the somatic level (see compartmental–volume–conduction model by Leung, 1995). The latter is in line with the observation that RE is able to discharge interneurons that are likely inhibitory and are known to contact the pyramidal cell bodies (see below). In CSDs, however, synaptically elicited activity by nonpyramidal cells can remain undetected, because these cells: (1) are widely distributed and largely outnumbered by CA1 cells, and (2) display a laminar dendritic orientation similar to that of pyramidal cells.

The RE-evoked dipole field, lacking a population spike, is remarkably similar to that evoked by stimulation of the excitatory entorhinal cortex (EC)– CA1 input in the rat (Colbert and Levy, 1992; Empson and Heinemann, 1995; Leung, 1995; Levy et al., 1995). Thus, like EC-evoked CA1 responses, RE-evoked fEPSPs may be mediated by non-NMDA as well as NMDA receptors (Colbert and Levy, 1992; Empson and Heinemann, 1995). However, the pharmacology of CA1 responses to RE stimulation awaits further investigation. The presently observed conspicuous RE-induced PPF of fEPSPs, noted to

be largely independent on stimulus intensity and IPI duration (at least under all tested conditions), indicates that RE can exert a persistent influence on the state of pyramidal cell excitability. This will probably keep the latter cells close to the firing threshold, allowing them to discharge under certain conditions, for instance, during periods of diminished inhibition. Previously, the findings by Hirayasu and Wada (1992a,b) also indirectly pointed to the ability of RE to modulate temporal limbic excitability. These investigators observed that NMDA injections in RE caused remarkable behavioral and temporal lobe EEG changes, i.e., tonic and/or clonic generalized convulsions, and seizure discharges.

Our interpretation that RE is able to elicit a suprathreshold activation of interneurons is based on the detection of elicited spikes in the stratum radiatum and at the oriens/ alveus border. Direct evidence for this interpretation (i.e., RE-evoked responses in morphologically identified interneurons) should be obtained in future studies using the in vivo intracellular recording and labeling technique (e.g., Sik et al., 1995). Nevertheless, the present assumption is consistent with the observations that: (1) stimulation of RE never elicited action potentials in the stratum pyramidale; (2) stimulus-triggered action potentials were found in strata containing interneurons that, from a morphological view point (see below), can be contacted by RE fibers; and (3) anatomically we found that RE– CA1 axons form asymmetrical synapses on GABA-positive dendrites in the stratum L-M (M. J. Dolleman- van der Weel and M. P. Witter, unpublished results). These latter observations support our interpretation that RE-elicited spiking of extracellularly recorded units reflects monosynaptic activation of interneurons. With respect to the observed radiatum spike events, however, we also have to address the possibility that these actually represented dendritic spiking in pyramidal cells. High intensity, low frequency stimulation of radiatum fibers and Schaffer collaterals (Herreras, 1990) has been shown to result in the consistent occurrence of dendritic spikes generated by CA1 pyramidal cells. In our hands, using a standard protocol of high intensity stimulation at 0.13 Hz, dendritic spiking thus should have been encountered on a far more regular basis than the two cases in which triggered spikes in the stratum radiatum were detected. Moreover, the latency of the radiatum spikes in those two experiments was highly comparable, despite a difference in latency between the respective fEPSPs. This supports the interpretation that RE-elicited radiatum spikes reflect synaptic discharges in radiatum interneurons.

According to their distinctive morphologies, axonal targets, and neurochemical markers, CA1 interneurons in strata oriens/ alveus and radiatum represent a heterogeneous class of nonpyramidal cells (McBain et al., 1994; Buckmaster and Soltesz, 1996; Freund and Buzs´aki, 1996; Maccaferri and McBain, 1996). A prerequisite for these interneurons to receive RE input is that their dendritic tree extends into the stratum L-M. This has been shown for a subpopulation of cells at the oriens/alveus border, the so-called vertical oriens/ alveus cells (McBain et al., 1994). These interneurons have an extensively arborizing

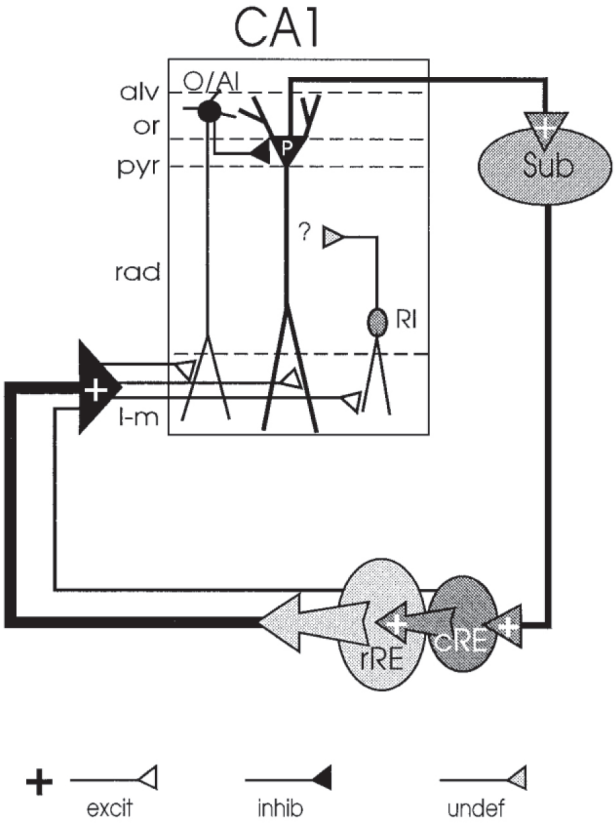

Fig. 6. Schematic representation of the RE– CA1– subiculum–RE loop. The RE– CA1 input is both monosynaptically and disynaptically organized. Monosynaptic input originates predominantly in the rRE; only a minor portion of the monosynaptic afferents arises from cRE. A dense intranucleus projection from cRE to rRE can account for the disynaptic cRE–rRE– CA1 input. In the stratum lacunosum-moleculare (l-m) of CA1, the RE axons form exclusively asymmetrical [i.e., excitatory (excit)] synapses on the apical dendrites of pyramidal cells [P; stratum pyramidale (pyr)], as well as on those of subtypes of interneurons located at the oriens (or)/alveus (alv) border [vertical oriens/ alveus interneuron (O/AI)] and in the distal stratum radiatum [rad; radiatum interneuron (RI)]. Electrical stimulation of RE in vivo elicits a subthreshold depolarization in pyrami- dal cells and the generation of synaptic spikes in oriens/alveus and radiatum interneurons. The vertical oriens/alveus interneurons are as- sumed to mediate feedforward inhibition (inhib) of pyramidal cells; the axonal targets of radiatum interneurons (the latter probably containing both inhibitory and excitatory transmitters [undefined (undef); see Dis- cussion], and thereby the role these interneurons play in the local circuit of CA1 awaits further investigation. Major output of CA1 is known to be transmitted to the subiculum (Sub), which, in turn, projects back to cRE. This suggests a closed rRE– CA1– subiculum– cRE–rRE loop that may enable RE to modulate the flow of information through CA1 depending on the output of the hippocampus.

axon that is largely confined to the stratum pyramidale, forming symmetrical (inhibitory) synapses on the somata and primary dendrites of numerous CA1 cells. Functionally, they are assumed to mediate both feed-forward and feedback inhibition of pyramidal cells (Lacaille et al., 1987; Lacaille and Schwarzkroin, 1988; Samulack et al., 1993). Interneurons located in the distal radiatum that fulfill the criterion to receive RE input are likely the ones containing GABA as well as the putative excitatory transmitters cholecystokinin (CCK) and/or vasoactive intestinal polypeptide (VIP) (Kosaka et al., 1985; Gulyás et al., 1991; Haas and Gáhwiler, 1992; Acsády et al., 1996a,b). GABA–CCK cells have been observed to form symmetrical synapses with pyramidal cell bodies (Harris et al., 1985; Nunzi et al., 1985); GABA–VIP cells have been shown to contact primarily other interneurons (Acsády et al., 1996a,b; Freund and Buzsáki, 1996). Although the function of these interneuron subtypes in the stratum radiatum remains to be established, based on their different axonal targets it can be assumed that each subtype plays a distinctive role in the local circuit of CA1. Thus, the ability to discharge interneuron subpopulations in strata oriens/alveus and radiatum (e.g., differing in discharge threshold, afferent and efferent targets, and transmitter contents) increases the flexibility of RE to modulate transmission in CA1. The possible interaction between the EC–CA1 and RE–CA1 inputs is also of interest in understanding the role RE might play in modulating the activity in the entorhinal–hippocampal circuit. In this respect, our preliminary results from paired stimulation of RE and EC revealed that an interaction (i.e., facilitation of elicited-fEPSPs, yet without inducing a population spike) between perforant path and RE inputs occurs in CA1 (M. J. Dolleman-van der Weel and F. H. Lopez da Silva, unpublished results).

Based on the previously demonstrated RE–CA1 (asymmetrical) synapses on spines and dendrites (Wouterlood et al., 1990), a monosynaptic RE input was to be expected. However, RE-evoked CA1 responses displayed a wide range of latency values, indicating that both monosynaptic and disynaptic RE inputs exist. Interestingly, our early (monosynaptic) and late (disynaptic) CA1 responses seemed associated with selective stimulation of rostral and caudal RE, respectively. Anatomically, rostral RE is the major source of CA1 afferents, whereas caudal RE contributes very modestly to this projection (Dolleman-van der Weel and Witter, 1996). We now report that caudal RE gives rise to a dense innervation of rostral RE. Taken together, our anatomical and electrophysiological data thus suggest that the caudal-to-rostral RE projection is involved in the disynaptic, or occasionally noted complex monosynaptic and disynaptic, fEPSPs in CA1 evoked by stimulation of caudal RE. In these latter complex responses, the early potential of a small amplitude likely represents the activation of few caudal RE neurons projecting monosynaptically to CA1; the late potential of a larger amplitude then reflects the activation of the presently described caudal RE–rostral RE–CA1 disynaptic input.

Because caudal RE receives input from the hippocampus via the subiculum (Herkenham, 1978; Witter and Groenewegen, 1990; Dolleman-van der Weel et al., 1993), we propose the existence of a closed circuit (see Fig. 6) between rostral RE–CA1–subiculum–caudal RE–rostral RE, which may allow RE to modulate the activity level in CA1 depending on the hippocampal output.

REFERENCES

Acsády L, Arabadzisz D, Freund TF (1996a) Correlated morphological and neurochemical features identify different subsets of vasoactive intestinal polypeptide-immunoreactive interneurons in rat hippocampus. Neuroscience 73:299 –315.

Acsády L, Görcs TJ, Freund TF (1996b) Different populations of vasoactive intestinal polypeptide-immunoreactive interneurons are specialized to control pyramidal cells or interneurons in the hippocampus. Neuroscience 73:317–334.

Bergles DE, Doze VA, Madison DV, Smith SJ (1996) Excitatory actions of norepinephrine on multiple classes of hippocampal CA1 interneurons. J Neurosci 16:572–585.

Braak H, Braak E (1991) Alzheimer's disease affects limbic nuclei of the thalamus. Acta Neuropathol (Berl) 81:261–268.

Braak H, Braak E (1992) The human entorhinal cortex: normal morphology and lamina-specific pathology in various diseases. Neurosci Res 15:6 –31.

Buckmaster PS, Soltesz I (1996) Neurobiology of hippocampal interneurons: a workshop review. Hippocampus 6:330 –339.

Colbert CM, Levy WB (1992) Electrophysiological and pharmacological characterization of perforant path synapses in CA1: mediation by glutamate receptors. J Physiol (Lond) 68:1– 8.

Dolleman-van der Weel MJ, Witter MP (1996) Projections from the nucleus reuniens thalami to the entorhinal cortex, hippocampal field CA1, and the subiculum in the rat arise from different populations of neurons. J Comp Neurol 364:637– 650.

Dolleman-van der Weel MJ, Ang W, Witter MP (1993) Afferent connections of the nucleus reuniens thalami: a neuroanatomical tracing study in the rat. Eur J Neurosci [Suppl] 6:247.

Dolleman-van der Weel MJ, Wouterlood FG, Witter MP (1994) Multiple anterograde tracing, combining Phaseolus vulgaris leucoagglutinin with rhodamine- and biotin-conjugated dextran amine. J Neurosci Methods 51:9 –21.

Empson RM, Heinemann U (1995) The perforant path projection to hippocampal area CA1 in the rat hippocampal-entorhinal cortex combined slice. J Physiol (Lond) 484:707–720.

Freeman JA, Nicholson C (1975) Experimental optimization of current-source-density technique for anuram cerebellum. J Neurophysiol 38:369 –382.

Freeman JA, Stone JA (1969) A technique for current source density analysis of field potentials and its application to the frog cerebellum. In: Neurobiology of cerebellar evolution and development (Llinás R, ed), pp 421– 430. Chicago: American Medical Association.

Freund TF, Buzsáki G (1996) Interneurons of the hippocampus. Hippocampus 6:347– 470.

Gulyás AI, Tóth K, Dános P, Freund TF (1991) Subpopulations of GABAergic neurons containing parvalbumin, calbindin D28k, and cholecystokinin in the rat hippocampus. J Comp Neurol 312:371–378.

Haas HL, Gáhwiler BH (1992) Vasoactive intestinal polypeptide modulates neuronal excitability in hippocampal slices of the rat. Neuroscience 47:273–277.

Harris KM, Marshall PE, Landis DM (1985) Ultrastructural study of cholecystokinin-immunoreactive cells and processes in area CA1 of the rat hippocampus. J Comp Neurol 233:147–158.

Herkenham M (1978) The connections of the nucleus reuniens thalami: Evidence for a direct thalamo-hippocampal pathway in the rat. J Comp Neurol 177:589 – 609.

Herreras O (1990) Propagating dendritic action potential mediates synaptic transmission in CA1 pyramidal cells in situ. J Neurophysiol 64:1429 –1441.

Hirayasu Y, Wada JA (1992a) N-methyl-D-aspartate injection into the massa intermedia facilitates development of limbic kindling in rats. Epilepsia 33:965–970.

Hirayasu Y, Wada JA (1992b) Convulsive seizures in rats induced by N-methyl-D-aspartate injection into the massa intermedia. Brain Res 577:36 – 40.

Kosaka T, Kosaka K, Tateishi K, Hamaoka Y, Yanaihara N, Wu J-Y, Hama K (1985) GABAergic neurons containing CCK-8-like and/or VIP-like immunoreactivities in the rat hippocampus and dentate gyrus. J Comp Neurol 239:420 – 430.

Lacaille J-C, Schwarzkroin PA (1988) Stratum lacunosum-moleculare interneurons of hippocampal CA1 region. II. Intrasomatic and intradendritic recordings of local circuit synaptic interactions. J Neurosci 8:1411–1424.

Lacaille J-C, Mueller AL, Kunkel DD, Schwarzkroin PA (1987) Local circuit interactions between oriens/alveus interneurons and CA1 pyramidal cells in hippocampal slices: electrophysiology and morphology. J Neurosci 7:1979 –1993.

Leung L-WS (1995) Simulation of perforant path evoked field and intracellular potentials in hippocampal CA1 area. Hippocampus 5:129 –136.

Levy WB, Colbert CM, Desmond NL (1995) Another network model bites the dust: entorhinal inputs are no more than weakly excitatory in the hippocampal CA1 region. Hippocampus 5:137–140.

Maccaferri GM, McBain CJ (1996) Long-term potentiation in distinct subtypes of

hippocampal nonpyramidal neurons. J Neurosci 16:5334 –5343.

McBain CJ, DiChiara TJ, Kauer JA (1994) Activation of metabotropic glutamate receptors differentially affects two classes of hippocampal interneurons and potentiates excitatory synaptic transmission. J Neurophysiol 14:4433– 4445.

Nunzi MG, Gorio A, Milan F, Freund TF, Somogyi P, Smith AD (1985) Cholecystokinin-immunoreactive cells form symmetrical synaptic contacts with pyramidal and non-pyramidal neurons in the hippocampus. J Comp Neurol 237:485–505.

Paxinos G, Watson C (1986) The rat brain in stereotaxic coordinates, Ed 2. New York: Academic.

Rousseau M (1994) Amnesias following limited thalamic lesions. In: The memory system of the brain, advanced series in neuroscience Vol 4 (Delacour J, ed), pp 241–277. Singapore: World Scientific.

Samulack DD, Williams S, Lacaille J-C (1993) Hyperpolarizing synaptic potentials evoked in CA1 pyramidal cells by glutamate stimulation of interneurons from the oriens/alveus border of rat hippocampal slices. I. Electrophysiological response properties. Hippocampus 3:331–344.

Sik A, Penttonen M, Ylinen A, Buzsáki G (1995) Hippocampal CA1 interneurons: an in vivo intracellular labeling study. J Neurosci 15:6651– 6665.

Steffensen SC (1995) Dehydroepiandrosterone sulfate suppresses hippocampal recurrent inhibition and synchronizes neuronal activity to theta rhythm. Hippocampus 5:320 –328.

Squire LR (1992) Memory and the hippocampus: a synthesis from findings with rats, monkeys and humans. Physiol Rev 99:195–231.

Vanderwolf CH, Leung L-WS, Cooley RK (1985) Pathways through cingulate, neo- and entorhinal cortices mediate atropine-resistant hippocampal rhythmical slow activity. Brain Res 347:58 –73.

Veenman CL, Reiner A, Honig MG (1992) Biotinylated-dextran amine as an anterograde tracer for single- and double labelings studies. J Neurosci Methods 41:239 –254.

Witter MP, Groenewegen HJ (1990) The subiculum: cytoarchitectonically a simple structure, but hodologically complex. Prog Brain Res 83:47–58.

Wouterlood FG, Saldana E, Witter MP (1990) Projection from the nucleus reuniens thalami to the hippocampal region: light and electron microscopic tracing study in the rat with the anterograde tracer Phaseolus vulgaris leucoagglutinin. J Comp Neurol 296:179 –203.

Chapter 5

NUCLEUS REUNIENS THALAMI INNERVATES GAMMA AMINOBUTYRIC ACID POSITIVE CELLS IN HIPPOCAMPAL FIELD CA1 OF THE RAT.

Neuroscience Letters (2000) 278: 145-146.

ABSTRACT

The aim of the present study was to investigate whether the nucleus reuniens thalami (RE) innervates inhibitory cells in hippocampal field CA1. Therefore, we examined the RE-CA1 input at the ultrastructural level. RE axons were anterogradely labeled with biotin-conjugated dextran amine (BDA), in combination with pre-embedding gamma aminobutyric acid (GABA)-immunolabeling of neurons in CA1. We observed that part of the BDA-labeled axons formed asymmetrical (i.e., excitatory) synapses on GABA-positive dendrites. Based on these data, which are in line with our previously published electrophysiological observations (see Dolleman-van der Weel et al. [7]), we propose that RE-CA1 input partially influences hippocampal transmission through activation of local inhibitory interneurons.

INTRODUCTION

The thalamic midline nucleus reuniens (RE) gives rise to strong projections to hippocampal field CA1, the subiculum, and the peri- and entorhinal cortices [8,13,24]. Based on the tracing study by Herkenham [13], who used the transport of tritiated amino acids, RE input was supposed to be of an excitatory nature. This assumption was confirmed by the findings of Wouterlood et al. [24], who revealed that at the ultrastructural level RE axons form exclusively asymmetrical (i.e., excitatory) synapses on spines (50%) and dendrites (50%). Therefore, RE fibers were assumed to contact the spinous apical dendrites of pyramidal cells, as well as the largely aspinous dendrites of interneurons. Recently, we showed that in the anesthetized rat stimulation of the RE-CA1 fibers at their origin resulted in a (subtreshold) depolarization of the apical dendrites of pyramidal cells, and RE-elicited spiking of extracellularly recorded units in strata oriens/alveus and distal radiatum [7]. The latter finding is indicative of the activation of local, putative inhibitory oriens/alveus and radiatum interneurons. In the present study, we examined the RE axo-dendritic contacts in CA1 at the ultrastructural level. The anterograde tracer biotin-conjugated dextran amine (BDA) was used to label RE axons, in combination with the immunocytochemical silver-gold intensified staining of GABA for the visualization of presumed local inhibitory interneurons.

MATERIALS AND METHODS

Two female Wistar rats (225 g) were used. Briefly, 5% BDA (MW 10000, Molecular Probes, Eugene, Oregon, USA), dissolved in 0.01 M phosphate buffer (PB), pH 7.4, was injected bilaterally into the rostral and caudal parts of RE. Coordinates for the injection sites were derived from the stereotaxic atlas of Paxinos and Watson [21]. BDA was applied iontophoretically with the use of glass micropipettes (tip diameter of 10-20 μm), and a positive pulsed DC current (7 sec on/off) at 5-6.5 μA, for 10-15 minutes. After 10-14 days survival, the animals were transcardially perfused with 0.9% saline solution, followed by 500 ml of 4% freshly depolymerized paraformaldehyde and 0.05% glutaraldehyde in 0.1 M PB, pH 7.4. Following postfixation in the same fixative for one hour at room temperature, the tissue was cryoprotected in a solution of 20% glycerine and 2% dimethylsulfoxide (DMSO) in PB, pH 7.4, for 24 hours at 4 ºC. The brains were cut on a freezing microtome into 40 μm thick sections. One brain was sectioned in the horizontal plane, the other in the coronal plane. One series of sections containing the injection sites, as well as one series of hippocampal sections were destined for light microscopic assessment of BDA-labeled neurons in RE and their projection fibers in CA1, respectively. Remaining series

of sections, destined for electron microscopic examination, were stored in 20% glycerine and 2% DMSO in PB at –20 ºC until processing.

For the light microscopic analysis, BDA was visualized according to a previously described procedure [9]. Briefly, all rinsing and incubations were performed in 0.05 M Tris-buffered saline and 0.5% Triton X-100 (TBS-TX), pH 7.6. Sections were incubated with avidine-biotin-peroxidase complex (prepared according to the manufacturer's recommendations; ABC kit, Vectastain, Vector, Burlingame, CA, USA), for 1.5 hour at room temperature. Subsequently, the sections were reacted with nickel-enhanced diaminobenzidine (DAB-Ni) as chromogen (i.e., 12.5 mg DAB/25 ml PB plus 1 ml of 1% ammonium nickel sulphate), mounted, dehydrated, and coverslipped with Entellan (Merck, Darmstadt, Germany). After the light microscopic assessment of the injection sites in RE and detection of satisfactory labeling of RE fibers in CA1, the stored hippocampal sections that matched the ones with the strongest anterograde labeling in CA1 were processed for electron microscopic examination. They were slowly thawed in a refrigerator, subjected to three additional freeze-thawing steps [25], and thoroughly rinsed in PB to remove glycerine and DMSO. Sections were then washed in TBS (without the addition of TX-100), pH 8.0, which was also used as the vehicle for the immunoreagents. First, GABA was visualized with the use of a monoclonal mouse-anti-GABA antiserum (Dr. I. Virtanen, Helsinki, Finland). Briefly, sections were incubated for 60 hours in mouse-anti-GABA (1:500) at room temperature, incubated with goat-anti-mouse (1:50, Dako, Copenhagen, Denmark) for 8 hours at 4 ºC, and finally incubated with a peroxidase-anti-peroxidase raised in mouse (1:100, Dako, Copenhagen, Denmark) overnight, at 4 ºC. The sections were then reacted with DAB and subjected to a slightly modified silver-gold intensification procedure [14]. Subsequently, BDA was visualized with an ABC-reaction (i.e., incubation with 8 µl of A and 8 µl of B/ml TBS, overnight) and DAB as chromogen [14]. After flat-embedding in epoxy resin, the hardened sections were taped on glass slides. Per rat brain, we used four 40 µm thick hippocampal sections (40-400 µm apart). One sample per section was cut out, mounted on pre-cured resin blocks, and cut on a Reichert OM 4 ultramicrotome into series of ultrathin sections (silver-gold colour, 80-90 nm), preferably from the superficial part of the tissue. Sections were collected on formvar-coated slot grids and scanned under a Philips EM 401 electron microscope. We focussed on the BDA-labeled axo-dendritic synapses. In order to avoid that the same synapse was sampled more than once, ultrathin sections (2-3 per sample) were examined at an interval of 400-500 nm. Initially, they were systematically scanned at a relatively low magnification for the occurrence of areas containing both BDA- and GABA-positive structures. Within these areas, in the material of the two animals every encountered BDA-labeled axo-dendritic synaptic contact was photographed, up to a total of 100 synapses. They were analyzed afterwards and categorized either as BDA/non-GABA synapses or as BDA/ GABA synapses.

RESULTS

At the light microscopic level, in both cases the injections with BDA appeared to be centered in RE, resulting in numerous BDA-labeled RE neurons. In the hippocampus, we detected (bilaterally) a dense plexus of BDA-labeled fibers throughout the depth of stratum lacunosum-moleculare, especially in the intermediate dorso-ventral parts of CA1 and the subiculum (Fig. 1 A-F).

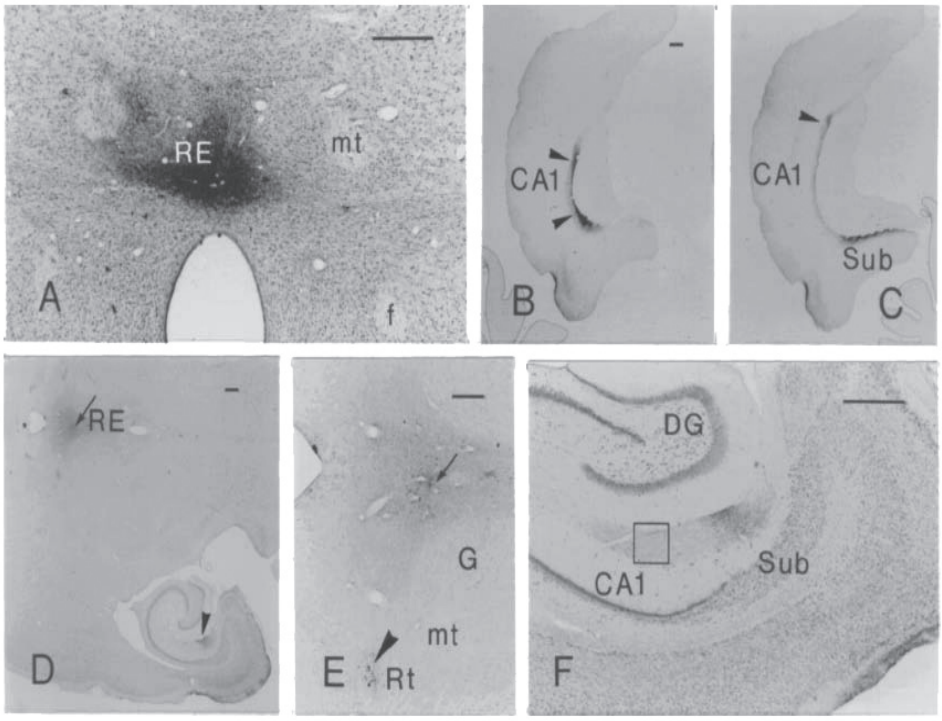

Fig. 1. Injection sites of BDA in RE and anterogradely labeled RE fibers in the hippocampus in coronal sections of rat 1 (A-C), and horizontal sections of rat 2 (D-F). (A) The BDA-injection site is strictly confined to RE. (B,C) A dense plexus of BDA-labeled RE fibers is detected in stratum lacunosum-moleculare of CA1 and in the ventral subiculum (Sub). Arrowheads indicate the approximate areas examined in adjacent sections at the ultrastructural level. (D) The BDA-injection site, photographed at low magnification, is centered in RE. Note the dense terminal labeling in the ventral subiculum (arrowhead). (E) Injection site at higher magnification. BDA-labeled RE neurons surround a necrotic spot within the nucleus (arrow). The arrowhead indicates retrogradely labeled cells in the reticular thalamic nucleus (Rt) [see 9, 24]. (F) BDA-labeled RE fibers in CA1 and subiculum. The square markes the approximate area in CA1 that was examined in an adjacent section in the electron microscope. Abbreviations: mt, mammillothalamic tract; f, fornix; G, gelatinosus nucleus; DG, dentate gyrus. Scale bars: 500 μm.

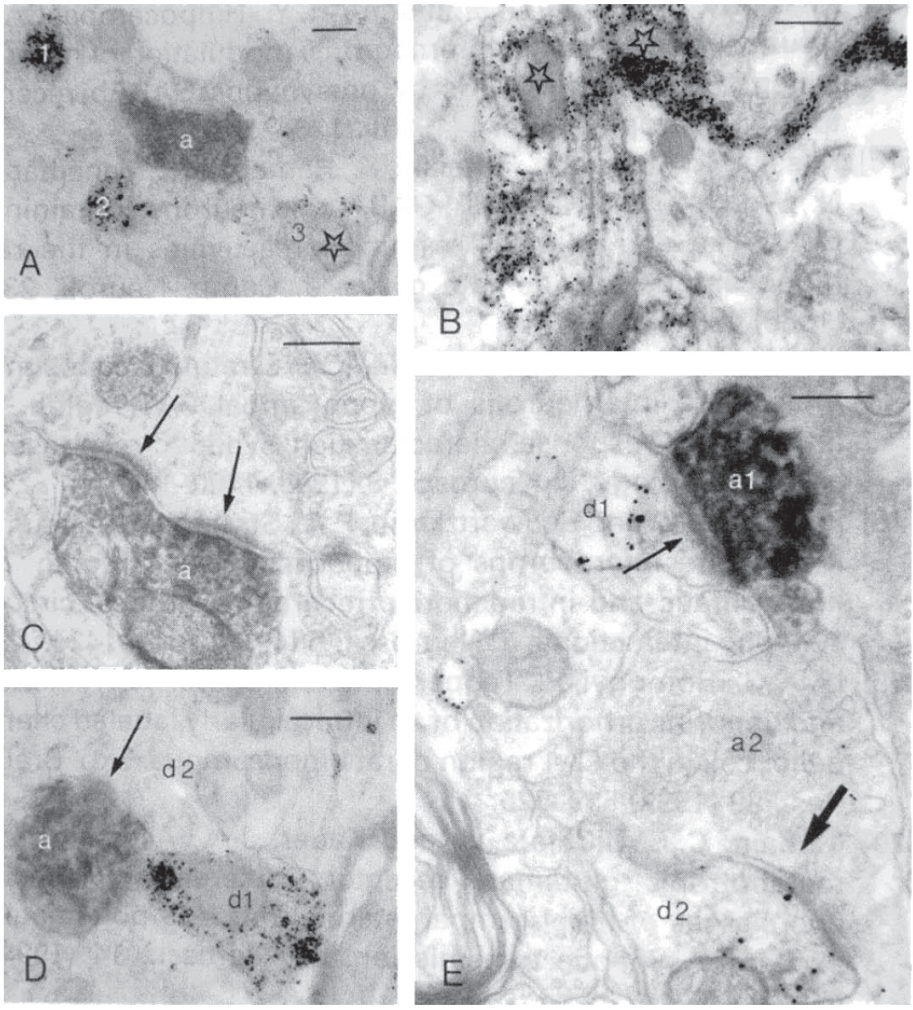

Fig. 2. Representative examples of BDA- and GABA-labeled structures in stratum lacunosum-moleculare of CA1 at the ultrastructural level. (A) Typical examples of densely (1), moderately (2), and lightly (3) GABA-immunolabeled structures, adjacent to a BDA-labeled axon (a). Notice the absence of a granular deposit in a mitochondrion (asterisk). (B) Mitochondria (asterisk) of densely and moderately labeled GABAergic elements are also free of granular deposit. (C) A BDA-labeled axon (a) forms an asymmetrical, perforated synapse (arrows) with a GABA-negative dendrite. (D) A GABA-positive dendrite (d1) adjacent to a BDA-labeled axon (a), the latter forming an asymmetrical synaptic contact (arrow) with a GABA-negative dendrite (d2). (E) Two GABA-positive dendrites, one of them (d1) forming an asymmetrical non-perforated synapse (small arrow) with a BDA-labeled axon (a1). The other GABAergic dendrite (d2) forms an asymmetrical perforated synapse (large arrow) with an unlabeled axon (a2). Scale bars: 0.25 μm.

At the electron microscopic level, the ultrastructure was satisfactorily preserved and allowed for a good detection of BDA- and GABA-labeled structures (see Fig. 2A-E). The reaction product in the GABA-positive structures consisted of a granular silver-gold deposit which had superseded the DAB reaction product. We noticed densely, moderately, and lightly labeled GABAergic elements which were usually found in one and the same ultrathin section (Fig. 2A, B). A common feature of all GABA-labeled structures was the absence of a granular deposit within mitochondria. BDA-labeled fibers contained a homogeneously distributed black precipitate. In most cases the DAB reaction product was rather fuzzy; occasionally spherical vesicles were recognizable within terminals. The anterogradely labeled RE-axons formed exclusively asymmetrical, perforated as well as non-perforated, synaptic contacts with both GABA-negative and GABA-positive dendrites (Fig. 2C-E). In general, BDA/GABA synapses were observed in ultrathin sections from each of the hippocampal samples examined. Of the photographed BDA-labeled synapses, on average 17% turned out to be on GABAergic dendrites (i.e., 16% in the one rat and 18% in the other; Fig. 2E).

DISCUSSION

The present observations provide the first anatomical evidence that RE innervates GABAergic cells in hippocampal field CA1 of the rat. The similarity in the ratio of BDA/GABA- and BDA/non-GABA synapses in both cases clearly reflects the reliability of the immunocytochemical procedure used. The intensity of GABA-labeling was rather variable (e.g., see [6]). Because densely labeled GABA-structures were commonly found immediately adjacent to lightly labeled ones, this variation can not be explained by differences in the penetration of antibodies. A possibility is that labeling intensity is related to the actual amount of GABA within the labeled structures.

The present anatomical evidence supports our previous electrophysiological observations [7] which indicated that RE-CA1 input is able to drive putative inhibitory interneurons in the strata oriens/alveus and radiatum. A prerequisite for all cells in CA1 to receive RE input is that their dendritic tree extends into the stratum lacunosum-moleculare. So far, several interneuron subtypes in all strata of CA1 have been described that fulfil this criterion. In line with our electrophysiological data [7], the so-called vertical oriens/alveus cells [20] and the radiatum interneurons containing GABA as well as CCK and/or VIP [1,2,11,16] are likely to be innervated by RE axons. Based on their anatomical features, in stratum pyramidale the candidates for RE input are basket cells [1,3,5,12], some supposedly containing GABA/CCK [12] and others containing GABA/VIP [1], as well as axo-axonic or chandelier cells [4,19,23]. Furthermore, the

lacunosum-moleculare interneurons [15,17,18] and the VIP-containing interneurons located at the radiatum/lacunosum-moleculare border [1] are also in a position to receive RE input. All aforementioned interneuron subtypes are likely to have different in- and/or output connections, and therefore are supposed to play different roles in the regulation of transmission in CA1 (for review, see [10]). Unfortunately, there are no specific neurochemical markers known that can differentiate unequivocally at the ultrastructural level between these non-pyramidal cells. For they all contain GABA, and in multiple instances there is co-localization reported of CCK and/or VIP (see above). Moreover, several interneuron subtypes contain the same calcium binding proteins [10]. Therefore, future studies using the in vivo intracellular recording and labeling technique [22] may reveal more detail about the RE innervation of specific inhibitory interneuron subtypes in CA1, and thereby about the role RE plays in the functioning of the hippocampus.

This work was supported by NWA Grant 90-20 from the Graduate School for Neurosciences Amsterdam. The authors thank Barbara Jorritsma-Byham, Peter Goede, and Shimon Paniry for their expert technical assistance.

REFERENCES

[1] Acsády, L., Arabadzisz, D. and Freund, T.F., Correlated morphological and neurochemical features identify different subsets of vasoactive intestinal polypeptide-immunoreactive interneurons in rat hippocampus, Neurosci., 73 (1996) 299-315.

[2] Acsády, L., Görcs, T.L. and Freund, T.F., Different populations of vasoactive intestinal polypeptide-immunoreactive interneurons are specialized to control pyramidal cells or interneurons in the hippocampus, Neurosci., 73 (1996) 317-334.

[3] Buhl, E.H., Halasy, K. and Somogyi, P., Diverse sources of hippocampal unitary inhibitory postsynaptic potentials and the number of synaptic relase sites, Nature, 368 (1994) 823-828.

[4] Buhl, E.H., Han, Z.S., Lörinczi, Z., Stezhka, V.V/, Karnup, S.V. and Somogyi, P., Physiological properties of anatomically identified axo-axonic cells in the rat hippocampus, J. Neurophysiol., 71 (1994) 1289-1307.

[5] Buhl, E.H., Szilágyi, T., Halasy, K. and Somogyi, P., Physiological properties of anatomically identified basket and bistratified cells in the CA1 area of the rat hippocampus in vitro, Hippocampus, 6 (1996) 294-305.

[6] Commons, K.G., Kow, L-M., Milner, T.A. and Pfaff, D.W., In the ventromedial

nucleus of the rat hypothalamus, GABA-immunolabeled neurons are abundant and are innervated by both enkephalin- and GABA-immunolabeled axon terminals, Brain Res., 816 (1999) 58-67.

[7] Dolleman-van der Weel, M.J., Lopes da Silva, F.H. and Witter, M.P., Nucleus reuniens thalami modulates activity in hippocampal field CA1 through excitatory and inhibitory mechanisms, J. Neurosci., 17 (1997) 5640-5650.

[8] Dolleman-van der Weel, M.J. and Witter, M.P., Projections from the nucleus reuniens thalami to the entorhinal cortex, hippocampal field CA1, and the subiculum in the rat arise from different populations of neurons, J. Comp. Neurol., 364 (1996) 637-650.

[9] Dolleman-van der Weel, M.J., Wouterlood, F.G. and Witter, M.P., Multiple anterograde tracing, combining Phaseolus vulgaris leucoagglutinin with rhodamine- and biotin-conjugated dextran amine, J. Neurosci. Methods, 51 (1994) 9-21.

[10] Freund, T.F. and Buszáki, G., Interneurons of the hippocampus, Hippocampus, 6 (1996) 347-470.

[11] Gulyás, A.I., Tóth, K., Dános, P. and Freund, T.F., Subpopulations of GABAergic neurons containing parvalbumin, calbindin D28k, and cholecystokinin in the rat hippocampus, J. Comp. Neurol., 312 (1991) 371-378.

[12] Halasy, K., Buhl, E.H., Lörinczi, Z., Tamás, G. and Somogyi, P., Synaptic target selectivity and input of GABAergic basket and bistratified interneurons in the CA1 area of the rat hippocampus, Hippocampus, 6 (1996) 306-329.

[13] Herkenham, M., The connections of the nucleus reuniens thalami: Evidence for a direct thalamo-hippocampal pathway in the rat, J. Comp. Neurol., 177 (1978) 589-609.

[14] Jorritsma-Byham, B., Witter, M.P. and Wouterlood, F.G., Combined anterograde tracing with biotinylated dextran-amine, retrograde tracing with Fast Blue and intracellular filling of neurons with Lucifer Yellow: an electron microscopic method, J. Neurosci. Methods, 52 (1994) 153-160.

[15] Khazipov, R., Congar, P. and Ben-Ari, Y., Hippocampal CA1 lacunosum-moleculare interneurons: Modulation of monosynaptic GABAergic IPSCs by presynaptic GABAb receptors, J. Neurophysiol., 74 (1995) 2126-2137.

[16] Kosaka, T., Kosaka, K., Tateishi, K., Hamaoka, Y., Yanaihara, N., Wu, J-Y., Hama, K., GABAergic neurons containing CCK-8-like and or VIP-like immunoreactivities in the rat hippocampus and dentate gyrus, J. Comp. Neurol., 239 (1985) 420-430.

[17] Lacaille, J-C. and Schwartzkroin, P.A., Stratum lacunosum-moleculare interneurons of hippocampal CA1 region. I. Intracellular response characteristics, synaptic

responses, and morphology, J. Neurosci., 8 (1988) 1400-1410.

[18] Lacaille, J-C. and Schwartzkroin, P.A., Stratum lacunosum-moleculare interneurons of hippocampal CA1 region. II. Intrasomatic and intradendritic recordings of local circuit synaptic interactions, J. Neurosci., 8 (1988) 1411-1424.

[19] Li, X-G., Somogyi, P., Tepper, J.M. and Buszáki, G., Axonal and dendritic arborization of an intracellularly labeled chandelier cell in the CA1 region of rat hippocampus, Exp. Brain Res., 90 (1992) 519-525.

[20] McBain, C.J., DiChiara, J. and Kauer, J.A., Activation of metabotropic glutamate receptors differentially affects two classes of hippocampal interneurons and potentiates excitatory synaptic transmission, J. Neurosci., 14 (1994) 4433-4445.

[21] Paxinos, G. and Watson, C., The rat brain in stereotaxic coordinates, 2nd ed., Academic Press, Sydney, 1986.

[22] Sik, A., Penttonen, M., Ylinen, A. and Buszáki, G., Hippocampal CA1 interneurons: an in vivo intracellular labeling study, J. Neurosci., 15 (1995) 6651-6665.

[23] Somogyi, P., Freund, T.F., Hodgson, A.J., Somogyi, J., Beroukas, D. and Chubb, I.W., Identified axo-axonic cells are immunoreactive for GABA in the hippocampus and visual cortex of the cat, Brain Res., 332 (1985) 143-149.

[24] Wouterlood, F.G., Saldana, E. and Witter, M.P., Projections from the nucleus reuniens thalami to the hippocampal region: Light and electron microscopic tracing study in the rat with the anterograde tracer Phaseolus vulgaris-leucoagglutinin, J. Comp. Neurol., 296 (1990) 179-203.

[25] Wouterlood, F.G. and Jorritsma-Byham, B., The anterograde tracer biotinylated dextran-amine: comparison with the tracer PHA-L in preparations for electronmicroscopy, J. Neurosci. Methods, 48 (1993) 75-87.

Chapter 6

NEUROTOXIC LESIONS OF THE THALAMIC REUNIENS OR MEDIODORSAL NUCLEUS IN RATS AFFECT NON-MNEMONIC ASPECTS OF WATERMAZE LEARNING.

Brain Struct Funct (2009) 213:329-342.

ABSTRACT

Rats with bilateral neurotoxic reuniens (RE), mediodorsal (MD), hippocampal (HIPP) or sham- (SH) lesions were tested in a standard watermaze task, together with unoperated rats. RE-rats and SH-controls readily learned to swim directly to a hidden platform. In contrast, MD-rats displayed a transient deficit characterized initially by thigmotaxis. Like in previous studies, HIPP-rats had long latencies throughout training and displayed more random swims than the other groups. In a memory probe test with the platform removed, SH- and RE-rats approached the correct location relatively directly but, whereas SH-controls persistently searched in the training quadrant, RE-rats switched to searching all over the pool. The MD-group swam in loops to the platform, but then displayed persistent searching in the training quadrant. The HIPP-group performed at chance. These distinct patterns indicate that, although their search strategies were different, RE-and MD-rats had acquired sufficient knowledge about the platform location and could recall information in the probe test. All groups performed well in a subsequent cue test with a visible platform, with RE-rats initially escaping faster than the SH- and HIPP-groups, and MD-rats improving from an initially poorer level of performance to control level. This indicates that there were no sensorimotor or motivational deficits associated with any of the lesions.

In conclusion, while the RE and MD nuclei seem not to be critical for the learning and memory of a standard watermaze task, they may contribute to non-mnemonic strategy shifting when animals are challenged in ways that do not occur during training.

INTRODUCTION

Diencephalic (thalamic) amnesia is characterized by deficits resembling those of medial temporal lobe (hippocampal) amnesia or prefrontal dysfunctions (for reviews, Rousseau 1994; Van der Werf et al. 2000, 2003). Thalamic midline nuclei are connected with either the medial temporal lobe, or the prefrontal cortex (PFC), or both. Therefore, thalamic amnesia may result from either 1) disconnecting the temporal and prefrontal systems at the thalamic level, or 2) the loss of specific thalamic contributions to these systems.

Recently, Cain et al. (2006) reported that the medial thalamus of the rat is essential for acquiring watermaze behavioral strategies. However, the role of individual thalamic nuclei is not yet clear. The aim of the present study was to investigate and compare the impact of reuniens (RE) and mediodorsal (MD) lesions upon spatial learning and memory, with their impact on the flexible use of task-relevant strategies.

In the rat, both RE and MD are heavily, and reciprocally connected with the medial (m) PFC (Krettek and Price 1977; Groenewegen 1988; Vertes 2002, 2004; McKenna and Vertes 2004; Rotaru et al. 2005; Vertes et al. 2006). RE is also heavily connected with hippocampal structures (Herkenham 1978; Wouterlood et al. 1990; Dolleman-van der Weel and Witter 1996, 2000). It has been proposed that RE is an important link between mPFC and the hippocampus (Vertes 2006; Vertes et al. 2007), and may play a role in a large-scale limbic network engaged in mnemonic processes (Braak and Braak 1991; Vann et al. 2000). Flämig and Klingberg (1978) conducted, to our knowledge, the only previous behavioral study of RE-lesioned rats. Surprisingly, they reported that learning and memory of a conditioned avoidance task in a Y-maze was unaffected by destruction of RE.

A specific role of MD in cognitive processes is still controversial (e.g., Markowitsch 1982; Stokes and Best 1990; Peinado-Manzano and Pozo-Garcia 1996; Chauveau et al. 2005; Mitchell et al. 2007a, b). Lesions of MD can result in deficits that resemble those of mPFC lesions (Hunt and Aggleton 1991; McAlonan et al. 1993). Hunt and Aggleton (1998) suggest that acquisition deficits arising from MD lesions may be due to disruption of processes that interact with task performance (e.g., strategy learning, response flexibility), rather than with mnemonic processes.

In the present study, we examined whether RE and/or MD input is essential for the functioning of the hippocampal/mPFC memory systems, or for the normal behavioral expression of information acquired by these memory systems. Based on changes in c-fos activity, Vann et al. (2000) suggested that RE plays a role in working memory. However, c-fos imaging yields complex and sometimes controversial results (e.g., Aggleton et al. 2000; Bertaina-Anglade et al. 2000; Jenkins et al. 2003; Santin et al. 2003), while the precise role of c-fos in memory formation and the underlying mechanisms remain

unknown (Herrera and Robertson 1996; Zhang et al. 2002). Therefore, we used a conventional (reference memory) watermaze task, known to be sensitive to dysfunction of both the hippocampal and prefrontal systems, with each system mediating different aspects of watermaze learning. Whereas the hippocampal formation is engaged in the spatial aspects of learning and memory, the role of mPFC in this task appears to involve behavioral flexibility and the execution of spatial strategies, rather than encoding or storage of spatial information (De Bruin et al. 1994; Ragozzino et al, 1999a, b; De Bruin et al. 2001; Lacroix et al. 2002; Passetti et al. 2002; Ragozzino et al, 2003). Therefore, a RE lesion, that could affect both the hippocampal and mPFC memory systems, might be expected to cause a mixture of hippocampal (spatial learning/memory) and mPFC (behavioral flexibility/strategy learning) related impairments. An MD lesion, likely affecting primarily mPFC memory functions more specifically, was expected to result in an acquisition deficit in behavioral flexibility when task conditions change.

MATERIALS AND METHODS

Subjects

We used 42 male Lister hooded rats (weighing 280-400 gm at the time of surgery) from breeding stock in the University of Edinburgh. They were housed individually in plastic cages with ad libitum access to food and tap water at all times. A normal 12 h dark/light cycle was maintained, with all behavioral training and testing carried out in the light phase.

All experiments described here have been conducted in accordance with the European Communities Council Directive (1986), and with the approval of the local Animal Experimentation Committee of the VU University medical centre, Amsterdam. All efforts were made to minimize any suffering and the number of animals used.

Surgery

Restricted lesions in RE and MD were created by injecting small amounts of ibotenic acid (IBO, Cambridge Research Biochemicals, Cambridge, UK) into the respective nuclei, resulting in local cell death with minimal damage to fibres of passage (Köhler and Schwarcz 1983). The animals were anaesthetized with tribromethanol (10 ml/kg, i.p.) and placed in a Kopf stereotaxic frame. The skull was exposed and burr holes were made to accommodate injections of IBO (10 mg/ml phosphate buffered saline), applied with the use of a glass micropipette that was glued to the end of the needle of a 1 µl Hamilton syringe. IBO was infused slowly in a volume of 0.10 µl per injection site over a period of 10 min. After leaving the pipette in situ for another 5 min, to ensure diffusion of IBO

into the target structure, it was slowly retracted. Stereotaxic coordinates were derived from Paxinos and Watson (1986), aligned with respect to bregma (Br.), the midline of the superior sagittal sinus (medial-to-lateral, ML), and the surface of the dura (dorsal-to-ventral, DV). Because RE is a very small nucleus, difficult to lesion selectively, the RE-group contained more animals than the other groups. Rats in the RE-group (n=12) received bilateral injections in the rostral as well as in the caudal part of the nucleus (rostral RE, Br, - 1.80 mm; ML, 2.0 mm, at an angle of 15 degrees in the coronal plane; DV, 6.9 mm; caudal RE, Br, -2.30 mm; ML, 1.4 mm, at an angle of 10 degrees in the coronal plane; DV, 7.0 mm). Rats in the MD-group (n=6) received bilateral injections that were placed according to the RE coordinates, except that at the rostral injection sites the pipette was lowered to a depth of 4.8 mm, and at the caudal sites to 5.2 mm. Sham (SH)-controls underwent anaesthesia/surgical procedures that were similar to those for RE- and MD-rats, except that 1) in the SH-hippocampus-group (SH-HIPP, n=6) a needle was lowered through the dorsal hippocampus, a structure implicated in spatial memory (Moser et al 1993; Moser and Moser 1998), but no IBO was injected (i.e., a procedure which causes mechanical hippocampal damage that is identical to that necessarily caused in creating the RE and MD lesions), and 2) in the SH-dura-group (n=6) only the dura was cut.

Under certain training conditions, animals with damage to the hippocampal formation are capable of acquiring a place response (Whishaw and Tomie 1997; Gerlai et al. 2002; Pouzet et al. 2002). Therefore, a HIPP-group was added to establish the degree of hippocampal related spatial impairment under our training and test conditions. Rats in the HIPP-group (n=6) received 26 injections along the entire longitudinal axis of the hippocampus, completely destroying the hippocampal formation (procedure previously described by Jarrard 1989). Following surgery all rats were allowed two weeks recovery.

It is well known that anaesthetics can affect cognitive functions (e.g., Culley et al. 2003, 2004; Baxter et al. 2008). There are no specific reports whether or not tribromethanol affects learning and memory, but it can have various side effects (e.g., Zeller et al. 1998; Thompson et al. 2002; Meyer and Fisch 2005; Lieggi et al. 2005) which may affect behavior. In order to control for any effect of the anaesthesia/surgical procedure, unoperated rats (UNOP-group, n=6) were added as well.

Behavioral training and testing procedures

All rats were well handled before being trained in a 2 m open-field watermaze, filled with water (25 +/- 1 ºC) made opaque by the addition of powdered milk. An escape platform (10 cm in diameter) was placed at a fixed position in one of the quadrants of the pool, arbitrarily designated NE, NW, SE and SW. The pool was situated in a diffusely

illuminated room, containing prominent extra-maze cues to enable the rats to learn the platform's location. A curtain hanging from the ceiling could be drawn around the pool to obscure the room cues. A video camera mounted on the ceiling was connected with a computerized tracking system (HVS image analyser and Acorn Archimedes computer; Hawk Track, Watermaze program) to monitor and store the swim paths of the animals for off-line analysis. In general, at the start of each trial the rat was placed in the pool facing the wall, and then allowed to search for the submerged (i.e., 1 cm below the water surface) escape platform for a maximum of 120 s. The rat remained on the platform for 30 s, after which the next trial was run immediately. If the animal failed to escape from the water within 120 s, it was guided to the platform by hand. After finishing the trials, the animals were dried and warmed before being returned to their home cage.

Pre-training (day 1) consisted of 4 swim trials to familiarize the animals with the general procedures of the task (e.g., searching the pool, climbing onto the platform). Spatial learning was prevented by drawing curtains around the pool to exclude room cues. The starting point and position of the submerged platform differed per trial.

Spatial training (days 2-4) consisted of 18 trials (i.e., 6 trials/day), with room cues visible. For each group, half of the rats were trained to find the submerged platform at a fixed location in the NE quadrant, for the other half of the group the platform was located in the SW quadrant. The starting points (N, S, E or W) were varied in a semi-random way across trials.

A single *transfer (or "memory probe") test* (day 5) was run during which the escape platform was removed from the pool, and the rats allowed a free swim of 60 s. Performance in the probe test is generally accepted to reflect the rats' memory for the learned platform location, which is behaviorally shown as the proportion of time spent in the training quadrant.

Finally, a *cue test* consisting of 4 trials (day 6) was given with the platform visible (i.e., 1 cm above the water surface), and curtains surrounding the pool to exclude extra maze cues. This test served a dual purpose: i) due to a change in task demands, performance in the cue test will reflect the animals' ability to switch to a different problem solving strategy, and ii) the cue test is assumed to reflect the occurrence of any gross sensorimotor and/or motivational deficiencies.

Data collection and statistics

The behavior of the animals was analyzed off-line, focusing upon performance during the spatial training (submerged platform), the transfer test (platform removed), and the

cue test (visible platform). Parameters computed by the software were: escape latency, path length, swim speed, quadrant time, and directionality. We also performed an analysis of the swim paths recorded during the spatial training phase. This was done in order to examine whether the different groups made use of particular search strategies. Distinctive swim paths were categorized according to a system that was modified and expanded after Whishaw and Jarrard (1995). We distinguished the following categories: A) edge, B) random, C) circle, D) loop, E) direct, F) indirect, and G) near miss (for typical examples, see figure 4a). Accordingly, the 18 swim paths of each rat were blindly analyzed by an observer and attributed to these categories. Whenever a path showed multiple characteristics, it was attributed to the category that dominated the swim. For each group the number of swim paths per category per group across spatial training trials was used for statistical analyses. For representation in a figure, the scores were normalized by expressing them as percentage of swims belonging to a particular category.

Statistical analyses used an ANOVA for overall comparison, and Dunnett's test for comparison between groups. Statistical packages used were ALICE (System for manipulating and analyzing multidimensional data) and SPSS (Statistical Package for the Social Sciences). Significance was set at $p<0.05$.

Variability in performance within groups may be related to differences in lesion size (including inadvertent damage to adjacent structures). This possibility was investigated using the Spearman rank correlation coefficient. During the training trials the most efficient strategies are the relatively direct (E+F+G) routes. These strategies are associated with short escape latencies, and clearly reflect the rats' knowledge of the hidden platform location. Therefore, the ranking of smallest to largest lesion was compared to the ranking of most to least frequent use of E+F+G paths (i.e., best to worst performance, respectively). In addition, the ranking according to lesion size was compared to ranking of the highest to lowest training quadrant time in the transfer test (i.e., a memory measure).

Histology

At the end of the experiment, the animals received an injection of sodium pentobarbital (Euthatal, 200 mg/kg, i.p.) and were transcardially perfused with physiological saline and 10% formalin fixative. The brains were removed and stored in fixative for at least 24 hours. Subsequently, they were cryoprotected in 2% dimethyl sulfoxide and 20% glycerin in phosphate buffer. On a freezing microtome the brain tissue was cut to either coronal (RE-, MD-, SH- and UNOP-groups) or horizontal (HIPP-group) sections of 40 um thickness. Every fifth section was Nissl-stained with cresyl violet or thionin, and analyzed to determine the extent of the IBO lesions in the RE-, MD-, and HIPP-rats, and

the mechanical damage caused by the sham-lesioning procedure in the SH-HIPP and SH–dura controls.

RESULTS

Histological observations

The brains of the RE-rats (n=12) showed that RE was completely destroyed in all but one animal. In the latter case, approximately 90% of the nucleus was lesioned, leaving only its very rostral part in tact. In 2 rats the lesion was strictly confined to RE. In the other 10 animals, due to leakage of IBO along the injection tract, the extent of the lesion ranged from a minor involvement of the rhomboid, anteromedial, interanteromedial and gelatinosus nuclei (n=4), to a moderate damage in the midline including a part of the intralaminar central medial nucleus (n=6). In most cases, some mechanical damage was noticed in MD. Commonly, the tract through the overlying hippocampus was accompanied by a restricted cell death and gliosis in CA1 and/or the dentate gyrus (not illustrated). Because the variability of RE lesions was relatively small, and later statistical analysis did not show any correlation between lesion size and behavior (see below), all animals were included in the RE-group. The extent of the smallest and largest RE-lesion is schematically represented in Fig. 1a. A photomicrograph of a lesion confined to RE, taken approximately at the level illustrated in Fig. 1a (bregma -2.30), is shown in Figs. 2a, a'.

In all MD-rats (n=6) the lesion was centred in MD. The estimated extent of the MD-lesions, however, varied from 50-80% of the nucleus. In all cases, the most caudal part of MD appeared to be intact. In 3 rats, the intralaminar and paratenial/paraventricular nuclei showed partial cell loss as well. In all animals but the one with the smallest MD-lesion, we noticed some damage in the anterodorsal nucleus. Inadvertent hippocampal damage along the injection tract (not illustrated) was comparable to that noticed in the RE-group. The extent of the smallest and largest MD-lesion is schematically represented in the Fig. 1b. A photomicrograph of the largest MD lesion, taken approximately at the level illustrated in Fig. 1b (bregma -2.30), is shown in Figs. 2b, b'.

The brains of all HIPP-rats (n=6) displayed a massive destruction of the dentate gyrus, the CA fields and the subiculum, although in three cases partial (restricted) sparing of neurons in the intermediate hippocampal region was noticed. In addition, the entorhinal cortex showed minor damage in all but one animal, whereas the neocortex (i.e., mainly visual areas overlying the hippocampus) was moderately, but comparably damaged in all cases (not illustrated). In all 6 rats, the thalamus was unaffected. Figure 1c shows the

extent of the smallest and largest HIPP-lesion. Photomicrographs in Fig. 2c illustrate the smallest (i.e., least complete) HIPP lesion at a dorsal (left) and ventral (right) level, approximately at interaural 6.90 and 3.90, respectively (see Fig. 1c).

The brains of the rats in the SH-dura- (n=6) and SH-HIPP-groups (n=6), showed minimal cell loss and/or some gliosis in the superficial cortical layers. In the SH-HIPP-group we also noticed restricted damage in CA1 and the dentate gyrus, directly bordering the needle tract (not illustrated).

Based on these histological observations, none of the lesioned animals had to be excluded.

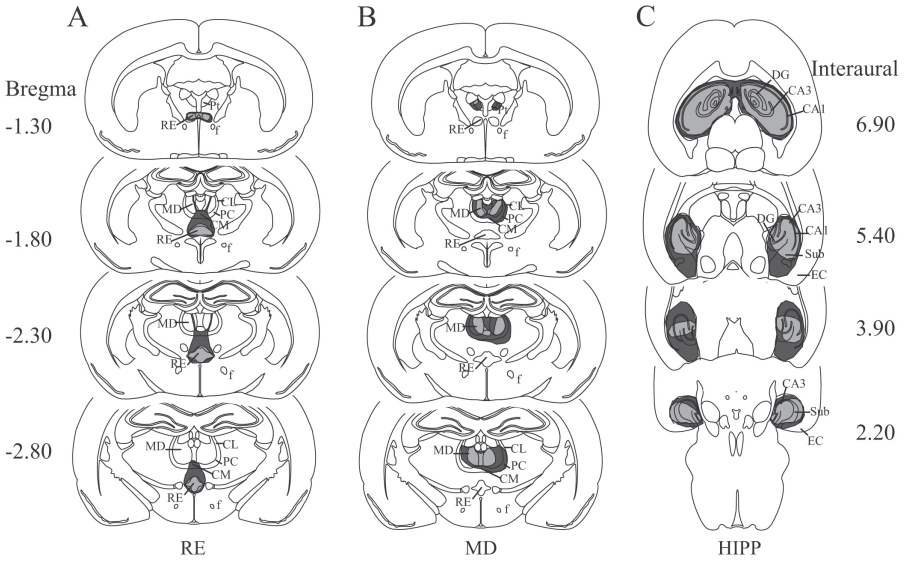

Fig. 1. Schematical representation of smallest (light grey area) and largest lesions (dark grey area) of RE (a), MD (b), and HIPP (c) in a series of sections at four rostro-to-caudal (a, b), and dorsal-to-ventral levels (c) through the rat brain. Abbreviations: CA1-3 = cornu ammonis field 1-3; CL = centrolateral nucleus; CM = centromedial nucleus; DG = dentate gyrus; EC = entorhinal cortex; f = fornix; HIPP = hippocampal formation; MD = mediodorsal nucleus; PC = paracentral nucleus; Pt = paratenial nucleus; RE = nucleus reuniens; Sub = subiculum.

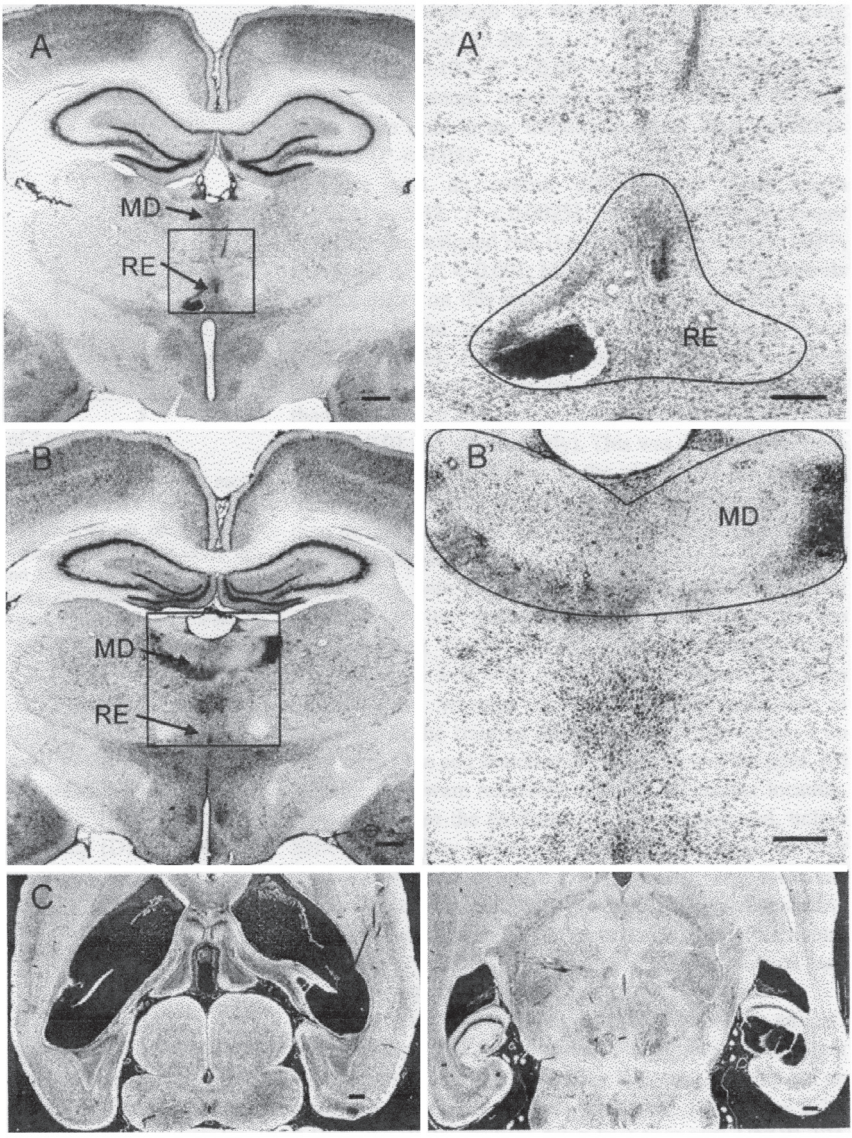

Fig. 2. Photomicrographs of representative examples of Nissl-stained coronal sections illustrating a RE-lesion (a), a MD-lesion (b), and horizontal sections of a HIPP-lesion (c) at a dorsal (left) and a ventral level (right). Boxed areas in (a) and (b) are shown at higher magnification in (a') and (b'), respectively. The lines delineate the lesioned area. In case of HIPP-lesions (c), almost all of the structure has disappeared, similar to what is shown for the left side of the (bilateral) RE-lesion (a, a'). On the right side of the RE-lesion, as well as within the (bilaterally) lesioned MD (b,b') there are numerous Nissl-stained astrocytes present, yet only a few if any surviving neurons can be detected.

Behavioral observations

During training and testing, it became clear that one of the SH-dura rats displayed a serious visual deficit. Therefore, this rat was excluded from the behavioral analyses, reducing the SH-dura-group to n=5. All the remaining rats swam in a normal way, using the adult swimming posture. They had no difficulty climbing onto the platform, or using it as a suitable means of escape from the water.

Spatial training

Because of a lack of significant differences between the SH-HIPP- and SH-dura-groups (data not shown), they were combined into a single sham lesion (SH) group (n=11). Thus, all following analyses dealt with five groups, i.e., UNOP-rats, and RE-, MD-, HIPP-, and SH-lesioned animals.

The 18 training trials (days 2-4) were grouped into 6 blocks of 3 trials each (i.e., 2 blocks/day) and analyzed for escape latencies. Figure 3 shows the mean escape latencies of the five groups across blocks. An ANOVA revealed that these latencies differed significantly between groups {$F(4,36)=5.87$, $p<0.001$}, blocks {$F(5,180)=44.38$, $p<0.001$} and there was a significant groups x blocks interaction {$F(20,180)=2.17$, $p<0.005$)}, the latter likely due to the long latencies of the MD- and HIPP-groups. Subsequently, we compared group latencies per block, showing that on day 1 (block 2) the SH-group had longer escape latencies than the UNOP-group ($p<0.05$). This small, yet significant difference (as well as a significant difference in transfer test performance, see below) indicated an effect of the anaesthesia/surgical procedure that should be taken into account when analyzing the performance of the three lesion groups. Therefore, the SH- and UNOP-rats were not combined into one group. In all analyses, the behavior of the RE-, MD-, and HIPP-lesioned rats was compared to that of the SH-controls, as well as to each other; comparisons between lesion groups and UNOP-rats were not conducted.

Further comparison of group latencies per block revealed that, compared to SH-controls, the MD-group displayed longer latencies on the first block of each training day (block 1: $p< 0.005$; block 3: $p<0.05$; block 5: $p<0.025$), whereas the RE-group was not significantly different from the SH-group (block 3: $0.10>p>0.05$, trend). The HIPP-group had long latencies throughout spatial training (HIPP vs. SH; blocks 2 and 3, $0.10>p>0.05$, trend; block 4, $p<0.001$; block 5, $p<0.05$; block 6, $p<0.005$). A comparison of the three lesion groups revealed that the RE-group was significantly faster than the MD- and HIPP-groups (RE vs. MD: blocks 1 and 4, $p<0.005$, $p<0.05$, respectively; RE vs. HIPP: blocks 4, 5, and 6, $p<0.05$, $p<0.05$, and $p<0.0025$, respectively).

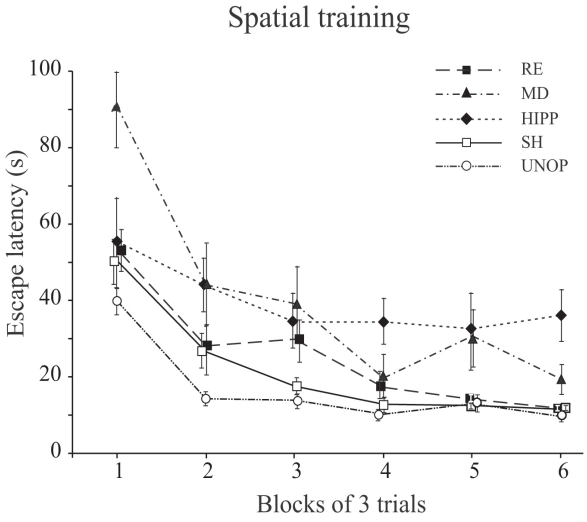

Fig. 3. Mean escape latencies against blocks of three trials each during spatial training, days 2-4. The SH-control group had significantly longer latencies than the UNOP-group on block 2. Notice the long latencies of the MD-group during the first block of each day (i.e. blocks 1, 3, and 5), and their improvement on the second block of each day. The HIPP-group displayed long latencies throughout training, whereas the RE-group was not significantly different from the SH-controls.

There was no overall difference in swim speed {mean speed (m/sec) +/- SEM: RE, 0.29 +/- 0.003; MD, 0.29 +/-0.01; HIPP, 0.30 +/-0.01; SH, 0.28 +/-0.01; UNOP, 0.29 +/-0.01}, and the analysis of path length therefore closely followed the pattern of the analysis of escape latencies (data not shown).

The different lesions had a distinct effect on the use of distinctive swim strategies. In Fig. 4a, the categories A-G (see Materials and methods) are illustrated by examples of swim paths that show the range for each category. The differential use of these search strategies across the 3 days of spatial training is represented in Fig. 4b. The UNOP-, SH-control, and RE-rats quickly learned to swim a direct path (E) to the hidden escape platform. In contrast, particularly on the first block of trials of each day, the MD-group persistently used the least efficient strategy {i.e., edge swimming (A), associated with long latencies, see also Fig. 3}, with little chance to encounter the submerged platform. Their behavior gradually changed to swimming loops (D) and indirect routes (F). The HIPP-group displayed the highest percentage of random paths (B) throughout training, although these were often alternated with circle swims (C) and loops (D). An ANOVA revealed that group differences in the overall use of strategies reached significance for the categories edge (A) {$F(4,36)=6.89$, $p<0.001$}, random (B) {$F(4,36)=9.39$, $p<0.001$}, loop (D) {$F(4,36)=2.65$, $p<0.05$}, and direct (E) {$F(4,36)=7.14$, $p<0.001$}. Further analyses

showed that both SH-controls and RE-rats swam significantly more direct routes (E) than the MD- and HIPP-groups (SH vs. MD, $p< 0.005$, and SH vs. HIPP, $p<0.001$; RE vs. MD, $p<0.05$, and RE vs. HIPP, $p<0.0025$, respectively). In turn, the MD-group displayed significantly more edge (A) swims than the SH-, RE- and HIPP-rats (MD vs. SH, $p<0.005$; MD vs. RE, $p<0.001$; MD vs. HIPP, $p<0.025$), whereas the HIPP-group swam more random paths (B) than the SH-, RE-, and MD-animals (HIPP vs. SH, $p<0.001$; HIPP vs. RE, $p< 0.001$; HIPP vs. MD, $p<0.005$). Regarding the category loop (D), differences were only found between the three lesion groups, i.e., the RE-group swam less loops than the MD- and HIPP-groups (RE vs. MD, $p< 0.01$; RE vs. HIPP, $p<0.005$).

Transfer test

To examine the rats' memory for the learned platform location, a single trial was run during which the platform was removed from the pool. An overall ANOVA showed a highly significant difference across groups in the distribution of time spent in the four quadrants {$F(3,108)=34.08, p<0.001$} and a group x quadrant interaction {$F(12,108)=3.35, p<0.001$}. A separate analysis was conducted of time spent in the training quadrant only, showing a highly significant difference between groups {$F(4,36)=7.45$, $p<0.001$}. Further analyses revealed that the SH-controls spent significantly less time in the training quadrant than the UNOP-group ($p<0.05$). The HIPP-group was significantly impaired (SH vs. HIPP, $p<0.05$), with a training quadrant time indistinguishable from chance level (see Fig. 5, quadrant time expressed in percentages: 26.7% +/- 3.9; chance=25%). Comparison of the SH- versus the RE- and MD-groups did not reach significance, although the RE-group (see Fig. 5, training quadrant time of 33.2% +/- 1.7) performed rather poorly (SH vs. RE, $0.10>p>0.05$, trend). Comparison of the three lesion groups, however, revealed that the RE-rats spent more time in the training quadrant than the HIPP-animals ($p<0.05$).

There was an overall difference in path length {$F(4,36)=5.42$, $p<0.0025$}, with significantly longer paths for the lesioned rats (i.e., versus SH-controls: HIPP, $p<0.05$; RE, $p<0.001$; MD, $p<0.05$). The SH-controls did not differ on this measure from the UNOP-rats (n.s.). We also found an overall difference in swim speed {$F(4,36)=4.24$, $p<0.01$)}, with the three lesion groups swimming slightly faster (mean speed 0.33 +/-0.02 m/sec) than the SH- and UNOP-rats (mean speed 0.29 +/-0.01, and 0.28 +/-0.01 m/sec, respectively). This was due to the animals of control groups dwelling in the vicinity of the platform location, frequently stopping and turning around, rather than differences in the actual speed of swimming when it occurred. Figure 5 also shows, for each group, a representative swim path during the transfer test, with the initial approach of the platform location represented by the thickened line. UNOP- and SH-rats swam relatively direct (i.e., using E+F+G paths) to the learned platform location, yet whereas the UNOP-group

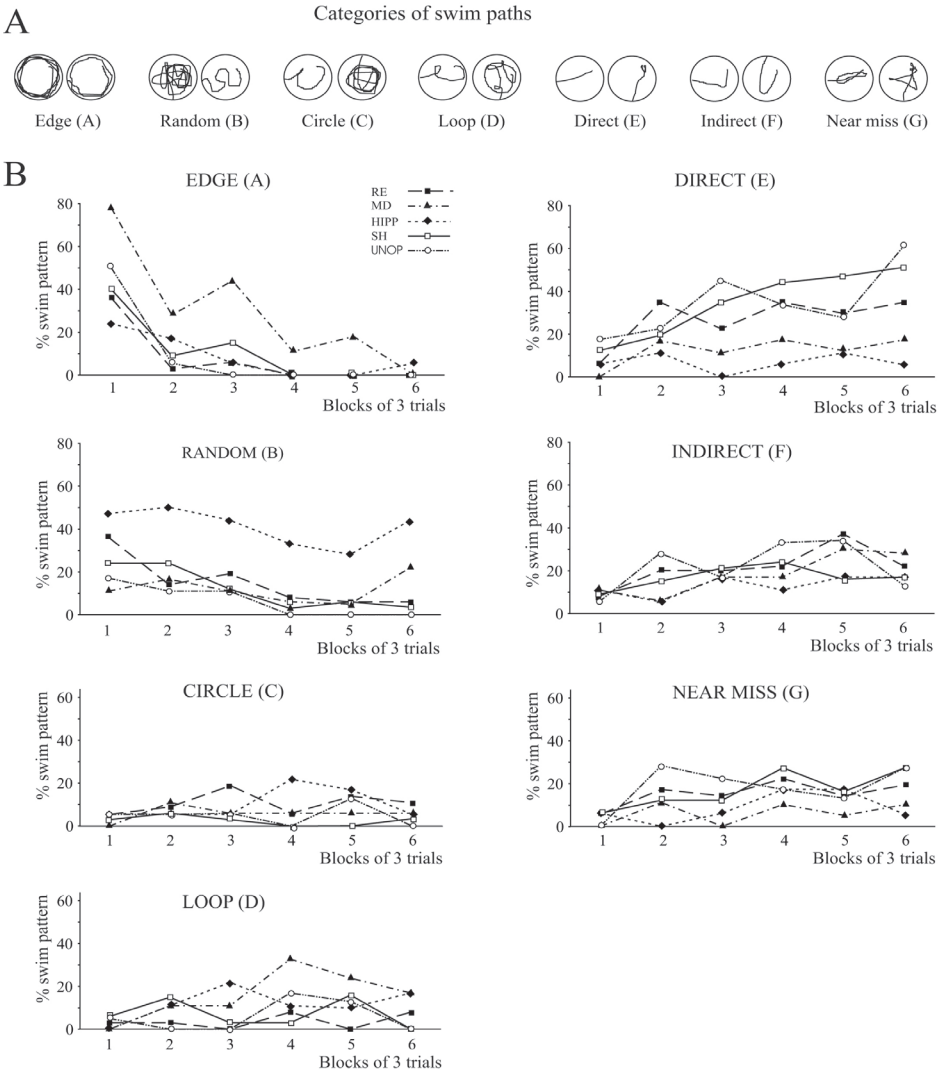

Fig. 4. Search strategies during spatial training. (a) Examples of swim paths illustrating the range for each category. (b) Differential use of strategies across blocks of trials, as indicated by the percentage of swim patterns used by the five groups. The exceptional display of edge swimming by MD-rats closely followed their pattern of escape latencies (see figure 2). HIPP-rats displayed the most random swims throughout training, whereas SH-, RE- and UNOP-rats rapidly learned to swim mainly direct paths, occasionally alternated with near miss and indirect paths.

persisted in searching in the training quadrant, the SH-group gave up after some time and searched in a larger area of the pool. All RE-rats also swam relatively direct to the correct location. However, when the platform was not encountered, unlike SH-controls, they carried on swimming to search all over the pool. In contrast, MD-rats swam mainly in loops to the platform and then, once they got there, continued searching in the training quadrant. HIPP-rats swam mainly in circular paths, often crossing the former platform location and possibly using the wall as reference for their search.

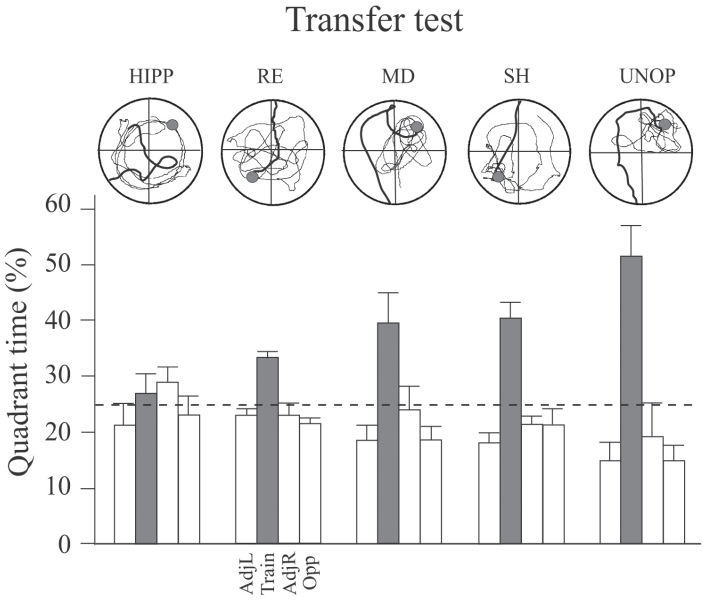

Fig. 5. Distribution of time (expressed as mean percentage) spent in the 4 quadrants of the pool during the transfer test, with emphasis on time spent in the training quadrant (grey bars; the dotted line represents chance level = 25 %). The statistical analysis of actual quadrant time revealed that the SH-group spent significantly less time in the training quadrant than the UNOP-group, but more time than the HIPP-group. Despite of rather poor performance in the RE-group, RE- and MD-rats were not significantly different from SH-controls. For each group a representative swim path is shown; grey dots mark the location of the (removed) platform. The initial part of the swim path is marked by the thickened line, illustrating the differences in approaches of the learned location between groups. While UNOP-rats persistently searched in the training quadrant, SH-rats also searched at the correct location, but gave up after some time and then swam over a larger area of the pool. RE-rats swam directly towards the learned location, but when the platform was not encountered they switched immediately to searching all over the pool. MD-rats swam in loops towards the platform and then kept searching that area. HIPP-rats mainly circled at a certain distance from the pool wall, often crossing the former platform location.
Abbreviations: train=training quadrant; adj/l=adjacent left; adj/r=adjacent right, opp=opposite.

We also included an assessment of whether the animals were heading for the platform 50 cm away from their starting point (i.e., a directionality measure). A trend but no significant difference was observed {$F(4,36)=2.23$, $0.10>p>0.05$; ranking from best to worst: UNOP, SH, RE, MD, HIPP}, reflecting that the UNOP- and SH-rats showed a tendency to be heading more accurately for the platform location than the lesion groups. Unfortunately, variability in this measure makes it difficult to secure clear cut results for "heading-direction".

Cue test

A final test with a visible platform was conducted on day 6 (see Fig. 6). An ANOVA showed a significant difference in overall latencies for groups {$F(4,159)=3.70$, $p<0.01$}, trials {$F(3,108)=6.56$, $p<0.001$}, and a groups x trials interaction ($F(12,108)=1.96$, $p<0.05$). No differences were found between SH-controls, UNOP-, and HIPP-groups. However, RE-rats had significantly shorter latencies than SH- and HIPP-rats on trial 2 (RE vs. SH, $p<0.01$; RE vs. HIPP, $p<0.05$). The extremely long latencies of the MD-group (trials 1 and 2, likely due to swimming mainly loops and indirect paths, ignoring the visible platform and searching for the hidden one) failed to reach significance versus both the SH-controls and the RE-group ($0.10>p>0.05$, trend), most likely due to the rather large variation. Therefore, cue test analyses were also conducted using non-parametrical tests. This yielded similar statistical results (data not shown).

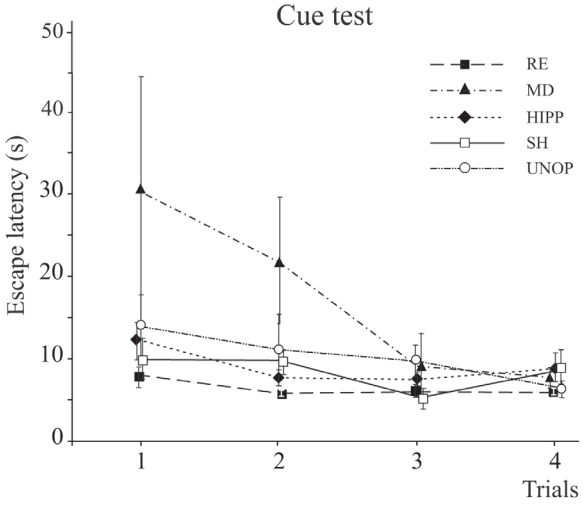

Fig. 6. Mean escape latencies in the cue test (visible platform). The RE-group displayed significantly shorter latencies than the SH- and HIPP-groups on trial 2. The initially poor performance of the MD-group (trials 1 and 2) did not reach significance versus the SH-controls, and showed a trend ($0.10>p>0.05$) versus the RE-group.

Relation between lesion size and behavior

On the acquisition measure (i.e., use of E+F+G paths, associated with short escape latencies) there was no significant correlation with lesion size for any of the lesion groups (RE, rs= - 0.2; MD, rs=0.7; HIPP, rs= - 0.3), although there was a slight tendency towards a positive correlation in the MD-group. On the memory measure (i.e., training quadrant time in the transfer test) we found also no significant correlation (RE, rs= - 0.4; MD, rs= - 0.4; HIPP, rs= - 0.6). The lack of significant correlations largely reflects the lesions being relatively complete as intended.

DISCUSSION

We examined the role of the thalamic RE and MD nuclei in spatial learning and memory, using a conventional (reference memory) watermaze task. The main findings were that 1) RE-lesioned rats, like SH-controls, rapidly learned the task and swam mainly direct paths to the invisible platform, whereas MD-lesioned rats displayed a transient acquisition deficit, characterized initially by perseveration of edge-swims; 2) when the platform was removed (probe test), RE-lesioned rats swam relatively direct to the correct location, but did not stop and search locally. Instead, they carried on swimming around the pool. In contrast, MD-lesioned rats swam in loops to the former platform location, but then displayed persistent searching in the training quadrant; 3) when task conditions were altered (visible platform test), RE-lesioned rats escaped initially faster than SH-controls. MD-lesioned rats, however, initially displayed abnormalities in the paths taken to the escape target, but eventually recognized and used the visible platform as refuge. These findings argue against a role for RE and MD in mnemonic aspects of spatial learning, but instead point to a role in the behavioral strategy used to express spatial information and the flexibility with which environmental changes can be accommodated.

Effects of anaesthesia/surgical procedure

Small, yet significant differences between the SH- and UNOP-groups were found in two measures: 1) SH-rats had longer escape latencies in the early phase of spatial training, and 2) in the transfer test they spent less time in the training quadrant. These differences between the SH- and UNOP-groups imply that (at least with our training and test protocols) sustained tribromethanol anaesthesia and/or a sham lesion is sufficient to bring about a partially impaired performance that should be taken into account when examining lesion effects. Therefore, in this study the SH-group (and not the UNOP-, or a combined

SH/UNOP-group) was considered the appropriate control for comparison with the RE-, MD-, and HIPP-groups.

Effects of hippocampal versus thalamic lesions

In line with previous reports, HIPP-rats were considerably impaired and their escape latencies improved only slightly across training trials. Most conspicuous was that, unlike any of the other groups, HIPP-rats displayed random swims throughout acquisition that, eventually, often alternated with circling. These strategies also characterized the search of the HIPP-group in the transfer test. Despite of a clear navigational deficit, their "platform biased circling" suggested that they had acquired at least some knowledge of the (now absent) platform location, but probably used distance to the wall to guide their search rather than integrating spatial cues in a normal way (e.g., Morris et al. 1990; Whishaw and Jarrard 1995; Whishaw and Tomie 1997; Pouzet et al. 2002). These results show that the present behavioral protocol is sensitive to dysfunction of the hippocampal formation.

We therefore expected that depriving the entorhinal-hippocampal circuitry from RE input, which had been hypothesized to be crucial for (hippocampal-related) spatial aspects of watermaze learning, should in principle be detected with our training and test procedure. Surprisingly, the RE-group displayed no lasting acquisition deficit. They learned the task rapidly and, like SH-controls, swam with significantly more direct routes to the platform than the HIPP- and MD-groups. This indicates that RE afferents to the hippocampal formation may not be critical for either hippocampal-related spatial learning and memory encoding, or the learning of mPFC-related procedural strategies necessary for a reference memory watermaze task.

In contrast, the MD-group displayed a transient acquisition deficit with a specific pattern of long latencies, which closely matched the pattern of gradual decline in edge-swims across blocks of training. Overall, the MD-group showed significantly more swimming at the edge (sometimes referred to as "thigmotaxis") than the SH-, RE- and HIPP-groups. Commonly, thigmotaxis is only noticed during the first trials after introduction (i.e., in this study during pretraining) to the pool. When this behavior appears ineffective, the animals will subsequently explore the pool by a rapid shift to other strategies (e.g., random, loop) and after only a few spatial training trials they have learned to swim directly to the correct location. Figure 4 clearly illustrates that, in the first block of spatial training, MD-rats displayed far more edge swimming than the four other groups. This suggests that, in this respect, the MD-group had experienced a less beneficial effect from the pretraining trials than the other lesion and control groups. Obviously, perseveration of edge-swims will hamper the rate of learning, because MD-rats will then have less chance to encounter

the hidden platform and so be rewarded for a more efficient navigational strategy. It has been reported that mice with large MD lesions extending into CM, showed an increased fear reactivity (elevated-plus maze, GO/NOGO temporal alternation tasks, Chauveau et al. 2005). The latter authors suggested that a cognitive deficit of MD-lesioned animals (characterized by a difficulty in maintaining an alternation rule with procedural variance) could stem primarily from increased fear. We cannot entirely rule out the possibility that the acquisition deficit of the MD-group was (partly) due to an increased level of fear. Yet, to our knowledge, there are no reports available to support the idea that MD-lesioned rats can display "fear for the open field", which otherwise might have contributed to the presently observed perseveration of edge-swims. The long latencies of the MD-group during acquisition do not, however, necessarily imply a spatial learning/memory deficit (see below).

Despite of normal acquisition, the RE-group spent an unexpectedly poor percentage of their time in the training quadrant in the transfer test. In the initial phase of the test, all RE-rats (like SH-controls) approached the correct location relatively direct, indicative of normal learning and memory. Unlike SH-controls, when the platform was not encountered at the learned location, RE-rats continued swimming and searched all over the pool. This resulted in a training quadrant time that was poor, yet significantly better than that of the HIPP-group, which displayed mainly "platform biased circling" throughout the transfer test and performed at chance (see above). The rapid behavioral shift by the RE-group indicates an interference with the suppression of strategy shifting, which normally occurs whenever the most effective strategy has been selected, and resembles old observations by Flämig and Klingberg (1978). They found no effects of a RE lesion on learning of a conditioned avoidance task in a Y-maze, but noticed a significant increase in anticipatory responses. In contrast to our initial hypothesis, we found no major hippocampal related effects of a RE lesion on standard reference memory watermaze learning. There is the possibility that RE is more involved in working memory (e.g., see Vann et al. 2000), and thus other tests would be more suited to investigate the effects of a RE lesion.

The initial phase of the transfer test of MD-rats was characterized by mainly loops to the platform location. This was followed by persistent searching in the training quadrant, which indicates that MD-rats had learned and remembered the correct location. Therefore, it is unlikely that the transient acquisition deficit of MD-rats was due to a deficit in learning of the task or in using spatial cues, but was initially due to perseveration of an ineffective strategy (i.e., thigmotaxis) and an impaired ability to switch to other strategies. In this respect, it might also be of interest to examine the effects of RE- and MD-lesions, using the egocentric response-learning version of the watermaze task (e.g., De Bruin et al. 2001).

The differences in the ability/readiness of RE- and MD-lesioned rats to use strategies in

a flexible way (i.e, RE-rats being very flexible; MD-rats showing perseveration), is further supported by our observations in the cue test. Specifically, there were no indications that any of the lesion groups had sensorimotor deficiencies, or a lack of motivation. HIPP-rats showed normal latencies compared to controls, as in previous studies (Morris et al. 1982; Pouzet et al. 2002), whereas RE-rats initially escaped onto the platform even faster than SH- and HIPP-rats. Although the MD-group had long latencies in the first trials, likely because of searching for the submerged platform, it improved across trials to the control level. In the cue test, the only intramaze cue is the platform itself, and therefore this task is far less demanding than the hidden platform version. Nevertheless, it still requires a shift in strategy, prompts the suppression of the previously learned response (i.e., swim to the hidden platform), and the subsequent selection and facilitation of a new response (i.e., swim to the visible platform). Our results show that the RE-lesioned rats were very fast in shifting to a new strategy, whereas the MD-group was probably hampered by initial perseveration of the previously learned hidden platform response. This suggests that, in contrast to RE-lesioned rats, MD-lesioned rats have a problem in shifting strategy when task demands are altered (Kolb et al. 1982; Hunt and Aggleton 1998; Block et al. 2007).

An important qualification is that the observed effects of a HIPP-, RE- and MD-lesion appear to be primarily due to destruction of the intended area, with little if any contribution of (minor) damage in adjacent structures. In comparison, our RE lesions were more selective than the RE lesions in the study by Flämig and Klingberg (1978). Our MD lesions also appeared more selective than the ones described in previous reports (e.g., Kolb et al. 1982; Beracochea et al. 1989; Hunt and Aggleton, 1991; Cain et al. 2006), although a straightforward comparison is hampered by the use of different lesion methods (e.g., chemical, electrolytic, radiofrequency). We failed to observe any significant correlations between lesion size and two measures of performance – acquisition (as indicated by the use of relatively direct E+F+G paths, associated with short escape latencies), and memory for the platform location (as indicated by training quadrant time). It should, however, be mentioned that the variation in extent of the MD lesions showed a slight tendency towards a correlation on the acquisition measure (i.e., strategy use). This might suggest that rats with small MD lesions (in this study involving approximately 50 % of MD) were more likely to use relatively direct strategies (i.e., suggestive for somewhat less perseverative behavior) than rats with larger, near complete MD lesions.

Behavioral considerations in relation to thalamic-mPFC connectivity

Afferents from RE were shown to exert excitatory effects on mPFC, similar to actions in the hippocampus, and thus RE appears to be in a position to influence and/or coordinate

activity in both systems (Dolleman-van der Weel et al. 1997; Di Prisco and Vertes 2006). RE neurons, receiving input from mPFC, have been shown to innervate the hippocampal CA1 area. Hence, RE is assumed to represent a critical link in a HIPP-mPFC-RE-HIPP neuronal circuitry (Vertes et al. 2007). Based on its strong reciprocal connections with the mPFC, and the involvement of the latter area in behavioral flexibility, it has been suggested that RE might play a role in the selection of appropriate responses (Vertes 2006; Vertes et al. 2006). The present observations, however, show that rats in which RE is destroyed can rapidly display the most appropriate response in both the hidden platform and cue tasks. Therefore, it is unlikely that RE plays a critical role in response selection - at least not in these two tasks. Instead, our results yield a clue towards involvement of RE in shifting strategy. Kolb et al. (1982, 1983) showed that mPFC-lesioned rats can fail to learn a watermaze task. Later studies revealed that mPFC lesions can also cause no impairment in spatial navigation, but rather result in a deficit of behavioral flexibility (De Bruin et al. 1994, 2001; Lacroix et al. 2002). In various tests, it has been shown that destruction or inactivation of mPFC does not affect learning and memory per se, but impairs the animals' ability to shift strategy, or rule out inappropriate strategies when task demands are changed or environmental conditions are altered (Ragozzino et al. 1999a, b; Delatour and Gisquet-Verrier 2000; Dias and Aggleton 2000; Lacroix et al. 2002; Sullivan and Gratton 2002; Passetti et al. 2002; Ragozzino et al. 2003; Ragozzino 2007). At first sight, in relation to RE-mPFC connectivity, these reports seem contradictory to the rapid strategy shifting by RE-rats. However, abnormalities in behavioral flexibility can be due to a disturbance of mPFC-mediated inhibitory response control (e.g., Carli et al. 2006), resulting in 1) a failure of response inhibition, expressed as inappropriate anticipatory or "impulsive" responding (see RE-lesioned rats), or 2) a failure to suppress/inhibit an aimless repetition of an irrelevant response/strategy, causing perseverative behavior (see MD-lesioned rats). Therefore, the ability of RE-lesioned rats to shift very rapidly from one strategy to another might have been due to the loss of excitatory RE input to mPFC, causing a dysfunction of inhibitory response control mechanisms (e.g., Murphy et al. 2005). Hence, RE may be of importance for the suppression of (inappropriate/impulsive) strategy shifting, thereby opposing the role of MD (see below).

Only a few studies have used the watermaze to examine the effects of a MD or medial thalamus lesion on spatial learning (e.g., Kolb et al. 1982; Cain et al. 2006). A comparison with previous observations, however, is complicated due, for instance, to considerable differences in actual extent of the lesions, as well as in training and test procedures. In general, the deficits in watermaze performance resulting from a MD lesion resemble those seen after an mPFC lesion, i.e., little or no effect on spatial aspects, but slower acquisition and/or reversal training which is proposed to reflect deficits in non-mnemonic processes as reduced behavioral flexibility (e.g., Lacroix et al. 2002). Perseveration by

MD-rats, or an impaired ability to shift strategies, appears to be a consistent finding and has been reported in various studies with a variety of tests (e.g., Stokes and Best 1988; Beracochea et al. 1989; McAlonan et al. 1993; Hunt and Aggleton 1991, 1998). Interestingly, Floresco and Grace (2003) showed that MD-to-mPFC projection neurons exert a complex excitatory-inhibitory gating action over hippocampal input in PFC. They suggested that MD-PFC input may be able to facilitate or inhibit hippocampal input upon mPFC, supposedly permitting strategy switching by facilitation of a new strategy while at the same time inhibiting a previously learned one. More recently, using a cross-maze-based strategy set-shifting task, Block et al. (2007) provided further evidence that MD is involved in behavioral flexibility. Inactivation of MD disturbed the flow of information from MD to mPFC, resulting in a perseverative deficit. They proposed that the MD-to-mPFC connection may play a role in signaling the need to shift strategy. In turn, the mPFC then serves to suppress perseveration of the now irrelevant response. Our results appear in accordance with such a role for MD in strategy shifting.

In summary, while HIPP-lesions cause the expected deficit in the protocol used here, lesions of RE or MD did not prevent the learning or later memory of a standard watermaze task. Instead, lesions of RE or MD appeared to affect the normal flexible use of search strategies and/or the flexibility with which a change in task conditions can be accommodated (i.e., a RE lesion resulted in very flexible/impulsive behavior; a MD lesion caused perseverative behavior). Based on the present observations, and in line with described modulatory effects of RE-to-PFC and MD-to-PFC projections (Floresco and Grace 2003; Di Prisco and Vertes 2006), we hypothesize that RE and MD play opposing roles in non-mnemonic processes like strategy shifting, or in general aspects of behavioral flexibility. This hypothesis should be tested in future research, using electrophysiological methods and additional appropriate behavioral tests.

Acknowledgements

We thank J.P.C. de Bruin and F.H. Lopes da Silva for stimulating discussions and reading of an early version of the manuscript. We gratefully acknowledge the technical assistance by the technicians at the Department of Neuroscience, University of Edinburgh, at the Department of Anatomy, VU University Medical Centre, Amsterdam, and at the Netherlands Institute for Neuroscience, Amsterdam. We also thank G. Docter for helping with statistical analyses, and D. de Jong for processing of the microphotographs. This work was supported by NWA Grant 90-20 from the Graduate School for Neurosciences Amsterdam.

REFERENCES

Aggleton JP, Vann SD, Oswald CJ, Good M (2000) Identifying cortical inputs to the rat hippocampus that subserve allocentric spatial processes: a simple problem with a complex answer. Hippocampus 10:466-474

Baxter MG, Murphy KL, Crosby G, Culley DJ (2008) Different behavioral effects of neurotoxic dorsal hippocampal lesions placed under either isoflurane or propofol anesthesia. Hippocampus 18:245-250

Beracochea DJ, Jaffard R, Jarrard LE (1989) Effects of anterior or dorsomedial thalamic ibotenic lesions on learning and memory in rats. Behav Neural Biol 51:364-376

Bertaina-Anglade V, Tramu G, Destrade C (2000) Differential learning-stage dependent patterns of c-Fos protein expression in brain regions during the acquisition and memory consolidation of an operant task in mice. Eur J Neurosci 12:3803-3812

Block AE, Dhanji H, Thompson-Tardif SF, Floresco SB (2007) Thalamic-prefrontal cortical-ventral striatal circuitry mediates dissociable components of strategy set shifting. Cereb Cortex 17:1625-1636

Braak H, Braak E (1991) Alzheimer's disease affects limbic nuclei of the thalamus. Acta Neuropathol 81:261-268

Cain PP, Boon F, Corcoran M. (2006) Thalamic and hippocampal mechanisms in spatial navigation: a dissociation between brain mechanisms for learning how versus learning where to navigate. Behav Brain Res 170:241-256

Carli M, Baviera M, Invernizzi RW, Balducci C (2006) Dissociable contribution of 5-HT 1A and 5-HT 2A receptors in the medial prefrontal cortex to different aspects of executive control such as impulsivity and compulsive perseveration in rats. Neuropsychopharmacol 31:757-767

Chauveau F, Celerier A, Ognard R, Pierard C, Beracochea D (2005) Effects of ibotenic acid lesions of the mediodorsal thalamus on memory: relationship with emotional processes in mice. Behav Brain Res 156:215-223

Culley DJ, Baxter M, Yukhananov R, Crosby G (2003) The memory effects of general anesthesia persist for weeks in young and aged rats. Anesth Analg 96:1004-1009

Culley DJ, Baxter MG, Yukhananov R, Crosby G (2004) Long-term impairment of acquisition of a spatial memory task following isoflurane-nitrous oxide anesthesia in rats. Anesthesiology 100:309-314

De Bruin JPC, Sanchez-Santed F, Heinsbroek RPW, Donker A, Postmes P (1994) A behavioral analysis of rats with damage to the medial prefrontal cortex using the Morris water maze: evidence for behavioral flexibility, but not for impaired spatial navigation. Brain Res 652:323-333

De Bruin JP, Moita MP, de Brabander HM, Joosten RN (2001) Place and response learning

of rats in a Morris water maze: differential effects of fimbria fornix and medial prefrontal cortex lesions. Neurobiol Learn Mem 75:164-178

Delatour B, Gisquet-Verrier P (2000) Functional role of rat prelimbic-infralimbic cortices in spatial memory: evidence for their involvement in attention and behavioral flexibility. Behav Brain Res 109:113-128

Dias R, Aggleton JP (2000) Effects of selective excitotoxic prefrontal lesions on acquisition of nonmatching- and matching-to-place in the T-maze in the rat: differential involvement of the prelimbic-infralimbic and anterior cingulate cortices in providing behavioral flexibility. Eur J Neurosci 12:4457-4466

Di Prisco GV, Vertes RP (2006) Excitatory actions of the ventral midline thalamus (rhomboid/reuniens) on the medial prefrontal cortex in the rat. Synapse 60, 45-55

Dolleman-van der Weel MJ, Witter MP (1996) Projections from the nucleus reuniens thalami to the entorhinal cortex, hippocampal field CA1, and the subiculum in the rat arise from different populations of neurons. J Comp Neurol 364:637-650

Dolleman-van der Weel MJ, Lopes da Silva FH, Witter MP (1997) Nucleus reuniens thalami modulates activity in hippocampal field CA1 through excitatory and inhibitory mechanisms. J Neurosci 17:5640-5650

Dolleman-van der Weel MJ, Witter MP (2000) Nucleus reuniens thalami innervates gamma aminobutyric acid positive cells in hippocampal field CA1 of the rat. Neurosci Lett 278:145-148

Flämig R, Klingberg F (1978) Die Beteiligung thalamischer Kerne an der Ausbildung bedingter Fluchtreflexe der Ratte. IV. Läsionen des nucleus reuniens. Acta Biol Med Germ 37:1779-1782

Floresco SB, Grace AA (2003) Gating of hippocampal-evoked activity in prefrontal cortical neurons by inputs from the mediodorsal thalamus and ventral tegmental area. J Neurosci 23:3930-3943

Gerlai RT, NcNamara A, Williams S, Philips HS (2002) Hippocampal dysfunction and behavioral deficit in the water maze in mice: An unresolved issue? Brain Res Bull 57:3-9

Groenewegen HJ (1988) Organization of the afferent connections of the mediodorsal nucleus in the rat, related to the mediodorsal-prefrontal topography. Neurosci 24:379-431

Herkenham M (1978) The connections of the nucleus reuniens thalami: evidence for a direct thalamohippocampal pathway. J Comp Neurol 177:589-609

Herrera DG, Robertson HA (1996) Activation of c-fos in the brain. Prog Neurobiol 50:83-107

Hunt PR, Aggleton JP (1991) Medial dorsal thalamic lesions and working memory in the rat. Behav Neur Biol 55:227-246

Hunt PR, Aggleton JP (1998) Neurotoxic lesions of the dorsomedial thalamus impair acquisition but not the performance of delayed matching to place by rats: a deficit in shifting response rules. J Neurosci 18:10045-10052

Jarrard LE (1989) On the use of ibotenic acid to lesion selectively different components of the hippocampal formation. J Neurosci Meth 29:251-259

Jenkins TA, Amin E, Harold GT, Pearce JM, Aggleton JP (2003) Distinct patterns of hippocampal formation activity associated with different spatial tasks: a Fos imaging study in rats. Exp Brain Res 151:514-523

Köhler C, Schwarcz R (1983) Comparison of ibotenate and kainate neurotoxicity in rat brain: a histological study. Neuroscience 8:819-835

Kolb B, Pittman K, Sutherland RJ, Whishaw IQ (1982) Dissociation of the contributions of the prefrontal cortex and dorsomedial thalamic nucleus to spatially guided behavior in the rat. Behav Brain Res 6:365-378

Kolb B, Sutherland RJ, Whishaw IQ (1983) A comparison of the contributions of the medial frontal and parietal association cortex to spatial localization in rats. Behav Neurosci 97:13-27

Krettek JE, Price JL (1977) The cortical projections of the mediodorsal nucleus and adjacent thalamic nuclei in the rat. J Comp Neurol 171:157-192

Lacroix I, White I, Feldon J (2002) Effect of excitotoxic lesions of rat medial prefrontal cortex on spatial memory. Behav Brain Res 133:69-81

Lieggi CC, Artwohl JE, Leszcynski JK, Rodriguez NA, Fickbohm BL, Fortmann JD (2005) Efficacy and safety of stored and newly prepared tribromoethanol in ICR mice. Contemp Top Lab Anim Sci 44:17-22

Markowitsch HJ (1982) Thalamic mediodorsal nucleus and memory: a critical evaluation of studies in animal and man. Neurosci Biobehav Rev 6:351-380

McAlonan GM, Robbins HE, Everitt BJ(1993) Effects of medial dorsal thalamic and ventral pallidal lesions on the acquisition of a conditioned place preference: further evidence for the involvement of the ventral striatopallidal system in reward-related processes. Neuroscience 52:605-620

McKenna JT, Vertes RP (2004) Afferent projections to nucleus reuniens of the thalamus. J Comp Neurol 480:115-142

Meyer RE, Fisch RE (2005) A review of tribromoethanol anesthesia for production of genetically engineered mice and rats. Lab Anim (NY) 34:47-52

Mitchell AS, Browning PG, Baxter MG (2007a) Neurotoxic lesions of the mediodorsal nucleus of the thalamus disrupt reinforcer devaluation effects in rhesus monkeys. J Neurosci 27:11289-11295

Mitchell AS, Baxter MG, Gaffan D (2007b) Dissociable performance on scene learning and strategy implementation after lesions to magnocellular mediodorsal thalamic

nucleus. J Neurosci 31:11888-11895

Morris RGM, Garrud P, Rawlins JNP (1982) Place navigation impaired in rats with hippocampal lesions. Nature 297:681-683

Morris RGM, Schenk F, Tweedie F, Jarrard LE (1990) Ibotenate lesions of hippocampus and/or subiculum: dissociating components of allocentric spatial learning. Eur J Neurosci 2:1016-1028

Moser E, Moser M-B, Andersen P (1993) Spatial learning impairment parallels the magnitude of dorsal hippocampal lesions, but is hardly present following ventral lesions. J Neurosci 13:3916-3925

Moser M-B, Moser EI (1998) Distributed encoding and retrieval of spatial memory in the hippocampus. J Neurosci 15:7535-7542

Murphy ER, Daley JW, Robbins TW (2005) Local glutamate receptor antagonism in the rat prefrontal cortex disrupts response inhibition in a visuospatial attentional task. Psychopharmacol 179:99-107

Passetti F, Chudasama Y, Robbins TW (2002) The frontal cortex of the rat and visual attentional performance: dissociable functions of distinct medial prefrontal subregions. Cereb Cortex 12:1254-1268

Paxinos G, Watson C (1986) The rat brain in stereotaxic coordinates. Academic Press, Sidney

Peinado-Manzano MA, Pozo-Garcia R (1996) Retrograde amnesia in rats with dorsomedial thalamic damage. Behav Brain Res 80:177-184

Pouzet B, Zhang WN, Feldon J, Rawlins JN (2002) Hippocampal lesioned rats are able to learn a spatial position using non-spatial strategies. Behav Brain Res 133:279-291

Ragozzino ME, Detrick S, Kesner RP (1999a) Involvement of the prelimbic-infralimbic areas of the rodent prefrontal cortex in behavioral flexibility for place and response learning. J Neurosci 19:4585-4594

Ragozzino ME, Wilcox C, Raso M, Kesner RP (1999b) Involvement of rodent prefrontal cortex subregions in strategy switching. Behav Neurosci 113:32-41

Ragozzino ME, Kim J, Hasser D, Minniti N, Kiang C (2003) The contribution of the rat prelimbic-infralimbic areas to different forms of task switching. Beh Neurosci 117:1054-1065

Ragozzino ME (2007) The contribution of the medial prefrontal cortex, orbitofrontal cortex, and dorsomedial striatum to behavioral flexibility. Ann N Y Acad Sci 1121:355-375

Rotaru DC, Barrionuevo G, Sesack SR (2005) Mediodorsal thalamic afferents to layer III of the rat prefrontal cortex: synaptic relationships to subclasses of interneurons. J Comp Neurol 490:220-238

Rousseau M (1994) Amnesia following limited thalamic lesions. In Delacour, J. (ed.),

The memory system of the brain. World Scientific Publishers, Singapore, New Yersey, London, Adv. Series Neurosci. 4, pp. 241-277

Santin LJ, Aguirre JA, Rubio S, Miranda R, Arias JL (2003) c-Fos expression in supramammillary and medial mammillary nuclei following spatial reference and working memory tasks. Physiol Behav 78:733-739

Stokes KA, Best PJ (1988) Mediodorsal thalamic lesions impair radial maze performance in the rat. Beh Neurosci 102:294-300

Stokes KA, Best PJ (1990) Mediodorsal thalamic lesions impair "reference" and "working" memory in rats. Physiol Behav 47:471-476

Sullivan RM, Gratton A (2002) Behavioral effects of excitotoxic lesions of ventral medial prefrontal cortex in the rat are hemisphere-dependent. Brain Res 927:69-79

Thompson JS, Brown SA, Khurdayan V, Zeynalzadedan A, Sullivan PG, Scheff SW (2002) Early effects of tribromoethanol, ketamine/xylazine, pentobarbital, and isoflurane anesthesia on hepatic and lymphoid tissue in ICR mice. Comp Med 52:63-67

Van der Werf YD, Witter MP, Uylings HBM, Jolles J (2000) Neuropsychology of infarctions in the thalamus: a review. Neuropsychologia 38:613-627

Van der Werf YD, Jolles J, Witter MP, Uylings HB (2003) Contributions of thalamic nuclei to declarative memory functioning. Cortex 39:1047-1062

Vann SD, Brown MW, Aggleton JP (2000) Fos expression in the rostral thalamic nuclei and associated cortical regions in response to different spatial memory tests. Neuroscience 101:983-991

Vertes RP (2002) Analysis of projections from the medial prefrontal cortex to the thalamus in the rat, with emphasis on nucleus reuniens. J Comp Neurol 442:163-187

Vertes RP (2004) Differential projections of the infralimbic and prelimbic cortex in the rat. Synapse 51:32-58

Vertes RP (2006) Interactions among the medial prefrontal cortex, hippocampus and midline thalamus in emotional and cognitive processing in the rat. Neuroscience 142:1-20

Vertes RP, Hoover WB, do Valle AC, Sherman A, Rodriquez JJ (2006) Efferent projections of reuniens and rhomboid nuclei of the thalamus in the rat. J Comp Neurol 499:768-796

Vertes RP, Hoover WB, Szigeti-Buck K, Leranth C (2007) Nucleus reuniens of the midline thalamus: link between the medial prefrontal cortex and the hippocampus. Brain Res Bull 71:601-609

Whishaw IO, Jarrard LE (1995) Similarities vs. differences in place learning and circadian activity in rats after fimbria-fornix section or ibotenate removal of hippocampal cells. Hippocampus 5:595-604

Whishaw IQ, Cassel J-C, Jarrard LE (1995) Rats with fimbria-fornix lesions display a place response in a swimming pool: a dissociation between getting there and knowing where. J Neurosci 15:5779-5788

Whishaw IQ, Tomie J-A (1997) Perseveration on place reversals in spatial swimming pool tasks: further evidence for place learning in hippocampal rats. Hippocampus 7:361-370

Wouterlood FG, Saldana E, Witter MP (1990) Projections from the nucleus reuniens thalami to the hippocampal region: light and electron microscopic tracing study in the rat with the anterograde tracer Phaseolus vulgaris-Leucoagglutinin. J Comp Neurol 296:179-203

Zeller W, Meier G, Burki K, Panoussis B (1998) Adverse effects of tribromoethanol as used in the production of transgenic mice. Lab Anim 32:407-413

Zhang J, McQuade JM, Vorhees CV, Xu M (2002) Hippocampal expression of c-fos is not essential for spatial learning. Synapse 46:91-99

Chapter 7

INTERACTION OF NUCLEUS REUNIENS AND ENTORHINAL CORTEX PROJECTIONS IN HIPPOCAMPAL FIELD CA1 OF THE RAT.

Brain Struct Funct (2017) 222:2421-2438

ABSTRACT

The nucleus reuniens (RE) and entorhinal cortex (EC) provide monosynaptic excitatory inputs to the apical dendrites of pyramidal cells and to interneurons with dendrites in stratum lacunosum-moleculare (LM) of hippocampal field CA1. However, whether the RE and EC inputs interact at the cellular level is unknown. In this electrophysiological in vivo study, low frequency stimulation was used to selectively activate each projection at its origin; field excitatory postsynaptic potentials (fEPSPs) were recorded in CA1. We applied 1) paired pulses to RE or EC, 2) combined paired pulses to RE and EC, and 3) simultaneously paired pulses to RE/EC. The main findings are that: a) stimulation of either RE or EC evoked subthreshold fEPSPs, displaying paired pulse facilitation (PPF), b) subthreshold fEPSPs evoked by combined stimulation did not display heterosynaptic PPF, and c) simultaneous stimulation of RE/EC resulted in enhanced subthreshold fEPSPs in proximal LM displaying a nonlinear interaction.

CSD analyses of RE/EC-evoked depth profiles revealed a nonlinear enlargement of the 'LM sink-radiatum source' configuration and the appearance of an additional small sink-source pair close to stratum pyramidale, likely reflecting (peri)somatic inhibition. The nonlinear interaction between both inputs indicates that RE and EC axons form synapses, at least partly, onto the same dendritic compartments of CA1 pyramidal cells. We propose that low frequency activation of the RE-CA1 input facilitates the entorhinal-hippocampal dialogue, and may synchronize the neocortical-hippocampal slow oscillation which is relevant for hippocampal-dependent memory consolidation.

INTRODUCTION

Neural processing in the hippocampus and anatomically related cortices is crucial for learning and memory (Wang and Morris 2010). Activity of neurons in hippocampal field CA1 is generally considered to reflect the convergence of input from CA3 in stratum radiatum and direct EC-CA1 input in stratum lacunosum moleculare (LM; Brun et al. 2002; Remondes and Schuman 2002, 2003). Field CA1 is, however, also targeted by an excitatory subcortical input that arises from the ventral thalamic midline nucleus reuniens (RE), of which the terminal distribution of axons in LM overlaps with the terminations of the direct EC-CA1 projection (Herkenham 1978; Wouterlood et al. 1990; Dolleman-van der Weel et al. 1994; Vertes et al. 2006). In the rat, both RE and EC inputs affect the level of hippocampal excitability by targeting pyramidal cells as well as several types of local interneurons with a dendritic tree in LM (Wouterlood et al. 1990; Colbert and Levy 1992; Desmond et al. 1994; Empson and Heinemann 1995; Levy et al. 1995; Dolleman-van der Weel et al. 1997; Dolleman-van der Weel and Witter 2000; Bokor et al. 2002; Klausberger 2009). Surprisingly, the overlap of RE and EC projections in CA1 and its relevance for hippocampal functioning has received little attention.

Recent studies have indicated the importance of RE for cognitive processes, such as behavioral flexibility, strategy shifting, inhibitory response control, associative learning, memory consolidation, working memory, fear memory, memory generalization, goal-directed navigation, and executive behaviors (Dolleman-van der Weel et al. 2009; Davoodi et al. 2011; Eleore et al. 2011; Hembrook et al. 2011; Kincheski et al. 2012; Loureiro et al. 2012; Cholvin et al. 2013; Hallock et al. 2013; Prasad et al. 2013; Varela et al. 2013; Wheeler et al. 2013; Xu and Sűdhof 2013; Duan et al. 2015; Griffin 2015; Ito et al. 2015; Layfield et al. 2015; Anderson et al 2016; Prasad et al. 2017). This variety of memory-related behaviors has also been associated with the interplay between the medial prefrontal cortex (mPFC) and the hippocampus (Jin and Maren 2015). The mPFC receives a dense hippocampal input, but lacks a direct return projection to the hippocampus (Sesack et al. 1989; Jay and Witter 1991; Hoover and Vertes 2007). Since RE is reciprocally connected with mPFC (Vertes 2002; Vertes et al. 2006) the partially collateralized RE projections to CA1 and mPFC (Hoover and Vertes 2012; Varela et al. 2014), taken together with a closed RE-CA1-subiculum-RE circuit (Dolleman-van der Weel et al. 1997), have led to the notion that RE is an important link between mPFC and the hippocampus. Cognitive alterations resulting from experimental manipulations of RE (i.e., lesions, reversible inactivation, optogenetic stimulation) support the idea that, instead of specifically affecting the functioning of either the mPFC or hippocampus, RE is mainly involved in orchestrating the flow of hippocampal-mPFC information, likely by modulating the coupling between both structures (Di Prisco and Vertes 2006; Saalmann

2014; Cassel and Pereira de Vasconcelos 2015; Ito et al. 2015; Pereira de Vasconcelos and Cassel 2015). The EC has also been shown to play a role in various cognitive tasks (e.g., Skelton and McNamara 1992; Sybirska et al. 2000; Remondes and Schumann 2004; Brun et al. 2008; Deshmukh and Knierim 2011; Suh et al. 2011; Wilson et al. 2013; Chao et al. 2016; Anderson et al 2016), and both RE and EC appear to be involved in the consolidation of hippocampal-dependent memories (Remondes and Schumann 2004; Loureiro et al. 2012). Moreover, Xu and Sűdhof (2013) have proposed that the cooperativity between RE-CA1 and EC-CA1 input may reduce the threshold for synaptic plasticity, and thus for the incorporation of entorhinal-transmitted neocortical information in hippocampal memory representation and subsequent long-term storage.

As yet, the function of the RE input in hippocampal field CA1 is not fully understood. In particular, a possible interaction of the RE-CA1 and EC-CA1 pathways in LM has never been investigated. In the present study we therefore addressed whether an interaction of RE and EC projections in CA1 occurs, and its functional relevance. An important prerequisite to examine the convergence of RE-CA1 and EC-CA1 inputs is to be able to selectively activate each system. This has been achieved in this acute in vivo study in which we stimulated the RE-CA1 and lateral EC-CA1 projections at their respective origins, and recorded depth profiles of field potentials in CA1. Because both the RE and lateral EC inputs appear most excitable during low frequency activation or slow oscillations (<1 Hz) (Dolleman-van der Weel et al. 1997; Schall et al. 2008), we recorded depth profiles of field potentials in CA1 elicited by a range of low frequency stimulation protocols. Current-source-density (CSD) analyses of the evoked depth profiles were performed to provide the sites of synaptic activity in CA1. Our results show that co-activation of RE and EC inputs yields a major nonlinear enhancement of the elicited field potentials and associated sink in proximal LM. This indicates that RE and EC axons form synapses, at least partly, onto the same dendritic compartments of pyramidal cells. Moreover, the obtained CSD profiles reveal an additional (peri)somatic inhibition evoked by simultaneous activation of the RE-CA1 and EC-CA1 projections. We conclude that the influence of RE and EC on neural processing in CA1 is strongly enhanced during coincident low frequency activation of both inputs. We further suggest that the RE-CA1 input has the ability to synchronize the hippocampal and mPFC slow oscillations, which is important for memory consolidation.

MATERIALS AND METHODS

We used 15 male Wistar rats (Harlan CPB, Zeist, The Netherlands), weighing 275-375 g. Under halothane anesthesia the trachea was intubated. The rat was then placed in a

stereotaxic apparatus and throughout the experiment artificially ventilated by a mixture of O2 and N2O with 1% halothane. Body temperature was maintained using a heating pad. All experiments were carried out according to the guidelines laid down by the European Communities Council Directive (1986), and with the approval of the local Animal Experimentation Committee of the VU University Medical Centre, Amsterdam. All efforts were made to minimize any suffering and the number of animals used.

Based on anatomical observations (Dolleman-van der Weel et al. 1994), the stimulation sites in RE and lateral EC (layer III) were chosen such that the corresponding terminations would be optimally placed to overlap with the recording sites in stratum LM of CA1 (see Fig. 1). Stereotaxic coordinates were derived from Paxinos and Watson (1986). They were zeroed at bregma (Br), the midline of the midsagital sinus, and the dura surface. Stimulation electrodes in RE were lowered into position at an angle of 15 degrees in the coronal plane using the following coordinates: Br., -1.80 mm; lateral (L) 2.0 mm; ventral (V), 7.0 mm. The coordinates for stimulation electrodes in lateral EC were: Br., -5.8 mm; L, 6.0 mm; V, 6.1 mm, and for recording electrodes in CA1: Br., -5.6 mm, L, 4.3 mm; V, 1.6-3.1 mm. To prevent the exposed tissue from dehydration, the brain surface was covered with warm paraffin oil.

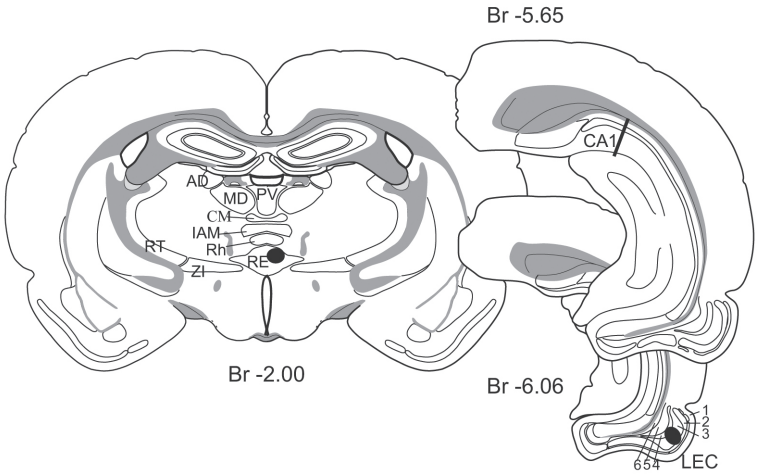

Fig. 1 Schematical representation of the stimulation sites in RE and lateral EC (black dots) and the recording site in CA1 (black line). Figures are modified from Swanson (1998). Abbreviations: RE = nucleus reuniens; AD = anterodorsal nucleus; MD = mediodorsal nucleus; PV = paraventricular nucleus; CM = central medial nucleus; IAM = interanteromedial nucleus; Rh = rhomboid nucleus; ZI = zona incerta; RT = reticular nucleus; CA1 = hippocampal field CA1; LEC = lateral entorhinal cortex; 1-6 = EC layers 1-6; Br = bregma.

Stimulation protocols and data acquisition

The RE-CA1 input elicits larger amplitude responses during stimulation at low frequencies (0.1-2 Hz) than at theta frequency (4-10 Hz) (Dolleman-van der Weel et al. 1997), and the lateral EC-CA1 projection also shows greater excitability during slow oscillations (< 1 Hz) than during oscillations in the theta range (Schall et al. 2008). Therefore, we choose low frequency (< 1 Hz) stimulation of RE and EC inputs to investigate their combined influence on neural excitability in CA1. Electrical stimulation of RE and EC was performed using an electrode array of three stainless steel wires (diameter 60 μm, insulated except the tip) that were obliquely arranged. This electrode array was positioned in RE, covering the rostro-caudal extent of the nucleus; within the EC it was predominantly aimed at layer III. To optimize evoked responses, stimulation of RE and EC was varied between different pairs of the electrode array. The standard stimulation protocol consisted of monopolar paired pulses of equal strength and duration [0.2 ms; interpulse interval (IPI) 100 ms, unless stated otherwise; intensity 350-650 μA; 0.13 Hz]. The first stimulus of a pair is referred to as the conditioning pulse, the second one as the test pulse. Protocols for combined stimulation of the RE-CA1 and EC-CA1 projections consisted of an RE-EC stimulation sequence (IPI 50 ms; occasionally IPI 25 ms) and/or a RE-EC-RE-EC sequence of stimuli (IPI range 25-100 ms), occasionally vice versa starting with EC stimulation. Simultaneous RE/EC stimulation consisted of standard paired pulses (IPI 100 ms) applied to each input structure. Whenever response latencies differed, the RE and EC stimulations were timed such that the peaks of the conditioning RE- and EC-evoked fEPSPs coincided. For nearby inputs onto neocortical pyramidal cells, Nettleton and Spain (2000) have reported that two synaptic events, occurring within a 5 ms time window, were integrated as coinciding events. Therefore, we occasionally timed RE and EC stimulations such that the peaks of their respective responses had a 4 ms delay.

CA1 depth profiles of fEPSPs were obtained using an array of six equally spaced stainless steel wires (diameter 60 μm, insulated except the tip; inter-electrode distance 250 μm; n=12), arranged in the same plane. To obtain depth profiles for CSD analyses (n=3), we used a specially constructed probe of 18 electrodes (stainless steel wires, diameter 60 μm, insulated except the tip; electrode heart-to-heart distance, 100 μm, along the sloping side of the probe, see Fig. 4F), tightly glued together in the same plane. Both types of recording probes were cut at an angle of approximately 30 degrees (Dolleman-van der Weel et al., 1997). They covered the depth of CA1 from the deep cortical layer/white matter down to the hippocampal fissure, or just into the dentate gyrus. The shape of these electrode arrays allowed for recordings approximately perpendicular to the curved longitudinal axis of the hippocampus, i.e., corresponding to the orientation of the apical dendrites of the pyramidal cells (see Figs. 1, 4F). Evoked field potentials were amplified

and digitized by way of an interface (CED 1401 plus) connected to a personal computer. They were sampled at a rate of 5000/sec, averaged (n = 32), and stored for off-line analysis.

Off-line analysis

Characteristics of CA1 fEPSPs were studied in laminar depth profiles. Response latencies were defined as the time from the onset of the stimulus artefact to the peak of the conditioning response. Paired pulse facilitation (PPF) was expressed as the ratio between test response amplitude/conditioning response amplitude. PPF was calculated for field potentials recorded in stratum LM, representing the summed active synaptic processes. Statistical analyses of heterosynaptic PPF, evoked by combined RE and EC stimulation and recorded with a six-electrode probe, were done with an ANOVA; significance was set at $p< 0.05$. In addition, the amplitude of conditioning responses in LM elicited by simultaneous RE/EC activation were compared with responses elicited by single RE or EC stimulation.

One-dimensional CSD analyses (Freeman and Nicholson, 1975) show estimates of the local trans-membrane currents, resulting from the excitatory and inhibitory synaptic inputs. We made a two-step CSD analysis of the recorded CA1 depth profiles according to the formula:

$$CSD(h) = \left[\frac{\emptyset(h-\Delta h) - 2 * \emptyset(h) + \emptyset(h+\Delta h)}{(\Delta h)^2}\right] * \sigma h$$

in which CSD(h) = current source density at depth h, $\phi(h)$ = averaged field potential at depth h, Δh = depth interval (100 μm), and σ_h = conductivity in the direction of the track, here assumed to be constant. Spontaneous activity (i.e., recorded 0-50 ms immediately before the first stimulus) was averaged and subtracted from each of the recorded traces. Smoothing of the depth profile was performed using a moving averaging window consisting of five points with weights: +1, 0, -2, 0, +1. Since the value of σ_h was not determined, CSDs (mV/mm2) were in arbitrary units.

We calculated the CSDs of CA1 depth profiles recorded following 1) stimulation of RE, 2) stimulation of EC, and 3) simultaneous RE/EC stimulation. We also calculated the CSD of a theoretical depth profile which consisted of the algebraic sum of the single RE- and EC-evoked depth profiles, i.e., a depth profile which was to be expected in case RE and EC inputs activated independently different subsets of CA1 neurons. In principle, comparison of the theoretical CSD with the experimental CSD reveals whether or not RE and EC inputs interact at the cellular level.

Histological control

At the end of the experiment, under deep anesthesia, the stimulation and recording

electrodes were marked by lesions (three pulses of 1 mA anodal current) that resulted in a blue spot, due to the potassium ferrocyanide in the fixative (see below), occasionally with a hole in the centre of the lesion. The rat was decapitated, the brain removed and stored for 3 days in 4% paraformaldehyde and 0.05% glutaraldehyde in 0.1 M phosphate buffer with potassium ferrocyanide. The tissue was cryoprotected in 2% dimethylsulfoxide and 20% glycerin, and cut on a freezing microtome in 40 µm thick coronal sections. Subsequently the sections were Nissl-stained and examined for verification of electrode placements.

RESULTS

CA1 responses to paired pulse stimulation of RE and EC

Stimulation of either RE or lateral EC at locations as represented in Fig. 1, resulted in field potentials in CA1. The elicited depth profiles showed a large negative-going deflection in the recordings from LM. In stratum radiatum the deflections were positive-going, and gradually decreased towards the alvear surface (Fig. 2, A-C).
RE- and EC-evoked field potentials displayed peak latencies ranging from 14-21 ms, varying with the relative positions of stimulating and recording electrodes. A common feature of RE-CA1 and EC-CA1 responses was the consistent lack of a population spike at all stimulation intensities used. These results are in accordance with previous findings (Colbert and Levy 1992; Empson and Heinemann 1995; Dolleman-van der Weel et al. 1997; Morales et al. 2007). Inadvertent co-stimulation of EC layer II cells elicited a large amplitude field potential, often with a population spike, in the dentate gyrus (DG; Fig. 2B, arrows) at slightly shorter latency than the co-evoked CA1 response. Stimulation of deeper EC layers (III/IV/V; Köhler 1985) resulted in eight cases in two negative-going deflections in LM, of which the first short latency peak (Fig 2C, white arrow) did not reverse polarity in stratum radiatum whereas the second LM peak did reverse (Fig. 2C black arrow). In contrast to the monosynaptic input from the rostral RE (Dolleman-van der Weel et al. 1997), we have to consider the possibility that EC-evoked responses can result from activation of multiple pathways, i.e., monosynaptic EC-CA1, disynaptic EC-CA3-CA1 and/or trisynaptic EC-DG-CA3-CA1 inputs. Yet, in our recordings di- or tri-synaptic CA1 responses can be ruled out, because 1) the latency difference between the evoked field potentials in DG and CA1 was very small, and thus a tri-synaptic input in CA1 is unlikely, and 2) the depth profile evoked by di- or tri-synaptic input to CA1, both via the Schaffer collaterals, is known to be opposite (i.e., positive-going in LM, negative-going in radiatum) to that of the actually recorded depth profiles in CA1 (i.e.,

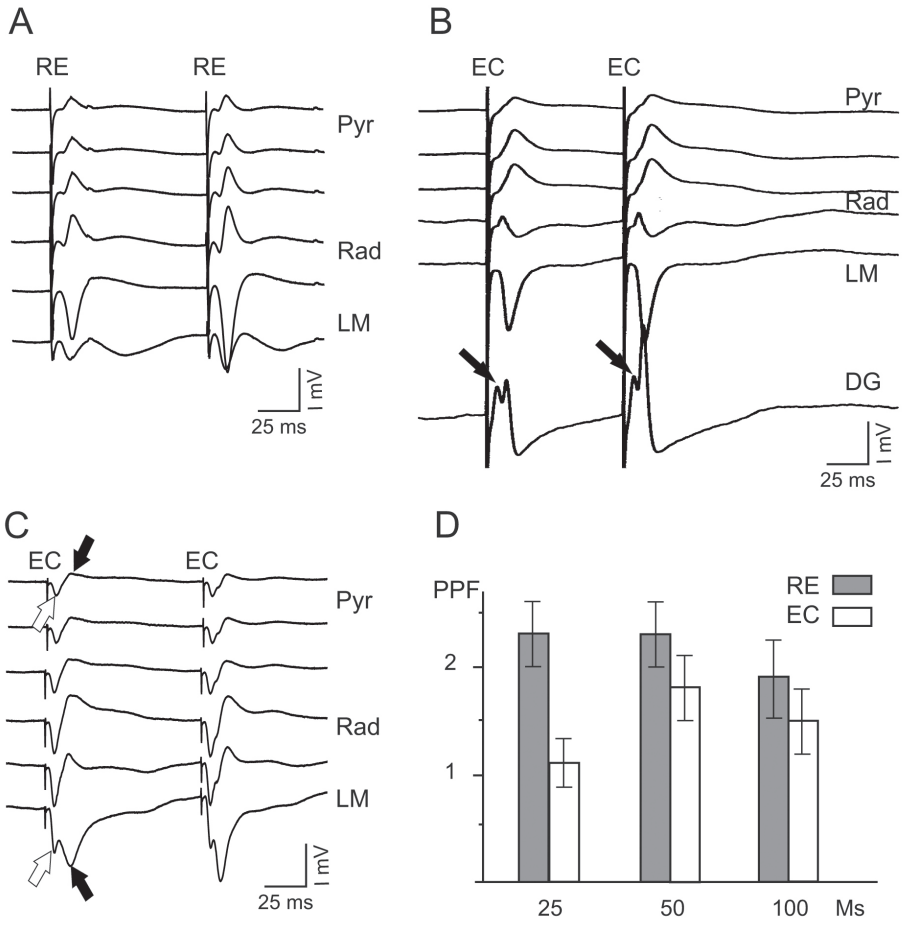

Fig. 2 CA1 responses to stimulation of reuniens (RE) and the lateral entorhinal cortex (EC), and paired pulse facilitation (PPF). **A-C** Subthreshold fEPSPs were evoked by stimulation of RE (**A**) or EC (**B,C**); RE- or EC-induced field potentials were negative-going in LM and positive-going in radiatum. **B** EC stimulation of layers II/III evoked field potentials in CA1 and in DG, the latter with a population spike (arrows) and at slightly shorter peak latency than the CA1 response. The DG field potential, recorded rather close to the cell layer, was positive-going. **C** When the stimulation electrode array covered the EC layers III/IV/V, the CA1 response displayed two negative-going waves in LM; the first one (open arrows) did not reverse polarity, whereas the second one (black arrows) reversed to a positive-going wave near the LM/radiatum border. **D** PPF was calculated for 25, 50, and 100 ms interpulse intervals (IPI). Both RE and EC stimulation resulted in robust PPF at IPIs of 50 and 100 ms. Yet, whereas at 25 ms IPI, RE-induced PPF was just a robust as at 50 ms, EC-induced PPF was hardly, if at all, noticeable. Abbreviations: Pyr = stratum pyramidale, Rad = stratum radiatum, LM = stratum lacunosum moleculare, DG = dentate gyrus.

negative-going in LM, positive-going in radiatum; Colbert and Levy, 1992). Therefore, we conclude that the recorded CA1 responses were monosynaptically elicited by direct EC-CA1 input. In addition, entorhinal fibres have been reported to reach CA1 via the alvear pathway. On the way to their terminal field in LM these alvear EC axons make synaptic contacts in the strata oriens, pyramidale and radiatum with pyramidal cells and, to a much higher extent, with inhibitory neurons (Deller et al. 1996; Takács et al. 2011). Hence, it is possible that the early negative deflections, recorded throughout the depth of the CA1 profile, may reflect EC input via the alvear pathway.

We next analyzed whether RE- and EC-evoked local field potentials displayed paired pulse facilitation (PPF) (Fig. 2D). Usually, low intensity stimulation of RE and EC evoked small and weak responses, particularly in case of the EC-evoked field potentials in LM. Therefore, we applied high intensity paired pulses (0.13 Hz; IPI range 25-50-100 ms), which resulted in reliably measurable RE- and EC-evoked responses (Dolleman-van der Weel et al. 1997; Di Prisco and Vertes 2006; Eleore et al. 2011; Aksoy-Aksel and Manahan-Vaughan 2013). RE-induced PPF was robust at the standard 100 ms IPI (PPF 1.9 ± 0.4, n=15), and even stronger at shorter intervals (IPI 25 and 50 ms; PPF 2.3 ± 0.3, n=6). This was also found for the EC-induced PPF both at IPI 100ms (PPF 1.5 ± 0.3, n=15) and IPI 50 ms (PPF 1.8 ± 0.3, n=5). However, at IPI 25 ms, EC-induced PPF was hardly noticeable (PPF 1.1 ± 0.2, n=4). These findings are in agreement with those reported in previous studies (Sloviter 1991; Leung et al. 1995; Dolleman-van der Weel et al. 1997; Eleore et al. 2011; Ito and Schuman 2012; Gonzalez et al. 2016).

Combined stimulation of RE and EC

In subsequent experiments we used various stimulation protocols to examine whether the responses to RE- and EC activation showed interaction or were independent. First, since there was a pronounced PPF of both RE- and EC-evoked responses at a 50 ms interval, we used this stimulation protocol as reference to examine the effects of heterosynaptic paired pulse stimulation. A representative example of such stimulation shows that a conditioning stimulus applied to RE did not significantly affect the amplitude of the field potential in LM evoked by a following EC test stimulus (Fig. 3A; mean peak amplitudes of a EC-elicited LM conditioning response 1.31 mV ± 0.32, and a heterosynaptic EC-elicited LM test response 1.36 mV ± 0.31, n=9; $F_{(1,16)}$=0.078, p=0.783, n.s.).
Second, in some instances, we applied a conditioning stimulus to EC and a test stimulus to RE, which did not affect the RE-evoked LM response (mean peak amplitudes of a RE-elicited LM conditioning response 0.98 mV ± 0.43, and a heterosynaptic RE-elicited LM test response 1.03 mV ± 0.49, n=4; $F_{(1,6)}$=0.017, p=0.899, n.s.; not illustrated, but see also

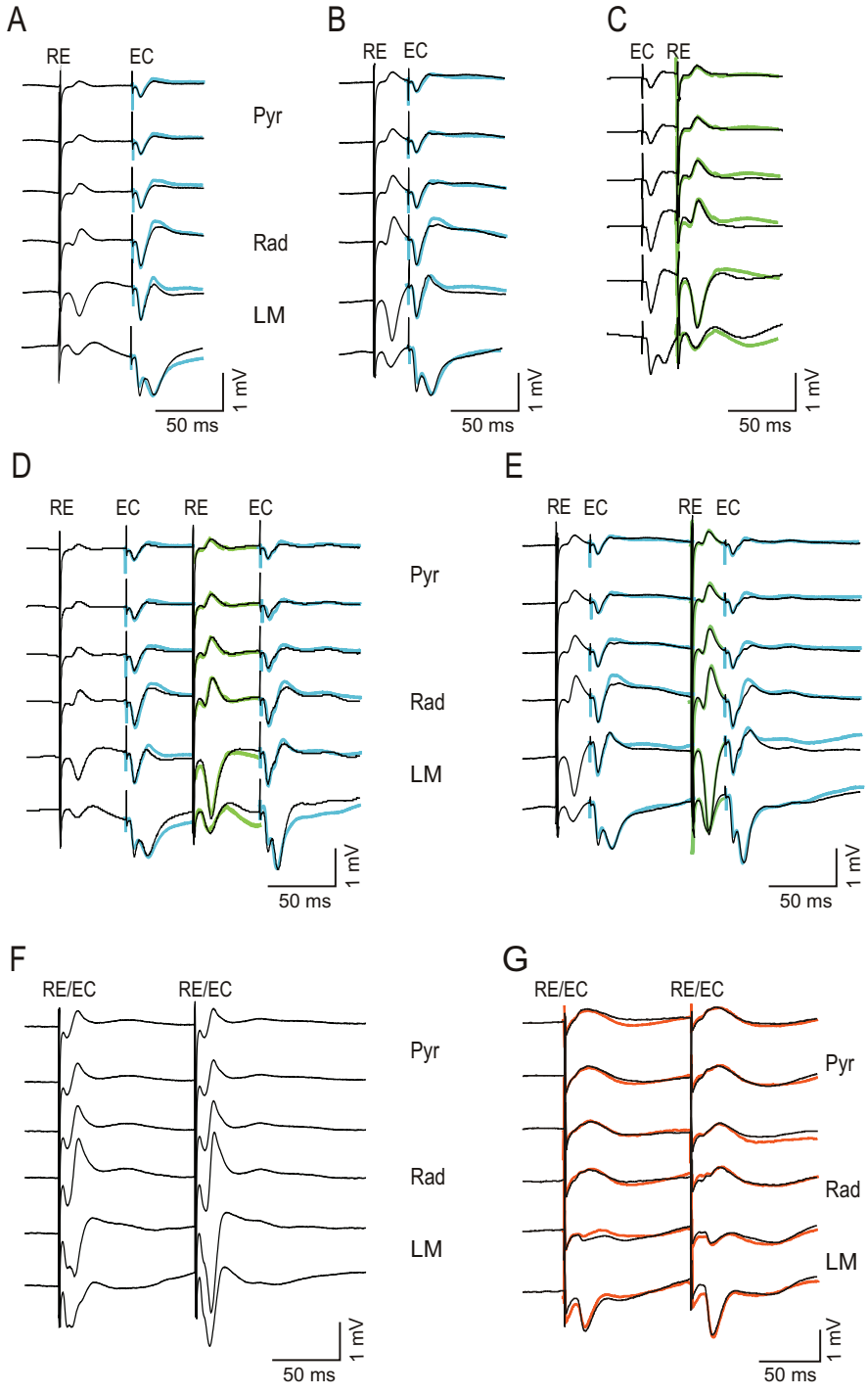
A
RE
EC
Pyr
Rad
LM
1 mV
50 ms
B
RE
EC
1 mV
50 ms
C
EC
RE
1 mV
50 ms
D
RE
EC
RE
EC
Pyr
Rad
LM
1 mV
50 ms
E
RE
EC
RE
EC
1 mV
50 ms
F
RE/EC
RE/EC
Pyr
Rad
LM
1 mV
50 ms
G
RE/EC
RE/EC
Pyr
Rad
LM
1 mV
50 ms

⇦ Fig. 3 Absence of heterosynaptic facilitation following combined stimulation of RE and EC (**A-F** show recordings from one rat; **G** shows recordings from a different rat). **A** A conditioning pulse to RE followed by a test pulse to EC (IPI 50 ms) did not result in heterosynaptic facilitation, as shown by comparison with an EC conditioning response (superimposed blue traces). **B** Similar results were obtained at 25 ms IPI. **C** Vice versa, a conditioning pulse to EC followed by a RE test pulse (IPI 25 ms) had no effect on the RE-evoked field potential, as compared with a RE conditioning pulse (green traces). **D,E** Combining paired pulses to RE and EC at various intervals also had no effect on their respective field potentials or PPF, as indicated by comparison with their separately evoked responses (RE = green traces; EC = blue traces). **F** Simultaneous paired pulse stimulation of RE/EC (IPI 100 ms) resulted in a markedly enlarged field potential in LM. **G** Applying paired pulses to RE and EC, either simultaneously (black traces) or with a 4 ms delay (red traces) between RE and EC stimulation, yielded similar responses.

figure 3D). Even at a shorter interval of 25 ms, RE stimulation did not affect the amplitude of the EC test response in LM (Fig. 3B); the reversed stimulation sequence (i.e., an EC conditioning pulse followed by a RE test pulse; Fig. 3C) yielded similar results. In addition, we employed RE-EC-RE-EC stimulation sequences. As shown in Figs. 3D-E, RE- and EC-induced PPF was comparable to PPF evoked by paired pulse stimulation of RE or EC separately. Thus, in line with earlier reports, indicating that PPF is specific to the set of afferents excited by the first stimulus (Creager et al. 1980; Grover and Teyler 1992), heterosynaptic PPF between RE and EC, or vice-versa, was not observed. Third, we applied paired pulses (IPI 100 ms) to RE/EC simultaneously (Fig. 3F). Compared to a RE- or EC-elicited LM conditioning response (mean peak amplitude 0.76 mV ± 0.22, and 0.86 mV ± 0.11, respectively; n=6), the RE/EC-elicited LM conditioning response (mean peak amplitude 1.53 mV ± 0.26, n=6) was significantly enlarged (RE/EC versus RE stimulation alone, $F_{(1,10)}$=7.264, p=0.022; RE/EC versus EC stimulation alone, $F_{(1,10)}$=6.920, p=0.025). Compared to an RE- or EC-elicited LM test response (mean peak amplitude 1.37 mV ± 0.52, and 1.45 mV ± 0.35, respectively), the enlargement of the RE/EC-elicited LM test response (mean peak amplitude 2.14 mV ± 0.30) just did not reach significance (RE/EC versus RE stimulation alone, $F_{(1,10)}$=4.357, p=0.063, trend; RE/EC versus EC stimulation alone, $F_{(1,10)}$=4.359, p=0.063, trend). Because depth profiles recorded with an 18-electrode array yielded more detail, the interaction between both inputs underlying the RE/EC-evoked enlargement of the fEPSP in LM will be described below while examining the CSD's.

Since RE- and EC-evoked response latencies could be different, we timed the stimuli so that the position of the initial response peaks in LM coincided. In addition, based on observations of Nettleton and Spain (2000) that nearby inputs occurring within a 5 ms time window may be integrated as coinciding events, we also recorded RE/EC-evoked responses of which the initial LM peaks had a 4 ms latency difference. Fig. 3G shows

superimposed the RE/EC-evoked response obtained with appropriately timed stimuli (in black) and those for which a delay of 4 ms was maintained (in red). These CA1 responses were very similar, which is in agreement with the report of Nettleton and Spain (2000).

Yet, despite the markedly increased amplitude of LM field potentials, simultaneous stimulation of RE/EC never elicited population spikes. This inability of RE and EC to drive pyramidal cells under all test conditions is likely due to inhibitory influences mediated by both inputs (see Discussion).

CSD analyses

Using an 18-electrode probe, we next investigated whether the superposition of RE and EC inputs would yield responses that may be interpreted as resulting from a summation process in case of independent inputs, or whether signs of an interaction at the cellular level could be found. Accordingly, we compared the responses evoked by simultaneous RE/EC stimulation with the corresponding RE- and EC-evoked responses added algebraically [i.e., (RE+EC)].

⇨ Fig. 4 Depths profiles of evoked field potentials in CA1; recordings from electrodes 4-18 are illustrated. **A** The RE-elicited depth profile has large negative-going potentials in LM, and positive-going ones in radiatum. **B** In this case, the EC-elicited depth profile shows two negative-going LM field potentials; the first, small one does not reverse polarity (open arrows) whereas the second, larger one reverses polarity close to the LM/radiatum border. **C** The experimental RE/EC depth profile, elicited by simultaneous stimulation, displays i) a small negative potential (open arrow), similar to that in the EC profile, and ii) a robust enhancement of the LM field potential. (Due to a large overlap of traces in the depth profile this is difficult to visualize in this plot; therefore, see LM traces in **E**). **D** The summated (theoretical) RE+EC depth profile is different from the experimentally induced one (see also overlays in **E**). **E** The peak amplitude of the experimental RE/EC-elicited field potential (black trace, open arrows) in proximal LM is much larger than the theoretical one (red trace, red arrows). In contrast, in distal LM, the peak amplitude of the theoretical RE+EC-elicited field potential (red trace, red arrows) is larger than the experimental RE/EC-induced one (black trace). **F** Micrograph showing the position of the 18-electrode recording probe in the dorsal part of the intermediate CA1, placed perpendicular to the hippocampal lamina. The most superficial electrode (1, small white arrow) and the deepest electrode (18, small white arrow) were marked by a lesion/blue spot. Electrode 1 was located in the white matter; electrode 18 was located just across the fissure (F) in the dentate gyrus. Large white arrow indicates the LM/radiatum border. Scale bar: 500 μm. Test response field potentials in LM are truncated in **B-E**. Abbreviations: LMp = proximal LM; LMd = distal LM.

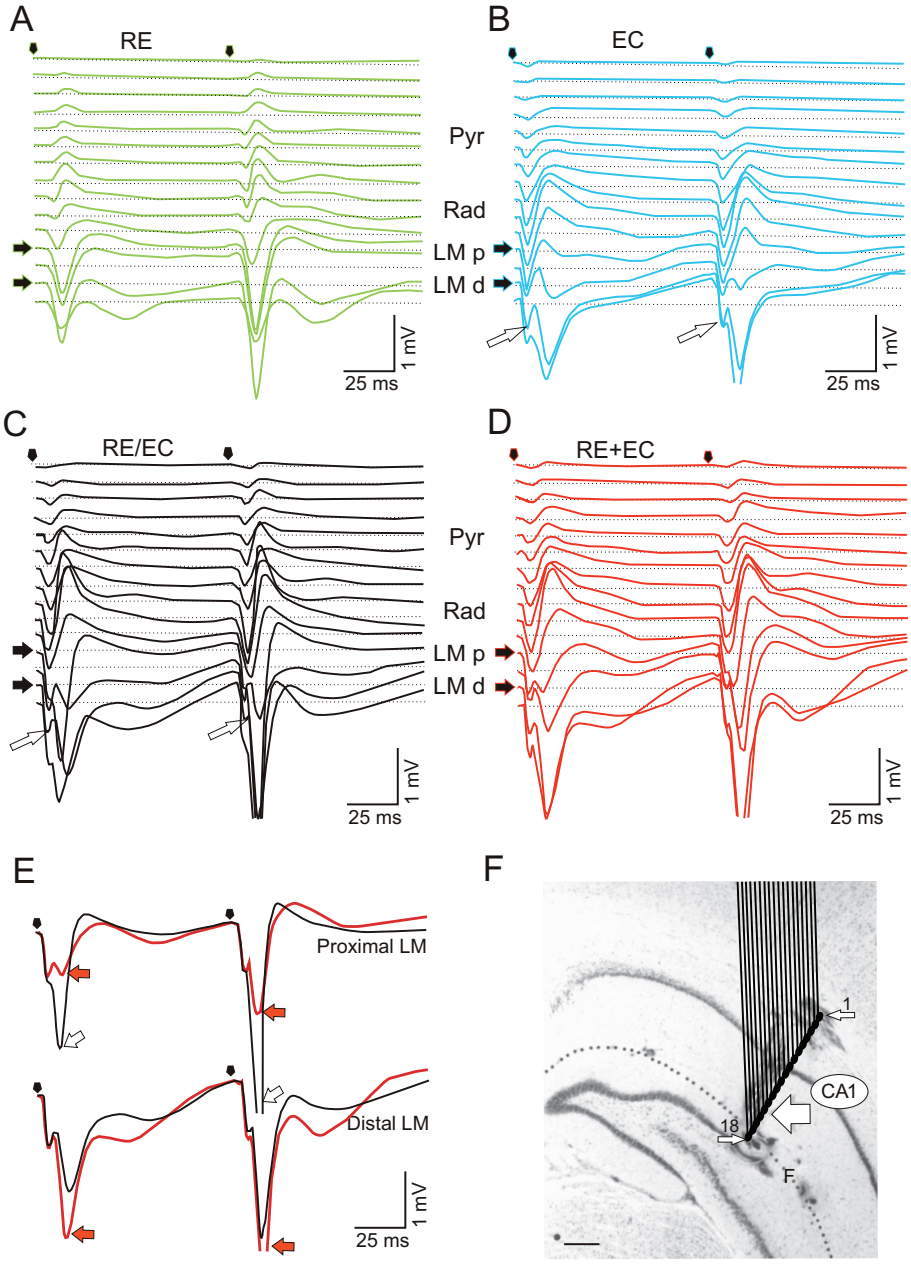
A
RE
B
EC
Pyr
Rad
LM p
LM d
1 mV
25 ms
C
RE/EC
D
RE+EC
E
Proximal LM
Distal LM
F
1
CA1
18

In general, following simultaneous RE/EC stimulation the CSD analyses from three different rats showed an enhancement of the evoked field potentials in LM and the associated LM sink. Because RE/EC stimulation appeared to affect the CA1 response in a complex way throughout the depth of the profile, we describe the observed effects in some detail. The results of a representative experiment are shown in Figs. 4 and 5, illustrating the single RE-, single EC-, simultaneous RE/EC- and theoretical (RE+EC)-elicited CA1 depth profiles, and CSDs, respectively. The EC stimulation electrode was positioned in layers III/IV and the RE stimulation electrode was placed in the mid rostro-caudal part of the nucleus, corresponding to the EC and RE stimulation sites represented in Fig. 1. The recording 18-electrode array was positioned in the dorsal part of the intermediate CA1, perpendicular to the curved axis of the CA1 field (see Fig. 4F). The most superficial electrode was located in the white matter and the deepest electrode just across the fissure in the dentate gyrus. Compared to the RE- and EC-elicited depth profiles (Fig. 4A,B), simultaneous stimulation of RE/EC (Fig. 4C) yielded a conspicuous effect: namely an enlargement of the field potentials in LM, especially of the deflections close to radiatum, i.e., in proximal LM (LMp). These observations are in agreement with earlier publications

⇨ Fig. 5 CSDs, corresponding to the depth profiles shown in Fig. 4. (sinks are downward, sources upward, in arbitrary units). **A** The RE CSD profile displays a clear 'LM sink-radiatum source' configuration. **B** The EC CSD shows a series of early small sink-source pairs (thick black lines) throughout the depth profile, followed by larger sinks and sources with a longer time course. **C** The experimental RE/EC CSD displays a markedly enlarged 'LM sink-radiatum source', but also maintains some of the characteristics of the EC CDS, i.e., i) the series of early sinks and sources (thick blue lines), ii) a sink in proximal radiatum (red circles; for comparison see circled areas in **B**, **C**, and **F** middle superimposed traces), and iii) the sink-source-sink sequence in distal LM (LMd, **B**-**C**; **F** lowest superimposed traces), respectively. There was also a small sink-source configuration close to stratum pyramidale (yellow box), which was not observed in any of the other CSDs (boxed areas in **A**,**B**,**D**, **F** upper superimposed traces). **D** The theoretical, summated (RE+EC) CSD profile was different from the experimental RE/EC CSD profile, especially in proximal LM (LMp). **E** Superimposed traces of the experimental RE/EC CSD (black lines) and the theoretical RE+EC CSD (red lines) show the substantial enlargement of the experimentally recorded sink in proximal LM (LMp). The experimental 1st small sink in distal LM (black line/open arrows, LMd) is slightly larger than the theoretical one (red line, LMd), while the experimental second LM sink (black arrows) is smaller than the summated one. **F** The upper two traces show superimposed the RE/EC CSD (black) and the summated RE+EC CSD (red) at the pyramidal cell level), clearly revealing the appearance of a small sink-source pair (boxed area) in the experimental CSD (black). Middle superimposed traces show the similarity of the radiatum sink (circled areas) in the EC CSD (blue) and in the experimental RE/EC CSD (black). Lowest superimposed traces show the similarity of the LMd sink-source-sink sequence in the EC (blue) and RE/EC (black) CSDs. They also reveal that compared to the EC CSD (blue) the RE/EC CSD (black) shows i) a slight enhancement of the early small sink, ii) a shorter duration of the experimental source (in black), and iii) some 'disinhibition' of the late LM sink in the test response of the RE/EC CSD (black).

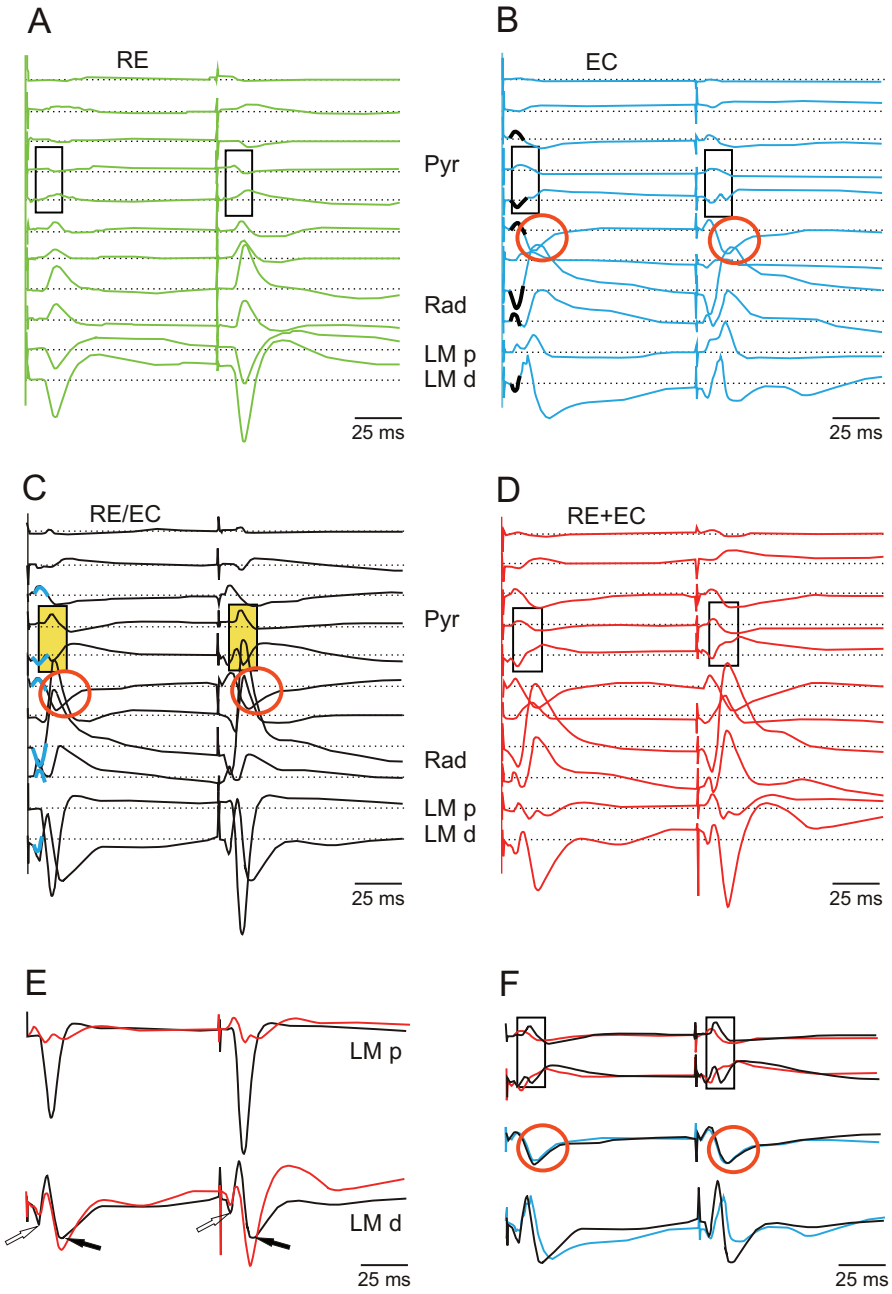
A
RE
Pyr
Rad
LM p
LM d
25 ms
B
EC
25 ms
C
RE/EC
Pyr
Rad
LM p
LM d
25 ms
D
RE+EC
25 ms
E
LM p
LM d
25 ms
F
25 ms

(e.g., Steward 1976; Witter et al. 1988; Wouterlood et al. 1990). Although we cannot entirely exclude some variation in specificity or efficacy, as hinted to in recent publications concerning EC projections to CA1 (e.g., Kitamura et al. 2014; Basu et al. 2016), it is unlikely that an (anatomical) uneven distribution of RE and/or EC fibres in LM underlies the predominant effect of coinciding RE/EC input in proximal LM.

To further clarify this finding, we made CSD analyses of the different depth profiles (Fig.5A-D). Whereas the RE CSD showed a clear LM sink-radiatum source configuration (Fig. 5A), the EC CSD showed multiple sinks and sources, which is likely due to a recruitment of EC-CA1 fibres in both perforant path and alveus (Fig. 5B). Comparison of the experimental RE/EC CSD (Fig. 5C), and the simply algebraically added (RE+EC) CSD profiles (Fig. 5D) revealed marked differences that are indicative for a nonlinear interaction, and where this interaction may take place. Specifically a very strong sink in proximal LM was observed in the RE/EC CSD but not in that of the simple summation model (Fig. 5E, LMp). In the experimental RE/EC CSD profile, in distal LM (Fig. 5C, LMd), we recognized a sink-source-sink sequence that was rather similar to the sink-source-sink sequence in the single EC CSD (Fig. 5B, LMd, 5F lowest superimposed traces), but the large distal LM sink is smaller in the experimental RE/EC CSD than in the theoretical one (Fig. 5E, LMd). Taken together, this suggests that the influence of RE input on the EC-elicited field potentials is more prominent in proximal versus distal LM (Fig 5E; see also Fig. 6, at 14 ms). Another remarkable feature of the RE/EC CSD was a small sink-source pair (Fig. 5C, yellow boxed area) close to stratum pyramidale, not seen in the RE, EC, and (RE+EC) CSDs (Fig. 5A,B,D,F; boxed areas). Similar small sink-source pairs close to the pyramidal cell level were detected in the CSDs from all three rats. This additional effect of RE/EC stimulation presumably represents an inhibitory input at the (peri)somatic level (see Discussion). In contrast, the small early sinks and sources in strata pyramidale and radiatum in the EC CSD (Fig. 5B, thick black lines), possibly reflecting alvear EC input, seemed unaffected by simultaneous RE/EC stimulation (Fig. 5C). Because a presumed alvear input was quite variable in our experiments, and the early pyramidal and radiatum sink-source pairs at 7 ms emerged just from the background, rendering them rather fragile, this precludes a detailed interpretation at this time. The sink in proximal radiatum (Fig. 5B, circled areas) was also unaffected by RE/EC input (Fig. 5B,C, and F, middle superimposed EC [blue] and RE/EC [black] traces). Although this sink is rather substantial, as yet its origin, and whether this is an active or passive sink, is not clear. More data are needed for a detailed interpretation of the underlying mechanism(s). Thus, we focus here on the more robust effects of RE/EC stimulation.

To further clarify the RE/EC interactions, we examined more in detail the CSD profiles at 6.5, 14 and 17 ms, resulting from the conditioning pulse (Fig. 6). These three

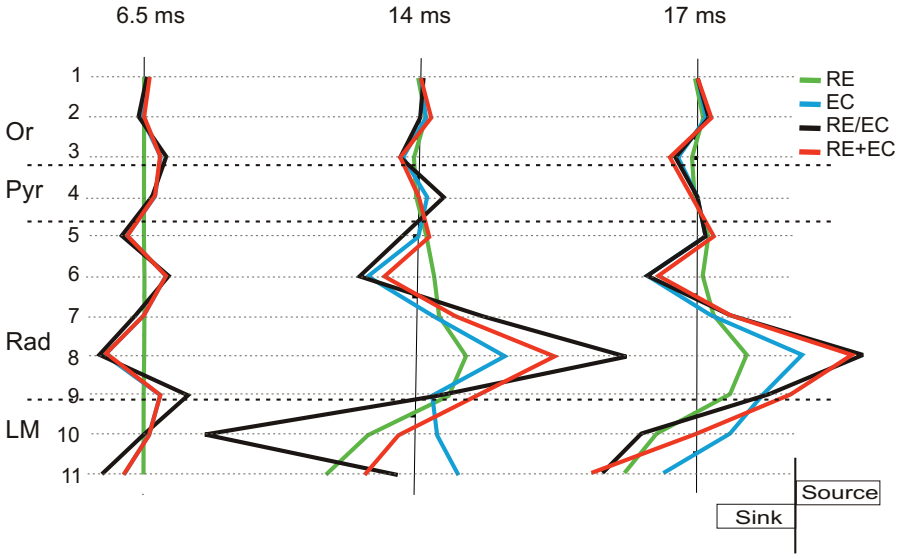

Fig. 6 Detailed cross section of the CSD profiles shown in Fig. 5 (t = 6.5 ms, t = 14 ms, and t = 17 ms correspond to time points of the conditioning response; sinks and sources are in arbitrary units). At 6.5 ms, there are no noticeable RE-elicited sink/source pairs, and thus a simple straight line is shown (green). The RE/EC-elicited experimental response (black) and theoretically (RE+EC) evoked response (red) are shown; the EC-elicited response is not shown because it coincides with the red line. Simultaneous input from RE/EC (black) yielded a small enlargement of the early LM sink and associated source at the LM-radiatum border. At t=14 ms, the RE/EC input resulted in a nonlinear summation of evoked potentials throughout the depth of the profile. Most obvious is the major increase in the amplitudes of the 'LM sink-radiatum source' (see thin lines 10 and 8, respectively), and the shift of the LM sink towards radiatum. In addition, a small source appeared at the pyramidal cell level (see thin line 4). At 17 ms the experimental RE/EC (black) and theoretical (RE+EC) (red) CDS profiles are largely similar, except for some minor broadening of the experimental LM sink towards radiatum, indicating ongoing interaction in proximal LM.

timepoints represent approximately the peak latencies of the early, small sinks-sources pairs and of the later, large sinks and sources in the CSD depth profiles of Fig. 5. First, at 6.5 ms there were no sinks and sources noticeable in the RE CSD profile, and thus the single EC- and theoretical (RE+EC) CSD depth profiles were largely similar, except for some enhancement of the early small sink-source pair in LM (Fig. 6, lines 11-9). This was suggestive for an unexpected, yet minor contribution of RE to the RE/EC evoked early synaptic response in LM (see also Discussion). Second, at 14 ms a large LM sink (towards radiatum) was most pronounced for the RE/EC case, suggesting that the main site of interaction between RE and EC takes place on dendritic compartments of CA1 cells in proximal LM. Thus, coinciding RE input appears, at least partly, to 'overrule' an

EC-induced inhibition onto the apical dendrites of the pyramidal cells. This inhibitory effect is likely represented by the occurrence of the LM source, of which the decay phase (at 14 ms) seems to mask the onset of the EC-elicited LM sink (see Fig. 5B). Third, at 17 ms, comparison of the experimental RE/EC and the theoretical (RE+EC) CSDs revealed that summation throughout the depth of the CA1 profile was mainly linear, except for minor broadening of the LM sink towards radiatum, indicating ongoing interaction in the apical dendrites in proximal LM.

DISCUSSION

The present findings form a strong indication that RE and EC axons actually converge, at least partly, onto the same apical dendritic compartment of CA1 pyramidal cells. Following simultaneous low frequency stimulation of both inputs the elicited CA1 response shows 1) a major nonlinear enhancement of subthreshold RE- and EC-evoked fEPSPs in proximal LM, and 2) a small sink-source pair at the pyramidal cell level, likely reflecting an additional (peri)somatic inhibition.

The analysis of inputs to CA1 shows a strong focus on the excitatory projections from EC and CA3, and how they might interact with each other as well as with local connectivity, mainly originating from the many classes of interneurons (Klausberger and Somogyi 2008; Klausberger 2009). Entorhinal axons in LM form asymmetrical synaptic contacts on spines and shafts of CA1 cells (Desmond et al. 1994), and it is generally accepted that the EC and CA3 inputs converge onto single pyramidal cells (Kajiwara et al. 2008). RE-CA1 axons also form asymmetrical synapses on spines and dendritic shafts in LM (Wouterlood et al. 1990). Preliminary ultrastructural data have confirmed that RE forms synapses on spines and shafts of identified (i.e., intracellularly labelled) CA1 pyramidal cells (own unpublished observations). Previous light microscopical data support a convergence of RE as well as EC axons onto the apical dendrites of CA1 cells (Dolleman-van der Weel et al. 1994). Here, we provide the first data indicating that RE and EC inputs indeed converge, at least partly, onto single pyramidal neurons.

Many (in vitro) electrophysiological studies have examined the interplay between CA3-CA1 and direct EC-CA1 inputs stimulated via the Schaffer collaterals in radiatum and perforant path fibres in LM, respectively, and the spatial distribution of activated synapses (e.g., Judge and Hasselmo 2004; Ang et al. 2005; Dudman et al. 2007; Izumi and Zorumski 2008; Takahashi and Magee 2009; Pissadaki et al. 2010; McQuiston 2010). Yet, the contribution of inadvertently co-activated RE axons in LM was not taken into consideration. The present in vivo results are the first to shed light on the individual contributions of RE and EC to a coinciding RE/EC input in CA1. This implies that, in

case of in vitro stimulation of axons in radiatum and LM, the observed effects of CA3 and EC interactions on transmission in CA1 may in fact reflect, at least partly, the converging inputs from RE and EC, together with CA3 input. Such reported effects are: 1) changes in spiking activity of pyramidal cells, (Remondes and Schuman 2002; Takahashi and Magee 2009; Pissadaki et al. 2010), 2) modification of long-term synaptic changes in both inputs (Remondes and Schuman 2003; Judge and Hasselmo 2004; Dudman et al. 2007), 3) gating of Schaffer collaterals input by preceding LM stimulation (McQuiston 2010) and, vice versa, gating of EC input by preceding Schaffer collaterals stimulation (Ang et al. 2005). Overall, these differential effects appeared dependent on timing, spatial synaptic arrangement, and stimulation frequencies of LM axons and Schaffer collaterals.

There is evidence that convergent inputs onto the dendrites of CA1 pyramidal cells result in a nonlinear summation of evoked potentials (Wei et al. 2001; Poirazi et al. 2003; Liang 2006). Gasparini and Magee (2006) demonstrated that the response patterns of CA1 pyramidal cells depend on whether the converging inputs are either asynchronous and distributed in space, resulting in linear processing, or are synchronous and spatially clustered, resulting in nonlinear processing. The latter form of integration is in line with the present results, thus suggesting that RE-CA1 and EC-CA1 inputs converge on the same dendritic branch of a pyramidal cell.

Synaptic summation in CA1 cells is also controlled by GABAergic inputs (Enoki et al. 2001). In general, an inhibitory control mechanism is necessary to coordinate the activities of numerous principal cells. At least 21 classes of functionally different interneurons in CA1 allow for the flexibility with which pyramidal cells can enhance their computational abilities. Thirteen of these interneuron types have dendrites in LM and thus, in theory, can be activated by RE and EC inputs (Klausberger and Somogyi 2008; Klausberger 2009; Roux and Buzsáki 2015). As schematically summarized in Fig. 7, the excitatory RE and EC innervation of several classes of interneurons provides potentially a powerful inhibitory influence covering the entire depth of field CA1. RE has been shown to drive vertical oriens/alveus (O/A) cells, mediating feedforward perisomatic inhibition of CA1 cells (Lacaille et al. 1987; Samulack et al. 1993; McBain et al. 1994; Dolleman-van der Weel et al. 1997). Furthermore, RE drives interneurons in distal radiatum, that fire only in response to low frequency (0.1-2 Hz) stimulation of RE, but are silent during stimulation at theta (4-10 Hz) frequencies (Dolleman-van der Weel et al. 1997). These interneurons are presumably Schaffer collaterals-associated cholecystokinin-positive (CCK^+) cells which innervate pyramidal cells and other classes of interneurons, as well as each other (Nunzi et al. 1985; Acsady et al. 1996; Gulyás et al. 1996; Vida et al. 1998; Somogyi and Klausberger 2005; Klausberger 2009; Chamberland and Topolnik 2012). The excitatory RE innervation of GABAergic cells in CA1 has also been confirmed at the ultrastructural level (Dolleman-van der Weel and Witter 2000). EC axons in LM

innervate parvalbumine-positive (PV^+) basket cells and chandelier or axo-axonic cells, providing powerful feedforward somatic and axonal inhibition, respectively (Somogyi et al. 1983; Li et al. 1992; Kiss et al. 1996. In addition, the presently described small sink-source pair at the pyramidal cell level in the RE/EC CSD (see Fig. 5C) may reflect a RE/EC-mediated (peri)somatic inhibition. Because RE and EC do not provide an excitatory input in stratum pyramidale, we propose that this small sink-source pair represents an active (i.e., inhibitory) source and a passive sink, probably originating from RE/EC-induced activation of a subclass of CCK/vasoactive intestinal polypeptide (VIP)-positive (CCK^+/VIP^+) basket cells located at the LM/radiatum border (Klausberger and Somogyi 2008; Kajiwara et al. 2008). These CCK^+/VIP^+ basket cells exert a powerful feedforward inhibitory influence at the (peri-)somatic level, which effectively suppresses the generation of action potentials in CA1 cells (Freund and Katona, 2007). EC-activated PV^+ basket cells and presumed RE/EC-activated CCK^+/VIP^+ basket cells are thought to have different functions, such as distinct contributions to network oscillations, and/or targeting different subtypes of pyramidal cells (e.g., Klausberger et al. 2005; Klausberger and Somogyi 2008; Lee et al. 2014; Donato et al. 2015; Roux and Buzsáki 2015). Although this awaits further investigation, such an RE/EC-evoked activation of CCK^+/VIP^+ basket cells can exert a strong inhibitory influence on the output abilities of CA1 cells. Furthermore, in LM a variety of interneurons is supposed to gate the entorhinal-hippocampal dialogue (Capogna 2011). Price et al. (2005, 2008) have shown that LM neurogliaform (LM-NG) cells are monosynaptically activated by stimulation of EC fibres in LM in a slice preparation. They suggested that, next to innervating other LM interneurons, LM-NG cells might be specialized for shunting inhibition of EC-CA1 input. In line with this idea, we propose that the sink-source-sink sequence in LM in the EC CSD (see Fig. 5B) consists of 1) a small early sink, presumably reflecting the excitatory EC input onto LM-NG cells. Because these interneurons have all their dendrites and a very compact axonal plexus in LM, they may generate currents strong enough to be detected in a CSD. 2) The succeeding LM source may than reflect the (EC-mediated) feed forward inhibitory input of LM-NG cells onto the apical dendrites of the pyramidal cells (Price et al. 2008), and 3) the large LM sink, of which the onset likely summates with the preceding (inhibitory) source, represents the direct EC excitatory input onto the CA1 cell dendrites in LM. So far, there is no evidence for RE innervation of LM-NG cells, and/or other subclasses of LM interneurons. Yet, the presently observed small enhancement of the early sink in LM in the RE/EC CSD (see Fig.6 at 6.5 ms) seems at least suggestive for a minor RE input on presumed LM-NG cells. Since these effects are small, a presumed RE innervation/activation of LM-NG cells requires further confirmation, both at the electrophysiological (e.g., pair-wise recordings) as well as at the anatomical (e.g., intracellular labeling, or ultrastructural) level.

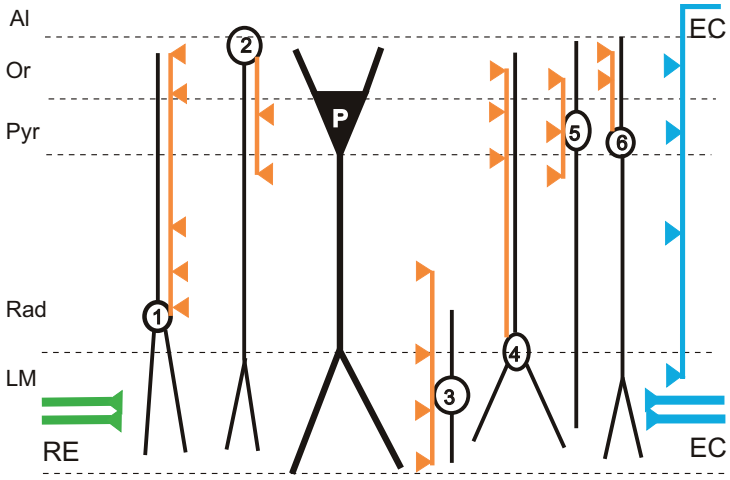

Fig. 7 Schematical representation of excitatory RE and EC inputs in CA1 onto pyramidal cells and interneurons (modified from Klausberger and Somogyi, 2008). The CA1 pyramidal cell (in thick black, white P) receives presumed inhibitory synaptic inputs represented by the orange triangles, and excitatory inputs corresponding to the blue and green triangles. The inhibitory inputs are presented alongside the axons (in orange) of the corresponding interneurons and not next to the pyramidal cell for clarity. RE (green) and EC input (via perforant path and alveus; blue) innervate the apical dendrites of CA1 pyramidal cells as well as several subclasses of interneurons with a dendritic tree (black) in LM (for clarity these excitatory inputs are not presented next to their dendritic targets). RE innervates presumed Schaffer collaterals-associated cells (1) which are thought to inhibit pyramidal cells and other (unidentified) interneurons, and vertical oriens/alveus cells (2), mediating feedforward perisomatic inhibition of CA1 cells. EC innervates LM-neurogliaform cells (3), providing feedforward inhibition of pyramidal cells as well as other interneurons in LM, and parvalbumine-positive basket cells (5) and chandelier or axo-axonic cells (6), providing feedforward somatic and axonal inhibition, respectively. Synaptic targets of alvear EC input (blue) are pyramidal cells, and to a larger extent, unspecified interneurons (Takács et al., 2011). The present results indicate that RE and EC inputs converge onto the same dendritic branch of a pyramidal cell in proximal LM, and presumably also on a specific set of interneurons, possibly a subclass of basket cells located at the LM/radiatum border (4), which provide (peri) somatic inhibition of CA1 cells. Abbreviations: Al = alveus; Or = stratum oriens; Pyr = stratum pyramidale; Rad = stratum radiatum; LM = stratum lacunosum moleculare; RE = nucleus reuniens; EC = entorhinal cortex.

Overall, the present data reveal that simultaneous RE/EC activation resulted in an increased excitation level of the pyramidal cell dendrites, predominantly in proximal LM. This indicates that convergence of EC- and RE inputs onto the same dendritic compartments of CA1 pyramidal cells partly ‘overrules’ the ‘on-the-path’ shunting inhibition (Koch et al.

1983; Hao et al. 2009) exerted by EC-activated LM-NG cells. Such an enhanced dendritic excitation level in the apical tuft of pyramidal cells can lead to the generation of dendritic spikes which, reliant on the presence/modulation of voltage dependent channels and the level of synaptic inhibition (Jarski et al. 2005; Ibarz et al. 2006; Hao et al. 2009), may propagate towards the CA1 soma, initiating action potentials. Although it is possible that dendritic spikes were overlooked, all aforementioned RE- and EC-mediated inhibitory influences together (see Fig.7) offer an adequate explanation for the absence of dendritic spikes and the consistent lack of pyramidal cell firing in our recordings.

Functional relevance

Regarding the interactions of RE and EC input in CA1, there are two important questions: 1) whether coincident low frequency input of the RE-CA1 and the lateral EC-CA1 pathways is a natural occurring phenomenon, and 2) what the functional importance of such interactions might be. As yet, there are no studies available, showing that during low frequency oscillations (as in slow-wave-sleep, or during immobility) the RE-CA1 and the EC-CA1 projections are simultaneously active. In fact, the coincidence of RE and EC inputs in hippocampal field CA1 has never been examined. Nonetheless, Xu and Sűdhof (2013) have suggested that the cooperative activation of RE-CA1 and EC-CA1 synapses may reduce the threshold for synaptic plasticity, thereby facilitating transmission in CA1 and subsequent memory consolidation, a process that is improved by slow oscillations (Heib et al. 2013). In line with this idea, the present data show at least that coinciding low frequency activation of the RE and EC inputs results in a strongly enhanced excitation level of the CA1 cell apical dendrites in LM.

Recent studies in freely-moving rats have shed some light on the physiological properties of RE neurons (Jankowski et al. 2014, 2015). Next to a relatively small percentage of cells with diverse spatial properties, the vast majority of RE neurons (~64%) appeared to be low frequency firing cells without spatial properties, of which approximately 17% fired only at frequencies below 1 Hz (Jankowski et al. 2014). Thus low frequency stimulation of RE, as applied in this study, appears to mimic the physiological properties of a large group of RE neurons. Previously, we have stimulated the RE-CA1 projection at frequencies ranging from 0.13-10 Hz, and found that low frequency (0.13-2 Hz) activation of RE evokes the largest LM field potentials (Dolleman-van der Weel et al. 1997). Therefore, we suggest that the RE-CA1 input shows enhanced synaptic excitability during slow oscillations. Since interneurons play important roles in the regulation of oscillations (Jonas et al. 2004; Somogyi and Klausberger 2005; Klausberger 2009), it is noteworthy that low frequency ($\leq$ 2 Hz) RE input is also able to drive interneurons

in distal radiatum (Dolleman-van der Weel et al. 1997) that inhibit both pyramidal cells and other inhibitory interneurons. Driving these particular radiatum interneurons may thus provide a possible mechanism for RE to impose a slow oscillation on CA1 cells, as previously reported by Zhang et al. (2012). RE-induced oscillatory activity in CA1 may be in synchrony with slow oscillations in mPFC. This idea is supported by the fact that the RE-CA1 projecting neurons receive input from mPFC (Vertes et al. 2007). In addition, a small percentage of these RE neurons project via collateralized axons to CA1 as well as back to mPFC, and thus have the potential to directly synchronize the activity in both target areas (Hoover and Vertes 2012; Varela et al. 2014). Moreover, paired pulse stimulation at 0.1 Hz of the RE-mPFC projection has been shown to exert pronounced excitatory effects in mPFC, displaying strong PPF similar to RE-induced PPF in CA1 (Dolleman-van der Weel et al. 1997; Di Prisco and Vertes 2006; Eleore et al. 2011; present study). Taken together, these findings are supportive for a pivotal role of RE in synchronizing the activities in hippocampus and mPFC. Such synchronous slow oscillations, occurring during slow-wave-sleep, are crucially important for the consolidation of hippocampal-dependent memories (Sirota et al. 2003; Sirota and Buzsáki 2005; Marshall et al. 2006; Wolansky et al. 2006; Isomura et al. 2006; Wang and Morris 2010; Mölle and Born 2011; Heib et al. 2013; Binder et al. 2014). It has also been assumed that hippocampal theta oscillations may play a role in memory processes. Recently, causal evidence was presented for the role of rapid eye movement (REM) sleep theta rhythm in contextual memory consolidation (Boyce et al. 2016). Therefore, it is timely to investigate the interaction of coinciding RE-CA1 and EC-CA1 inputs with hippocampal theta oscillations in future studies.

A growing number of behavioral studies has provided evidence that RE is indeed involved in cognitive functions, most likely by coordinating neuronal activities in hippocampus and mPFC (Dolleman-van der Weel et al., 2009; Davoodi et al. 2011; Eleore et al. 2011; Hembrook et al. 2011; Loureiro et al. 2012; Prasad et al. 2013; Cholvin et al. 2013; Hallock et al. 2013; Xu and Sűdhof 2013; Saalmann 2014; Bobal and Savage 2015; Ito et al. 2015; Layfield et al. 2015; Prasad et al. 2017). Because mPFC lacks a direct return projection to the hippocampus (Sesack et al. 1989; Jay and Witter 1991), RE might relay mPFC-processed information back to the hippocampus as part of a closed CA1-mPFC-RE-CA1 circuit (Vertes et al. 2007; Xu and Sűdhof 2013). In addition, mPFC-processed information can be transmitted to CA1 via the lateral EC (Preston and Eichenbaum 2013; Takehara-Nishiuchi 2014; Chao et al. 2016), an area that can also be influenced by RE input (Wouterlood 1991; Dolleman-van der Weel and Witter 1996; Zhang and Bertram 2002; Wouterlood et al. 2008).

In summary, viewed in the context discussed above, we propose that low frequency RE input in CA1 is potentially important for the synchronization of hippocampal and

mPFC slow oscillations. Whether synchronization actually takes place, however, has to be tested quantitatively. Furthermore, the present electrophysiological data strongly suggest that, by directly and indirectly facilitating the EC-CA1 input during slow oscillations, RE can contribute to the dialogue between hippocampus and mPFC which is of crucial importance for the consolidation of hippocampal-dependent memories.

Acknowledgements
This work was supported by NWA grant 90-20 from the Graduate School for Neurosciences Amsterdam. We thank A.J.A. Juta for helping with the calculation of the CSDs.

REFERENCES

Acsady L, Gorcs TJ, Freund TF (1996) Different populations of vasoactive intestinal polypeptide-immunoreactive interneurons are specialized to control pyramidal cells or interneurons in the hippocampus. Neuroscience 73:317-334.

Aksoy-Aksel A, Manahan-Vaughan D (2013) The temporoammonic input to the hippocampal CA1 region displays different synaptic plasticity compared to the Schaffer collateral input in vivo: significance for synaptic information processing. Front Syn Neurosci 5:5. doi: 10.3389/fsyn.2013.00005.

Anderson MC, Bunce JG, Barbas H (2016) Prefrontal-hippocampal pathways underlying inhibitory control over memory. Neurobiol Learn Mem 134 PtA:145-161.

Ang CW, Carlson GC, Coulter DA (2005) Hippocampal CA1 circuitry dynamically gates direct cortical inputs preferentially at theta frequencies. J Neurosci 25:9567-9580.

Basu J, Zaremba JD, Cheunh SK, Hitti FL, Zemelman BV, Losonezy A, Siegelbaum SA (2016) Gating of hippocampal activity, plasticity, and memory by entorhinal cortex long-range inhibition. Science 351,aaa5694 doi: 101126/science.aaa5694.

Binder S, Rawohl J, Born J, Marshall L (2014) Transcranial slow oscillation stimulation during NREM sleep enhances acquisition of the radial maze task and modulates cortical network activity in rats. Front Behav Neurosci 7, doi: 10.3389/fnbeh.2013.00220.

Brun VH, Otnass MK, Moiden S, Steffenach HA, Witter MP, Moser MB, Moser EI (2002) Place cells and place recognition maintained by direct entorhinal-hippocampal circuitry. Science 296:2243-2246.

Brun VH, Leutgeb S, Wu HQ, Schwarcz R, Witter MP, Moser EI, Moser MB (2008) Impaired spatial representation in CA1 after lesion of direct input from entorhinal cortex. Neuron 57:290-302.

Bobal MG, Savage LM (2015) The role of ventral midline thalamus in cholinergic-based recovery in the amnestic rat. Neuroscience 285:260-268.

Bokor H, Csaki A, Kocsis K, Kiss J (2002) Cellular architecture of the nucleus reuniens thalami and its putative aspartatergic/glutamatergic projection to the hippocampus and medial septum in the rat. Eur J Neurosci 16:1227-1239.

Boyce R, Glasgow SD, Williams S, Adamantidis A (2016) Causal evidence for the role of REM sleep theta rhythm in contextual memory consolidation. Science 352: 812-816.

Capogna M (2011) Neurogliaform cells and other interneurons of stratum lacunosum-moleculare gate entorhinal-hippocampal dialogue. J Physiol 589:1875-1883.

Cassel JC, Pereira de Vasconcelos A (2015) Importance of the ventral midline thalamus in driving hippocampal functions. Prog Brain Res 219:145-161.

Chamberland S, Topolnik L (2012) Inhibitory control of hippocampal inhibitory neurons. Front Neurosci 6:165. doi: 10.3389/fnins.2012.00165.

Chao OY, Huston JP, Li JS, Wang AL, de Souza Silva MA (2016) The medial prefrontal cortex-lateral entorhinal cortex circuit is essential for episodic-like memory and associative object-recognition. Hippocampus 26:633-645.

Cholvin T, Loureiro M, Cassel R, Cosquer B, Geiger K, De Sa Nogueira D, Raingard H, Robelin L, Kelche C, Pereira de Vasconcelos A, Cassel JC (2013) The ventral midline thalamus contributes to strategy shifting in a memory task requiring both prefrontal cortical and hippocampal functions. J Neurosci 33:8772-8783.

Colbert CM, Levy WB (1992) Electrophysiological and pharmacological characterization of perforant path synapses in CA1: mediation by glutamate receptors. J Neurophysiol 68:1-8.

Creager R, Dunwiddie T, Lynch G (1980) Paired-pulse and frequency facilitation in the CA1 region of the in vitro rat hippocampus. J Physiol 299:409-424.

Davoodi FG, Motamedi F, Akbari E, Ghanbarian E, Jila B (2011) Effect of reversible inactivation of reuniens nucleus on memory processing in passive avoidance task. Behav Brain Res 221:1-6.

Deller T, Adelmann G, Nitsch R, Frotscher M (1996) The alvear pathway of the rat hippocampus. Cell Tissue Res 286:293-303.

Deshmukh SS, Knierim JJ (2011) Representation of non-spatial and spatial information in the lateral entorhinal cortex. Front Behav Neurosci 5:69. doi: 10.3389/fnbeh.2011.00069.

Desmond NL, Scott CA, Jane Jr JA, Levy WB (1994) Ultrastructural identification of entorhinal cortical synapses in CA1 stratum lacunosum-moleculare of the rat. Hippocampus 4:594-600.

Di Prisco GV, Vertes RP (2006) Excitatory actions of the ventral midline thalamus

(rhomboid/reuniens) on the medial prefrontal cortex in the rat. Synapse 60:45-55.

Dolleman-van der Weel MJ, Wouterlood FG, Witter MP (1994) Multiple anterograde tracing, combining Phaseolus vulgaris leucoagglutinin with rhodamine- and biotin-conjugated amine. J Neurosci Methods 51:9-21.

Dolleman-van der Weel MJ, Witter MP (1996) Projections from the nucleus reuniens thalami to the entorhinal cortex, hippocampal field CA1, and the subiculum in the rat arise from different populations of neurons. J Comp Neurol 364:637-650.

Dolleman-van der Weel MJ, Lopes da Silva FH, Witter MP (1997) Nucleus reuniens thalami modulates activity in hippocampal field CA1 through excitatory and inhibitory mechanisms. J Neurosci 17:5640-5650.

Dolleman-van der Weel MJ, Witter MP (2000) Nucleus reuniens thalami innervates gamma aminobutyric acid positive cells in hippocampal field CA1 of the rat. Neurosci Lett 278:145-148.

Dolleman-van der Weel MJ, Morris RG, Witter MP (2009) Neurotoxic lesions of the thalamic reuniens or mediodorsal nucleus in rats affect non-mnemonic aspects of watermaze learning. Brain Struct Funct 213:329-342.

Donato F, Chowdhury A, Lahr M, Caroni P (2015) Early- and late-born parvalbumine basket cell subpopulations exhibiting distinct regulation and roles in learning. Neuron 85:770-786.

Duan AR, Varela C, Zhang Y, Shen Y, Xiong L, Wilson MA, Lisman J. (2015) Delta frequency optogenetic stimulation of the thalamic nucleus reuniens is sufficient to produce working memory deficits: relevance to schizophrenia. Biol Psychiatry 77:1098-1107.

Dudman JT, Tsay D, Siegelbaum SA (2007) A novel role for synaptic inputs at distal dendrites: instructive signals for hippocampal long-term plasticity. Neuron 56:866-879.

Eleore L, López-Ramos JC, Guerra-Narbona R, Delgado-Garcia JM (2011) Role of reuniens nucleus projections to the medial prefrontal cortex and to the hippocampal pyramidal CA1 area in associative learning. PloS One 6:e23538. Doi: 10.1371/journal.pone.0023538.

Empson RM, Heinemann U (1995) The perforant path projection to hippocampal area CA1 in the rat hippocampal-entorhinal cortex combined slice. J Physiol 484:707-720.

Enoki R, Inoue M, Hashimoto Y, Kudo Y, Miyakawa H (2001) GABAergic control of synaptic summation in hippocampal CA1 pyramidal neurons. Hippocampus 11:683-689.

Freeman JA, Nicholson C (1975) Experimental optimization of current-source-density techniques for anuram cerebellum. J Neurophysiol 38:369-382.

Freund TF, Katona I (2007) Perisomatic inhibition. Neuron 56:33-42.

Gasparini S, Magee JC (2006) State-dependent dendritic computation in hippocampal CA1 pyramidal neurons. J Neurosci 26:2088-2100.

Gonzalez J, Villarreal DM, Morales IS, Derrick BE (2016) Long-term potentiation at temporoammonic path-CA1 synapses in freely moving rats. Front Neural Circuits 10:2. Doi: 10.3389/fncir.2016.00002.

Griffin AL (2015) Role of the thalamic nucleus reuniens in mediating interactions between the hippocampus and medial prefrontal cortex during spatial working memory. Front Syst Neurosci 9:29. Doi: 10.3389/fnsys.201500029.

Grover LM, Teyler TJ (1992) N-methyl-D-aspartate receptor-independent long-term potentiation in area CA1 of rat hippocampus: input-specific induction and preclusion in a non-tetanized pathway. Neuroscience 49:7-11.

Gulyás AI, Hajos N, Freund TF (1996) Interneurons containing calretinin are specialized to control other interneurons in the rat hippocampus. J Neurosci 16:3397-3411.

Hallock HL, Wang A, Shaw CL, Griffin AL (2013) Transient inactivation of the thalamic nucleus reuniens and rhomboid nucleus produces deficits of a working-memory dependent tactile-visual conditional discrimination task. Behav Neurosci 127:860-866.

Hao J, Wang X-d, Dan Y, Poo M-m, Zhang X-h (2009) An arithmetic rule for spatial summation of excitatory and inhibitory inputs in pyramidal neurons. PNAS 106:21906-21911.

Heib DPJ, Hoedlmoser K, Anderer P, Zeitlhofer J, Gruber G, Klimesch W, Schabus M (2013) Slow oscillations amplitudes and up-state lengths relate to memory improvement. PloS One 8: e82049. Doi: 10.1371/journal.pone.0082049.

Hembrook JR, Onos KD, Mair RG (2011) Inactivation of ventral midline thalamus produces selective spatial delayed conditional discrimination impairment in the rat. Hippocampus 22:853-860.

Herkenham M (1978) The connections of the nucleus reuniens thalami: evidence for a direct thalamo-hippocampal pathway in the rat. J Comp Neurol 177:589-609.

Hoover WB, Vertes RP (2007) Anatomical analysis of afferent projections to the medial prefrontal cortex in the rat. Brain Struct Funct 212:149-179.

Hoover WB, Vertes RP (2012) Collateral projections from nucleus reuniens of thalamus to hippocampus and medial prefrontal cortex in the rat: a single and double retrograde fluorescent labeling study. Brain Struct Funct 217:191-209.

Ibarz JM, Makarova I, Herreras O (2006) Relation of apical dendritic spikes to output decision in CA1 pyramidal cells during synchronous activation: a computational study. Eur J Neurosci 23:1219-1233.

Isomura Y, Sirota A, Ozen S, Montgomery S, Mizuseki K, Henze DA, Buzsáki G

(2006) Integration and segregation of activity in entorhinal-hippocampal subregions by neocortical slow oscillations. Neuron 52:871-882.

Ito HT, Schuman EM (2012) Functional division of hippocampal area CA1 via modulatory gating of entorhinal cortical inputs. Hippocampus 22:372-387.

Ito HT, Zhang S, Witter MP, Moser EI, Moser MB (2015) A prefrontal-thalamo-hippocampal circuit for goal-directed spatial navigation. Nature 522:50-55.

Izumi Y, Zorumski CF (2008) Direct cortical inputs erase long-term potentiation at Schaffer collateral synapses. J Neurosci 28:9557-9563.

Jankowski MM, Islam MN, Wright NF, Vann SD, Erichsen JT, Aggleton JP, O'Mara SM (2014) Nucleus reuniens of the thalamus contains head direction cells. Elife 3. Doi: 10.7554/elife.03075.

Jankowski MM, Passecker J, Islam MN, Erichsen JT, Aggleton JP, O'Mara SM (2015) Evidence for spatially-responsive neurons in the rostral thalamus. Front Behav Neurosci 9:256. Doi: 10.3389/fnbeh.2015.00256.

Jarski T, Roxin A, Kath WL, Spruston N (2005) Conditional dendritic spike propagation following distal synaptic activation of hippocampal CA1 pyramidal neurons. Nat Neurosci 8:1667-1676.

Jay TM, Witter MP (1991) Distribution of hippocampal and subicular efferents in the prefrontal cortex of the rat studied by means of anterograde transport of Phaseolus vulgaris-leucoagglutinin. J Comp Neurol 313:574-586.

Jin J, Maren S (2015) Prefrontal-hippocampal interactions in memory and emotion. Front Syst Neurosci 9:170. Doi: 10.3389/fnsys.2015.00170.

Jonas P, Bischofberger J, Fricker D, Miles R (2004) Interneuron diversity series: fast in, fast out – temporal and spatial signal processing in hippocampal interneurons. Trends Neurosci 27:30-40.

Judge SJ, Hasselmo ME (2004) Theta rhythmic stimulation of stratum lacunosum moleculare in rat hippocampus contributes to associative LTP at a phase offset in stratum radiatum. J Neurophysiol 92:1615-1624.

Kajiwara R, Wouterlood FG, Sah A, Boekel AJ, Baks-te Bulte LT, Witter MP (2008) Convergence of entorhinal and CA3 inputs onto pyramidal neurons and interneurons in hippocampal area CA1—an anatomical study in the rat. Hippocampus 18:266-280.

Kincheski GC, Mota-Ortiz SR, Pavesi E, Canteras NS, Carobrez AP (2012) The dorsolateral periaqueductal gray and its role in mediating fear learning to life threatening events. PLoS One 7:e50361. Doi:10.1371/journal.pone.0050361.

Kiss J, Buzsaki G, Morrow JS, Glantz SB, Leranth C (1996) Entorhinal cortical innervation of parvalbumin-containing neurons (basket and chandelier cells) in the rat Ammon's horn. Hippocampus 6:239-246.

Kitamura T, Pignatelli M, Suh J, Kohara K, Yoshiki A, Abe K, Tonewaga S (2014) Island

cells control temporal association memory. Science 343:896-901.

Klausberger T, et al. (2005) Complementary roles of cholecystokinin- and parvalbumin-expressing GABAergic neurons in hippocampal network oscillations. J Neurosci 25:9782-9793.

Klausberger T (2009) GABAergic interneurons targeting dendrites of pyramidal cells in the CA1 area of the hippocampus. Eur J Neurosci 30:947-957.

Klausberger T, Somogyi P (2008) Neuronal diversity and temporal dynamics: the unity of hippocampal circuit operations. Science 321:53-57.

Koch C, Poggio T, Torre V (1983) Nonlinear interactions in a dendritic tree: Localization, timing, and role in information processing. Proc. Natl. Acad. Sci. USA 80:2799-2802.

Köhler C (1985) A projection from the deep layers of the entorhinal area to the hippocampal formation in the rat. Neurosci Lett 56:13-19.

Lacaille J-C, Mueller AI, Kunkel DD, Schwarzkroin PA (1987) Local circuit interactions between oriens/alveus interneurons and CA1 pyramidal cells in hippocampal slices: electrophysiology and morphology. J Neurosci 7:1979-1993.

Layfield DM, Patel M, Hallock H, Griffin AL (2015) Inactivation of the nucleus reuniens/rhomboid causes a delay-dependent impairment of spatial working memory. Neurobiol Learn Mem 125:163-167.

Lee SH, Marchionni I, Bezaire M, Varga C, Danielson N, Lovett-Barron M, Losonczy A, Soltesz I (2014) Parvalbumin-positive basket cells differentiate among hippocampal pyramidal cells. Neuron 82:1129-1144.

Leung LS, Roth L, Canning KJ (1995) Entorhinal inputs to hippocampal CA1 and dentate gyrus in the rat: A current-source-density study. J Neurophysiol 73:2392-2403.

Levy WB, Colbert CM, Desmond NL (1995) Another network model bites the dust: entorhinal inputs are no more than weakly excitatory in the hippocampal CA1 region. Hippocampus 5:137-140.

Li X-G, Somogyi P, Tepper JM, Buszáki G (1992) Axonal and dendritic arborization of an intracellularly labelled chandelier cell in the CA1 region of rat hippocampus. Exp Brain Res 90:519-525.

Liang CW (2006) One dendritic arbor, two modes of integration. J Neurosci 26:6664-6665.

Loureiro M, Colvin T, Lopez J, Merienne N, Latreche A, Cosquer B, Geiger K, Kelche C, Cassel J-C, de Vasconcelos AP (2012) The ventral midline thalamus (reuniens and rhomboid nuclei) contributes to the persistence of spatial memory in rats. J Neurosci 32:9947-9959.

Marshall L, Helgadóttir H, Mölle M, Born J (2006) Boosting slow oscillations during sleep potentiates memory. Nature 444:610-613.

McBain CJ, DiChiara TJ, Kauer JA (1994) Activation of metabotropic glutamate receptors differentially affects two classes of hippocampal interneurons and potentiates excitatory synaptic transmission. J Neurosci 14:4433-4445.

McQuiston AR (2010) Cholinergic modulation of excitatory synaptic input integration in hippocampal CA1. J Physiol 588:3727-3742.

Mölle M, Born J (2011) Slow oscillations orchestrating fast oscillations and memory consolidation. Prog Brain Res 193:93-110.

Morales GJ, Ramcharan EJ, Sundararaman N, Morgera SD, Vertes RP (2007) Analysis of the actions of nucleus reuniens and the entorhinal cortex on EEG and evoked population behavior of the hippocampus. Conf. Proc. IEEE Eng Med Biol Soc 2007:2480-2484.

Nettleton JS, Spain WJ (2000) Linear to supralinear summation of AMPA-mediated EPSPs in neocortical pyramidal neurons. J Neurophysiol 83:3310-3312.

Nunzi MG, Gorio A, Mila F, Freund TF, Somogyi P, Smith AD (1985) Cholecystokinin-immunoreactive cells form symmetrical synaptic contacts with pyramidal and non-pyramidal neurons in the hippocampus. J Comp Neurol 237:485-505.

Paxinos G, Watson C (1986) The rat brain in stereotaxic coordinates, 2nd ed., Academic Press, Sydney.

Pereira de Vasconcelos A, Cassel JC (2015) The nonspecific thalamus: a place in a wedding bed for making memories last? Neurosci Biobehav Rev 54:175-196.

Pissadaki EK, Sidiropoulou K, Reczko M, Poirazi P (2010) Encoding of spatio-temporal input characteristics by a CA1 pyramidal neuron model. PLoS Comput Biol 6:e1001038.

Poirazi P, Brannon T, Mel BW (2003) Arithmetic of subthreshold synaptic summation in a model CA1 pyramidal cell. Neuron 37:977-987.

Prasad JA, Macgregor EM, Chudasama Y (2013) Lesions of the thalamic reuniens cause impulsive but not compulsive responses. Brain Struct Funct 218:85-96.

Prasad JA, Abela AR, Chudasama Y (2017) Midline thalamic reuniens lesions improve executive behaviors. Neuroscience 345:77-88.

Preston AR, Eichenbaum H (2013) Interplay of hippocampus and prefrontal cortex in memory. Curr Biol 23:R764-R773.

Price CJ, Cauli B, Kovacs ER, Kulik A, Lambolez B, Shigemoto R, Capogna M (2005) Neurogliaform neurons form a novel inhibitory network in the hippocampal CA1 area. J Neurosci 25:6775-6786.

Price JC, Scott R, Rusakov D, Capogna M (2008) GABAb receptor modulation of feed-forward inhibition through neurogliaform cells. J Neurosci 28:6974-6982.

Remondes M, Schuman EM (2002) Direct cortical input modulates plasticity and spiking in CA1 pyramidal neurons. Nature 416:736-740.

Remondes M, Schuman EM (2003) Molecular mechanisms contributing to long-lasting synaptic plasticity at the temporoammonic-CA1 synapse. Learn Mem 10:247-252.

Remondes M, Schuman EM (2004) Role for a cortical input to hippocampal area CA1 in the consolidation of long-term memory. Nature 431:699-703.

Roux L, Buzsáki G (2015) Tasks for inhibitory interneurons in intact brain circuits. Neuropharmacology 88:10-23.

Saalmann YB (2014) Intralaminar and medial thalamic influence on cortical synchrony, information transmission and cognition. Front Syst Neurosci 8:83. Doi: 10.3389/fnsys.2014.00083.

Samulack DD, Williams S, Lacaille J-C (1993) Hyperpolarizing synaptic potentials evoked in CA1 pyramidal cells by glutamate stimulation of interneurons from the oriens/alveus border of rat hippocampus slices. Hippocampus 3:331-344.

Schall KP, Kerber J, Dickson CT (2008) Rhythmic constraints on hippocampal processing: State and phase-related fluctuations of synaptic excitability during theta and slow oscillation. J Neurophysiol 99:888-899.

Sesack SR, Deutch AY, Roth RH, Bunney BS (1989) Topographical organization of the efferent projections of the medial prefrontal cortex in the rat: an anterograde track-tracing study with Phaseolus vulgaris leucoagglutinin. J Comp Neurol 290:213-242.

Sirota A, Csicsvari J, Buhl D, Buzsáki G (2003) Communication between neocortex and hippocampus during sleep in rodents. PNAS 100:2065-2069.

Sirota A, Buzsáki G (2005) Interactions between neocortical and hippocampal networks via slow oscillations. Thalamus Relat Syst 3:245-259.

Skelton RW, McNamara RK (1992) Bilateral knife cuts to the perforant path disrupt spatial learning in the Morris water maze. Hippocampus 2:73-80.

Sloviter RS (1991) Feedforward and feedback inhibition of hippocampal principal cell activity evoked by perforant path stimulation: GABA-mediated mechanisms that regulate excitability. Hippocampus 1:31-40.

Somogyi P, Klausberger T (2005) Defined types of cortical interneuron structure space and spike timing in the hippocampus. J Physiol (Lond) 562:9-26

Somogyi P, Nunzi MG, Gorio A, Smith AD (1983) A new type of specific interneuron in the monkey hippocampus forming synapses exclusively with the axon initial segment of pyramidal cells. Brain Res 259:137-142.

Steward O (1976) Topographic organization of the projections from the entorhinal area to the hippocampal formation of the rat. J Comp Neurol 167:285-314.

Suh J, Rivest AJ, Nakashiba T, Tominaga T, Tonegawa S (2011) Entorhinal cortex layer III input to the hippocampus is crucial for temporal association memory. Science 334:1415-1420.

Swanson LW (1998) Brain maps: structure of the rat brain. 2. San Diego, Elsevier

Academic Press.
Sybirska E, Davachi L, Goldman-Rakic PS (2000) Prominence of direct entorhinal-CA1 pathway activation in sensorimotor and cognitive tasks revealed by 2-DG functional mapping in nonhuman primate. J Neurosci 20:5827-5834.
Takács VT, Klausberger T, Somogyi P, Freund TF, Gulyás AI (2011) Extrinsic and local glutamatergic inputs of the rat hippocampal CA1 area differentially innervate pyramidal cells and interneurons. Hippocampus 22:1379-1391.
Takahashi H, Magee JC (2009) Pathway interactions and synaptic plasticity in the dendritic tuft regions of CA1 pyramidal cells. Neuron 62:102-111.
Takehara-Nishiuchi K (2014) Entorhinal cortex and consolidated memory. Neurosci Res 84:27-33.
Varela C, Kumar S, Yang JY, Wilson MA (2014) Anatomical substrates for direct interactions between hippocampus, medial prefrontal cortex, and the thalamic nucleus reuniens. Brain Struct Funct 219:911-929.
Vertes RP (2002) Analysis of projections from the medial prefrontal cortex to the thalamus in the rat, with emphasis on nucleus reuniens. J Comp Neurol 442:163-187.
Vertes RP, Hoover WB, Do Valle AC, Sherman A, Rodriguez JJ (2006) Efferent projections of reuniens and rhomboid nuclei of the thalamus in the rat. J Comp Neurol 499:768-796.
Vertes RP, Hoover WB, Szigeti-Buck K, Leranth C (2007) Nucleus reuniens of the midline thalamus: link between the medial prefrontal cortex and the hippocampus. Brain Res Bull 71:601-609.
Vida I, Halasy K, Szinyei C, Somogyi P Buhl EH (1998) Unitary IPSPs evoked by interneurons at the stratum radiatum-stratum lacunosum-moleculare border in the CA1 area of the rats hippocampus in vitro. J Physiol 506:755-773.
Wang SH, Morris RG (2010) Hippocampal-neocortical interactions in memory formation, consolidation, and reconsolidation. Annu Rev Psychol 61: 49-79.
Wei DS, Mei YA, Bagal A, Kao JP, Thompson SM, Tang CM (2001) Compartmentalized and binary behavior of terminal dendrites in hippocampal pyramidal neurons. Science 293:2272-2275.
Wheeler AL, Teixera CM, Wang AH, Xiong X, Kovacevic N, Lerch JP, McIntosh AR, Parkinson J, Frankland PW (2013) Identification of a functional connectome for long-term fear memory in mice. PLoS Comput Biol 9: e1002853. Doi: 10.1371/journal.pcbi.1002853.
Wilson DIG, Watanabe S, Milner H, Ainge JA (2013) Lateral entorhinal cortex is necessary for associative but not nonassociative recognition memory. Hippocampus 23:1280-1290.
Witter MP, Griffioen AW, Jorritsma-Byham B, Krijnen JLM (1988) Entorhinal projections

to the hippocampal CA1 region in the rat: an underestimated pathway. Neurosci Lett 85:193-198.

Wolansky T, Clement EA, Peters SR, Palczak MA, Dickson CT (2006) Hippocampal slow oscillation: a novel EEG state and its coordination with ongoing neocortical activity. J Neurosci 26:6213-6229.

Wouterlood FG (1991) Innervation of entorhinal principal cells by neurons of the nucleus reuniens thalami. Anterograde PHA-L tracing combined with retrograde fluorescent tracing and intracellular injection with Lucifer yellow in the rat. Eur J Neurosci 3:641-647.

Wouterlood FG, Saldana E, Witter MP (1990) Projections from the nucleus reuniens thalami to the hippocampal region: light and electron microscopic tracing study in the rat with the anterograde tracer Phaseolus vulgaris-leucoagglutinin. J Comp Neurol 296:179-203.

Wouterlood FG, Aliane V, Boekel AJ, Hur EE, Zaborsky L, Barroso-Chinea P, Härtig W, Lanciego JL, Witter MP (2008) Origin of calretinin-containing, vesicular glutamate transporter 2-coexpressing fiber terminals in the entorhinal cortex of the rat. J Comp Neurol 506:359-370.

Xu W, Südhof TC (2013) A neural circuit for memory specificity and generalization. Science 339:1290-1295.

Zhang DX, Bertram EH (2002) Midline thalamic region: wide spread excitatory input to the entorhinal cortex and amygdala. J Neurosci 22:3277-3284.

Zhang Y, Yoshida T, Katz DB, Lisman JE (2012) NMDAR antagonist action in thalamus imposes delta oscillations on the hippocampus. J Neurophysiol 107:3181-3189.

Chapter 8

SUMMARY

The main objective of our research, using anatomical, electrophysiological, and behavioral approaches, was to study the functional organization of the ventral thalamic midline nucleus reuniens (RE), particularly regarding its connectivity with the hippocampus, and proposed importance for cognitive functions.

In *chapter 2*, using the multiple retrograde tracing technique, we showed that the projections from RE to the hippocampus (i.e., CA1, and subiculum), as well as those to the perirhinal and entorhinal cortices (EC) are non-collateralized. These predominant unilateral projections, displaying a topographical organization, arise from distinct although intermingled population of neurons located mainly in the rostral and mid rostral-to-caudal part of RE. Moreover, within each target area the terminal collateralization is locally restricted instead of distributing axon collaterals throughout the entire target structure. Since RE afferents are also topographically organized, it is conceivable that distinct clusters of RE projection cells may receive separate inputs, which in turn will be relayed to specific targets in the hippocampal-entorhinal complex.

In *chapter 3*, the RE-CA1 and direct EC-CA1 projections, both known to terminate in stratum lacunosum moleculare, were used as a model to explore and compare the sensitivity, specific properties, and the detectability of three different anterograde tracers, namely Phaseolus-vulgaris leucoagglutinin (PHA-L), rhodamine- (RDA) and biotin-conjugated dextran amine (BDA). We describe a newly developed method that can be used to examine the distribution of axonal terminations of three different afferent systems in a particular brain area, in one and the same animal. Using a simple application procedure, we injected the first tracer bilaterally in RE, a second tracer in the left EC, and a third tracer in the right EC. Subsequently, a newly developed triple staining procedure allowed for the simultaneous and permanent visualization of these three tracers, i.e., detectable as black, brown, and blue-green coloured labelled fibres, respectively. Not only offers this method an attractive approach for anatomical research in general, it also provided the necessary information to be used in our following electrophysiological experiments, i.e., choosing the optimal site for electrical stimulation in RE and EC, as well as the appropriate recording site in CA1 showing substantial overlap of RE and EC terminals in lacunosum moleculare (*see chapters 4 and 7*).

In *chapter 4*, we describe our electrophysiological in vivo experiments in which we stimulated the RE-CA1 projection at its origin, and studied the influence of RE input on the neuronal activity in hippocampal field CA1. Anatomically, RE axons in stratum lacunosum moleculare of CA1 are known to form asymmetrical (i.e., excitatory) synaptic contacts with spines and dendrites, suggesting that RE innervates the spinous apical dendrites of pyramidal cells, and presumably also the largely aspinous dendrites of interneurons with a dendritic tree in lacunosum moleculare. Paired pulse stimulation of RE elicited a clear dipole field in CA1, i.e., relatively large negative (subthreshold) deflections in lacunosum moleculare, reversing at the lacunosum moleculare-radiatum border to positive-going ones in strata radiatum and pyramidale, and steadily declining towards the alveus. A current source density (CSD) analysis revealed a clear lacunosum moleculare sink-radiatum source configuration, which is in agreement with an excitatory synaptic RE input onto the apical dendrites of CA1 pyramidal cells. Stimulation of RE at low frequencies (0.13-2 Hz) elicited the largest amplitude field excitatory postsynaptic potentials (fEPSPs). In contrast, stimulation of RE in the theta frequency range (4-10 Hz) evoked only small amplitude fEPSPs. Furthermore, low frequency paired pulse stimulation of the RE-CA1 input resulted in a robust form of short term plasticity, termed paired pulse facilitation (PPF). This appeared largely independent on stimulation (low-to-high) intensity or inter-pulse-interval duration (20-200 ms), indicating that RE can exert a persistent influence on the level of pyramidal cell excitability.

In contrast to subthreshold CA1 cell responses (i.e., we never observed action potential generation in pyramidal cells) we did notice the occurrence of RE-elicited spiking in two types of putative inhibitory CA1 interneurons, both known to mediate feedforward and feedback inhibition of pyramidal cells. Thus, RE-CA1 input partially influences hippocampal activity through activation of (at least two classes of) local inhibitory interneurons.

Next to a clear monosynaptic RE input, we found indications for complex and presumably di-synaptic elicited responses. Using additional anatomical tracing methods we showed that the basis for the observed di-synaptic input in CA1 was a projection from caudal RE-to-rostral RE.

Taken together, we concluded that RE can influence the CA1 pyramidal cell activity through direct excitatory and indirect inhibitory mechanisms. We proposed a closed circuit between rostral RE – CA1 – subiculum – caudal RE – rostral RE, which may allow RE to modulate the activity level in CA1 depending on the hippocampal output.

In *chapter 5*, we examined the RE axo-dendritic contacts in stratum lacunosum moleculare of hippocampal field CA1 at the ultrastructural level. To label RE axons, the anterograde tracer biotin-conjugated dextran amine (BDA) was injected into RE. Subsequently we

combined the visualization of BDA with staining of GABA, the latter to identify local inhibitory interneurons in CA1. Our results showed that a considerable part of the BDA-labeled RE axons form asymmetrical (i.e., excitatory) synapses on GABA-positive dendrites. These findings confirmed our previous electrophysiological observations, which indicated that RE is able to discharge inhibitory interneurons in CA1 (*see chapter 4*).

In *chapter 6*, we compared the effects of neurotoxic lesions of the RE or the mediodorsal (MD) thalamic nuclei on performance in a standard (reference memory) water maze task. Diencephalic or thalamic amnesia is characterized by deficits that resemble those of medial temporal lobe (hippocampal) amnesia or prefrontal dysfunction. Nuclei in the medial thalamus are connected with either the temporal lobe, or prefrontal cortex, or with both, and thus thalamic amnesia may be due to disconnecting the temporal and prefrontal systems at the thalamic level. Alternatively, it may result from the loss of specific thalamic contributions to these systems. In rats, both RE and MD are heavily and reciprocally connected with the medial prefrontal cortex (mPFC), but only RE innervates hippocampal field CA1, a structure of crucial importance for learning and memory. In the standard water maze task, the hippocampal formation is engaged in the spatial aspects of learning and memory, whereas the mPFC is more involved in behavioral flexibility and execution of strategies rather than in encoding or storage of spatial information. Therefore, a RE lesion was expected to cause a mixed deficit in hippocampal related spatial learning/memory as well as in mPFC related flexibility/strategy learning, while a MD lesion was assumed to result predominantly in an acquisition deficit in behavioral flexibility, i.e. a mPFC-related impairment. Unexpectedly, our observations during the acquisition phase (i.e., learning to located an invisible platform, using room cues to guide the search), probe test (i.e., a memory test, with room cues visible but platform removed), and cue test (i.e., a test to examine sensorimotor and/or motivational deficits; visible platform, but room cues no longer visible) revealed that neither RE, nor MD lesions did prevent learning and later memory of the task per se. Instead, RE and MD lesions affected the normal flexible use of search strategies and/or the flexibility with which a change in task conditions can be accommodated. That is, a RE lesion resulted in very flexible/impulsive behavior, whereas a MD lesion caused perseverative behavior, indicating that RE and MD may play opposing roles in non-mnemonic processes like strategy shifting, or in more general aspects of behavioral flexibility.

In *chapter 7*, using in vivo single and simultaneous low frequency stimulation of the RE-CA1 and lateral EC-CA1 projections, we investigated their combined effects on neuronal activity in hippocampal field CA1. Our results revealed that paired pulse stimulation of either RE or EC evokes subthreshold responses, showing strong homosynaptic paired

pulse facilitation (PPF), whereas combined paired pulse stimulation of RE and EC does not result in heterosynaptic PPF. Coinciding RE and EC inputs, however, resulted in a major enhancement of the fEPSPs in stratum lacunosum moleculare, yet action potential generation in pyramidal cells does not occur. This inability to induce CA1 cell firing is likely due to persistent inhibitory influences mediated by both inputs separately, as well as an additional peri-somatic inhibitory effect mediated by coinciding RE/EC inputs. A CSD analysis revealed complex interactions between RE and EC inputs throughout the depth profile of CA1, indicating an (at least partial) convergence of RE and EC synapses in lacunosum moleculare on the same dendritic branch of CA1 pyramidal cells, as well as on subclasses of inhibitory interneurons with dendrites in lacunosum moleculare. We discussed the functional relevance of coinciding RE and EC inputs in CA1, and proposed that low frequency RE-CA1 input is important for the synchronization of slow oscillations in hippocampus and mPFC. Furthermore, our data strongly suggested that by directly and indirectly facilitating the EC-CA1 input during slow oscillations, RE can contribute to the dialogue between hippocampus and mPFC which is of crucial importance for the consolidation of hippocampal-dependent memories.

Chapter 9

GENERAL DISCUSSION

Clinical evidence from patients with brain damage in the thalamus suggests that many thalamic nuclei play a role in cognitive functions, such as attention, executive functions and memory (e.g., Van der Werf, 2000, 2003a,b, Aggleton 2014). In clinical cases, lesions often result from vascular trauma and in most instances, but not always, include more than one nucleus. To experimentally determine the individual contribution of a particular thalamic nucleus to cognitive functioning we have to employ animal models (e.g., using permanent lesions, reversible inactivation, electrical stimulation/optogenetics), which can provide a far better anatomical specificity. Historically, most studies on thalamic (diencephalic) amnesia have focussed on the anterior nuclei, the rostral intralaminar nuclei, as well as on the mediodorsal nucleus. More recently a growing number of studies have provided evidence for the importance of the thalamic midline nuclei in cognitive functions (e.g., Saalmann 2014; Mitchell et al 2014).

The research described in this thesis focussed on the ventral midline nucleus reuniens (RE) in the rat. RE has long been considered a non-specific thalamic nucleus which, as a rostral non-discriminatory extension of the brainstem reticular arousal system, was thought to project diffusely to a large part of the cortical mantle. Using anatomical, electrophysiological, and behavioral methods, we investigated the anatomical and functional connectivity of RE, with emphasis on projections to structures belonging to the hippocampal region. In addition, we discuss a role for RE in coordinating the flow of information between hippocampus and mPFC in relation to cognitive functions, as well as in brain diseases such as schizophrenia and epilepsy.

Anatomical considerations

Understanding the functional role of a particular nucleus requires a detailed knowledge of its input and output connectivity. Herkenham (1978) performed the first systematic study of RE afferents and efferents. Later studies, using modern neuroanatomical tracing methods, have greatly expanded our knowledge of RE input and output systems, and their topographical organization.

Overall, RE input is very diverse and originates from widespread structures in brainstem, diencephalon and telencephalon (e.g., Dolleman-van der Weel et al 1993;

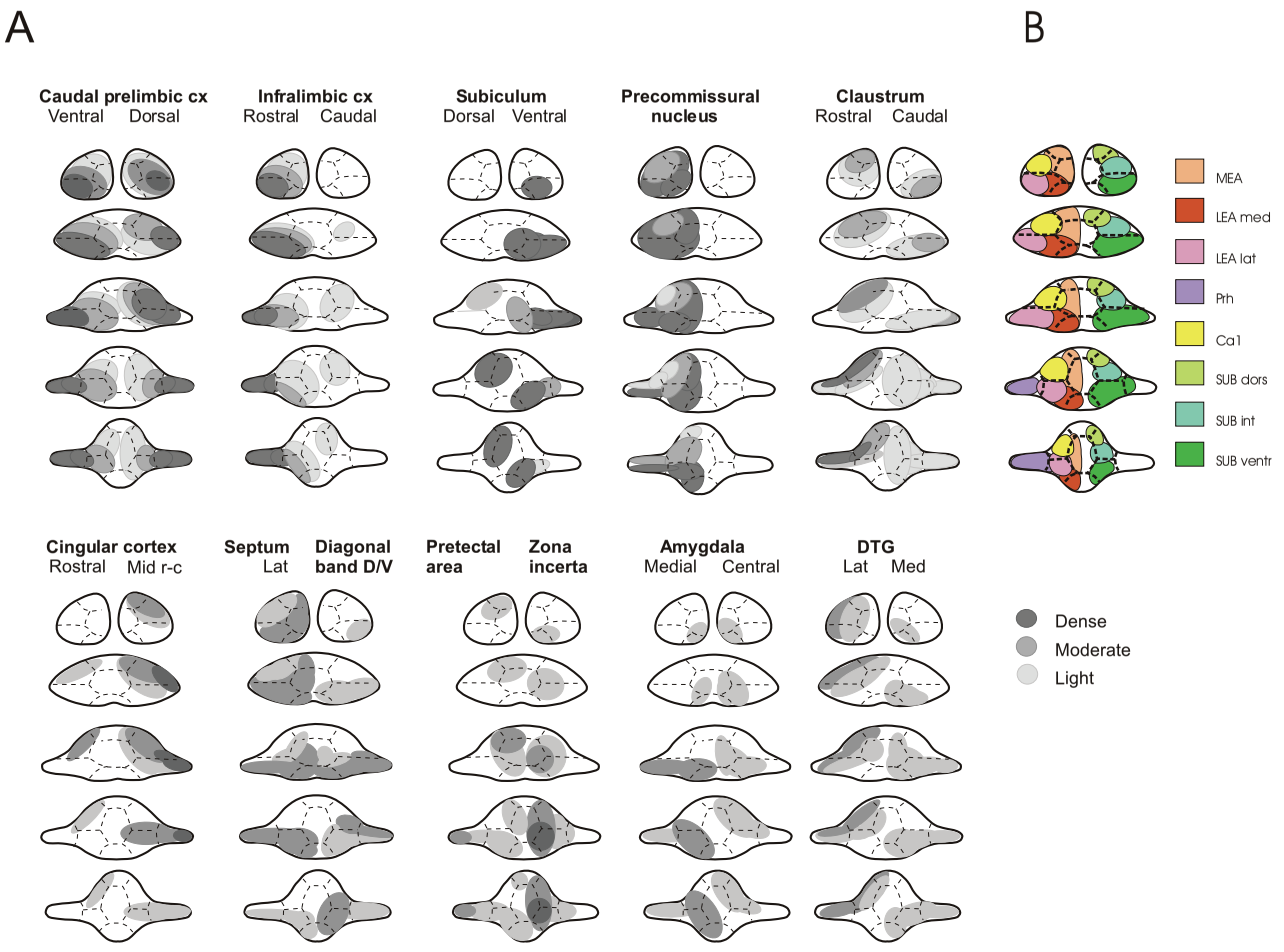
A
B
Caudal prelimbic cx
Ventral Dorsal
Infralimbic cx
Rostral Caudal
Subiculum
Dorsal Ventral
Precommissural nucleus
Claustrum
Rostral Caudal
MEA
LEA med
LEA lat
Prh
Ca1
SUB dors
SUB int
SUB ventr
Cingular cortex
Rostral Mid r-c
Septum
Lat
Diagonal band D/V
Pretectal area
Zona incerta
Amygdala
Medial Central
DTG
Lat Med
Dense
Moderate
Light

Krout et al 2002; Vertes 2002; McKenna and Vertes 2004; Cassel et al 2013), but RE output is slightly more restricted and mainly targets limbic structures, particularly the mPFC and the hippocampal region (Wouterlood et al 1990; Wouterlood 1991; Dolleman-van der Weel and Witter 1996; Van der Werf et al 2002; Vertes et al 2006, 2007; Varela et al 2014). Many of the RE input and output connections are reciprocal, predominantly those with limbic associated areas. Therefore, RE is thought of as a 'limbic thalamic nucleus' (Vertes et al 2015). Several thalamic nuclei, including RE, project to the subiculum. Yet, a unique feature of RE is that it is virtually the only thalamic nucleus (i.e., the RE/rhomboid complex) directly innervating hippocampal field CA1, but not the other CA fields or the dentate gyrus. The role of CA1 in learning and memory relies for a large part on its interaction with mPFC (e.g., Floresco et al 1997; Frankland et al 2001). The ventral and intermediate (but not dorsal) CA1/subiculum project to the mPFC, but there is no direct return projection from mPFC to the hippocampus (Jay and Witter 1991; Vertes et al 2004; Hoover and Vertes 2007). Since RE sends dense reciprocal projections to (especially the intermediate and ventral parts of) CA1/subiculum as well as to mPFC, it has been suggested that RE may serve as a critical functional link in the communication between mPFC and CA1 (Vertes et al 2007; Prasad and Chudasama 2013).

RE output pathways generally display a very low degree of collateralization (if at all present) between different target areas (Ohtake and Yamada 1989; Su and Bentivoglio 1990; Hoover and Vertes 2012; Varela et al 2014). Focussing on RE projections to the hippocampal formation and adjacent cortical areas, we showed that projections to CA1, subiculum, entorhinal and perirhinal cortices are non-collateralized, and arise from distinct topographically organized clusters of RE neurons (see *chapter 2*). RE projections to the medial septum or to CA1 also arise from different, topographically organized cell clusters (Bokor et al 2002). In contrast, a small percentage of the RE-CA1 projecting neurons has been shown to send collateralized axons to mPFC as well (Hoover and Vertes 2012; Varela et al 2014).

⇦ Fig. 1. Series of five coronal sections through the rostral-to-caudal (i.e., top to bottom) RE/periRE nucleus, illustrating the topographical organization of afferents and efferents. A. Schematic representation of the relative density of axon terminals originating in various afferent structures. B. Schematic representation of clusters of RE/periRE neurons projecting to CA1, subiculum, and entorhinal/perirhinal cortices, respectively. Abbreviations: cx=cortex; DTG=dorsal tegmentum; MEA=medial entorhinal area; LEA=lateral entorhinal area; Prh=perirhinal cortex; SUB=subiculum; lat=lateral; med=medial; int=intermediate; D/V=dorsal/ventral.

These findings raise some important questions, namely: 1) whether different clusters of RE neurons may each receive distinct inputs, or whether these cell clusters share, at least partly, the same information which is concurrently relayed via separate pathways to their respective targets, and 2) what might be the functional significance of the relatively few collateralized RE neurons innervating two different target areas (e.g., CA1 and mPFC)?

Regarding the first question, a comparison of the distribution of in- and output patterns in RE suggests that particular clusters of neurons, such as the ones projecting to the hippocampal region (Dolleman-van der Weel and Witter, 1996), have at least partly a higher probability of receiving a specific input that differs from that of other clusters (Fig 1). At the cellular level, however, the convergence of RE afferents is still unknown. It is also not fully known which of the numerous RE afferents can be considered 'drivers', targeting the proximal dendrites of RE neurons and carrying specific messages, and which ones may be 'modulators', targeting primarily the distal dendrites and fine-tuning transmission of the message (Groenewegen and Witter 2004; Varela, 2014). A high-order relay nucleus, such as RE, is considered to receive driver input from cortical layer V pyramidal cells, and modulator input from cortical layer VI pyramidal cells, and can be viewed as a link in cortico-thalamo-cortical processing (Sherman 2012). At the ultrastructural level, the mPFC-RE axons are known to form asymmetrical (excitatory) synapses on proximal dendrites of RE-CA1 projecting neurons (Vertes et al 2007). This suggests that the mPFC-RE projection transmits, at least partly, driver input arising from layer V pyramidal cells onto RE-CA1 projecting neurons, which are assumed to relay mPFC-processed information to the hippocampus. Whether the mPFC-RE input, arising from layer VI cells (McKenna and Vertes 2004), targets the distal dendrites of RE neurons (i.e., a modulator input) remains to be established. RE receives also 'classical' modulatory (e.g., cholinergic, dopaminergic, noradrenergic, serotonergic, and various neuropeptidergic), as well as inhibitory GABAergic inputs from the thalamic reticular nucleus and the zona incerta (e.g., Houser et al 1980; Barthó et al 2002; Halassa and Acsády 2016), mainly influencing how driver input is relayed through the thalamus (Mitchell et al 2014). Considering the wide variety of RE afferents (Vertes et al 2006), more detailed knowledge of specific input features (e.g., distal or proximal location of synaptic contacts on RE dendrites, presynaptic neurotransmitter) would greatly improve our understanding of the role(s) RE may play in cognitive and other functions (reviewed in Cassel et al 2013; Vertes et al 2015). Therefore, the convergence of RE afferents on identified RE projection cells should be addressed in future studies.

Regarding the second question, it has been suggested that the collateralized RE neurons projecting to CA1 and mPFC (Hoover and Vertes 2012) are particularly suited

to synchronize activities/oscillations in both areas (Varela et al 2014). However, the mechanism by which neuronal synchronization in distant brain areas can be accomplished is as yet unknown. Likewise, neither the target cells nor the electrophysiological properties of these collateralized RE-CA1/mPFC projecting neurons are known. From a functional view point, it may seem quite peculiar that synchronization of neural activities in these distant areas can be achieved by relatively few collateralized RE-CA1/mPFC projecting cells. In fact, their input will be outnumbered by a far denser RE input arising from the single CA1- and single mPFC-projecting neurons, respectively (Hoover and Vertes 2012; Varela et al 2014). The efficacy of a projection, however, is not determined by anatomical quantitative measures such as numbers of projection fibers, but depends on multiple complex factors, for example concerning the postsynaptic neuron (e.g., cell type, distribution of receptors, location of synaptic contacts on dendrites or soma), and the transmitter (excitatory or inhibitory) in the presynaptic neuron (e.g., Rockland 2015). So far, we have shown that the targets of RE-CA1 projecting neurons are pyramidal cells and several classes of local interneurons (Wouterlood et al 1990; see *chapters 4, 5, 7*; own unpublished results). In contrast, the target cells of RE-mPFC projecting neurons have not yet been identified, but it is assumed that, similar to the RE-CA1 input, pyramidal cells as well as interneurons in mPFC receive RE input (Di Prisco and Vertes, 2006; Eleore et al 2011; Cruikshank et al 2012). Since various types of interneurons are known to play important, diverse roles in controlling the activity of large numbers of principal cells (e.g., excitability level, formation of cell-ensembles, oscillatory behavior), an effective way to influence/synchronize large groups of pyramidal cells is through activation of local interneurons (e.g., Somogyi and Klausberger 2005; Klausberger and Somogyi 2008). Therefore, an interesting possibility is that the collateralized RE-CA1/mPFC projecting neurons innervate predominantly, or even exclusively, a specific class of interneurons in both CA1 and mPFC, which in turn may modulate (simultaneously) the excitability level and/or synchronize oscillations of a large group of pyramidal cells in each target area. This may create a window for coordinated input via single RE-mPFC, and RE-CA1 and/or CA1-mPFC pathways, thereby facilitating the communication between mPFC and hippocampus. Although speculative, this idea is at least supported by some interesting observations by Cruikshank et al (2012; see also Electrophysiological considerations). Using an optogenetic strategy, these investigators have shown that activation of matrix thalamo-cortical projection neurons, including cells in RE, resulted in excitation of mPFC layer I inhibitory interneurons, presumably the so-called late-spiking neurogliaform cells (e.g., Overstreet-Wadiche and McBain 2015). In turn, this resulted in feedforward inhibition of local layer 1 interneurons and pyramidal cells in layers 2/3. It was suggested that this thalamic-induced feedforward inhibition may impose a narrow window for excitation of mPFC pyramidal cells. It is thus timely to identify the target cells of

collateralized RE-CA1/mPFC projecting neurons, and to investigate their potential involvement in (possibly state-dependent) network synchronization.

The existence of collateralized RE 'feedback' inputs has also been reported (Varela et al 2014). Next to a small percentage of subicular neurons with collateralized axons to mPFC and RE, some cells in the dorsolateral entorhinal cortex layers III/IV, i.e., an area receiving RE input (Wouterlood et al 1990; Wouterlood 1991; Dolleman-van der Weel and Witter 1996), project via collaterals to mPFC and the hippocampus. As schematically summarized in figure 2, these small numbers of collateralized cells (i.e., RE–CA1/mPFC, subicular-mPFC/RE and entorhinal-hippocampus/mPFC projecting neurons), located in highly interconnected areas, may be of crucial importance for the synchronization of neuronal activities in a large scale hippocampal-mPFC-thalamic-entorhinal network, serving a critical role in cognitive processing (Varela et al 2014). Testing this hypothesis will, for instance, require simultaneous (intracellular) recording and labelling in multiple widespread areas. In this respect, however, a complicating factor may arise from the fact that these collateralized projection neurons are not only relatively sparse, but they are also intermingled amongst clusters of neurons projecting to just one of the two respective target areas. Targeting the collateralized neurons might be achieved with an optogenetic approach, using a dual retrograde viral labelling with each virus expressing part of the load needed to successfully express an opsin.

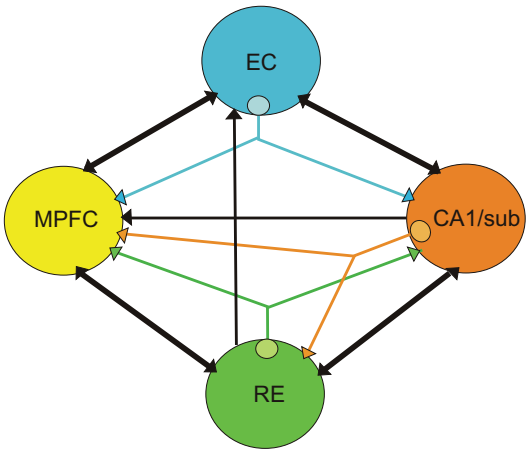

Fig. 2. Schematic representation of connectivity between CA1/subiculum, mPFC, entorhinal cortex, and RE. Thick black lines represent reciprocal connections; thin black lines represent a one-way projection. Coloured lines indicate sparse collateralized projections between the four areas.

The influence of a particular input structure is first of all determined by the neurotransmitter, i.e, excitatory or inhibitory, that is released onto the postsynaptic target cells. The primary neurotransmitter of RE neurons is most likely an excitatory amino acid, presumably aspartate and/or glutamate (e.g., Herkenham 1978; Bokor et al 2002; Cruikshank et al 2012). This assumption is also in agreement with observations at the ultrastructural level, revealing that RE neurons form exclusively asymmetrical (i.e., excitatory) synapses on target cells (i.e., pyramidal cells and local interneurons) in CA1, subiculum, and entorhinal cortex (Wouterlood et al 1990; Wouterlood 1991; Dolleman-van der Weel and Witter, 2000; own unpublished observations). In the rat brain, RE does not contain GABA-positive neurons. Recently, the existence of dopamine (DA) containing neurons in RE and zona incerta has been reported (Ogundele et al 2017). These thalamic DA neurons are suggested to be part of a hypothalamic neuroendocrine system involved in the control of appetite, fluid balance and metabolism.

RE neurons also contain the calcium-binding proteins calretinin (CR), calbindin (CB), or co-localized CR/CB, but parvalbumin (PV) is absent (Frassoni et al 1991; Arai et al 1994; Montpied et al 1995; Bokor et al 2002; Drexel et al 2011). Although little is known about the functional significance of these calcium-binding proteins, CB- and PV-positivity ($^+$) in thalamic neurons is used to distinguish two classes of thalamic relay cells, namely CB^+ 'matrix' cells with dense terminations in cortical layer 1, and PV^+ 'core' cells projecting to the middle cortical layers III/IV (Jones 1998). Although CB^+ matrix neurons can be found throughout the thalamus, unconstrained by nuclear boundaries, they are abundantly present in non-specific nuclei such as RE. Since RE is devoid of PV^+ cells (Arai et al 1994), RE neurons are thus considered to be matrix cells, projecting predominantly to cortical layer I. Nonetheless, RE axons in mPFC innervate both the superficial layer I as well as the deep layers V/VI (Vertes et al 2006), and the RE-EC projection innervates layers I and III/IV (Wouterlood et al 1990). Regarding the RE-CA1 projection, nearly all (94%) retrogradely labelled RE-CA1 neurons were CB-positive, whereas 66% contained CR (Bokor et al 2002). This indicates that roughly 2/3 of the RE-CA1 projecting neurons contain co-localized CB/CR, and that approximately 1/3 contains only CB. In addition, RE-EC and RE-subiculum projecting neurons have been shown to express CR (Wouterlood et al 2008; Drexel et al 2011). Interestingly, it was recently reported that midline thalamic CR^+ and CR-negative (CR^-) neurons are differentially active during hippocampal network oscillations (Lara-Vásquez et al 2016, see below). In this respect, the CB^+ and CR^+ RE neurons, projecting to CA1, subiculum, and EC may thus play different roles in state-dependent functioning of the hippocampus.

Electrophysiological considerations

Knowledge about the mechanisms through which RE can influence transmission of information in its main target structures (i.e., CA1, and mPFC) is still rather limited. Initially, most indications for a strong RE-mediated influence on hippocampal functioning came from epilepsy-related research. For instance, studies in the rat have shown that an injection of N-methyl-D-aspartate (NMDA) into RE produced strong hippocampal seizure activity (e.g., Hirayasu and Wada 1992). Although these findings pointed to an excitatory influence of RE on hippocampal neurons, at that time direct electrophysiological evidence was still lacking. In view of the prominent RE projections to the hippocampus and mPFC, it is surprising that so far only a few electrophysiological studies have provided evidence for RE-elicited excitatory responses in CA1 and mPFC (Dolleman-van der Weel et al 1997, 2017; Bertram and Zhang 1999; Di Priso and Vertes 2006; Eleore et al 2011). Our 1997 study was the first to reveal that RE modulates the excitability level of CA1 pyramidal cells through (direct) excitatory and (indirect) inhibitory mechanisms (see *chapter 4*). These findings are supported by our observations at the ultrastructural level, showing that RE axons in LM of CA1 form asymmetrical (i.e., excitatory) synaptic contacts onto GABA-positive dendrites of interneurons (see *chapter 5*), as well as on the dendrites and spines of identified (i.e., intracellularly labelled) pyramidal cells (own unpublished results). In spite of a strong and persistent RE-induced paired pulse facilitation of field excitatory post-synaptic potentials (fEPSPs) in CA1, population spikes, indicative for firing of principal cells, were never observed. In contrast, RE activation at low frequencies (ranging from 0.1-2 Hz) resulted in driving a subclass of radiatum interneurons, presumably Schaffer collaterals-associated cells mediating feedforward inhibition of pyramidal cells as well as inhibition of other interneurons. In addition, RE could drive vertical oriens/alveus interneurons also mediating feedforward inhibition (Dolleman-van der Weel et al 1997). Likewise, in mPFC (i.e., prelimbic and infralimbic areas) the RE-evoked fEPSPs seemed indicative for excitatory and inhibitory components in the elicited field potentials (Di Prisco and Vertes 2006). The inability to generate RE-induced pyramidal cell firing in CA1 and mPFC in the anaesthetized rat was confirmed in later studies (Morales et al 2007; Eleore at al 2011; Dolleman-van der Weel et al 2017). Only one study has reported that stimulation of the thalamic midline, including RE, resulted in the occurrence of CA1 population spikes, similar to the response evoked by contralateral CA3 stimulation (Bertram and Zhang 1999). However, this discrepancy with the aforementioned studies is most likely due to the much larger thalamic region that was stimulated by the latter investigators.

In conclusion, a strong RE-mediated feedforward inhibition may thus condition CA1 principal neurons to discharge only under certain circumstances, namely in the window when inhibition is diminished, and/or when the excitability level of the apical dendrites is further enhanced by other inputs, such as those from EC and/or CA3 (see below).

Physiological properties of reuniens neurons

Only recently it was reported that, in freely moving animals, a relatively small percentage of RE cells displayed various spatial properties, i.e., RE contains head direction cells, 'place cells' with low levels of spatial information, and perimeter/border or boundary cells (Jankowski et al 2014, 2015). Although these neurons showed activity in the theta frequency range, there was only a low coherence with hippocampal theta. The vast majority (~64%) of RE cells, however, were low frequency firing neurons without spatial properties, of which approximately 17% fired only at frequencies below 1 Hz (Jankowski et al 2014). Thus, low frequency stimulation, used in our studies (Dolleman-van der Weel et al 1997, 2017) as well as used by others (Di Prisco and Vertes 2006; Morales et al 2007; Eleore at al 2011), is at least consistent with these physiological properties of a large group of RE neurons. Using the patch clamp technique, the physiological diversity of RE neurons in the rostral part of the nucleus was recently examined in young adult mice (Walsh et al 2017). In this in vitro study, the recorded RE cell population had a mean membrane potential of -64 mV, and a mean high input resistance over 600 MΩ, which is much higher than is usually found for thalamic neurons (i.e., around 200 MΩ). Most RE cells displayed spontaneous firing at rest (i.e., without artificial stimulation), often in a tonic fashion at frequencies between 2-16 Hz. Only RE cells with very negative resting membrane potentials fired occasionally spontaneous high frequency (~ 200 Hz) bursts of spikes. Setting the membrane potential at -80 mV resulted in an absence of spontaneous activity. Subsequently, by applying a series of incremental depolarizing current injections at 1 Hz, RE cells could be divided into two groups, i.e., cells firing just one action potential, and cells firing in bursts of 2-6 action potentials. However, at a slightly more depolarized (i.e., -72 mV) membrane potential high frequency bursts were almost absent. The change in firing pattern is presumably due to the presence of low threshold T-type Ca^{2+} channels, which are largely inactivated at the latter resting potential. This assumption is supported by the observation that approximately 80% of T-type channels in RE neurons were deinactivated when the membrane potential was set at -85 mV for a short time (Walsh et al 2017). Therefore, it was suggested that the neurophysiological diversity of RE neurons could be associated with differences in calcium buffering capabilities, and a different expression of calcium binding proteins in RE cells (see below). In future in vivo

studies these findings need to be verified, e.g., in freely moving animals, and it should be further investigated how the membrane potential and firing behavior of RE cells can be influenced by various classical modulatory inputs.

Thalamic midline CR^- and CR^+ neurons, including the co-localized CR^+/CB^+ ones, are differentially active during hippocampal network oscillations (Lara-Vásquez et al 2016). This is of interest since RE projections to CA1, subiculum, and entorhinal cortex are known to arise for a large part from CR^+ RE cells (Bokor et al 2002; Wouterlood et al 2008; Drexel et al 2011), while approximately 1/3 of the RE-CA1 input arises from CB^+ (i.e. CR-negative) neurons (Bokor et al 2002). A general feature of the thalamic midline CR^+ neurons is their overall low level of discharges, whereas CR^- neurons display an overall higher level of activity (Lara-Vásquez et al 2016). Furthermore, at 4-10 Hz theta frequencies, occurring during exploratory behavior and REM sleep, and probably modulating memory processes, CR^- neurons display an increase in their discharge rates, whereas CR^+ neurons do not. In contrast, during high frequency sharp wave-ripples (SWR), occurring during quiet states, and ≤1 Hz slow oscillations in slow-wave sleep, likely reflecting memory consolidation, the firing rate of the CR^- neurons remains unaffected. CR^+ neurons, however, slightly increase their firing just before and just after SWR, but they are significantly inhibited during a SWR event (Lara-Vásquez et al 2016). Assuming that the aforementioned properties apply for the CR^+ and CR^+/CB^+, as well as CB^+ (i.e. CR-negative) RE neurons, this suggests that the majority of CR^+ RE neurons projecting to CA1, subiculum, and entorhinal cortex, display a specific discharge pattern during hippocampal slow oscillations. A minority of CR^- RE-CA1 projecting neurons (i.e., the single CB-containing ones), however, is particularly active during hippocampal theta waves.

The aforementioned physiological properties of RE neurons (Jankowski et al 2014, 2015; Lara-Vásquez et al 2016) are at least supportive for a predominant involvement of RE-CA1/subiculum and RE-EC projecting CR^+ neurons in slow oscillations. This is also in line with our electrophysiological results, showing that low (≤ 2 Hz) frequency stimulation of RE yielded much larger amplitude CA1 fEPSPs than following stimulation at theta frequencies (4-10 Hz). Through activation of particular CA1 interneurons in distal stratum radiatum (Dolleman-van der Weel et al 1997), RE may impose a slow oscillation on CA1 pyramidal cells, which is in accordance with recent reports by others (Zhang et al 2012; Duan et al 2015). Moreover, behavioral studies have indicated that RE is involved in memory consolidation, a process that depends on slow (<1 Hz) synchronized oscillations in hippocampus and mPFC (e.g., Loureiro et al 2012).

Next to slow oscillations, synchronized hippocampal-prefrontal activity in the theta frequency range (4-10 Hz, occurring during exploration, and REM sleep), is of crucial importance for (spatial) working memory and, as recently reported, also for memory consolidation (Boyce et al 2016). The role of hippocampal theta rhythm in plasticity, spatio-temporal coding of information, and learning and memory is well documented (e.g., Vertes et al 2004; Montgomery et al 2009; Boyce et al 2016). Whether RE plays an important role in hippocampal theta waves, and/or in theta-associated communication between hippocampus and mPFC, is as yet not entirely clear. For instance, RE lesions had no effect on atropine-resistant theta (Vanderwolf et al 1985). Only a few electrophysiological studies have specifically investigated RE involvement in hippocampal theta rhythm. It was reported that RE neurons increased their spiking activity during spontaneous or tail-pinch induced hippocampal theta oscillations, although their overall activity pattern, measured by steady discharges without bursting, displayed only a very low coherence with hippocampal theta (Morales et al 2007). In contrast, during goal directed navigation RE cells displayed trajectory-dependent activity, phase-locked to theta rhythm in CA1 (Ito et al 2015). Previously, we reported that, in the anesthetized rat, stimulation of RE at theta frequencies yielded only small amplitude CA1 responses (Dolleman-van der Weel et al 1997). Moreover, we often noticed that low frequency RE-CA1 input disrupted spontaneously occurring hippocampal theta oscillations, even up to a point of near complete suppression (own unpublished results). This disruption of theta waves may be due to a direct influence of RE input on CA1 pyramidal cells, and/or on local inhibitory interneurons. Alternatively, the suppression of hippocampal theta may also result from inadvertent co-activation of the RE-medial septum projecting neurons (Bokor et al 2002), which subsequently may interfere with the activity of the medial septum-CA1 projecting neurons and their role in the generation of hippocampal theta oscillations (Unal et al 2015; Vertes 2015). Recently, it was shown that in urethane-anesthetized rats pharmacological inactivation of RE resulted in a decreased coherence between PFC and hippocampus 2-5 Hz oscillations. In contrast, inactivation of RE had just a minimal effect on PFC and hippocampus coupling at theta frequencies (Roy et al 2017). Taken into account that the vast majority of RE neurons, specifically the CR^+ RE-CA1/subiculum projecting ones, generally fire at low frequencies while showing no (or very low) coherence with hippocampal theta (Jankowski et al 2014, 2015; Lara-Vasques et al 2016; Roy et al 2017), the proposed involvement of RE in hippocampal theta oscillations, and/or theta synchronization in hippocampus and mPFC, awaits further investigation.

RE-EC interactions

Based on the well-known overlap of RE and EC terminations in stratum lacunosum moleculare (LM) of CA1, it is to be expected that interactions between both inputs occur. Nevertheless, electrophysiological (in vitro) studies of converging inputs in CA1 commonly concern the direct EC-CA1 input in LM and the input from CA3 via the Schaffer collaterals in stratum radiatum. Dependent on input timing and stimulation frequency, combining in vitro stimulation of the EC-CA1 fibres in LM, and CA3-CA1 Schaffer collaterals inputs has been shown to result in a variety of effects, such as changes in spiking activity of pyramidal cells (Remondes and Schuman 2002; Takahasi and Magee 2009; Pissadaki et al 2010; Milstein et al 2015), modification of long-term synaptic changes in both inputs (Remondes and Schuman 2003; Judge and Hasselmo 2004; Dudman et al 2007), gating of Schaffer collateral input by preceding LM stimulation (McQuiston 2010) and, vice versa, gating of EC input by preceding Schaffer collateral stimulation (Ang et al 2005). However, in these instances inadvertent co-activation of RE and EC axons in LM in a slice preparation is usually not accounted for. In fact, our second electrophysiological study in the anesthetized rat (see *chapter 7*) was the first to examine the specific contributions of coinciding RE and direct EC inputs on neuronal activity of pyramidal cells and interneurons in hippocampal field CA1. In this study, we stimulated RE and EC at low (< 1Hz) frequency because: 1) this yields the largest RE-elicited fEPSPs amplitudes (Dolleman-van der Weel et al 1997), 2) the direct EC-CA1 input shows maximal synaptic excitability during hippocampal slow (~1 Hz) oscillations (Schall et al 2008; Schall and Dickson, 2010), and 3) both the EC-CA1 and RE-CA1 inputs have been proposed to coordinate neocortical and hippocampal slow oscillations (Wolanski et al 2006; Isomura et al 2006). The latter is also of interest since coordinated slow oscillations in the mPFC and hippocampus underlie the consolidation of hippocampal-dependent memories (e.g., Huber et al 2004; Mölle and Born, 2011), and both RE and EC have been shown to be involved in memory consolidation (Remondes and Schuman 2004; Loureiro et al 2012). In view of the well-established interconnectivity of RE with mPFC, hippocampus and EC, RE is thus in a key position to coordinate slow oscillatory states between these domains. We have shown that, due to at least partial convergence of RE and EC inputs on pyramidal cells, simultaneous low frequency RE/EC stimulation results in a major non-linear increase of the (still subthreshold) excitation level of CA1 cell apical dendrites, predominantly in proximal (i.e., towards radiatum) LM. Hence, we proposed that by facilitating the EC-CA1 input during hippocampal slow oscillations, RE can contribute significantly to the neocortical-hippocampal dialogue and subsequent memory consolidation (e.g., Xu and Südhof 2013).

In addition, we found that simultaneous RE/EC activation results in an additional perisomatic inhibition, presumably through driving a subclass of CCK^+/VIP^+ basket cells located at the radiatum/LM border (Dolleman-van der Weel et al 2017). Thus, persistent inhibitory influences, mediated by RE and EC separately as well as by coinciding RE/EC inputs, effectively precluded pyramidal cell firing in all tested conditions. Activation of CCK^+ interneurons, evoked by low-frequency (~1 Hz) stimulation of either the CA3-CA1 or EC-CA1 pathway, is known to produce a major feedforward inhibition of pyramidal cell activity. However, precisely timed pairing of the convergent inputs from CA3-CA1 and EC-CA1 can silence the CCK^+ interneuron microcircuit, resulting in enhanced excitatory drive which may allow information to flow through the hippocampus (Basu et al 2013, 2016). A dual role for distinctive CCK^+ interneuron subclasses in controlling excitatory transmission and plasticity in CA1 has also been suggested (Chevaleyre and Piskorowski 2014). The latter authors proposed that a decrease in GABA release from dendritic-targeting CCK^+ interneurons can facilitate the induction of long-term potentiation (LTP) at the CA3-CA1 synapses. Yet a decrease in GABA release from somatic-targeting CCK^+ basket cells (e.g., such as those activated by RE/EC input, see above) may directly increases the EPSP amplitude, and thereby the ability of CA1 pyramidal cells to evoke an action potential (the so-called E-S coupling). The additional perisomatic inhibition evoked by coincident activation of RE/EC inputs (Dolleman-van der Weel et al 2017) may add to the computational abilities of pyramidal cells, for instance associated with input-timing-dependent-plasticity (ITDP). In support of this idea, it has been shown that, in a slice preparation, ITDP is a form of heterosynaptic plasticity at the CA3-CA1 synapses, serving as a gating mechanism which is dependent on low frequency pairing of EC-CA1 and CA3-CA1 inputs, with EC input 20 ms prior to CA3 input (Dudman et al 2007). Since such in vitro stimulation of the EC-CA1 axons in lacunosum moleculare almost certainly involves inadvertent co-activation of RE fibers, it is conceivable that ITDP may in fact represent, at least partly, the effects of simultaneous RE/EC input, and thus their combined influence on plasticity.

Overall, it becomes increasingly clear that gating the flow of information through CA1 involves highly complex interactions of RE-, EC-, and simultaneous RE/EC-mediated excitatory/inhibitory mechanisms. A better insight requires a detailed investigation, first of all at the local CA1 circuit level. In addition, in freely moving animals, the CA1 circuit is also influenced by classical neuromodulator inputs such as the dopaminergic input from VTA (e.g., Ito and Schuman 2008; Xu and Südhof 2013), serotonergic input from raphe nuclei (Vertes 1991; Vertes et al 1999), and cholinergic input from the medial septum (McQuiston et al 2010; Lovett-Baron et al 2014; Vertes 2015). Solving these complex interactions may help to understand how the balance between RE-, EC-, and coincident

RE/EC-elicited excitation/inhibition is regulated, and thereby how (state-dependent) gating of information in CA1 can be achieved.

Behavioral considerations

RE has been implicated in the physiology of various behaviors, such as the regulation of circadian/seasonal adaptations, reproduction, feeding, nociception, arousal, stress and anxiety (Cassel et al 2013). In this thesis, however, the emphasis is on the involvement of RE in cognitive functions.

Learning and memory

Memory formation consists of different aspects (e.g., attention, arousal, motivation, strategy) and specific processes (e.g., encoding, storage, retrieval, consolidation). From a functional point of view, prefrontal-hippocampal synchrony appears necessary for effective transfer of information and neural plasticity in cognitive functioning (Saalman 2014). The thalamus also plays a crucial role in multiple thalamo-cortical functional circuits, but which thalamic nucleus is involved in certain aspects and/or specific processes of cognitive functioning is not yet fully known. Particularly the role of the ventral thalamic midline nuclei is still rather elusive. Using the rat as a model, our initial aim was to examine whether RE is important for mnestic processes, especially in relation to its connectivity with the hippocampus. However, the results from a growing number of behavioral studies (including our own study, see *Chapter 6*) have emphasized a more general role for RE in orchestrating the flow of information between hippocampus and mPFC.

Given the strong, reciprocal connections of RE with structures in the hippocampal region and mPFC (e.g., Herkenham, 1978; Wouterlood et al 1990; Dolleman-van der Weel and Witter, 1996; Van der Werf et al 2000; Vertes, 2002; Vertes et al 2006), i.e., with areas involved in various cognitive processes, it is surprising that for a long time RE has received very little attention. An initial behavioral study by Flämig and Klingberg (1978) revealed that a RE lesion had no effect on learning and memory of a conditioned avoidance task in a Y-maze, but instead caused an increase in anticipatory behavior in a jumping test. Nevertheless, the existence of a direct RE pathway to CA1/subiculum and EC on the one hand, and the observation of early neuronal degeneration in CA1, EC, and RE in Alzheimer's disease (Braak and Braak 1991, 1998; Llorens-Martin et al 2014) on the other, were regarded as a strong indication for the involvement of RE in hippocampal-associated memory processes. Our behavioral study, using a reference memory water maze task, was the first to reveal that a RE lesion affected non-mnemonic aspects of

behavioral flexibility (i.e., strategy shifting/ inhibitory response controle), although it had no effect on spatial (hippocampal-dependent) learning and memory per se (Dolleman-van der Weel et al 2009). Similar observations in later studies have largely confirmed our results (Loureiro et al 2012; Cholvin et al 2013; Prasad et al 2013). In contrast, it has also been reported that reversible inactivation of RE caused deficits in both spatial working and reference memory (Davoodi et al 2009). However, in the latter study the control rats performed at chance level, which makes it difficult to draw firm conclusions. Since that time, a growing number of behavioral studies have suggested possible roles of RE in various behavioral features in learning and memory tasks (Cassel et al 2013). In fact, RE has been proposed to be involved in an increasing variety of cognitive functions, such as working memory (Hembrook and Mair 2011; Hembrook et al 2012; Hallock et al 2013; Griffin 2015; Duan et al 2015; Layfield et al 2015; Hallock et al 2016), passive avoidance learning (Davoodi et al 2011), memory specificity/generalization (Xu and Südhof 2013), memory consolidation/remote memory (Loureiro et al 2012; Sierra et al 2017; Ali et al 2017), memory retrieval (Anderson et al 2016), impulsive behavior (Prasad et al 2013); executive behavior (Prasad et al 2017); goal directed navigation (Ito et al 2015); behavioral flexibility/strategy shifting (Dolleman-van der Weel et al 2009; Cholvin et al 2013; Prasad et al 2013; Linley et al 2016), and fear memory (Kincheski et al 2012; Wheeler et al 2013). Rats with RE lesions can display normal acquisition of a Morris water maze task, as well as normal performance on a probe trial after 5 days delay. Yet, after 25 days delay, their probe trial performance appeared significantly impaired (Loureiro et al 2012). Since in intact rats reversible inactivation of RE just before the probe trial did not affect their performance at either delay, it was suggested that RE may be a key structure for the long-term consolidation of spatial memories, i.e, a process that likely depends on synchronized slow oscillations in hippocampus and mPFC. In this context, it may be emphasized again that low frequency RE-CA1 stimulation has the potential to synchronize slow oscillations in CA1 and mPFC (Dolleman-van der Weel et al 2017; Roy et al 2017).

To further investigate the importance of RE as a functional link between mPFC and hippocampus, recent studies have combined behavioral and electrical stimulation/ optogenetics (e.g., silencing and/or activating RE neurons). For instance, spatial goal directed navigation was recently found to depend on trajectory-dependent firing in a circuit consisting of the mPFC, RE and hippocampal field CA1 (Ito et al 2015), with a key role for RE in the long-range communication between these areas. In classical eyeblink conditioning, involving hippocampal circuits, and in an object discrimination test, involving both the hippocampus and mPFC, high frequency stimulation of RE prevents the proper acquisition of associative learning (Eleore et al 2011). The authors

proposed that this was due to disruption of short-term plastic changes at the RE-hippocampus and RE-mPFC synapses. Alternatively, they suggested that high frequency stimulation may have modified the RE-mediated inhibitory control of CA1 pyramidal cells (see Electrophysiological considerations), resulting in inappropriate firing/output of CA1 neurons. Recently, optogenetic stimulation of RE at delta frequency (1-3 Hz) caused a strong working memory deficit in rats, performing a hippocampal-dependent delayed spatial working memory task in the T-maze (Duan et al 2015). It was speculated that, during a working memory task, delta activity in RE interfered with downstream theta/gamma-dependent hippocampal functioning. Interestingly, this suggestion is in accordance with our (unpublished) observations in anesthetized rats, revealing that low frequency stimulation of RE can disrupt hippocampal theta waves. Alternatively, the possibility that repetitive delta frequency firing of RE neurons simply 'jams' the necessary information flow through the thalamus was also considered (Duan et al 2015).

A more detailed insight in the functional role of RE results from a study by Xu and Südhof (2013). Using a contextual fear conditioning task, these authors have reported that RE can determine the degree of specificity/generalization of memories by processing information from the mPFC and relaying this to the hippocampus. The idea is that generalized memories are composed of only the most prominent features of an item, with a high probability of overlap with memories of quite similar items. But by increasing the incorporation of less prominent features or attributes of an item, memories will become more specific. It was demonstrated that either inactivation of mPFC-RE input, or direct silencing of the RE-hippocampus projection affected generalization of contextual fear memory. Interestingly, RE appeared to exert a bidirectional control, namely optogenetic burst stimulation of RE during memory acquisition induced phasic firing of RE neurons, which resulted in an enhanced memory generalization. In contrast, applying stimulus trains at 4 Hz induced tonic firing of RE neurons, which resulted in a decrease of memory generalization (i.e., memory becomes more specific). Refering to our electrophysiological results (see *Chapters 4 and 7*) it was suggested that RE may exert a persistent modulation of CA1 pyramidal cell excitability, which enables RE to control the levels of memory specificity or generalization. Specifically, during 'cooperative' RE and EC inputs an increase in excitability of pyramidal cells may reduce the threshold for synaptic plasticity at the EC-CA1 synapses (see above, RE/EC interactions), allowing less prominent features to become incorporated, thereby rendering memories more specific. Moreover, other possibilities such as an indirect (additional) influence of RE through its input of EC, and/or the ventral tegmental area (VTA) have been suggested (Xu and Südhof 2013). The first mechanism may result in an increased activity level in EC neurons and EC-CA1-mediated neocortical input; the latter may trigger/enhance DA release in the hippocampus, thereby reducing the threshold for synaptic plasticity (Ito and Schumann 2007, 2008, 2012;

Zimmerman and Grace 2016). In this respect, our electrophysiological findings are at least supportive for the 'cooperativity' proposal by Xu and Südhof, since we have clearly shown that coinciding RE/EC input significantly increases the excitability level of the principal cell apical dendrites in stratum lacunosum moleculare.

Recently, the first experimental evidence for a role of RE in memory in humans has become available (Reagh et al 2017). Using fMRI, the influence of repetition on recognition and discrimination memory judgements was examined. In agreement with the anatomical CA1-anterior cingulate cortex/mPFC-RE connectivity, the investigators detected a shift in the engagement of the anterior (=ventral) CA1-mPFC-RE network related to true and false recognition. These findings in the human brain not only offer new insights in how repeated experience can affect memory, they also reveal that the CA1-mPFC-RE functional connectivity shows important similarities in humans and animals (e.g., rodents). Therefore, cautious extrapolating experimental findings from animal models (mostly rodents) to humans may be justified.

Nucleus reuniens and brain diseases

Since a dysfunctioning of a hippocampal-mPFC-thalamic midline network is implicated in several brain pathologies, understanding the functioning of RE may not only improve our insight in cognitive processes, but may also have clinical relevance (e.g., Duan et al 2015; Prasad et al 2017). Patients with psychiatric or neurodegenerative diseases often display abnormalities in the hippocampal-prefrontal pathway, that may underlie cognitive impairment and emotional dysregulation. Disruption of the hippocampal-PFC circuit or their communication may thus be a common deficiency in diseases such as schizophrenia, major depression, and post-traumatic stress disorder (Small et al 2011; Godsil et al 2013). Here we focus on the hippocampal-mPFC-RE connectivity, and the presumed role of RE in abnormal functioning of circuitries involved in schizophrenia and (some forms of) epilepsy.

Schizophrenia

It has become clear that schizophrenia is a neurodevelopmental disorder instead of a neurodegenerative one, leading to dysfunctional circuits in early adulthood (Sigurdsson and Duvarci 2016). In relation to developmental anatomical abnormalities in the thalamus (with emphasis on RE), in schizophrenic patients the massa intermedia (MI) may be more

frequently absent, or is shorter/smaller than in healthy controls (e.g., Nopoulos et al 2001; Takahashi et al 2008; Ceyhan et al 2008; Trzesniak et al 2011, 2012; Landin-Romero et al 2016). Therefore, RE, as part of the MI, is one of the thalamic nuclei of interest. In addition, RE participates in the neural circuits that mediate the effects of antipsychotic drugs (Cohen et al 1998), and disturbed interactions between hippocampus and mPFC have been implicated as a major factor in schizophrenia (Godsil et al 2013). Although human mental illness is rarely applicable to animals, animal models are important to investigate how abnormal functioning may be due to an imbalance of excitation/inhibition, deficits in synaptic plasticity, abnormal (local and long-range) synchronzation of brain rhythms, as well as abnormal dopaminergic, glutamatergic and GABAergic signaling (Lodge and Grace 2011; Lisman 2012; Uhlhaas and Singer 2012; Schwartz et al 2012; Heckers and Konradi 2015; Spellman and Gordon 2015; Sigurdsson and Duvarci 2016).

According to the so-called glutamatergic theories (e.g., Javitt 2010), a commonly used rodent model of schizophrenia is based on the observation that a non-competative NMDAreceptor (-r) antagonist such as ketamine (e.g., Kocsis e al 2013), when given to healthy human subjects (i.e., adolescents and adults, but not children), can mimic the symptoms of the disease. This is associated with hyperactivity in CA1 and abnormal delta oscillations in the awake state, which are not seen in non-diseased brain, except during slow-wave-sleep (Boutros et al 2008). In the NMDAr rat model, either systemic applicaton or a local injection of ketamine into RE, has been shown to cause delta oscillations in RE, PFC, and hippocampus, as well as increased firing of RE and CA1 neurons. In addition, the ketamine/RE-induced abnormal activity may also cause tissue damage in CA1 and mPFC (Zhang et al 2012; Eggers 2013).

To explain the ketamine/RE-induced hyperactivity in CA1, Lisman (2012; Lisman et al 2010) proposed a model circuit consisting of a RE-CA1-ventral tegmental area (VTA) loop. They suggested that RE-induced hyperactivity in CA1 neurons can (polysynaptically) result in increased excitation of neurons in the VTA. This causes enhanced dopamine (DA) release, which may promote delta frequency bursts in the thalamic reticular nucleus, and subsequent bursting in RE, thereby closing the positive feedback loop (Zhang et al 2012). NMDA infusion in RE also increased the overall VTA DA cell activity, an effect that was dependent on activation of the ventral subiculum (Zimmerman and Grace 2016). In the same study it was also reported that infralimbic PFC modulation of DA cell activity in VTA was dependent on infralimbic-RE-subiculum-(multisynaptic) VTA activation. These observations are in line with the concept that RE serves as a functional link between mPFC and the (ventral) hippocampus.

It is also noteworthy to mention that RE might be able to directly influence the activity level of VTA DA neurons through its reciprocal connectivity with VTA (Herkenham 1978). In theory, RE may thus indirectly and directly modulate DA release in target areas

of VTA, such as hippocampus, mPFC, and presumably RE itself. RE-VTA connectivity, however, is as yet unexplored territory, but seems worth examining. Nonetheless, the implications of these processes to the pathology of schizophrenia are still unclear.

Epilepsy

Temporal lobe epilepsy

The 'functional anatomy' of epilepsy comprises 4 components: 1) the epileptic focus (site where the seizure starts), 2) the initiating circuit (interconnected areas that support the start of the epileptic focus to develop into a seizure, 3) recruiting regions that take care of spreading the seizure outside the initiating circuit to other brain areas, and 4) a modulatory centre, located outside the forementioned regions, that can influence the seizure threshold. Synchronization of seizure activity in temporal lobe epilepsy (TLE) can occur locally as well as over multiple brain areas, pointing to an activity-synchronizing structure that is connected to many if not all of the involved regions (Bertram 2013). The midline thalamus is proposed to function as a physiological synchronizer/recruiting area, and from an anatomical point of view RE is particularly well situated to play such a role in TLE (Bertram et al 1998, 2001, 2008). Given its strong excitatory projections to CA1, subiculum, and entorhinal cortex, RE may be involved in the development of an hyperexcitable entorhinal-hippocampal loop that often constitutes an epileptogenic network in limbic epilepsy, namely the mesial temporal lobe epilepsy syndrome (Stefan and Lopes da Silva 2013). Indeed there are experimental findings indicating a thalamic involvement in this syndrome (e.g., Hirayasu and Wada 1992; Bertram 2009). To test the role of thalamic nuclei in limbic seizures, Sloan et al (2011) investigated the effects of inactivating the midline thalamus (i.e., predominantly the MD nucleus) by injections of the sodium channel blocker tetrodotoxin (TTX) on local field potentials and on kindled seizures. Such TTX injections suppressed seizures, suggesting that the circuits connecting limbic cortical areas and thalamic midline nuclei can constitute an additional excitatory drive, facilitating seizures. However, injections outside the MD area appeared ineffective. For instance, one of their TTX injections was placed in RE but, notwithstanding the RE connectivity with mPFC and hippocampus, did not have a suppressive effect on kindled seizures. Despite this negative finding (Sloan et al 2011) RE may, in some other way, participate in modulating limbic seizures.

The RE projections to hippocampus and EC (Dolleman-van der Weel et al 1996) arise from neurons containing glutamate, and CB and/or CR (Bokor et al 2002; Wouterlood et al 2008). In genetically epilepsy-prone rats, CB is down-regulated in RE, which likely changes the calcium-buffering capacity and/or the regulation of calcium-mediated

processes, resulting in hyperactivity of RE neurons (Montpied et al 1995). After kainate-induced status epilepticus a reduced density of CR^+ fibres in CA1, subiculum, and EC layer I was found along with degeneration of CR^+ neurons in RE (Drexel et al 2011). This implies that the loss of CR^+ RE neurons projecting to CA1, subiculum, and EC may contribute to hyperexcitability by facilitating the transition from a normal to a hyperactive hippocampal-entorhinal network.

Another possible mechanism that may compromise inhibitory processes in RE, and thus assumed to contribute to hyperactivity and neuronal degeneration, involves changes in Zn^{2+} levels (Menqual e al 2001). Using a Timm staining, which mostly detects Zn^{2+} in synaptic vesicles in terminal boutons, it has been shown that in the midline thalamus of pilocarpine-induced epileptic rats, RE is the only nucleus displaying a lower staining-intensity compared to controls. Although the role of Zn^{2+} as neuromodulator in epilepsy is not entirely clear, there is experimental evidence that Zn^{2+} may have a protective function against excessive neuronal activity. For example, it was shown that transgenic mice lacking Zn^{2+} in synaptic vesicles had an enhanced seizure susceptibility compared to wild-type mice (Cole et al 2000). Furthermore, synaptically released Zn^{2+} may inhibit the activity of NMDA-receptors and thus excitation (Dominquez et al 2003). In a strain of adult epileptic rats, the incidence of seizures was markedly increased after administration of Zn^{2+} chelators that reduce the levels of synaptic Zn^{2+} (Takeda et al 2013). A reduced level of Zn^{2+} within RE may thus contribute to increased excitatory output, and ultimately to hyperexcitability causing neuronal damage within RE, as well as in the structures receiving enhanced RE input (Dominquez et al 2003; Hamani et al 2005; Sindreu and Storm 2011).

Due to the random nature of seizures, the mechanisms of ictogenesis are difficult to investigate. Essentially, there is a need for an endogenous pathway to modulate seizure threshold in a controlled manner. Based on the hypothesis that increased random afferent excitatory synaptic input (i.e., synaptic noise) within an epileptic focus can induce seizures, an in vivo model of ictogenesis was recently described (Luna-Munguia et al 2017). Using pilocarpine-induced epileptic rats, afferent synaptic activity in the hippocampus was modulated by injecting potassium chloride (KCl; this slightly depolarises neurons, and increases their firing) into RE in freely moving animals. This resulted in an increased risk of seizures that were qualitatively and quantitatively similar to spontaneous occurring seizures in the epileptic rats. Thus, at least in the pilocarpine-epilepsy model, increased RE-hippocampal input is suffient to induce seizures, likely by modulating the seizure threshold. In contrast, control rats never seized following a KCl injection in RE, indicating that (slightly) increased RE-hippocampal input by itself is not sufficient to induce seizure activity in non-epileptic rats. Therefore, other (additional) mechanisms must be involved

(e.g., a reduced level of Zn^{2+} in RE, see above), before enhanced RE input can facilitate the transition from a normal hippocampal network into an epileptic one. Nevertheless, using RE activation in models of TLE may prove useful to investigate basic control mechanisms of seizure threshold, and/or may be used to develop/optimize antiseizure therapies.

Atypical absence seizures

Briefly, patients with atypical absence seizures (AAS) have severe cognitive impairments which do not occur in the more benign type of typical absence seizures. Both types of absence seizures are thought to display activity in different neural circuits. RE is suggested to play a role in AAS as part of a hypothesized circuit comprising the mPFC, RE, CA1, and the reticular thalamic nucleus (NRT). The involvement of the hippocampus in this circuit is likely responsible for impaired cognitive functioning in AAS (Han et al 2012). The model of AAS is based on observations in transgenic mice with an over-expression of the GABAb-(1a) receptor, showing characteristics of the AAS syndrome in humans (Wu et al 2007; Wang et al 2009; Stewart et al 2009). In this mouse model, injections with a GABAb receptor agonist into RE and NRT can enhance slow spike-wave discharges, whereas injections with a GABAb receptor antagonist have an abolishing effect. In the proposed model circuit, the initiating event for an atypical absence seizure is assumed to originate in mPFC layer V/VI pyramidal cells which project to RE. RE, in turn, projects back to mPFC as well as forward to CA1/subiculum which also project to mPFC (Wang et al 2009). In theory, this creates a reverberating circuit that can be modulated by NRT, supposedly driven by reciprocal connections between RE and NRT (Çavdar et al 2008; Han et al 2012). However, the proposed involvement of RE in such an AAS circuit has to be verified in future studies.

Directions for future research

Based on a growing number of anatomical, electrophysiological, and behavioral data, the current view is that RE plays an important role in cognitive functioning, predominantly by orchestrating the communication between the hippocampus and mPFC.

As illustrated in the simplified schema of figure 3, the RE/periRE nucleus is, in theory, certainly in a position to influence neuronal activities in a large scale network of hippocampal and cortical structures, involved in learning and memory.

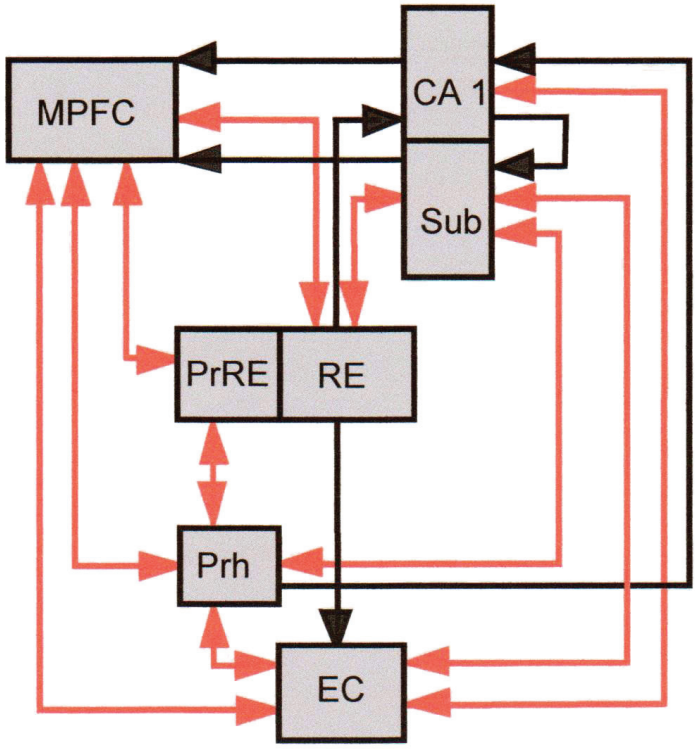

Fig. 3. Schematic representation of main connections between nucleus reuniens/perireuniens, hippocampal field CA1/subiculum, and the medial prefrontal, perirhinal and entorhinal cortices. Black lines represent one-way projections; red lines represent reciprocal connections. Abbereviations: MPFC=medial prefrontal cortex; Sub=subiculum; PrRE=perireuniens; RE=reuniens; Prh=perirhinal cortex; EC=entorhinal cortex.

Briefly, within this network CA1/subiculum project to mPFC, but a direct mPFC-hippocampal pathway is lacking. Instead, neocortical information can reach the hippocampus via the perirhinal and entorhinal cortices. In addition, RE can relay mPFC-processed information to the hippocampus. RE output is arranged such that different clusters of RE neurons give rise to separate projections to distinct subdivisions of the mPFC (i.e., infralimbic, prelimbic and anterior cingulate cortices), hippocampus (i.e., dorsal, intermediate, and ventral parts of CA1 and subiculum), perirhinal, and entorhinal cortices (i.e., lateral and medial entorhinal regions), with each target area contributing differently to cognitive and/or executive functions. This arrangement points

to the possibility that RE may directly and/or indirectly influence the flow of information between particular subdivisions of mPFC and the hippocampus. Behavioral studies have provided evidence that this tiny thalamic midline nucleus is indeed involved in a surprising variety of memory-related (i.e., mnemonic and non-mnemonic) processes. At present, however, we can only speculate whether the involvement of RE in these various processes reflects the presumably task- and/or state-dependent activation of specific clusters of RE output neurons. Overall, the convergence of RE afferent systems onto identified RE projection cells is unknown. Therefore, it is important to investigate 1) whether each cluster of RE projection neurons is innervated by different afferents, or that for instance some clusters share the same afferents, and 2) which afferents, based on proximal or distal location of their synapses on RE dendrites, can be considered driver or modulatory inputs. Elucidating these issues in future anatomical studies may further our insight in the functioning of RE. Nonetheless, understanding the mechanisms underlying the involvement of RE in so many aspects of cognitive behavior, will also require a more detailed neurophysiological knowledge of RE than presently known.

In general, the intrinsic physiological properties of neurons play an important role in determining their computational abilities to process and transmit information. Today, however, electrophysiological studies of RE are scarce, and knowledge of their intrinsic physiological properties is still limited to data from one in vitro study in the rostral part of RE in mice. Future in vivo studies are thus needed to substantiate and expand these findings, for instance in freely moving rodents. In addition, in view of the well known topographical organization of RE afferents and efferents, it is also important to investigate possible differences in intrinsic properties of rostral versus caudal RE/periRE neurons. Furthermore, bearing in mind that RE is likely subject to an abundance of neuromodulatory influences (i.e., inputs arising from telencephalic, diencephalic and brainstem structures), the question of how the membrane potential/firing mode (i.e., tonic or burst firing) of RE neurons is affected by different modulatory inputs also awaits answering. In this respect, it may be particularly interesting to study the involvement of low threshold T-type Ca^{2+} channels, and different Ca^{2+} binding abilities of RE neurons, in relation to specific patterns of output behavior. So far, only a few electrophysiological in vivo studies of RE have been performed, mainly focussing on RE-evoked responses in CA1 and mPFC, whereas our second electrophysiological study was the first to investigate the interaction of RE and EC inputs in CA1. However, the impact of RE input on neuronal activities in subiculum, perirhinal and entorhinal cortices, is largely unknown and thus requires future research. In addition, identification of the various target cells of RE in hippocampal and cortical structures may further our understanding of the mechanisms underlying modulation of excitability within local circuits.

Another interesting aspect that deserves more attention concerns the collateralized pathway arising from a small number of RE-CA1/mPFC projecting neurons. According to the broadly accepted idea that a collateralized output can synchronize neuronal activities in the respective target areas, such a role has been suggested for the collateralized RE-CA1/mPFC projection. Because the involvement of RE in cognitive functioning is largely based on its proposed ability to synchronize the activities in mPFC and hippocampus, it is thus opportune to investigate whether or not these RE-CA1/mPFC projecting neurons indeed play such a crucial role. Although challenging, an attractive approach might be the use of optogenetics to specifically activate these RE-CA1/mPFC cells, in combination with simultaneous recordings of field potentials/oscillations and unit activity (e.g., intracellular recording and labeling to identify target cells) in CA1 and mPFC, to substantiate their synchronizing potential.

In conclusion, a more detailed multidisciplinary research is needed, not just to explain the involvement of RE in a variety of cognitive functions, but also regarding a possible involvement of RE in a dysfunctional hippocampus-mPFC-thalamic midline connectivity, likely underlying neuropathological conditions displaying a cognitive deficit.

REFERENCES

Aggleton JP (2014) Looking beyond the hippocampus: old and new neurological targets for understanding memory disorders. Proc R Soc B 281:20140565.

Ali M, Cholvin T, Antoine Muller M, Cosquer B, Kelche C, Cassel JC, Pereira de Vasconcelos A (2017) Environmental enrichment enhances systems-level consolidation of a spatial memory after lesions of the ventral midline thalamus. Neurobiol Learn Mem 141:108-123.

Anderson MC, Bunce JC, Barbas H (2016) Prefrontal-hippocampal pathways underlying inhibitory control over memory. Neurobiol Learn Mem 134:Pt A:145-161.

Arai R, Jacobowitz DM, Deura S (1994) Distribution of calretinin, calbindin-D28k, and parvalbumin in the rat thalamus. Brain Res Bull 33:595-614.

Ang CW, Carlson GC, Coulter DA (2005) Hippocampal CA1 circuitry dynamically gates direct cortical inputs preferentially at theta frequencies. J Neurosci 25:9567-9580.

Ang CW, Carlson GC, Coulter DA (2006) Massive and specific dysregulation of direct cortical input to the hippocampus in temporal lobe epilepsy. J Neurosci 26:11850-11856.

Barthó P, Freund TF, Acsády L (2002) Selective GABAergic innervation of thalamic nuclei from zona incerta. Eur J Neurosci 16:999-1014.

Basu J, Srinivas KV, Cheung SK, Taniguchi H, Huang ZJ, Siegelbaum SA (2013) A cortico-hippocampal learning rule shapes inhibitory microcircuit activity to enhance hippocampal information flow. Neuron 79:1208-1221.

Basu J, Zaremba JD, Cheung SK, Hitti FL, Zemelman BV, Losonczy A, Siegelbaum SA (2016) Gating of hippocampal activity, plasticity, and memory by entorhinal cortex long-range inhibition. Science 351: aaa5694. Doi: 10.1126/science.aaa5694.

Bentivoglio M, Balercia G, Kruger L (1991) The specificity of the nonspecific thalamus: The midline nuclei. Prog Brain Res 87:53-80.

Bertram EH, Mangan PS, Zhang D, Scott CA, Williamson JM (2001) The midline thalamus: alterations and a potential role in limbic epilepsy. Epilepsia 42:967-978.

Bertram EH, Zhang DX, Mangan P, Fountain N, Rempe D (1998) Functional anatomy of limbic epilepsy: a proposal for central synchronization of a diffusely hyperexcitable network. Epilepsy Res 32:194-205.

Bertram EH, Zhang D (1999) Thalamic excitation of hippocampal CA1 neurons: a comparison with the effects of CA3 stimulation. Neurosci 92:15-26.

Bertram EH, Zhang D, Williamson JM (2008) Multiple roles of midline dorsal thalamic nuclei in induction and spread of limbic seizures. Epilepsia 49:256-268.

Bertram EH (2013) Neuronal circuits in epilepsy: do they matter? Exp Neurol 244:67-74.

Bokor H, Csáki A, Kocsis K, Kiss J (2002) Cellular architecture of the nucleus reuniens thalami and its putative aspartatergic/glutamatergic projection to the hippocampus and medial septum in the rat. Eur J Neurosci 16:1227-1239.

Boutros NN, Arfken C, Galderisi S, Warrick J, Pratt G, Iacono W (2008) The status of spectral EEG abnormality as a diagnostic test for schizophrenia. Schizophr Res 99:225-237.

Boyce R, Glasgow SD, Williams S, Adamantidis A (2016) Causal evidence for the role of REM sleep theta rhythm in contextual memory consolidation. Science 352:812-816.

Braak H, Braak E (1991) Alzheimer's disease affects limbic nuclei of the thalamus. Acta Neuropath 81:261-268.

Braak H, Braak E (1998) Evolution of neuronal changes in the course of Alzheimer's disease. J Neural Transm Suppl 53:127-140.

Cassel JC, Pereira de Vasconcelos A, Loureiro M, Cholvin T, Dalrymple-Alford JC, Vertes RP (2013) The reuniens and rhomboid nuclei: neuroanatomy, electrophysiological characteristics and behavioral implications. Prog Neurobiol 111:34-52.

Çavdar S, Onat FY, Cakmak YO, Yananli HR, Gűlçebi M, Aker R (2008) The pathways connecting the hippocampal formation, the thalamic reuniens nucleus and the thalamic reticular nucleus in the rat. J Anat 212:249-256.

Ceyhan M, Adapinar B, Aksaray G, Ozdemir F, Colak E (2008) Absence and size of massa intermedia in patients with schizophrenia and bipolar disorder. Acta Neuropsychiatr 20:193-198.

Chevaleyne V, Piskorowski R (2014) Modulating excitation through plasticity at inhibitory synapses. Front Cell Neurosci 8:93. Doi: 10.3389/fncel.2014.00093.

Cholvin T, Loureiro M, Cassel R, Cosquer B, Geiger K, De Sa Nogueira D, Raingard H, Robelin L, Kelche C, Pereira de Vasconcelos A, Cassel JC (2013) The ventral midline thalamus contributes to strategy shifting in a memory task requiring both prefrontal cortical and hippocampal functions. J Neurosci 33:8772-8783.

Cohen BM, Wan W, Froimowitz MP, Ennulat DJ, Cherkerzian S, Konieczna H (1998) Activation of midline thalamic nuclei by antipsychotic drugs. Psychopharmacol (Berl) 135:37-43.

Cole TB, Robbins CA, Wenzel HJ, Schwartzkroin PA, Palmitter RD (2000) Seizures and neuronal damage in mice lacking vesicular zinc. Epilepsy Res 39:153-169.

Cruikshank SJ, Ahmed OJ, Stevens TR, Patrick SL, Gonzales AN, Elmaleh M, Connors BW (2012) Thalamic control of layer 1 circuits in prefrontal cortex. J Neurosci 32:17813-17823.

Davoodi FG, Motamedi F, Nagdhi N, Akbari E (2009) Effect of reversible inactivation of the reuniens nucleus on spatial learning and memory in rats using Morris water maze. Beh Brain Res 198:130-135.

Davoodi FG, Motamedi F, Akbari E, Ghanbarian E, Jila B (2011) Effect of reversible inactivation of reuniens nucleus on memory processing in passive avoidance task. Behav Brain Res 221:1-6.

Di Prisco GV, Vertes RP (2006) Excitatory actions of the ventral midline thalamus (rhomboid/reuniens) on the medial prefrontal cortex in the rat. Synapse 60:45-55.

Dolleman-van der Weel MJ, Ang W, Witter MP (1993) Afferent connections of the nucleus reuniens thalami: a neuroanatomical tracing study in the rat. Eur J Neurosci Suppl 6:65.

Dolleman-van der Weel MJ, Witter MP (1996) Projections from the nucleus reuniens thalami to the entorhinal cortex, hippocampal field CA1, and the subiculum in the rat arise from different populations of neurons. J Comp Neurol 364:637-650.

Dolleman-van der Weel MJ, Lopes da Silva FH, Witter MP (1997) Nucleus reuniens thalami modulates activity in hippocampal field CA1 through excitatory and inhibitory mechanisms. J Neurosci 17:5640-5650.

Dolleman-van der Weel MJ, Witter MP (2000) Nucleus reuniens thalami innervates gamma aminobutyric acid positive cells in hippocampal field CA1 of the rat. Neurosci Lett 278:145-148.

Dolleman-van der Weel MJ, Morris RG, Witter MP (2009) Neurotoxic lesions of the

thalamic reuniens or mediodorsal nucleus in rats affect non-mnemonic aspects of watermaze learning. Brain Struct Funct 213:329-342.

Dolleman-van der Weel, Lopes da Silva FH, Witter MP (2017) Interactions of nucleus reuniens and entorhinal cortex projections in hippocampal field CA1 of the rat. Brain Struct Funct 222:2421-2438.

Dominguez MI, Blaso-Ibanez JM, Crespo C, Marques-Mari AI, Martinez-Guijarro FJ (2003) Zinc chelation during non-lesioning overexcitation results in neuronal death in the mouse hippocampus. Neurosci 116:791-806.

Drexel M, Preidt AP, Kirchmair E Sperk G (2011) Parvalbumin interneurons and calretinin fibers arising from the thalamic nucleus reuniens degenerate in the subiculum after kainic acid-induced seizures. Neurosci 189:316-329.

Duan AR, Varela C, Zhang Y, Shen Y, Xiong L, Wilson MA, Lisman J (2015) Delta frequency optogenetic stimulation of the thalamic nucleus reuniens is sufficient to produce working memory deficits: relevance to schizophrenia. Biol Psychiatry 77:1098-1107.

DudmanJT, Tsay D, Siegelbaum SA (2007) A novel role for synaptic inputs at distal dendrites: instructive signals for hippocampal long-term plasticity. Neuron 56:866-879.

Eggers AE (2013) An explanation of why schizophrenia begins with excitotoxic damage to the hippocampus. Med Hypotheses 81:1056-1058.

Eleore L, López-Ramos JC, Guerra-Narbona R, Delgado-Garcia JM (2011) Role of reuniens nucleus projections to the medial prefrontal cortex and to the hippocampal pyramidal CA1 area in associative learning. PLoS One 6:e23538. Epub 2011

Flämig R, Klingberg F (1978) Participation of thalami nuclei in the elaboration of conditioned avoidance reflexes of rats. IV. Lesions of the nucleus reuniens. Acta Biol Med Germ 37:1779-1782.

Floresco SB, Seamans JK, Phillips AG (1997) Selective roles for hippocampal, prefrontal cortical, and ventral striatal circuits in radial-arm maze tasks with or without a delay. J Neurosci 17:1880-1890.

Frassoni C, Bentivoglio M, Spreafico R, Sánchez MP, Puelles L, Fairen A (1991) Postnatal development of calbindin and parvalbumin immunoreactivity in the thalamus of the rat. Develop Brain Res 58:243-249.

Godsil BP, Kiss JP, Spedding M, Jay TM (2013) The hippocampal-prefrontal pathway: the weak link in psychiatric disorders? Eur Neuropsychopharmacol 23:1165-1181.

Griffin AL (2015) Role of the thalamic nucleus reuniens in mediating interactions between the hippocampus and medial prefrontal cortex during spatial working memory. Front Syst Neurosci 9:29 doi: 10.3389/fnsys.2015.00029.

Groenewegen HJ and Witter MP (2004) Thalamus. In: The Rat Nervous System, third ed.

Paxinos G, Paxinos G (Eds). Elsevier Academic Press. Pp 407-453.
Halassa MM, Acsády L (2016) Thalamic inhibition: diverse sources, diverse scales. Trends Neurosci 39:680-693.
Hallock HL, Wang A, Shaw CL, Griffin AL (2013) Transient inactivation of the thalamic nucleus reuniens and rhomboid nucleus produces deficits of a working-memory dependent tactile-visual conditional discrimination task. Behav Neurosci 127:860-866.
Hallock HL, Wang A, Griffin AL (2016) Ventral midline thalamus is critical for hippocampal-prefrontal synchrony and spatial working memory. J Neurosci 36:8372-8389.
Han HA, Cortez MA, Snead OC III (2012) GABAB receptor and absence epilepsy. In: Noebels et al, editors. Jasper's Basic Mechanisms of the Epilepsies. 4th edition Bethesda (MD): Nat Center for Biotechnol Information (US).
Heckers S, Konradi C (2015) GABAergic mechanisms of hippocampal hyperactivity in schizophrenia. Schozophr Res 167:4-11.
Hembrook JR, Mair RG (2011) Lesions of reuniens and rhomboid thalamic nuclei impair radial maze win-shift performance. Hippocampus 21:815-826.
Hembrook JR, Onos KD, Mair RG (2012) Inactivation of ventral midline thalamus produces selective delayed conditional discrimination impairment in the rat. Hippocampus 22:853-860.
Herkenham M (1978) The connections of the nucleus reuniens thalami: evidence for a direct thalamo-hippocampal pathway in the rat. J Comp Neurol 177:589-610.
Hirayasu Y, Wada JA (1992) Convulsive seizures in rats induced by N-methyl-D-aspartate injection into the massa intermedia. Brain Res 577:36-40.
Hoover WB, Vertes RP (2007) Anatomical analysis of afferent projections to the medial prefrontal cortex in the rat. Brain Struct Funct 212:149-179.
Hoover WB, Vertes RP (2012) Collateral projections from nucleus reuniens of thalamus to hippocampus and medial prefrontal cortex in the rat: a single and double retrograde fluorescent labeling study. Brain Struct Funct 217:191-209.
Houser CR, Vaughn JE, Barber RP, Roberts E (1980) GABA neurons are the major cell type of the nucleus reticularis thalami. Brain Res 200:341-354.
Huber R, Ghilardi MF, Massimini M, Tononi G (2004) Local sleep and learning. Nature 430:78-81.
Ito HT, Schuman EM (2007) Frequency-dependent gating of synaptic transmission and plasticity by dopamine. Frontiers Neural Circuits 1:1 doi: 10.3389/neuro.04/001.2007.
Isomura Y, Sirota A, Ozen S, Montgomery S, Mizuseki K, Henze DA, Buszáki G (2006) Integration and segregation of activity in entorhinal-hippocampal subregions by neocortical slow oscillations. Neuron 52:871-882.

Ito HT, Schuman EM (2008) Frequency-dependent signal transmission and modulation by neuromodulators. Front Neurosci 2:138-144.

Ito HT, Schuman EM (2012) Functional division of hippocampal area CA1 via modulatory gating of entorhinal cortical inputs. Hippocampus 22:372-387.

Ito HT, Zhang SJ, Witter MP, Moser EI, Moser MB (2015) A prefrontal-thalamo-hippocampal circuit for goal-directed navigation. Nature 522:50-55.

Jankowski MM, Islam MN, Wright NF, Vann SD, Erichsen JT, Aggleton JP, O'Mara SM (2014) Nucleus reuniens of the thalamus contains head direction cells. Elife 3:e03075. Doi: 10.7554/elife.03075.

Jankowski MM, Passecker J, Islam MN, Erichsen JT, Aggleton JP, O'Mara SM (2015) Evidence for spatially-responsive neurons in the rostral thalamus. Front Behav Neurosci 9:256. Doi: 10.3389/fnbeh.2015.00256.

Javitt DC (2010) Glutamatergic theories of schizophrenia. Isr J Psychiatry Relat Sci 47:4-16.

Jay TM, Witter MP (1991) Distribution of hippocampal and subicular efferents in the prefrontal cortex of the rat studied by means of anterograde transport of Phaseolus vulgaris-leucoagglutinin. J Comp Neurol 313:574-586.

Jones EG. (1998) A new view of specific and non-specific thalamocortical connections. Adv Neurol 77:49-71.

Judge SJ, Hasselmo ME (2004) Theta rhythmic stimulation of stratum lacunosum moleculare in rat hippocampus contributes to associative LTP at a phase offset in stratum radiatum. J Neurophysiol 92:1615-1624.

Kincheski GC, Mota-Ortiz SR, Pavesi E, Canteras NS, Carobrez AP (2012) The dorsolateral periaqueductal gray and its role in mediating fear learning to life threatening events. PLoS One 7:e50361. Doi: 10.1371/journal.pone.0050361.

Klausberger T, Somogyi P (2008) Neuronal diversity and temporal dynamics: the unity of hippocampal circuit operations. Science 321:53-57.

Kocsis B, Brown RE, McCarley RW, Hajos M (2013) Impact of ketamine on neural network dynamics: translational modelling of schizophrenia-relevant deficits. CNS Neurosci Ther 19:437-447.

Krout KE, Belzer RE, Loewy AD (2002) Brainstem projections to midline and intralaminar thalamic nuclei of the rat. J Comp Neurol 448:53-101.

Landin-Romero R et al (2016) Midline brain abnormalities across psychotic and mood disorders. Schizophr Bull 42:229-238.

Lara-Vásquez A, Espinosa N, Durán E, Stockle M, Fuentealba P (2016) Midline thalamic neurons are differentially engaged during hippocampal network oscillations. Sci Rep 6:29807. Doi: 10.1038/srep29807.

Layfield DM, Patel M, Hallock H, Griffin AL (2015) Inactivation of the nucleus reuniens/

rhomboid causes a delay-dependent impairment of spatial working memory. Neurobiol Learn Mem 125:163-167.

Linley SB, Gallo MM, Vertes RP (2016) Lesion of the ventral midline thalamus produce deficits in reversal learning and attention on an odor texture set shifting task. Brain Res 1649 (PtA):110-122.

Lisman JE, Pi HJ, Zhang Y, Otmakhova NA (2010) A thalamo-hippocampal-ventral tegmental area loop may produce the positive feedback that underlies the psychotic break in schizophrenia. Biol Psychiatry 68:17-24.

Lisman J (2012) Excitation, inhibition, local oscillations, or large-scale loops: what causes the symptoms of schizophrenia? Curr Opinion Neurobiol 22:537-544.

Llorens-Martin M, Blazquez-Llorca L, Benavides-Piccione R, Rabano A, Hernandez F, Avila J, DeFelipe J, (2014) Selective alterations of neurons and circuits related to early memory loss in Alzheimer's disease. Front Neuroanat 8:38. Doi: 10.3389/fanat.2014.00038.

Lodge DJ, Grace AA (2011) Hippocampal dysregulation of dopamine system function and the pathophysiology of schizophrenia. Trends Pharmacol Sci 32:507-513.

Loureiro M, Cholvin T, Lopez J, Merienne N, Latreche A, Cosquer B, Geiger K, Kelche C, Cassel JC, Pereira de Vasconcelos A (2012) The ventral midline thalamus (reuniens and rhomboid nuclei) contributes to the persistence of spatial memory. J Neurosci 32:9947-9959.

Lovett-Baron M et al (2014) Dendritic inhibition in the hippocampus supports fear learning. Science 343:857-863.

Luna-Munguia H, Starski P, Chen W, Gliske S, Stacey WC (2017) Control of in vivo ictogenesis via endogenous synaptic pathways. Sci Rep 7:1311.

McKenna JT, Vertes RP (2004) Afferent projections to nucleus reuniens of the thalamus. J Comp Neurol 480:115-142.

McQuiston AR (2010) Cholinergic modulation of excitatory synaptic input integration in hippocampal CA1. J Physiol 588:3727-3742.

Menqual E, Casanovas-Aquilar C, Perez-Clausell J, Gimenez-Amaya JM (2001) Thalamic distribution of zinc-rich terminal fields and neurons of origin in the rat. Neurosci 102:863-884.

Milstein D, Bloss EB, Apostolides PF, Vaidya SP, Dilly GA, Zemelman BV, Magee JC (2015) Inhibitory gating of input comparison in the CA1 microcircuit. Neuron 87: 1274-1289.

Mitchell AS, Sherman SM, Sommer MA, Mair RG, Vertes RP, Chudasama Y (2014) Advances in understanding mechanisms of thalamic relays in cognition and behavior. J neurosci 34:15340-15346.

Mölle M, Born J (2011) Slow oscillations orchestrating fast oscillations and memory

consolidation. Prog Brain res 193:93-110.

Montgomery SM, Betancur MI, Buzsaki G (2009) Behavior-dependent coordination of multiple theta dipoles in the hippocampus. J Neurosci 29:1381-1394.

Montpied P,Winsky L, Dailey JW, Jobe PC, Jacobowitz DM (1995) Alteration in levels of expression of brain calbindin D-28k and calretinin mRNA in genetically epilepsy-prone rats. Epilepsia 36:911-921.

Morales GJ, Ramcharan EJ, Sundararaman N, Morgera SD, Vertes RP (2007) Analysis of the actions of nucleus reuniens and the entorhinl cortex on EEG and evoked population behavior of the hippocampus. Conf Proc IEEE Eng Med Biol Soc 2007:2480-2484.

Nopoulos PC, Rideout D, Crespo-Facorro B, Andreasen NC (2001) Sex differences in the absence of massa intermedia in patients with schizophrenia versus healthy controls. Schizophr Res 48:177-185.

Ohtake T, Yamada H (1989) Efferent connections of the nucleus reuniens and the rhomboid nucleus in the rat: an anterograde PHA-L tracing study. Neurosci Res 6:556-568.

Ogundele OM, Lee CC, Francis J (2017)Thalamic dopaminergic neurons project to the paraventricular nucleus-rostral ventrolateral medulla/C1 neural circuit. Anat Rec (Hoboken) 300:1307-1314.

Overstreet-Wadiche L, McBain CJ (2015) Neurogliaform cells in cortical circuits. Nat Rev Neurosci 16:458-468.

Pissadaki EK, Sidiropoulou K, Reczko M, Poirazi P (2010) Encoding of spatio-temporal input characteristics by a CA1 pyramidal neuron model. PLoS Comput Biol 6:e1001038.

Prasad JA, Chudasama Y (2013) Viral tracing identifies parallel disynaptic pathways to the hippocampus. J Neurosci 33:8494-8503.

Prasad JA, Macgregor EM, Chudasama Y (2013) Lesions of the thalamic reuniens cause impulsive but not compulsive responses. Brain Struct Funct 218: 85-96.

Prasad JA, Abela AR, Chudasama Y (2017) Midline thalamic reuniens lesions improve executive behaviors. Neurosci 14:77-88.

Reagh ZM, Murray EA, Yassa MA (2017) Repetition reveals ups and downs of hippocampal, thalamic, and neocortical engagement during mnemonic decisions. Hippocampus 27:169-183.

Remondes M, Schuman EM (2002) Direct cortical input modulates plasticity and spiking in CA1 pyramidal neurons. Nature 416:736-740.

Remondes M, Schuman EM (2003) Molecular mechanisms contibuting to long-lasting synaptic plasticity at the temperoammonic-CA1 synapse. Learn Mem 10:247-252.

Remondes M, Schuman EM (2004) Role for a cortical input to hippocampal area CA1 in the consolidation of long-term memory. Nature 431:699-703.

Rockland KS (2015) About connections. Front Neuroanat 9:61 doi 10.3389/

fnana.2015.00061.
Roy A, Svensson FP, Mahez A, Kocsis B (2017) Prefrontal-hippocampal coupling by theta rhythm and by 2-5 Hz oscillation in the delta band: the role of the nucleus reuniens of the thalamus. Brain Struct Funct 222:2819-2830.
Saalman YB (2014) Intralaminar and medial thalamic influence on cortical synchrony, information transmission and cognition. Front Syst Neurosci 8:83 doi: 10.3389/fnsys.2014.00083.
Schall KP, Kerber J, Dickson CT (2008) Rhythmic constraints on hippocampal processing: state and phase-related fluctuations of synaptic excitability during theta and slow oscillations. J Neurophysiol 99:888-899.
Schall KP, Dickson CT (2010) Changes in hippocampal excitatory synaptic transmission during cholinergically induced theta and slow oscillation states. Hippocampus 20:279-292.
Schwartz TL, Sachdeva S, Stahl SM (2012) Glutamate neurocircuitry: theoretical underpinning in schizophrenia. Front Pharmacol 3:195.
Sherman SM (2012) Thalamocortical interactions. Curr Opin Neurobiol 22:575-579.
Sierra RO, Pedraza LK, Zanona QK, Santana F, Boos FZ, Crestani AP, Haubrich J, de Oliveira Alvares L, Calcagnotto ME, Quillfeldt JA (2017) Reconsolidation-induced rescue of a remote fear memory blocked by an early cortical inhibition: involvement of the anterior cingulate cortex and the mediation by the thalamic nucleus reuniens. Hippocampus 27:596-607.
Sigurdsson T, Duvarci S (2016) Hippocampal-prefrontal interactions in cognition, behavior and psychiatric disease. Front Syst Neurosci 9:109. Doi: 10.3389/fnsys.2015.00190.
Sindreu C, Storm DR (2011) Modulation of neuronal signal transduction and memory formation by synaptic zinc. Front Behav Neurosci 5:68. Doi:10.3389/fnbeh.2011.00068.
Sloan DM, Bertram EH 3rd (2011) Excitatory amplification through divergent-convergent circuits: the role of the midline thalamus in limbic seizures. Neurobiol Dis 43:435-445.
Small SA, Schobel SA, Buxton RB, Witter MP, Barnes A (2011) A pathophysiological framework of hippocampal dysfunction in ageing and disease. Nat Rev Neurosci 12:585-601.
Somogyi P, Klausberger T (2005) Defined types of cortical interneuron structure space and spike timing in the hippocampus. J Physiol 562(Pt 1):9-26.
Spellman TJ, Gordon JA (2015) Synchrony in schizophrenia: a window into circuit-level pathophysiology. Curr Opin Neurobiol 30:17-23.
Stefan H, Lopes da Silva FH (2013) Epileptic neuronal networks: methods of identification and clinical relevance. Front Neurol 4:8. Doi: 10.3389/fneur.2013.00008.

Su H-S, Bentivoglio M (1990) Thalamic midline cell populations projecting to the nucleus accumbens, amygdala, and hippocampus in the rat. J Comp Neurol 297:582-593.

Takahashi T, Suzuki M, Nakamura K, Tanino R, Zhou SY, Hagino H, Kawasaki Y, Kurachi M (2008) Association between absence of the adhesio interthalamica and amygdala volume in schizophrenia. Psychiatry Res 162:101-111.

Takahashi H, Magee JC (2009) Pathway interactions and synaptic plasticity in the dendritic tuft region of CA1 pyramidal cells. Neuron 62:102-111.

Trzesniak C et al (2011) Adhesio interthalamica alterations in schizophrenia spectrum disorders: a systematic review and meta-analysis. Prog Neuropsychopharmacol Biol Psychiatry 35:877-886.

Trzesniak C et al (2012) Longitudinal follow-up of cavum septum pellucidum and adhesio interthalamica alterations in first-episode psychosis: a population-based MRI study. Psychol Med 42:2523-2534.

Uhlhaas PJ, Singer W (2012) Neuronal dynamics and neuropsychiatric disorders: toward a translational paradigm for dysfunctional large-scale networks. Neuron 75:963-980.

Unal G, Joshi A, Viney TJ, Kis V, Somogyi P (2015) Synaptic targets of medial septal projections in the hippocampus and extrahippocampal cortices of the mouse. J Neurosci 35:15812-15826.

Van der Werf YD, Witter MP, Groenewegen HJ (2002) The intralaminar and midline nuclei of the thalamus. Anatomical and functional evidence for participation in processes of arousel and awareness. Brain Res Rev 39:107-140.

Van der Werf YD, Jolles J, Witter MP, Uylings HBM (2003a) Contributions of thalamic nuclei to declarative memory functioning. Cortex 39:1047-1062.

Van der Werf YD, Scheltens P, Lindeboom J, Witter Mp, Uylings HB, Jolles J (2003b) Deficits of memory, executive functioning and attention following infarctions in the thalamus: a study of 22 cases with localised lesions. Neuropsychol 41:1330-1344.

Vanderwolf CH, Leung LW, Cooley RK (1985) Pathways through cingulate, neo- and entorhinal cortices mediate atropine-resistant hippocampal rhythmical slow activity. Brain Res 347:58-73.

Varela C (2014) Thalamic neuromodulation and its implications for executive networks. Front Neural Circuits 8:69 doi: 10.3389/fncir.2014.00069.

Varela C, Kumar S, Yang JY, Wilson MA (2014) Anatomical substrates for direct interactions between hippocampus, medial prefrontal cortex, and the thalamic nucleus reuniens. Brain Struct Funct 219:911-929.

Vertes RP (1991) A PHA-L analysis of ascending projections of the dorsal raphe nucleus in the rat. J Comp Neurol 313:643-668.

Vertes RP, Fortin WJ, Crane AM (1999) Projections of the median raphe nucleus in the

rat. J Comp Neurol 407:555-582.
Vertes RP (2002) Analysis of projections from the medial prefrontal cortex to the thalamus in the rat, with emphasis on nucleus reuniens. J Comp Neurol 442:163-187.
Vertes RP, Hoover WB, DiPrisco VG (2004) Theta rhythm of the hippocampus: subcortical control and functional significance. Behav Cogn Neurosci Rev 3:173-200.
Vertes RP, Hoover WB, Do Valle AC, Sherman A, Rodriguez JJ (2006) Efferent projections of reuniens and rhomboid nuclei of the thalamus in the rat. J Comp Neurol 499:768-796.
Vertes RP, Hoover WB, Szigeti-Buck K, Leranth C (2007) Nucleus reuniens of the midline thalamus: link between the medial prefrontal cortex and the hippocampus. Brain Res Bull 71:601-609.
Vertes RP, Linley SB, Hoover WB (2015) Limbic circuitry of the midline thalamus. Neurosci Biobeh Rev 54:89-107.
Vertes RP (2015) Major diencephalic inputs to the hippocampus: supramammillary nucleus and nucleus reuniens. Circuitry and function. Prog Brain Res 219:121-144.
Walsh DA, Brown JT, Randall AD (2017) In vitro characterization of cell-level neurophysiological diversity in the rostral nucleus reuniens of adult mice. J Physiol 595:3549-3572.
Wang X, Stewart L, Cortez MA, Wu Y, Velazquez JC, Liu CC, Shen L, Snead OC 3rd (2009) The circuitry of atypical absence seizures in GABA(B)R1a transgenic mice. Pharmacol Biochem Behav 94:124-130.
Wheeler AL, Teixera CM, Wang AH, Xiong X, Kovacevic N, Lerch JP, McIntosh AR, Parkinson J, Frankland PW (2013) Identification of a functional connectome for long-term fear memory in mice. PLoS Comput Biol 9: e1002853. Doi: 10.1371/journal.pcbi.1002853.
Wolanski T, Clement EA, Peters SR, Palczak MA, Dickson CT (2006) Hippocampal slow oscillation: a novel EEG state and its coordination with ongoing neocortical activity. J Neurosci 26:6213-6229.
Wouterlood FG, Saldana E, Witter MP (1990) Projections from the nucleus reuniens thalami to the hippocampal region: light and microscopic tracing study in the rat with the anterograde tracer Phaseolus vulgaris-leucoagglutinin. J Comp Neurol 296:179-203.
Wouterlood FG (1991) Innervation of entorhinal principal cells by neurons of the nucleus reuniens thalami. Anterograde PHA-L tracing combined with retrograde fluorescent tracing and intracellular injection with Lucifer Yellow in the rat. Eur J Neurosci 3:641-647.
Wu Y et al (2007) Transgenic mice over-expressing GABA(B)Ra receptors acquire an atypical absence epilepsy-like phenotype. Neurobiol Dis 26:439-451.

Xu W, Südhof TC (2013) A neural circuit for memory specificity and generalization. Science 339:1290-1295.

Zhang Y, Yoshida T, Katz DB, Lisman JE (2012) NMDA antagonist action in thalamus imposes delta oscillations on the hippocampus. J Neurophysiol107:3181-3189.

Zimmerman EC, Grace AA (2016) The nucleus reuniens of the midline thalamus gates prefrontal-hippocampal modulation of ventral tegmental area dopamine neuron activity. J Neurosci 36:8984-8977.

DANKWOORD

"Waarom doe je dit allemaal Oma?" vroeg laatst een van mijn kleindochters toen ze me zag zitten tussen stapels artikelen, druk tikkend op m'n pc. Goeie vraag natuurlijk, want welbeschouwd leek het erg op huiswerk maken, en dan moest je in de ogen van een 'brugpieper' wel hartstikke gek zijn om dat zomaar voor je plezier te doen. Toch is dat laatste het geval, want alles wat leeft en groeit, heeft altijd mijn onbegrensde interesse gehad. Dus ging ik in een ver verleden biologie studeren aan de UVA. Door de inspirerende colleges van Fernando ontdekte ik al gauw dat ik vooral nieuwsgierig was naar de werking van ons brein. Helemaal geweldig vond ik het dat ik als kersverse, doch ietwat oudere doctorandus de kans kreeg om wetenschappelijk neurobiologisch onderzoek te doen in een combi-project van VU en UVA. Dat ik nog nooit had gehoord van de nucleus reuniens, het onderwerp van de studie, was geen bezwaar. Ik kwam er al snel achter dat ik daarin niet de enige was; over de reuniens was nog maar weinig bekend. Er was dus een wereld aan kennis te winnen, een hele uitdaging waar ik met veel plezier aan begon.

Hoewel ik alle experimenten tijdig heb kunnen afronden, heeft de finish van het project nogal op zich laten wachten. Dat was beslist niet volgens plan, maar de dingen gaan in het leven zoals ze gaan. Niettemin zijn in de loop der jaren de onderzoeksresultaten gepubliceerd, en ligt er nu dan eindelijk een proefschrift. Daarmee is het hoog tijd dat ik iedereen die mij ooit op een of andere manier heeft geholpen, leden van de wetenschappelijke staf, laboranten en ondersteunend personeel, fotografen, aio's, medewerkers van het secretariaat, bij Anatomie van de VU, Neurobiologie van de UVA, het Nederlands Hersen Instituut, en de Universiteit van Edinburgh, hartelijk bedank voor alle steun en hulp tijdens én zeker ook ná mijn onderzoeksperiode.

Maar mijn speciale dank gaat uit naar de volgende mensen.

Beste Menno en Fernando, tijdens mijn aioschap en ook gedurende de vele jaren daarna, hadden we regelmatig (nou ja, om de paar jaar, of op het laatst toch minstens om de paar maanden) contact en wisten jullie, ondanks drukke werkzaamheden, steeds weer tijd voor mij vrij te maken. Ik heb veel van jullie deskundige en vooral ook prettige begeleiding geleerd. Zonder jullie inspanningen, zoals het kritisch lezen en bediscussiëren van mijn schrijfsels en het publicatie-klaar maken ervan, was dit proefschrift immers nooit tot stand gekomen. En niet alleen stonden jullie klaar om mij met wetenschappelijke vragen te helpen, ook in moeilijke periodes in mijn privéleven kon ik op jullie steun en hulp rekenen. Heel bijzonder !!!

Beste Henk, je hebt wat meer op de achtergrond mijn hele aio-periode (en alles daarna) gevolgd. Bij mijn aanstelling stond je al genoteerd als promotor, met Menno en Fernando als copromotoren. Later werd de rol van promotor officieel door Menno overgenomen. Echter, tijdens mijn 'eeuwig aio-zijn' is er nogal wat veranderd. Menno, jij bent een aantal jaren geleden niet mét, maar wel náár de noorderzon vertrokken om in Trondheim aan een verdere succesvolle carrière te werken. En Fernando, jij geniet al jaren van je pensioen, ook al ben je nog volop actief in de neurowetenschappen. Henk, inmiddels ook met 'actief pensioen', jij bent tot mijn blijdschap weer tot mijn promotor benoemd toen bleek dat Menno al te lang 'weg' was om die rol nog te mogen vervullen. Reuze bedankt dat je deze taak weer op je hebt willen nemen. Zo lijkt de cirkel rond, op een manier die niemand had kunnen bedenken.

Rest mij nog het thuisfront te bedanken. Stapels artikelen die af en toe elk vrij plekje in huis bevolkten, mijn geestelijke afwezigheid tijdens het schrijven aan artikel en/of proefschrift, jullie hebben het allemaal geduldig getrotseerd. Mijn pogingen om uit te leggen waar ik mee bezig was, werden vaak met een glazige blik beantwoord. Toch hebben jullie me steeds aangemoedigd om het project af te ronden; al was het maar 'om een feestje te kunnen vieren' was dan de standaardgrap.

In ieder geval ben ik tevreden dat ik de eindstreep heb gehaald, en wat kennisstukjes (hoe klein ook) heb kunnen bijdragen aan het oplossen van die voor mij nog altijd fascinerende puzzel: onze hersenen.

Margriet

BIBLIOGRAPHY

- Dolleman-van der Weel MJ, Lopes da Silva FH, Witter MP (2017) Interaction of nucleus reuniens and entorhinal cortex projections in hippocampal field CA1 of the rat. Brain Struct Funct 222:2421-2438.

- Dolleman-van der Weel MJ, Morris RG, Witter MP (2009) Neurotoxic lesions of the thalamic reuniens or mediodorsal nucleus in rats affect non-mnemonic aspects of watermaze learning. Brain Struct Funct 213:329-342.

- Dolleman-van der Weel MJ, Witter MP (2000) Nucleus reuniens thalami innervates gamma aminobutyric acid positive cells in hippocampal field CA1 of the rat. Neurosci Lett 278:145-148.

- Dolleman-van der Weel MJ, Lopes da Silva FH, Witter MP (1997) Nucleus reuniens thalami modulates activity in hippocampal field CA1 through excitatory and inhibitory mechanisms. J Neurosci 17:5640-5650.

- Dolleman-van der Weel MJ, Witter MP (1996) Projections from the nucleus reuniens thalami to the entorhinal cortex, hippocampal field CA1, and the subiculum in the rat arise from different populations of neurons. J Comp Neurol 364:637-650.

- Dolleman-van der Weel MJ, Wouterlood FG, Witter MP (1994) Multiple anterograde tracing, combining Phaseolus vulgaris leucoagglutinin with rhodamine- and biotin-conjugated dextran amine. J Neurosci Methods 51:9-21.

- Dolleman-van der Weel MJ, Nijssen A, Steinbuch HW (1993) Morphological and behavioral drawbacks of fetal dopaminergic grafts, prelabeled with Phaseolus vulgaris leucoagglutinin. Exp Neurol 122:260-272.

- Pennartz CM, Dolleman-van der Weel MJ, Kitai ST, Lopes da Silva FH (1992) Presynaptic dopamine D1 receptors attenuate excitatory and inhibitory limbic inputs to the shell region of the rat nucleus accumbens studied in vitro. J Neurophysiol 67:1325-1334.

- Pennartz CM, Dolleman-van der Weel MJ, Lopes da Silva FH (1992) Differential membrane properties and dopamine effects in the shell and core of the rat nucleus accumbens studied in vitro. Neurosci Lett 136:109-112.

- Dolleman-van der Weel MJ, Nijssen A, De Vente J, Ramaekers FCS, Cordell B, Fuller F, Steinbusch HWM (1991) Morphological and behavioral effects of basic fibroblast growth factor and heparin on transplanted fetal dopaminergic neurons and astrocytes in the denervated rat caudate-putamen. In: Growths factors and Alzheimer's disease. Eds. Hefti F, Brachet P, Will B, Christen Y. Springer-Verlag Berlin Heidelberg New York, pp:149-164.

- Drukarch B, Schepens E, Dolleman-van der Weel MJ, De Boer P, Van Vliet BJ, Stoof JC (1990) Lack of a dopamine autoreceptor selective profile of B-HT 920 in functional in vitro model systems of D2 receptors in rat striatum. Eur J Pharmacol 187:257-269.